Enantioselective Preparation of a *cis*-*β*-Boronyl Cyclobutylcarboxyester Scaffold and Its Highly Diastereoselective Nickel/Photoredox Dual-Catalyzed Cross-Coupling

by

Kevin Nguyen

A thesis submitted in partial fulfillment of the requirements for the degree of

Master of Science

Department of Chemistry
University of Alberta

Abstract

Chiral polyfunctionalized cyclobutanes are components of numerous bioactive natural products and pharmaceutical agents. As a consequence, they have gained significant attention in medicinal chemistry. Optically enriched cyclobutylboronates can serve as valuable synthetic intermediates for the synthesis of a broad range of chiral cyclobutanes through exploiting the versatility of the boronic ester functionality. In this regard, the asymmetric synthesis of enantioenriched cyclobutylboronates is highly desirable. This Thesis describes recent efforts on the preparation of optically enriched polyfunctionalized cyclobutanes with an emphasis on cyclobutylboronates.

Chapter 1 provides examples of bioactive natural products and pharmaceutical agents containing the cyclobutane motif and describes the value of the rigid cyclobutane structure in drug discovery. A summary of recent methods for the preparation of optically enriched cyclobutanes along with the asymmetric functionalization of prochiral cyclobutane rings is described.

Chapter 2 describes the efforts made toward the synthesis of an optically enriched *cis*-β-boronyl cyclobutylcarboxyester by way of the enantioselective copper-catalyzed conjugate borylation reaction of a prochiral cyclobutene 1-carboxyester. Details on the optimization of this methodology are described, including a ligand high-throughput screening approach. Computational modelling was conducted in an effort to rationalize the high enantioselectivity observed. Furthermore, extension of the catalytic asymmetric conjugate borylation reaction to a three-component aldol reaction with an aldehyde, and the mild and stereospecific oxidation of the carbon-boron bond afforded valuable enantioenriched cyclobutane products.

In Chapter 3, the resulting optically enriched *cis*-*β*-boronyl cyclobutylcarboxyester were examined as a potential cross-coupling partner. A highly diastereoselective nickel/photoredox dual-catalyzed $C(sp^3)$–$C(sp^2)$ cross-coupling of the corresponding trifluoroborate salt with aryl/heteroaryl bromides and cycloalkenyl nonaflates was developed, providing access to a wide diversity of *trans*-*β*-aryl/heteroaryl and cycloalkenyl cyclobutylcarboxyesters with excellent diastereoselectivity and retention of optical purity. Despite the radical nature of the cross-coupling conditions, the flanking carboxyester proved to be a reliable chirality relay group to maintain the stereochemical integrity of the organoboron intermediate.

Due to the potential synthetic versatility of optically enriched allylic cyclobutylboronates, methods for their efficient synthesis are highly desirable. In Chapter 4, allylic cyclobutylphosphates were prepared for the copper-catalyzed allylic borylation reaction in an effort to access allylic cyclobutylboronates.

Preface

Research reported in this thesis was completed under the direct supervision of Prof. Dennis G. Hall and in collaboration with Pfizer, led by Dr. Jack C. Lee. As outlined in Chapter 2, the preparation of compound **2-13** was completed by Dr. Helen Clement, the ligand high-throughput screen was conducted by our collaborators at Pfizer, and the computational modelling was performed by Prof. Dennis G. Hall. I was responsible for the remaining experimental studies and data analysis. I was also responsible for the experimental and data analysis described in Chapters 3 and 4 under the guidance of Prof. Dennis G. Hall.

Acknowledgements

Over the past two years and 4 months, I had the chance to work with extremely talented people who have helped me grow as an individual. First and foremost, I would like to thank my supervisor Prof. Dennis Hall who welcomed me into his research group. I am truly thankful for his continuous support and guidance both inside and outside the laboratory, which has been nothing but extraordinary. The training that Prof. Hall provided myself allowed me to acquire a broad set of chemistry and interpersonal skills. I felt that I have accumulated a tremendous amount of knowledge from Prof. Hall during my short stay in his research group. I feel extremely fortunate to have an amazing supervisor that has my best interest in mind. I would also like to thank my supervisory committee, Prof. Frederick West and Prof. Ratmir Derda for their guidance and feedback during the annual progress reports. The Hall research group consists of amazing individuals that has made my stay extremely enjoyable in the laboratory. I am particularly thankful to Dr. Marco Paladino, Hwee Ting Ang, Mohamad Estaitie, Jason Rygus, and Zain Kazmi for their friendships and Dr. Helen Clement for also her friendship and guidance when I first started in the laboratory

My appreciation is also extended to the excellent administration and research services at the University of Alberta. In particular, I would like to thank Anita Weiler for administrative assistance, and all the staff from the NMR, mass spectrometry, analytical laboratory, and X-ray crystallography facilities. I would like to also give a big thank you to Dr. Ed Fu for his help with chiral HPLC. Last but not least, I would like to thank my significant other Lena Choon Moy Li Chun Fong and my family for their love and support throughout my studies, I will forever be grateful.

Table of Contents

List of Figures

List of Schemes

List of Tables

List of Abbreviations

AIBN 2,2′-Azobis(2-methylpropionitrile)

Am Amyl

app q Apparent quartet

Ar Aryl group

AQ Aminoquinoline

BARF Tetrakis[3,5-bis(trifluoromethyl)phenyl]borate

Bn Benzyl

bpy Bipyridine

br Broad

nBu Butyl

tBu *tert*-Butyl

calcd Calculated

CFL Compact fluorescent bulbs

cm^{-1} Wavenumber

COD 1,5-Cyclooctadiene

CPME Cyclopentyl methyl ether

Cy Cyclohexyl

dan 1,8-Diaminonaphthalene

dba Dibenzylideneacetone

DBU 1,8-Diazabicyclo[5.4.0]undec-7-ene

DCE 1,2-Dichloroethane

DCM Dichloromethane

dd Doublet of doublets

ddd Doublet of doublet of doublets

dFCF$_3$ppy 2-(2,4-Difluorophenyl)-5-trifluoromethylpyridine

DFT Density functional theory

DIBAL-H Diisobutylaluminum hydride

DIPPF 1,1′-Bis(diisopropylphosphino)ferrocene

DMAP 4-Dimethylaminopyridine

dmpe 1,2-Bis(dimethylphosphino)ethane

DPEPhos Bis[(2-diphenylphosphino)phenyl] ether

dppf 1,1′-Ferrocenediyl-bis(diphenylphosphine)

dr Diastereomeric ratio

dt Doublet of triplets

ee Enantiomeric excess

EI Electron impact

equiv Equivalents

ESI Electrospray ionization

Et Ethyl

Et$_2$O Diethyl ether

EtOAc Ethyl acetate

G Generation

h Hour

Het Hetero

HFIP Hexafluoro-2-propanol

HPLC High performance liquid chromatography

HRMS High resolution mass spectrometry

HTS High-throughput screening

IR Infrared spectroscopy

KHF_2 Potassium hydrogen difluoride

LDA Lithium diisopropyl amide

m Multiplet

M Metal

MeCN Acetonitrile

MeOH Methanol

MS Mass spectrometry

MTBE *tert*-Butyl methyl ether

NBS *N*-BromoSuccinimide

NMR Nuclear magnetic resonance

ORTEP Oak Ridge thermal ellipsoid plot

OTf Trifluoromethanesulfonate

Pd Palladium

Ph Phenyl

pin Pinacol

Pn Pentoxide

iPr Isopropyl

q Quartet

rt Room temperature

SCE Saturated calomel electrode

SET Single electron transfer

SPhos 2-Dicyclohexylphosphino-2′,6′-dimethoxybiphenyl

t Triplet

TBS *tert*-Butyldimethylsilyl

TFA Trifluoroacetic acid

THF Tetrahydrofuran

TMS Trimethylsilyl

TROSEY Transverse relaxation optimized spectroscopy

Xantphos 4,5-Bis(diphenylphosphino)-9,9-dimethylxanthene

XPhos [2-Dicyclohexylphosphino-2′,4′,6′-triisopropylbiphenyl]

Chapter 1. Introduction: Preparation of Cyclobutane Building Blocks

1.1 Cyclobutane motifs in biologically relevant compounds

Cyclobutane rings are a common structural motif found in a variety of natural products which have been sourced from bacteria, fungi, plants and marine invertebrates. Many exhibit biological activities and may serve as a potential drug leads.[1] Cyclobutane-containing natural products are of particular interest because many of these compounds exhibit important biological activity, displaying anti-tumor, anti-bacterial, anti-fungal and immunosuppressive properties.[1] For example, a family of dimeric and tetrasubstituted piperarborenines were isolated from the stems of *Piper arboresens* (Figure 1-1).[2] Isolation of the many stereoisomeric cyclobutane derivatives of piperarborenine suggests that such compounds were constructed from a non-selective photolytic [2 + 2] cycloaddition of alkenes. These compounds can be classified based on their stereochemical structure: *cis-trans-cis* and *trans-trans-trans* (Figure 1-1). This family of cyclobutanes displayed *in vitro* cytotoxicity against cancer cell lines.[2] Another example of a natural product is the *cis*-1,2-disubstituted cyclobutane quassidine A, which was isolated from the stems of *Picrasma quassiodies* (Figure 1-1).[3] It was the first reported *bis-β*-carboline natural product with a cyclobutane motif. This compound was tested for, and successfully displayed, anti-inflammatory activity. Moreover, Hippolachnin A, a cyclobutane-containing natural product with a unique carbon skeleton was isolated from the sea sponge *Hippospongia lachne* from South China (Figure 1-1).[4] This natural product showed potent antifungal activity against three pathogenic fungi. Overall, cyclobutane-containing natural products have been found with a vast

array of substitution patterns as well as distinct combinations of stereogenic centers which make them non-trivial to access synthetically.

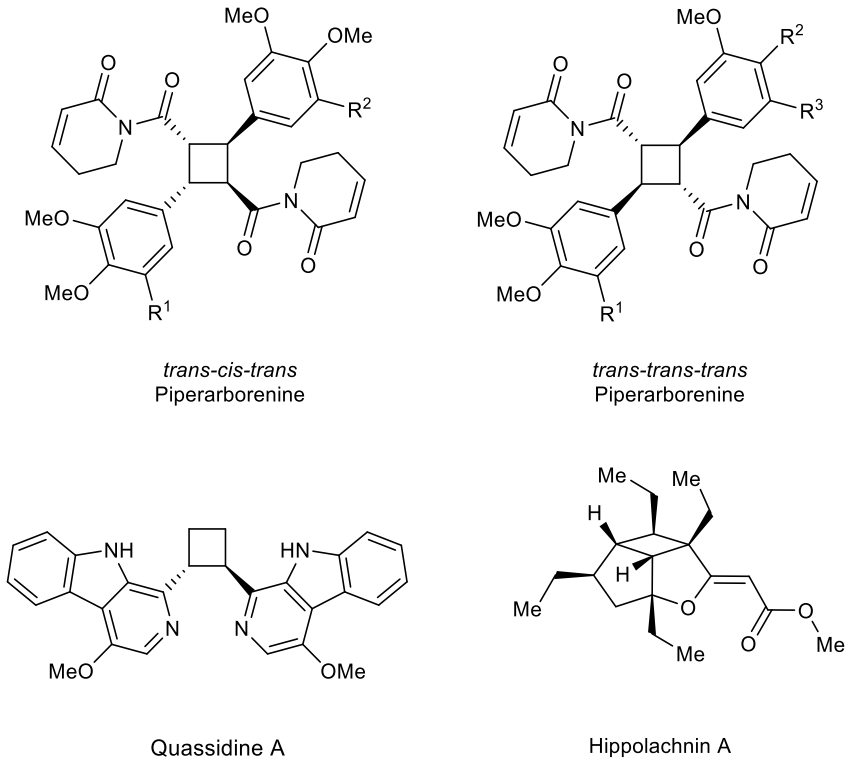

Figure 1-1. Examples of cyclobutane-containing natural products

The cyclobutane motif is also a core subunit in several synthetic and medicinally relevant compounds. For instance, Lobucavir, a cyclobutylguanosine nucleoside analogue, is an anti-viral drug that exhibits activity against herpes viruses, hepatitis B, HIV/AIDS and cytomegalovirus (Figure 1-2).[5] Another example of a medicinally relevant compound with a cyclobutane core is the discovery of Histamine H_3 receptor antagonists (Figure 1-2).[6] This potent compound was developed by Pfizer and is currently under clinical trials. Furthermore, the merit of the cyclobutane structure as a pharmacophore was displayed in the development of a novel series of cyclobutane derived potent and selective NK_1 selective antagonist (Figure 1-2).[7] The cyclobutane ring was found to provide comparable NK_1 receipt binding affinity compared to the phenyl

glycine-based analog.[7] As a result of the structural rigidity of the cyclobutane ring, this motif has often been employed in drug discovery to impose spatial rigidification and/or serve as a bioisostere of arenes (Figure 1-3).[8]

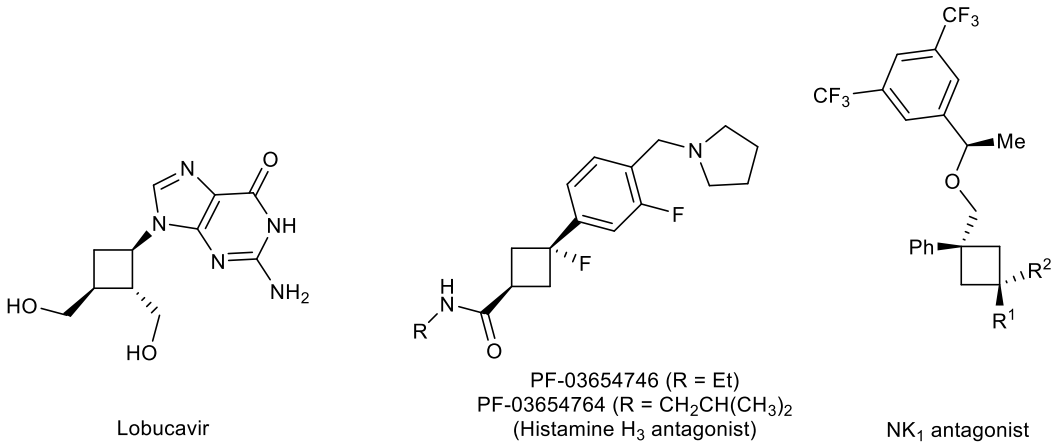

Figure 1-2. Examples of synthetic bioactive cyclobutane-containing compounds

Figure 1-3. Cyclobutane as a bioisostere for an arene

1.2 Recent methods for the synthesis of optically enriched cyclobutanes and cyclobutenes

In the last decade, new methods for the synthesis of optically enriched cyclobutane and cyclobutene rings have been developed. While cyclobutane and cyclobutenes are typically constructed by way of a [2 + 2] cycloaddition reaction, this method requires the synthesis of a new cyclobutane ring for every new or different substituent that is desired on the ring. In an alternative and complementary approach, the asymmetric functionalization of readily available cyclobutanes and prochiral cyclobutenes can provide access to a diverse range of functionalized

cyclobutanes from a single scaffold. Herein, a survey of recent methods concerning the enantioselective synthesis and asymmetric functionalization of cyclobutanes and prochiral cyclobutenes is described.

1.2.1. Enantioselective synthesis of cyclobutanes by [2 + 2] cycloaddition

1.2.1.1 Enantioselective Lewis acid catalyzed formal [2 + 2] cycloaddition

In 2016, Li and co-workers reported a highly enantio- and diastereoselective copper-catalyzed [2 + 2] cycloaddition of methylidenemalonate and alkenes using the chiral ligand **1-1**. This method provided highly functionalized donor-acceptor cyclobutanes **1-2** in moderate to high yields, with up to 99% ee and >99:1 dr (Scheme 1-1).[9] Control experiments suggested that the resulting cyclobutane product **1-2** can dissociate into a zwitterion pair at room temperature in the presence of a Lewis acid, resulting in racemization of the product. However, it was found that performing and stopping the reaction at –70 °C could inhibit the racemization process to obtain the product in excellent enantioselectivity. Due to the nature of this reaction, the alkene partners are limited to methylidenemalonate and electron-rich styrenes.

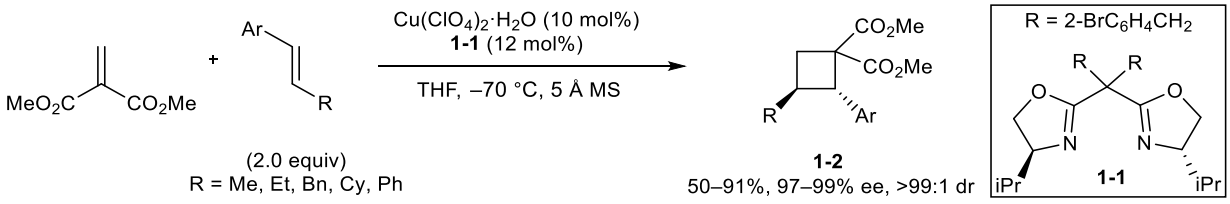

Scheme 1-1. Synthesis of donor-acceptor cyclobutanes

1.2.1.2 Enantioselective amine-catalyzed [2 + 2] cycloaddition

In 2013, Xu and co-workers reported the enantioselective organocatalytic formal [2 + 2] cycloaddition based on a tandem iminium-enamine activation of *α,β*-unsaturated aldehydes (Scheme 1-2a).[10] The secondary chiral amine catalyst **1-3** was found to readily promote the reaction. This method was applicable with functionalized 2-vinyl pyrroles and *α,β*-unsaturated aldehydes to afford pyrrole-containing cyclobutanes **1-4** in good yields and complete control of the three contiguous stereogenic centers. In 2012, Jorgenson and co-workers described an enantioselective [2 + 2] cycloaddition of nitroalkenes and enolizable *α,β*-unsaturated aldehydes (Scheme 1-2b).[11] The bifunctional chiral squaramide catalyst **1-5** enabled dual activation of both the *α,β*-unsaturated aldehyde and nitroalkene by way of dienamine formation and hydrogen-bonding of the oxygen atoms on the nitro group. Computational studies support the role of the bifunctional squaramide catalyst **1-5** in the formation of transition state **TS1.** Using this method, fully substituted cyclobutanes **1-6** were constructed in moderate to high yields with excellent enantioselectivity and complete diastereocontrol (Scheme 1-2b).

1.2.1.3 Enantioselective Lewis acid catalyzed [2 + 2] photochemical cycloaddition

In 2014, Yoon and co-workers discovered that the use of Lewis acids can accelerate visible light photoinduced electron transfer [2 + 2] cycloadditions of *α,β*-unsaturated ketones (Scheme 1-3a).[12] The amino acid-based chiral ligand **1-7** in tandem with the Lewis acid $Eu(OTf)_3$ was found to effectively promote the photochemical cycloaddition and afford trisubstituted cyclobutanes **1-8** with high enantioselectivity and good diastereoselectivity. Interestingly, changing the amino acid ligand to the reduced form **1-9** enabled access to a different diastereomer (**1-10**) with high enantioselectivity (Scheme 1-3a). A mechanistic feature

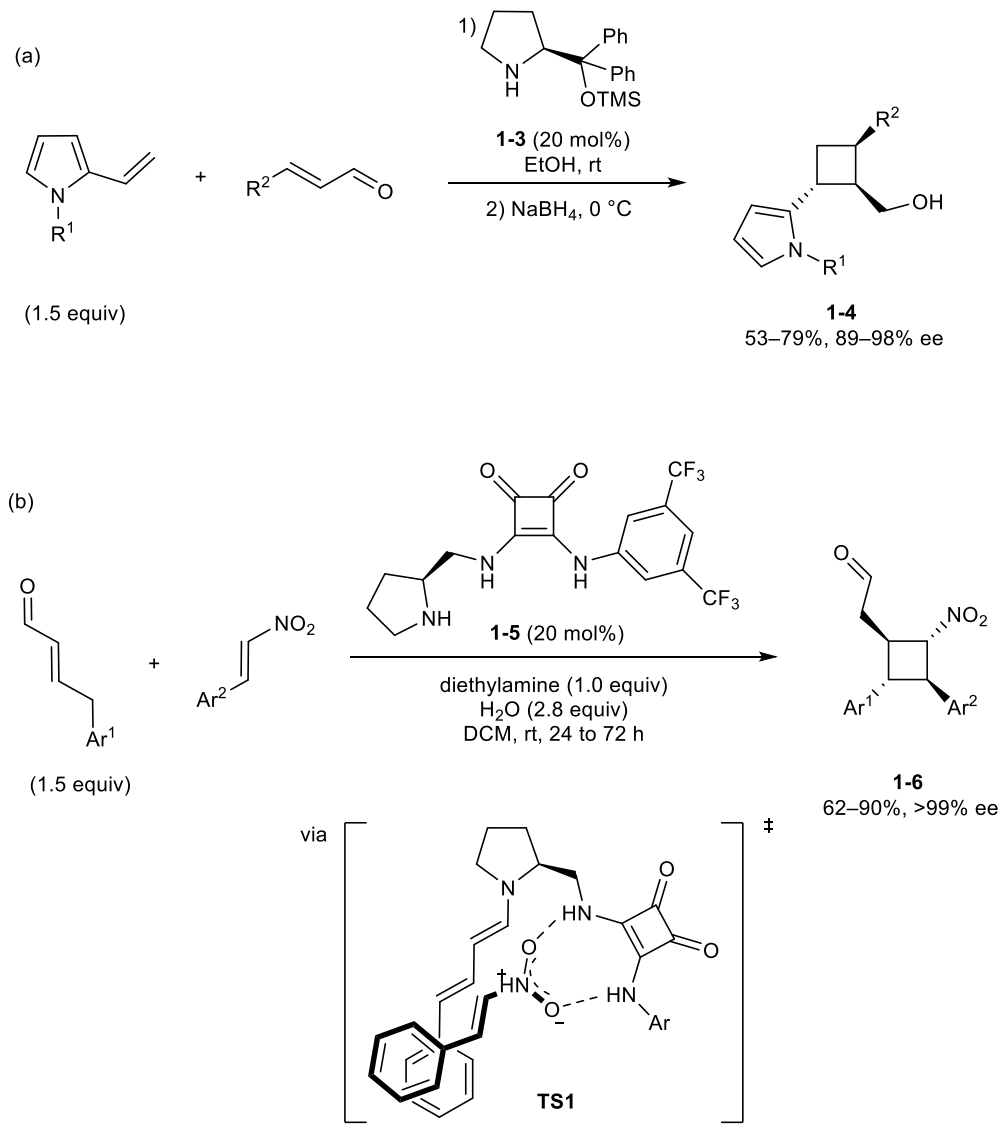

Scheme 1-2. Amine-catalyzed [2 + 2] cycloaddition methods

of this reaction is the crucial activation step involving the single electron reduction of the Lewis acid activated aryl enone **1-11** by the Ru(II) complex (Figure 1-3b). High enantioselectivities could be obtained due to the lack of racemic background reactions from the direct photoexcitation of the uncomplexed enone substrates. In 2017, the Yoon Group reported the Lewis acid-catalyzed sensitization of chalcones, enabling highly enantioselective [2 + 2] cycloadditions with styrenes to afford trisubstituted cyclobutanes **1-12** in good to excellent yields

and enantioselectivity (Scheme 1-4a).[13] Although the diastereoselectivity of the reaction was low, the authors noted that the diastereomers could be separated by silica column chromatography. The requirement of a bidentate chelating 2'-hydroxychalcone is a synthetic limitation as the resulting 2'-phenoxyketones are uncommon functional groups and difficult to manipulate. In a follow-up report in 2019, the Yoon Group applied their methodology towards a more general class of enoates substrates (Scheme 1-4b).[14]

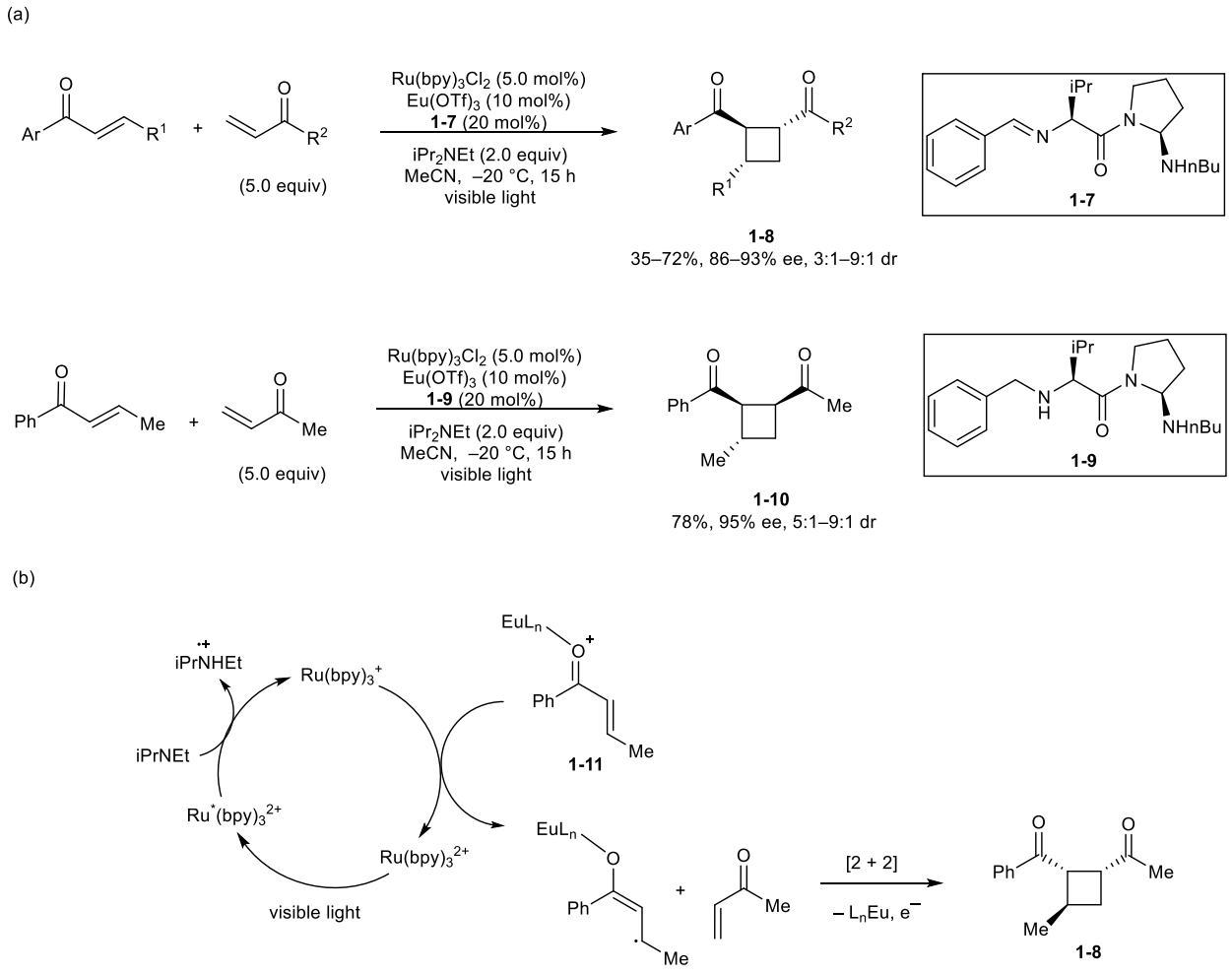

Scheme 1-3. (a) Lewis acid/photosensitizer dual-catalyzed [2 + 2] cycloaddition and (b) proposed mechanism

The cyclobutane products **1-14** were generally obtained in good to excellent yields and enantioselectivity, albeit with low diastereoselectivity. Optimization for the Lewis acid **1-15** and the appropriate photocatalyst was required to avoid racemic background reactions. A limitation to this method is the requirement of 5.0 or 10 equivalents of the styrene coupling partner.

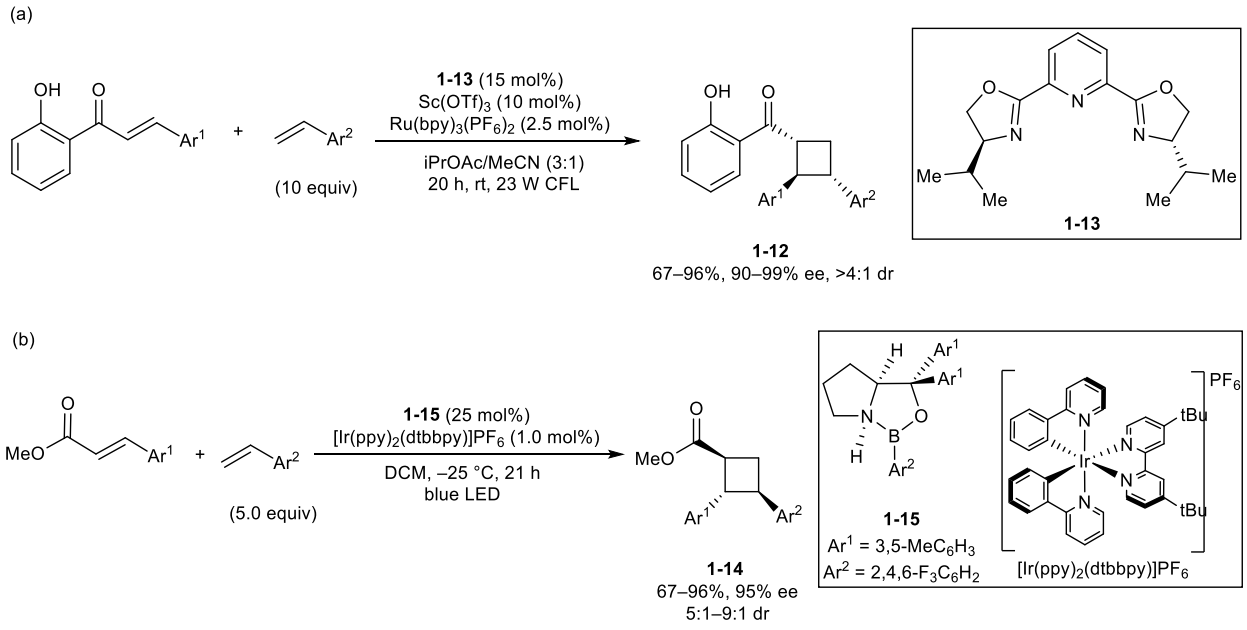

Scheme 1-4. Extension of the Lewis acid/photosensitizer dual-catalyzed [2 + 2] cycloaddition reaction towards other of *α,β*-unsaturated carbonyl compounds

1.2.1.4. Enantioselective chiral Lewis acid catalyzed [2 + 2] photochemical cycloaddition

In an alternative approach to Lewis acid-promoted [2 + 2] photocycloadditions mediated by a photosensitizer, in 2017, Meggers and co-workers developed a catalytic system in which a chiral Lewis acid bound substrate is directly activated by visible light towards a stereocontrolled reaction (Scheme 1-5).[15] Only the Rh(I) catalyst **1-16** was required in this system, which combined visible light activation of the substrate with a chiral environment for a stereocontrolled

reaction. Highly functionalized cyclobutanes **1-17** were obtained in excellent enantioselectivity and good diastereoselectivity. However, limitations remain in the requirement of an amide auxiliary on the substrate to chelate catalyst **1-16** and effectively facilitate the reaction.

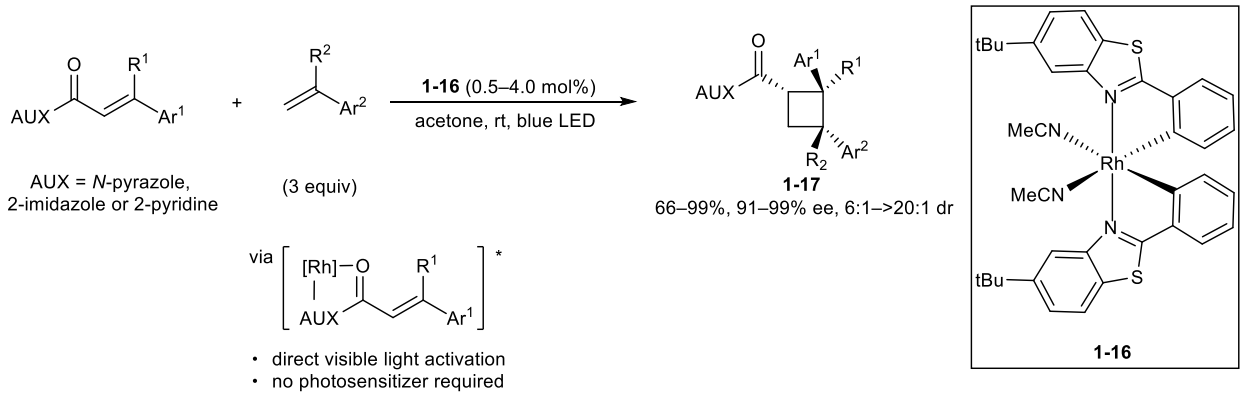

Scheme 1-5. Chiral Lewis acid-catalyzed [2 + 2] cycloaddition activated by visible light

1.2.1.5. Enantioselective diamine-catalyzed [2 + 2] photochemical cycloaddition of alkynes

In 2020, Aleman and co-workers reported a metal-free enantioselective [2 + 2] cycloaddition facilitated by a diamine catalyst (Scheme 1-6).[16] In general, highly functionalized cyclobutanes **1-18** were obtained in moderate to good enantio- and diastereoselectivity, and moderate to excellent yields. Substitution on the aryl moiety of the enone was mostly limited to alkyl groups with different substitution patterns on the aryl ring. A narrow subset of electron-rich and electron-deficient aryl rings was demonstrated. Moreover, a number of mono- and disubstituted arylated alkenes were found to be suitable under the optimized reaction conditions. The role of the diamine catalyst involved the formation of an active iminium ion species. DFT calculations revealed that upon visible light irradiation, charge transfer excited state complexes **1-19** and **1-20** are formed in equilibrium, in which the later can undergo photocycloaddition.

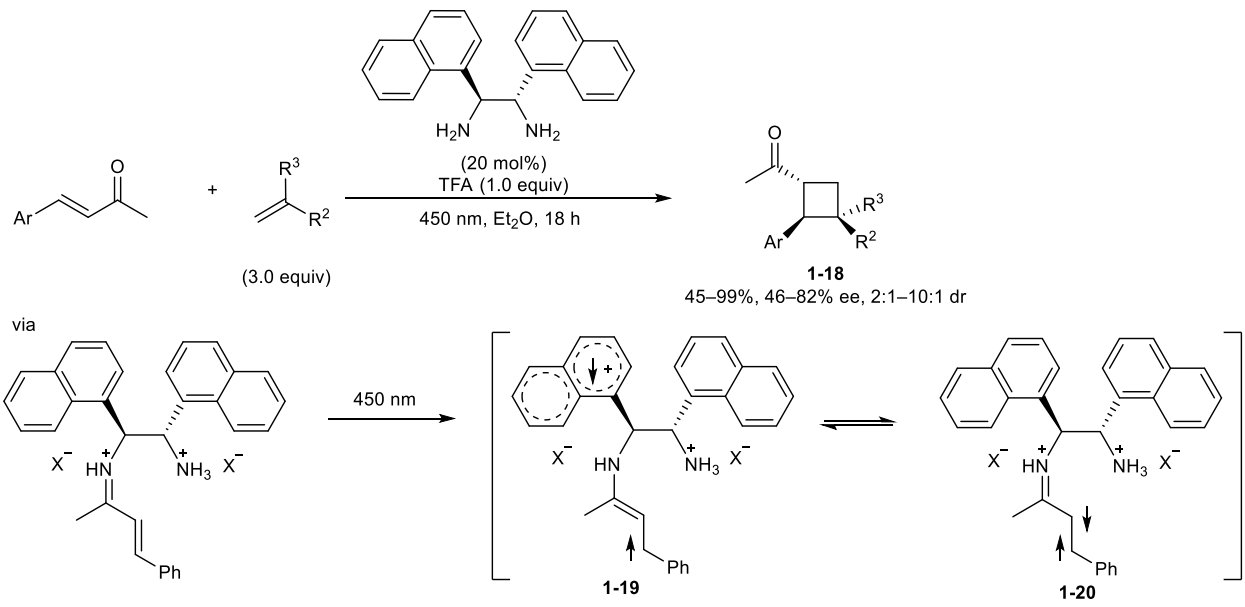

Scheme 1-6. Diamine-catalyzed [2 + 2] cycloaddition *via* a charge transfer complex

1.2.2 Enantioselective synthesis of cyclobutenes by [2 + 2] cycloaddition

1.2.2.1 Enantioselective [2 + 2] cycloaddition catalyzed by a digold complex

In 2017, the first intermolecular and enantioselective gold(I) catalyzed [2 + 2] cycloaddition of terminal alkynes and alkenes using the Josiphos digold(I) catalyst **1-21** was developed by Echavarren and coworkers (Scheme 1-7).[17] By carrying out the reaction at a low temperature (–20 °C), a good to excellent enantioselectivity of cyclobutenes **1-22** could be obtained with moderate to high yields. The reaction was found to accommodate a broad scope of aryl substrates for both the alkyne and alkene reaction partner. DFT studies indicated that only one of the gold(I) centers is directly involved in alkyne activation, while, the second gold(I) center is required to induce enantioselectivity.

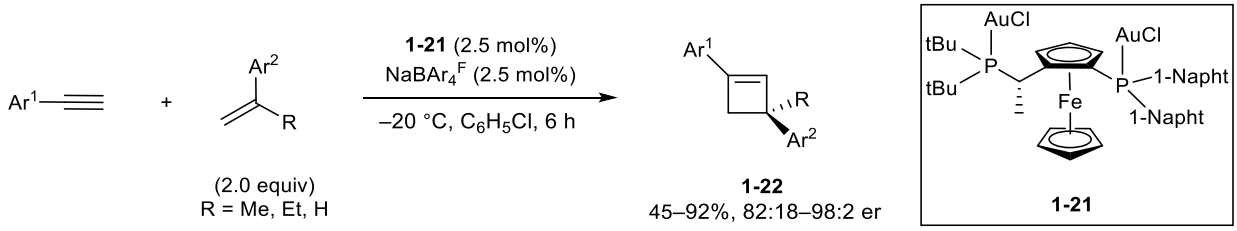

Scheme 1-7. Gold-catalyzed [2 + 2] cycloaddition

1.2.2.2 Enantioselective cobalt-catalyzed [2 + 2] cycloaddition

In 2019, RajanBabu and co-workers reported a broadly applicable enantioselective cobalt-catalyzed [2 + 2] cycloaddition between a wide variety of alkynes and alkenes.[18] Using ligand **1-23**, highly functionalized cyclobutanes **1-24** could be obtained in excellent enantioselectivity and high yields (Scheme 1-8). With a diverse range of heteroatoms (B, N, O, Si) that could be tolerated by this method, further diastereoselective transformations could be conducted towards the synthesis of other useful cyclobutene intermediates. Control experiments indicated the role of a cationic Co(I) species as the active catalyst.

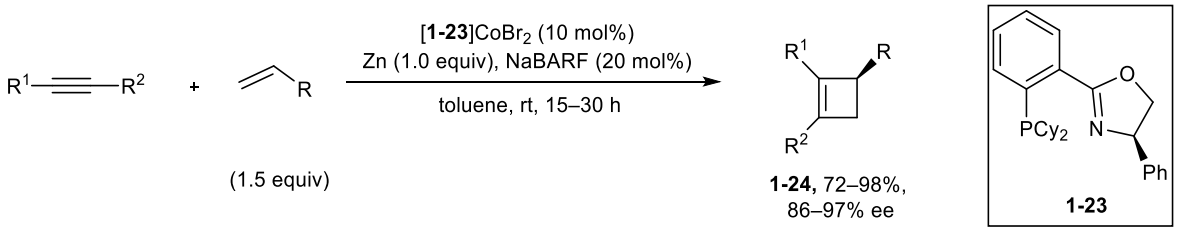

Scheme 1-8. Cobalt-catalyzed [2 + 2] cycloaddition

1.2.3 Enantioselective asymmetric functionalization of cyclobutanes

1.2.3.1 Enantioselective Pd-catalyzed C–H activation of cyclobutanes

In 2014, the enantioselective Pd(II)-catalyzed cross-coupling of a β-methylene C–H bond in cyclobutylcarboxyamide derivatives with arylboron reagents was reported by Yu and co-workers (Scheme 1-9a).[19] High yields and enantioselectivity of *cis*-1,2 disubstituted cyclobutanes **1-26** were achieved through the development of the chiral ligand **1-25**. Despite this advancement, the method suffered from a distinct limitation as cyclobutylcarboxyamide substrates bearing an α-hydrogen were incompatible. The authors attributed this lack of reactivity to the Thorpe-Ingold effect. The presence of a substituent larger than a hydrogen increases the C–C–C bond angle between the carbons of the α-substituent, the α-carbon, and the carboxyamide carbonyl to effectively promote the reaction. The presence of a small α-hydrogen atom compared to a bulkier alkyl group rendered enantioselective differentiation more challenging as the alkyl groups could provide steric influence. In 2018, the authors found that using the chiral ligand **1-27** overcame this substrate limitation in their previous Pd-catalyzed system when the chiral ligand **1-25** was employed (Scheme 1-9b).[20] The newly optimized method was now capable of promoting C–H arylation and vinylation with the corresponding iodide coupling partners to give cyclobutane products **1-28** and **1-29** in good yields and excellent enantioselectivity. It should be mentioned that a significant excess (3.0 equiv) of the more reactive iodide coupling partner is required. Treatment of cyclobutane **1-30** with sodium *tert*-butoxide successfully epimerized a stereocenter to give the *trans* product **1-31** with no erosion in enantioselectivity (Scheme 1-9c).

Notwithstanding the exceptional results obtained from these Pd-catalyzed directed C–H activation methods, limitations remain in the requirement of a directing amido group to facilitate

the reaction and its subsequent removal. In 2020, the Yu Group described a Pd-catalyzed enantioselective *β*-methylene C–H arylation reaction of aliphatic ketones using the chiral transient directing group **1-32** (Scheme 1-10).[21] The use of an electron deficient pyridine ligand proved to be crucial in obtaining cyclobutanes **1-33** in high enantioselectivity by serving as an acetate surrogate to accelerate C–H bond cleavage. An interesting silver salt additive effect was

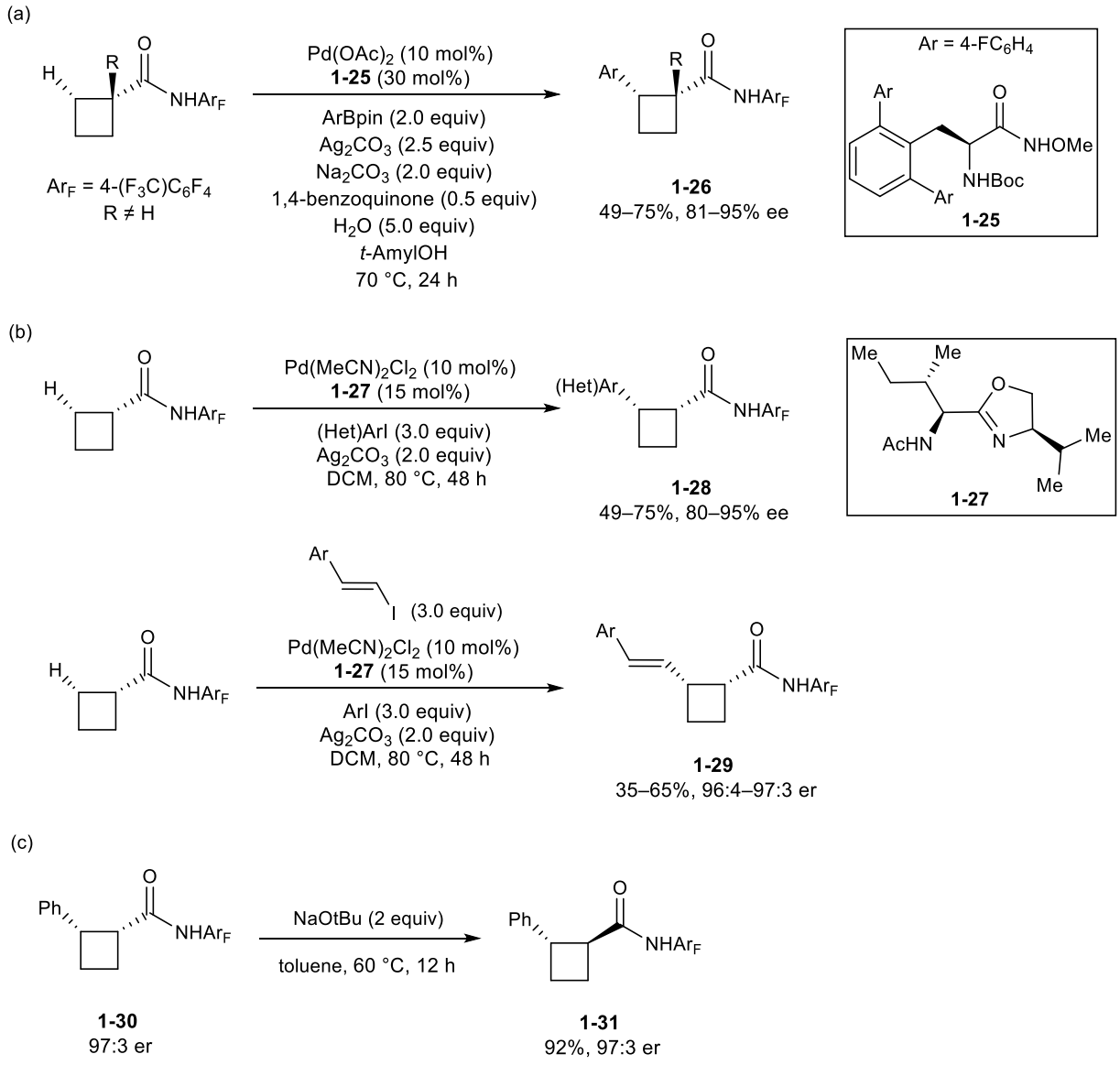

Scheme 1-9. (a, b) Enantioselective Pd-catalyzed C–H arylation and/or vinylation of an cyclobutylcarboxyamide and (c) epimerization of product

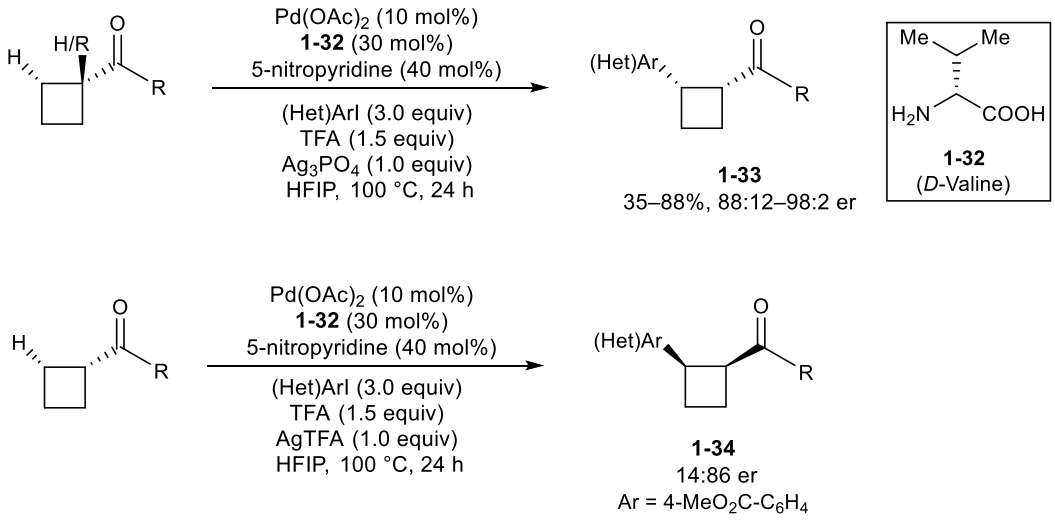

Scheme 1-10. Enantioselective Pd-catalyzed C–H arylation of cyclobutylketone using a transient directing group

observed where using silver trifluoroacetate could reverse the enantioselectivity to provide access to cyclobutane **1-34** in good enantioselectivity. However, limitations remain in the use of a significant excess (3.0 equiv) of the more reactive aryl and/or heteroaryl iodide electrophile.

1.2.3.2 Pd-catalyzed C–H activation of an optically enriched cyclobutane

In 2019, Reisman and co-workers reported the Pd-catalyzed directed C–H arylation of an optically enriched cyclobutane to afford *gem*-dimethyl cyclobutanes **1-35** with high retention of optical purity (Scheme 1-11).[22] In this protocol, heteroaryl iodides were found to be suitable coupling partners for the incorporation of pyridine, pyrimidine or indole rings. It should be mentioned that only *gem*-dimethyl cyclobutanes were examined as substrates for their optimized Pd-catalyzed C–H activation method.

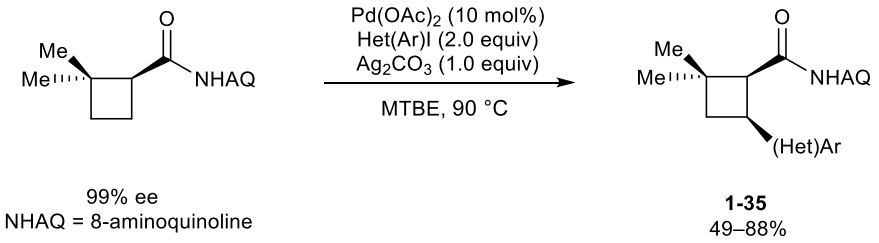

Scheme 1-11. Pd-catalyzed C–H activation of an optically enriched cyclobutane

1.2.4 Asymmetric functionalization of prochiral cyclobutenes

1.2.4.1 Enantioselective rhodium-catalyzed arylation of a cyclobutene 1-carboxyester

In 2016, Liu and co-workers reported the enantio- and diastereoselective rhodium-catalyzed arylation of a cyclobutene 1-carboxyester using aryl boronic acids.[23] Chiral diene ligand **1-36** was found to be crucial for high diastereoselectivity. This method afforded *trans*-1,2-disubstituted cyclobutanes **1-37** in moderate to excellent yields and enantioselectivity (Scheme 1-12). The scope of the reaction was not expanded towards heteroaryl derivatives.

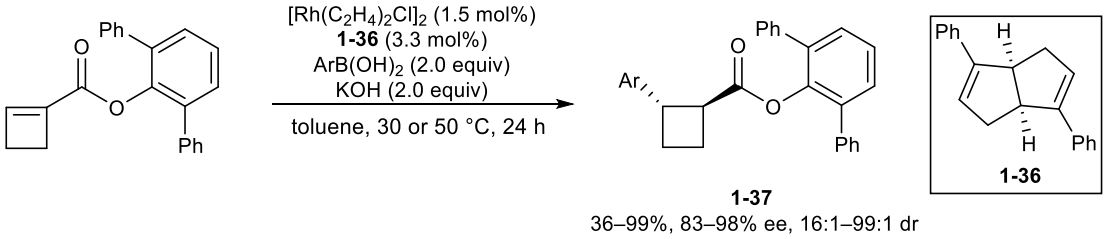

Scheme 1-12. Enantioselective rhodium-catalyzed arylation of cyclobutene

1.2.4.2. Enantioselective tandem copper-catalyzed conjugate addition or reduction/trapping reaction

In 2020, Lu and co-workers reported a tandem process that involved the enantioselective copper-catalyzed conjugate addition or reduction of prochiral cyclobutenones.[24] Rather than

quenching the resulting metal enolate intermediate with a proton source to give an achiral cyclobutanone, the intermediate was instead trapped with a chlorophosphate reagent to afford enantioenriched cyclobutenylphosphates (**1-39** or **1-41**) in moderate to good yield and excellent enantioselectivity (Scheme 1-13a). Various 3-aryl and 3-alkyl-substituted cyclobutenones were compatible with the reaction conditions. Furthermore, a wide range of dialkylzinc reagents, including a few diarylzinc reagents, were effectively employed for the conjugate addition reaction. Subsequent nickel-catalyzed Negishi cross-coupling of the enol phosphate moiety provided cyclobutene derivatives **1-42** without erosion in optical purity (Scheme 1-13b).

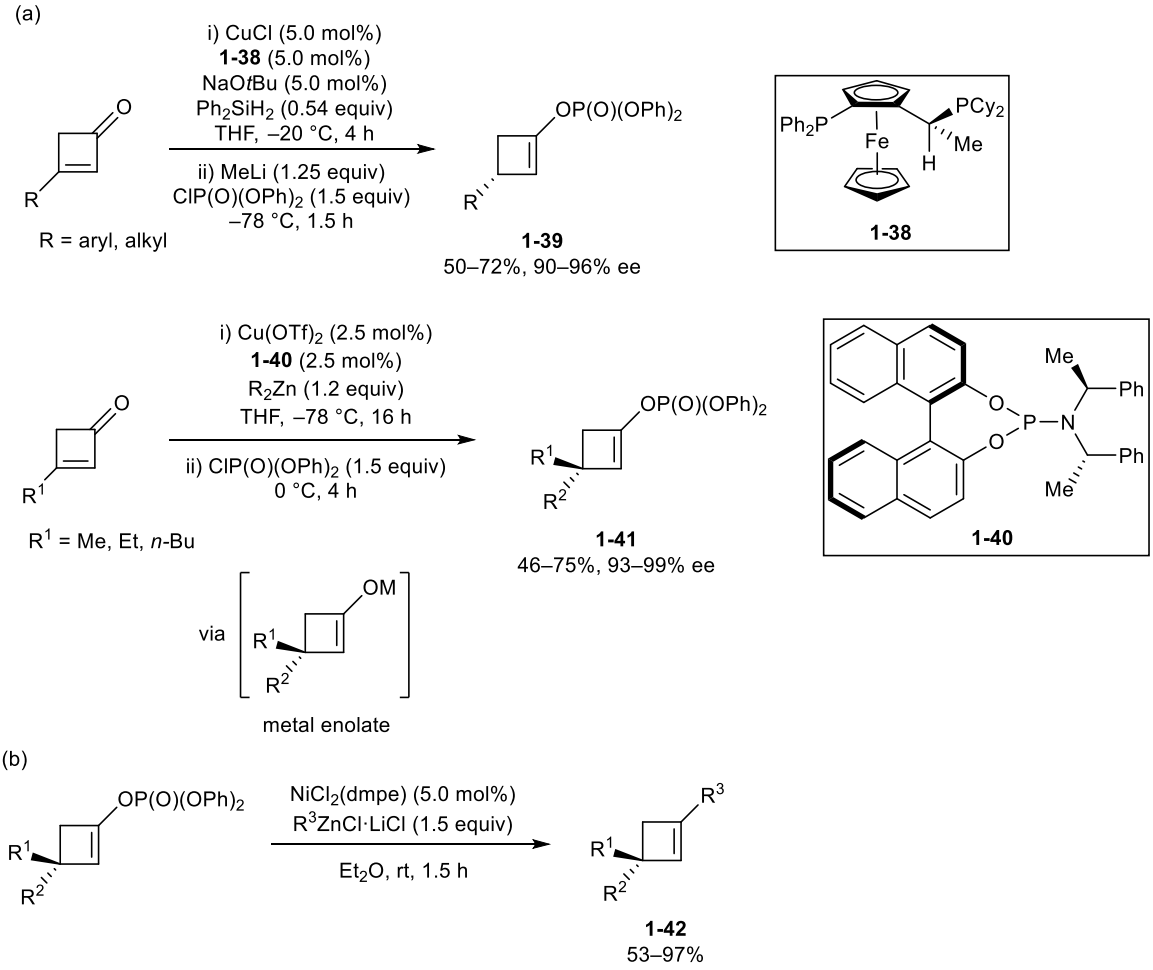

Scheme 1-13. (a) Synthesis of cyclobutenylphosphates and (b) application in Negishi cross-coupling

1.2.5. Miscellaneous methods for the enantioselective synthesis of cyclobutanes and cyclobutenes

1.2.5.1 Multistep rhodium-catalyzed bicyclobutanation/copper-catalyzed homoconjugate addition

In 2013, Fox and co-workers described the preparation of a series of optically enriched cyclobutanes by way of a three-component process. First, a diazo-enoate is treated with the rhodium catalyst **1-43** to give optically enriched bicyclobutanes **1-44** (Scheme 1-14a).[25] A subsequent copper-catalyzed homoconjugation addition reaction followed by enolate trapping with a proton source or carbon electrophile afforded highly substituted cyclobutanes **1-45** or **1-46** with retention in enantiomeric purity, respectively. In all cases, cyclobutane **1-47**, could be epimerized with potassium *tert*-butoxide for a more desirable dr (Scheme 1-14b). Furthermore, the diastereoselectivity could be reversed to give cyclobutane **1-48** by stopping the reaction with the sterically demanding proton source, 2,6-di-*tert*-butyl-4-methylphenol (Scheme 1-14c). Grignard reagents such as MeMgCl, EtMgCl, BnMgCl and PhMgCl were found to be applicable in the copper-catalyzed homoconjugation addition step.

1.2.5.2 Enantioselective intramolecular copper-catalyzed hydroalkylation

In 2015, Buchwald and co-workers reported the intramolecular hydroalkylation of alkyl halide tethered styrene derivatives through an enantioselective copper hydride-catalyzed process (Scheme 1-15).[26] This method provided access to *trans*-1,2-disubstituted cyclobutanes in good yields and excellent enantio- and diastereoselectivity. The presence of the lithium methoxide

additive proved critical to regenerate the copper hydride catalytic species. Of note, this method was only applied towards the synthesis of methyl-substituted cyclobutanes **1-50.**

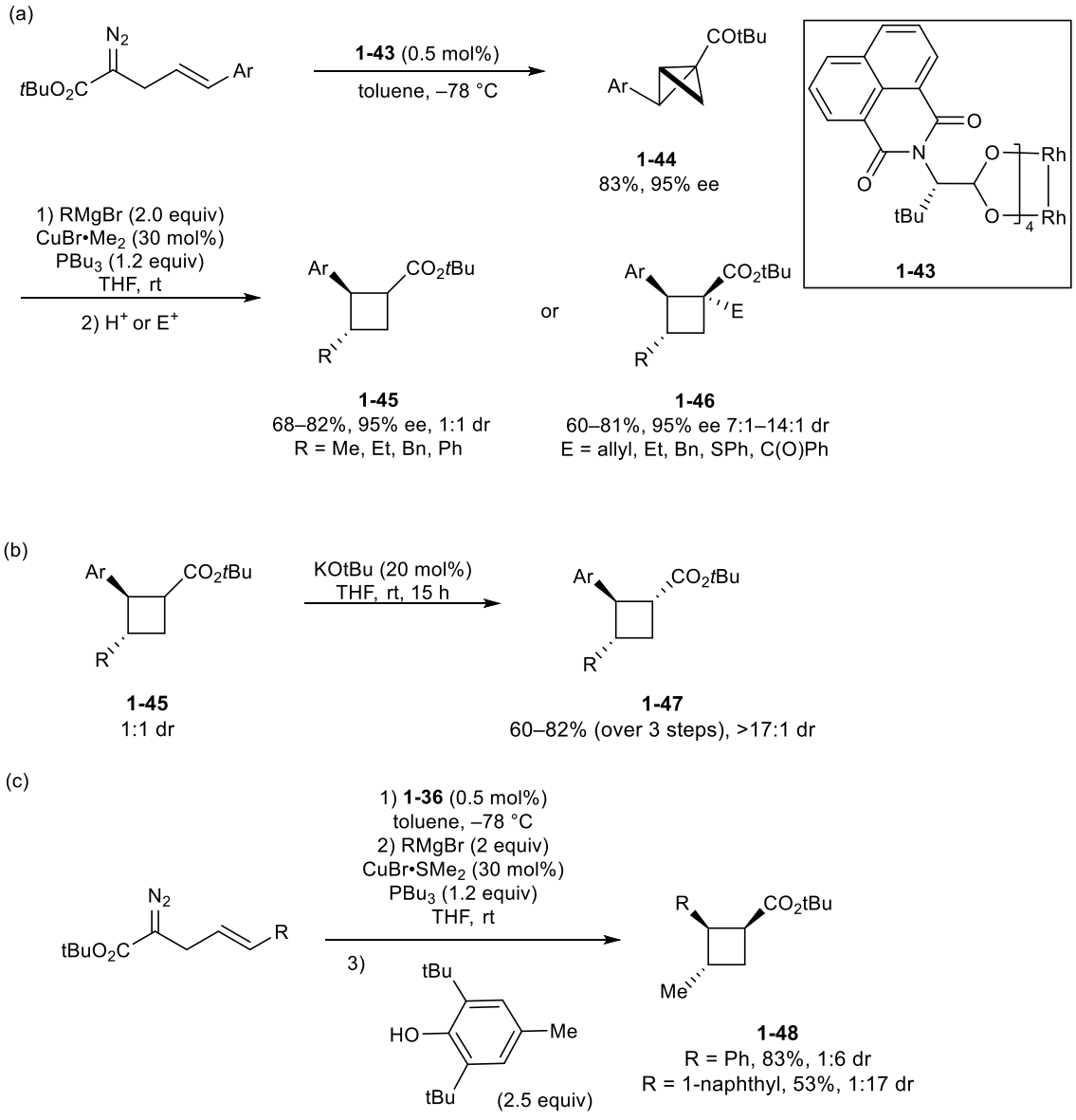

Scheme 1-14. (a, c) Rhodium-catalyzed bicyclobutanation/copper-catalyzed homoconjugate addition towards highly substituted cyclobutanes and (b) epimerization of product

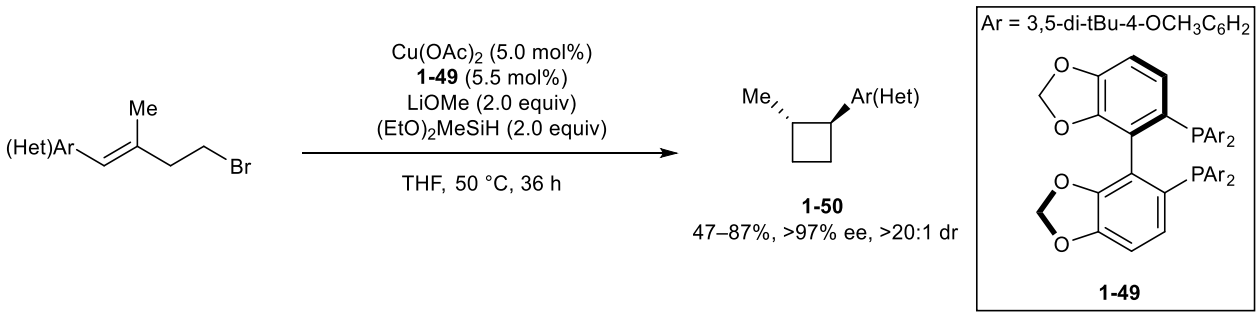

Scheme 1-15. Intramolecular copper-catalyzed hydroalkylation

1.2.5.3. Enantioselective phosphine-catalyzed Michael addition/Wittig olefination reaction

In 2019, Voituriez and co-workers reported an enantioselective phosphine-catalyzed tandem Michael addition/Wittig reaction via a phosphorus (III)/phosphorus(V) oxide cycle (Scheme 1-16a).[27] Employing the phosphorus-containing catalyst **1-51**, reactions of 4,4,4-trifluoro-1-arylbutane-1,3-dione and acetylenedicarboxylate afforded highly substituted trifluoromethyl-containing cyclobutenes **1-52** with predominantly the *trans* stereoisomer in high yield and enantioselectivity. This reaction mechanism was proposed to begin with the addition of the phosphorus catalyst onto acetylenedicarboxylate to form a zwitterionic intermediate which can subsequently deprotonate the 1,3-diketone substrate (Scheme 16b). The resulting enolate undergoes a Michael addition to from a phosphorus ylide. An intramolecular Wittig reaction affords the desired cyclobutene product and phosphine oxide, which is reduced by silane *in situ* to regenerate the active catalyst species.

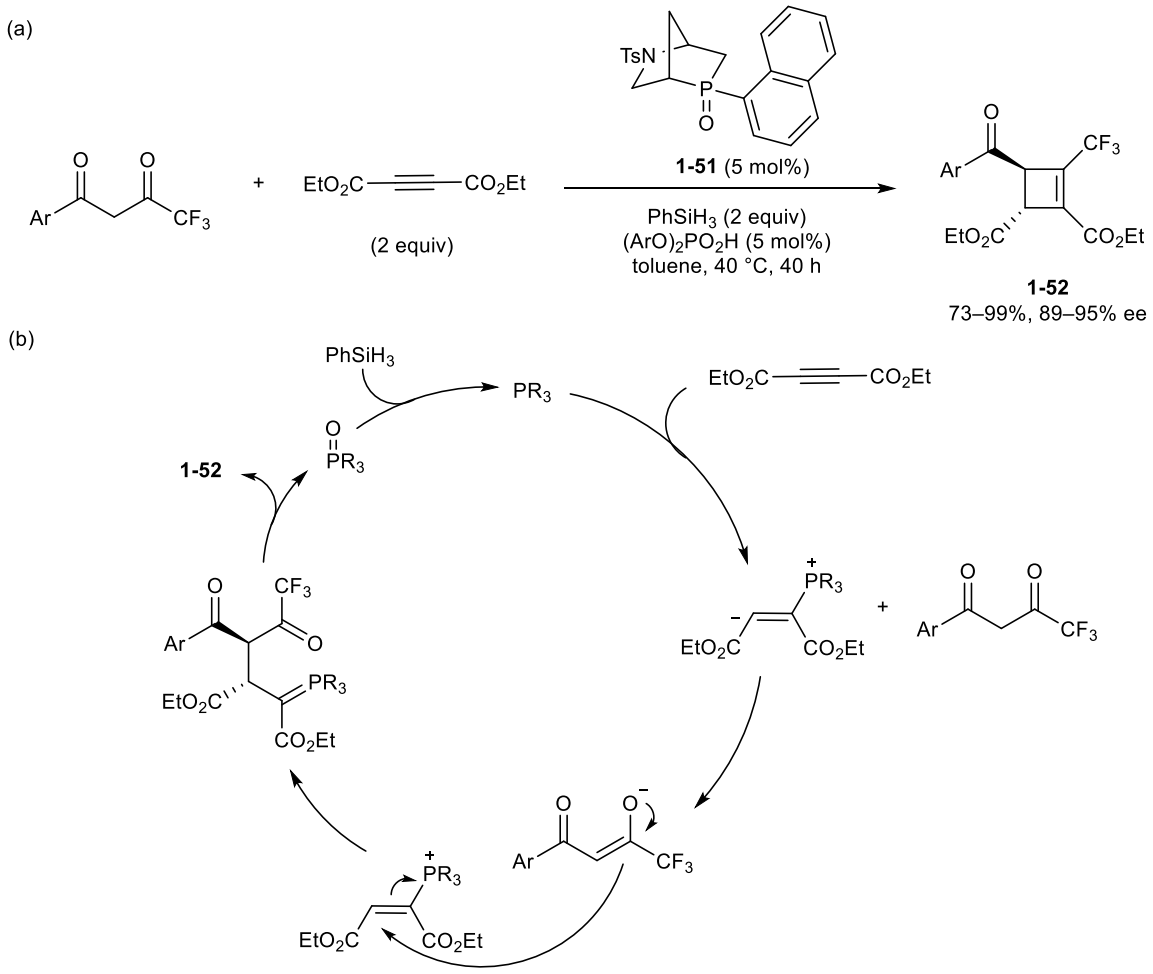

Scheme 1-16. (a) Enantioselective phosphine-catalyzed synthesis of cyclobutenes and (b) proposed mechanism

1.3. Preparation of optically enriched cyclobutylboronates

Optically enriched organoboron compounds can serve as valuable synthetic intermediates due to the growing number of stereospecific transformations they can undergo.[28] In this regard, the presence of a boronic ester group on a cyclobutane motif would result in a highly versatile intermediate. Only a few methods exist to prepare optically enriched cyclobutylboronates.

In 1999, Matteson and co-workers reported a multi-step synthetic approach based on the stereospecific cyclization of a stabilized carbanion onto a chiral α-chloroboronic ester to give cyclobutylboronates **1-53** (Scheme 1-17a).[29] In 2013, Bach and co-workers described a single example of an enantioselective intermolecular [2 + 2] photocycloaddition of isoquinolone with a vinylboronate to give cyclobutylboronate **1-55** as the major diastereomer (Scheme 17b).[30] The photocycloaddition was achieved in the presence of the chiral hydrogen bonding template **1-54**, which effectively shielded one face of the isoquinolone substrate through the formation of a hydrogen-bonded supramolecular complex.

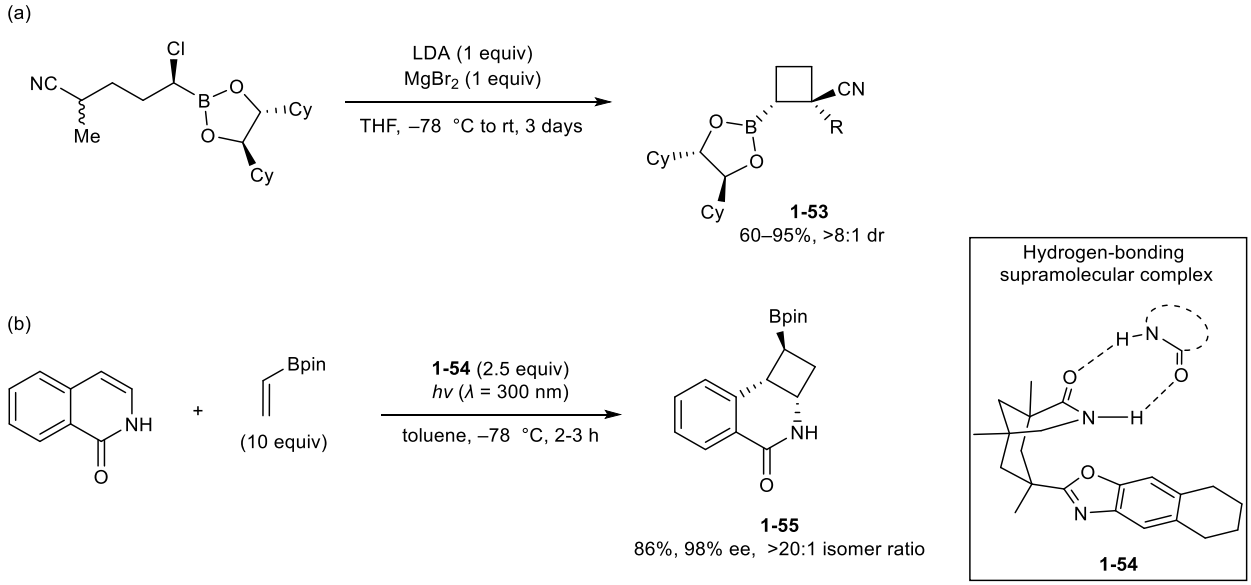

Scheme 1-17. Early examples on the preparation of enantioenriched cyclobutylboronates

More recently, catalytic enantioselective methods have been reported for the preparation of cyclobutylboronates. In 2016, Tortosa and co-workers reported the first catalytic enantioselective synthesis of cyclobutylboronates using a chiral copper(I) complex by way of a formal hydroboration of *meso* 2,3-disubstituted cyclobutenes **1-57** (Scheme 1-18a).[31] As a

desymmetrization method, this approach is limited to prochiral *meso* 2,3-disubstituted cyclobutene substrates. Moreover, in 2019, the Hall Group disclosed an enantioselective copper-catalyzed conjugate borylation of α-alkyl, β-aryl cyclobutenones to afford tertiary cyclobutylboronates **1-59** in good to excellent enantioselectivity. The reaction was found to accommodate a broad scope of aryl groups on the cyclobutenone, with a single example of an α, β-dialkyl cyclobutenone. A ligand high-throughput screening approach proved pivotal to overcome the challenge associated with identifying an optimal chiral ligand (Scheme 1-18b).[32] In addition to copper-catalyzed approaches to access chiral cyclobutylboronates, Yu and co-workers described a Pd-catalyzed enantioselective C–H borylation of a cyclobutylcarboxyamide to afford the corresponding β-borylated cyclobutane **1-61** in excellent enantio- and diastereoselectivity (Scheme 1-18c).[33] Limitations of this method include the requirement of the directing amide group to facilitate the reaction and its subsequent removal as it is an unconventional amide in organic molecules. In 2019, RajanBabu and co-workers disclosed the enantioselective colbalt-catalyzed [2 + 2]-cycloaddition between an alkyne and vinylboronate to afford 1,2,3-trisubstituted cyclobuteneboronates **1-62** in high yield and enantioselectivity (Scheme 1-18d).[18] With a diverse range of heteroatoms (B, N, O, Si) that could be tolerated on the alkyne, further diastereoselective transformations could be performed to afford valuable enantioenriched cyclobutane products. Enantioenriched allylic cyclobutylboronates can serve as an attractive class of intermediates since allyl boronates are well-known to undergo allyl transfer reactions with an appropriate electrophile efficiently.[34] In 2016, Didier and co-workers reported a one-pot asymmetric boron-homologation and allylboration strategy towards the synthesis of optically enriched allylic cyclobutylboronates **1-64** (Scheme 1-19). The reaction begins with the asymmetric boron-homologation of **1-63** with 1,2-dicyclohexylethanediol as the chiral ligand on

the boron atom, originally pioneered by Matteson.[35] The presence of zinc dichloride is known to give high levels of stereocontrol by positioning the migratory group antiperiplanar to one of the diastereotopic chlorine atoms to promote the 1,2-metalate rearrangement.[36] The metallated cyclobutene species is subsequently added to the reaction mixture resulting in a second

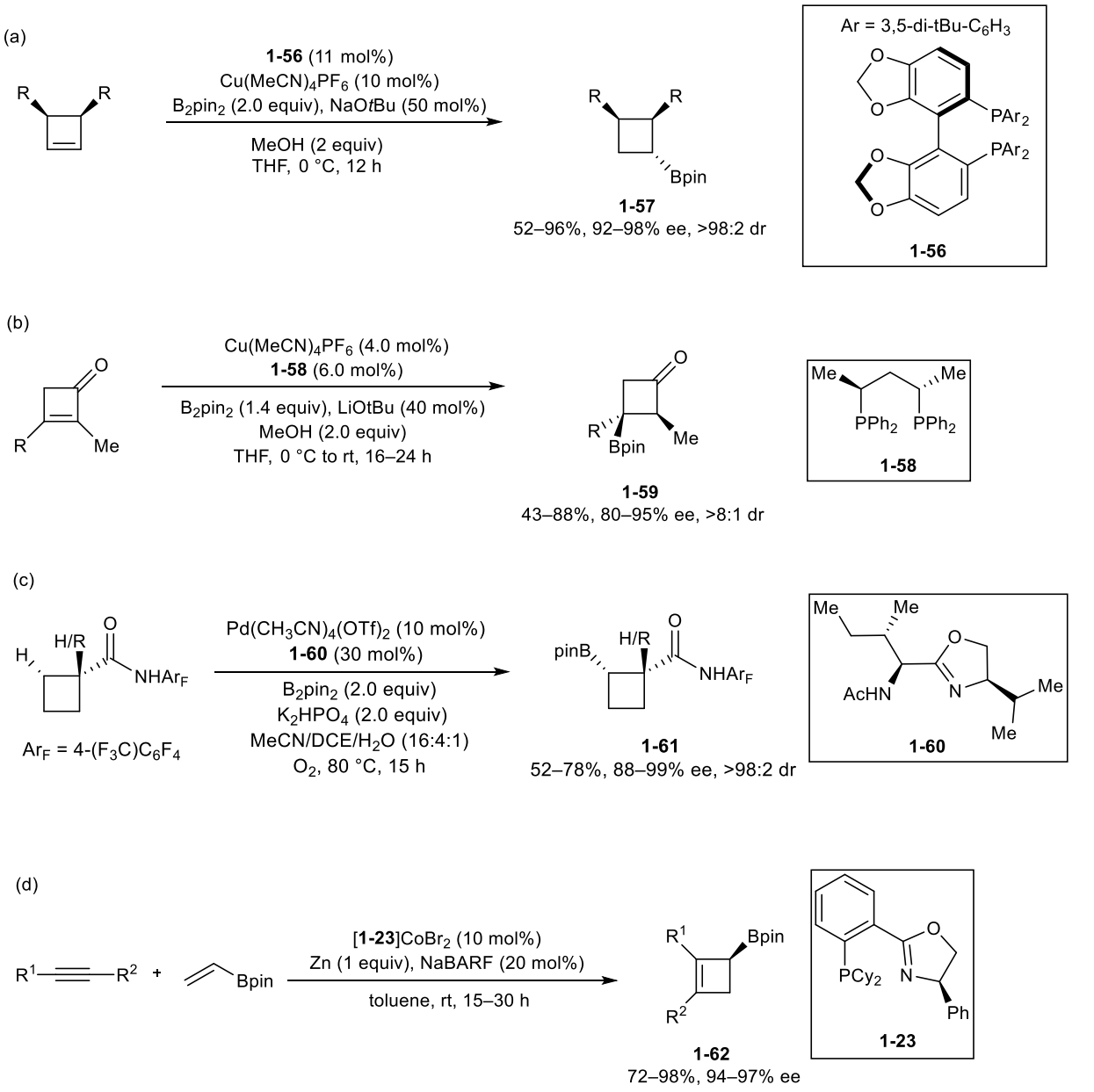

Scheme 1-18. Catalytic enantioselective preparation of cyclobutylboronates

1,2-metalate rearrangement. In the same pot, solvent exchange for dichloromethane and addition of an aldehyde resulted in a carbonyl allylboration reaction in a highly diasterecontrolled fashion through a cyclic 6-membered chair-like transition state. A broad scope of aryl and heteroaryl aldehydes were successfully employed.

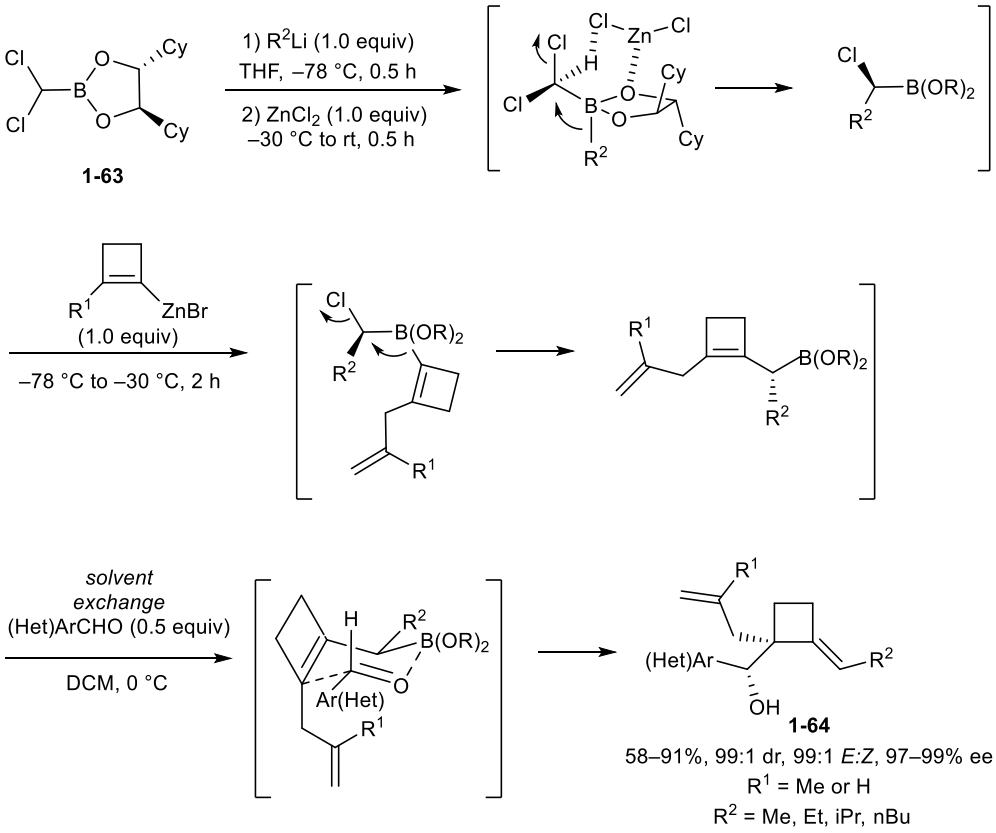

Scheme 1-19. Synthesis of enantioenriched alkylidenecyclobutanes via aldehyde allylboration

Furthermore, the Didier Group demonstrated two examples using an enantiomerically enriched allylic cyclobutylboronates scaffold in the regioselective Suzuki-Miyaura cross-coupling (Scheme 1-20).[37] The scope of the reaction was relatively unexplored. The coupling reactions were performed using an electron-rich aryl and heteroaryl bromide to afford the corresponding γ-coupled products **1-65** in excellent yields with high control of stereochemistry and retention in optical purity. The high levels of regio- and stereoselectivity observed was

attributed to a 6-membered cyclic transmetallation transition state. Attempts were made towards developing an enantioselective variant, however, only modest enantioselectivity induced into compound **1-67** could be achieved with the Josiphos ligand **1-66** (Scheme 1-20b).

In 2019, the Lautens Group reported the enantioselective 1,2-borylcupration of an olefin, followed by trapping with a tethered ketone to afford boron-containing cyclobutanols **1-68** with two contiguous quaternary stereogenic centers in excellent diastereo- and enantioselectivity (Scheme 1-21).[38]

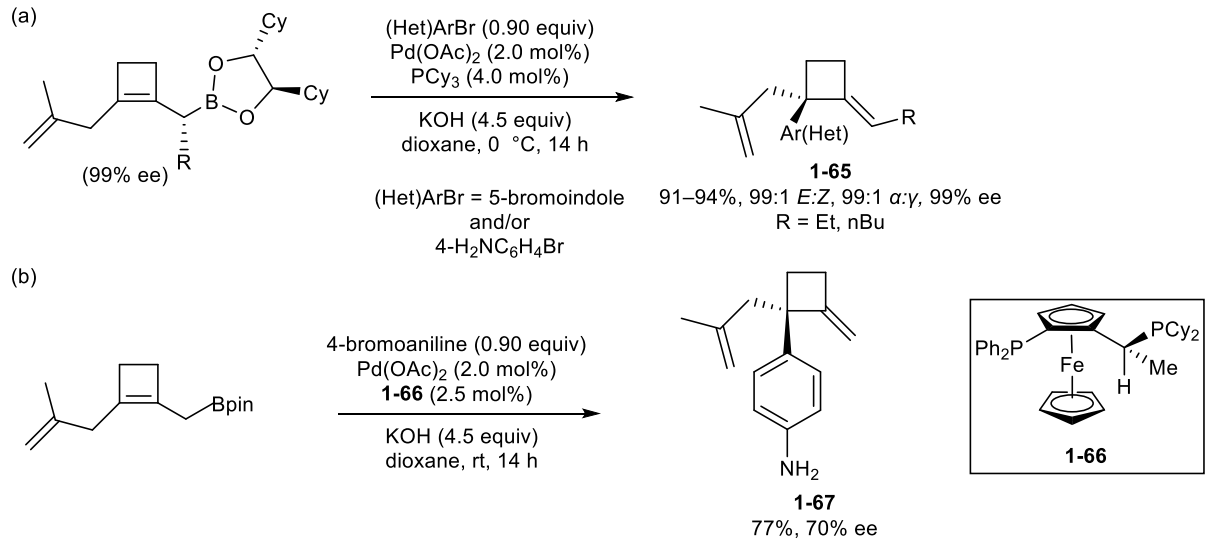

Scheme 1-20. Regio- and stereoselective cross-coupling of optically enriched allylic cyclobutylboronates

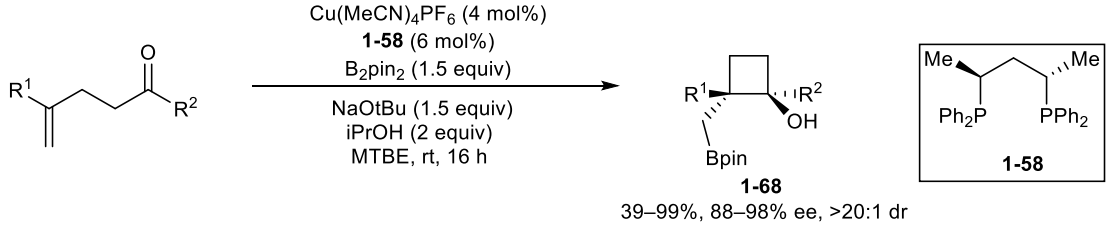

Scheme 1-21. Enantioselective synthesis of a boron-containing cyclobutanol

1.4 Thesis objectives

Accessing cyclobutanes with a specific substitution pattern and configuration is a challenge in modern organic synthesis. Boronic esters are desirable substituents that can serve in a growing number of stereospecific transformations.[28] As described in this chapter, cyclobutanes represent an important structural motif found in many natural products and pharmaceutical agents. Consequently, methods for the catalytic enantioselective preparation of cyclobutylboronates are highly desired, yet still relatively limited. While significant efforts have been made in the construction of cyclobutane rings, the asymmetric functionalization of prochiral cyclobutenes can provide a complementary approach towards chiral cyclobutanes. The latter strategy can be achieved using accessible starting material and avoid the difficult construction of strained cyclobutane rings. Only a few methods to prepare optically enriched 1,2-disubstuted cyclobutanes have been developed, which includes those reported by the Yu and Liu Group as described in this Chapter. The goal of this thesis is to provide a robust and complementary alternative towards optically enriched 1,2-disubstituted cyclobutanes.

The asymmetric copper-catalyzed conjugate borylation of *α,β*-unsaturated carbonyl compounds has emerged as a reliable and efficient method to access chiral organoboron compounds. In this regard, studies began with the optimization of the enantioselective copper-catalyzed conjugate borylation reaction of a cyclobutene 1-carboxyester to give the corresponding *cis*-*β*-boronyl cyclobutylcarboxyester. Next, the optically enriched cyclobutylboronate scaffold was investigated in cross-coupling chemistry to afford the corresponding *trans*-aryl and heteroaryl cyclobutylcarboxyester products with high retention in optical purity and diastereocontrol.

1.5 References

[1] Dembitsky, V. M. *Phytomedicine* **2014**, *21*, 1559–1581.

[2] Tsai, I-L.; Lee, F-P.; Wu, C-C; Duh, C-Y.; Ishikawa, T.; Chen, J-J.; Chen, Y. C.; Seki H.; Chen, I. S. *Planta Med.* **2005**, *71*, 535–542.

[3] Jiao, W. H.; Gao H.; Li, C. Y.; Zhao, F.; Jiang, R. W.; Wang, Y.; Zhou, G. X.; Yao, X. S. *J. Nat. Prod*. **2010**, *73*, 167-171.

[4] Piao, S-J.; Song, Y-L.; Jiao, W-H.; Yang, F.; Liu, X-F.; Chen, W-S.; Han, B. N.; Lin, W-H. *Org. Lett*. **2013**, *15*, 3526–3529.

[5] a) Field, A.; Tuomari, A.; Mcgeever-Rubin, B.; Terry, B.; Mazina, K.; Haffey, M.; Hagen, M. E.; Clark, J. M.; Braitman, A.; Slusarchyk, W. A.; Young, M. G.; Zahler, R. *Antiviral Res.* **1990**, *13*, 41–52. b) Yamanaka, G.; Wilson, T.; Innaimo, S.; Bisacchi, G. S.; Egli, P.; Rinehart, J. K.; Zahler, R.; Colonno, R. J. *Antimicrob. Agents Chemother.* **1999**, *43*, 190–193. c) Hoffman, V. F.; Skiest, D. J. *Exp. Opin. Invest. Drugs* **2000**, *9*, 207–220.

[6] Wager, T. T.; Pettersen, B. A.; Schmidt, A. W.; Spracklin, D. K.; Mente, S.; Butler, T. W.; Howard, H.; Lettiere, D. J.; Rubitski, D. M.; Wong, D. F.; Nedza, F. M.; Nelson, F. R.; Rollema, H.; Raggon, J. W.; Aubrecht, J.; Freeman, J. K.; Marcek, J. M.; Cianfrogna, J.; Cook, K. W.; James, L. C.; Chatman, L. A.; Iredale, P. A.; Banker, M. J.; Homiski, M. L.; Munzner, J. B.; Chandrasekaran, R. Y. *J. Med. Chem*. **2011**, *54*, 7602−7620.

[7] Wrobleski, M. L.; Reichard, G. A.; Paliwal, S.; Shah, S.; Tsui, H. C.; Duffy, R. A.; Lachowicz, J. E.; Morgan, C. A.; Varty, C. B.; Shiha, Y. N. *Bioorg. Med. Chem. Lett.* **2006,** *16*, 3859–3863.

[8] Stepan, A. F.; Subramanyam, C.; Efremov, I. V.; Dutra, J. K.; O'Sullivan, T. J.; DiRico, K. J.; McDonald, W. S.; Won, A.; Dorff, P. H., Nolan, C. E.; Becker, S. L.; Pustilnik, L. R.; Riddel,

D. R.; Kauffman, G. W.; Kormos, B. L.; Zhang, L.; Lu, Y.; Capetta, S. H.; Green, M. E.; Karki, K.; Sibley, E.; Atchison, K. P.; Hallgren, A. J.; Oborski, C. E.; Robshaw, A. E.; Sneed, B.; O'Donnell, C. J. *J. Med. Chem.* **2012**, *55*, 3414–3424.

[9] Hu, J.-L.; Feng, L.-W.; Wang, L.; Xie, Z.; Tang, Y.; Li, X. *J. Am. Chem. Soc.* **2016**, *138*, 13151–13154.

[10] Duan, G.-J.; Ling, J.-B.; Wang, W.-P.; Luo, Y.-C.; Xu, P.-F. *Chem. Commun.* **2013**, *49*, 4625–4627.

[11] Albrecht, L.; Dickmeiss, G.; Acosta, F. C.; Rodriguez-Escrich, C.; Davis, R. L.; Jørgensen, K. A. *J. Am. Chem. Soc*. **2012**, *134*, 2543–2546.

[12] Du, J.; Skubi, K. L.; Schultz, D. M.; Yoon, T. P. *Science* **2014**, *344*, 392–396.

[13] Miller, Z. D.; Lee, B. J.; Yoon, T. P. *Angew. Chem. Int. Ed.* **2017**, *56*, 11891–11895.

[14] Daub, M. E.; Jung, H.; Lee, B. J.; Won, J.; Baik, M.-H.; Yoon, T. P. *J. Am. Chem. Soc.* **2019**, *141*, 9543–9547.

[15] Huang, X.; Quinn, T. R.; Harms, K.; Webster, R. D.; Zhang, L.; Wiest, O.; Meggers, E. *J. Am. Chem. Soc.* **2017**, *139*, 9120–9123.

[16] Rigotti, T.; Mas-Balleste, R.; Aleman, J. *ACS Catal*. **2020**, *10*, 5335−5346.

[17] García-Morales, C.; Ranieri, B.; Escofet, I.; López-Suarez, L.; Obradors, C.; Konovalov, A. I.; Echavarren, A. M. *J. Am. Chem. Soc.* **2017,** *139*, 13628–13631.

[18] Parsutkar, M. M.; Pagar, V. V.; Rajanbabu, T. V. *J. Am. Chem. Soc.* **2019**, *141*, 15367–15377.

[19] Xiao, K.-J.; Lin, D. W.; Miura, M.; Zhu, R.-Y.; Gong, W.; Wasa, M.; Yu, J.-Q. *J. Am. Chem. Soc*. **2014**, *136*, 8138–8142.

[20] Wu, Q.-F.; Wang, X.-B.; Shen, P.-X.; Yu, J.-Q. *ACS Catal.*, **2018,** *8*, 2577–2581.

[21] Yu, J.-Q.; Xiao, L.-J.; Hong, K.; Luo, F.; Hu, L.; Ewing, W. R.; Yeung, K.-S. *Angew. Chem*. Int. Ed. **2020**, *59*, 2–9.

[22] Beck, J. C.; Lacker, C. R.; Chapman, L. M.; Reisman, S. E. *Chem. Sci.*, **2019**, *10*, 2315–2319.

[23] Chen, Y-J.; Hu, T-J.; Feng, C-G.; Lin, G-Q. *Chem. Commun.* **2015**, *51*, 8773–8776.

[24] Zhong, C.; Huang, Y.; Zhang, H.; Zhou, Q.; Liu, Y.; Lu, P. *Angew. Chem. Int. Ed*. **2020**, *59*, 2750 –2754.

[25] Panish, R.; Chintala, S. R.; Boruta, D. T.; Fang, Y.; Taylor, M. T.; Fox, J. M. *J. Am. Chem. Soc*. **2013**, *135*, 9283–9286.

[26] Wang, Y.-M.; Bruno, N. C.; Placeres, Á. L.; Zhu, S.; Buchwald, S. L. *J. Am. Chem. Soc.* **2015**, *137*, 10524–10527.

[27] Lorton, C.; Castanheiro, T.; Voituriez, A. *J. Am. Chem. Soc.* **2019**, *141*, 10142−10147.

[28] Sandford, C.; Aggarwal, V. K. *Chem. Commun.* **2017**, *53*, 5481–5494.

[29] Man, H-W.; Hiscox, W. S.; Matteson, D. S. *Org. Lett.* **1999**, *1*, 379–381.

[30] Coote, S. C.; Bach, T. *J. Am. Chem. Soc.* **2013**, *135*, 14948–14951.

[31] Guisán-Ceinos, M.; Parra, A.; Martín-Heras, V.; Tortosa, M. *Angew. Chem. Int. Ed.* **2016**, *128*, 7038–7086.

[32] Clement, H. A.; Boghi, M.; Mcdonald, R. M.; Bernier, L.; Coe, J. W.; Farrell, W.; Helal, C. J.; Reese, M. R.; Sach, N. W.; Lee, J. C.; Hall, D. G. *Angew. Chem. Int. Ed*. **2019**, *131*, 18576–18580.

[33] Shen, P.-X.; Hu, L.; Shao, Q.; Hong, K.; Yu, J.-Q. *J. Am. Chem. Soc.* **2018**, *140*, 6545–6549.

[34] Eisold, M.; Kiefl, G. M.; Didier, D. *Org. Lett.* **2016**, *18*, 3022−3025.

[35] Matteson, D. S.; Ray, R. *J. Am. Chem. Soc.* **1980**, *102*, 7590–7591.

[36] Matteson, D. S.; Sadhu, K. M. *J. Am. Chem. Soc.* **1983**, *105*, 2077–2078.

[37] Eisold, M.; Didier, D. *Org. Lett.* **2017**, *19*, 4046−4049.

[38] Whyte, A.; Mirabi, B.; Torelli, A.; Prieto, L.; Bajohr, J.; Lautens, M. *ACS Catal.* **2019**, *9*, 9253–9258.

Chapter 2. Catalytic Enantioselective Preparation of a *cis*-*β*-Boronyl Cyclobutylcarboxyester Scaffold

2.1 Introduction

2.1.1 Copper-catalyzed conjugate borylation reaction

The conjugate borylation of *α,β*-unsaturated carbonyl compounds is the 1,4-addition of a nucleophilic boryl group. This reaction has allowed for the efficient synthesis of chiral organoboron compounds that are highly versatile intermediates, owing to the growing number of stereospecific transformations that a boryl group can undergo. In over a decade, tremendous progress has been made in this reaction since the first racemic report. In 2000, the Hosomi and Miyaura Groups independently reported the first conjugate borylation of enones using a copper(I) source and bis(pinacolato)diboron. Hosomi and co-workers found a the combination of catalytic Cu(OTf) and tri-*n*-butylphosphine to be effective for the conjugate borylation of enones to afford *β*-boronyl ketones **2-1** in good to excellent yields (Scheme 2-1a).[1] At the same time, Miyaura and co-workers disclosed the conjugate borylation of *α,β*-unsaturated ketones, esters and nitriles to give the corresponding *β*-borylated products **2-2** using stoichiometric amounts of CuCl/LiCl and potassium acetate (Scheme 2-1b).[2] In 2006, Yun and co-workers made a major advancement in this area of research; the authors reported the use of an alcohol additive, which dramatically accelerated the copper-catalyzed conjugate borylation of *α,β*-unsaturated ketones,

esters and nitriles to give the corresponding *β*-borylated products **2-3** (Scheme 2-2a).[3] Although the seminal work by the Yun Group greatly enhanced the reaction rate, the presence of an alcohol additive caused racemic background reactions as a result of a reactive ligand-free copper species. In 2008, Yun and co-workers disclosed a seminal report of a catalytic enantioselective conjugate borylation protocol with acyclic *α,β*-unsaturated esters and nitriles in the presence of 2 equivalents of methanol (Scheme 2-2b).[4] The use of the bidentate Josiphos **2-4** or Mandyphos **2-5** ligands were found to be optimal to afford the *β*-borylated products **2-6** in good to excellent enantioselectivity.

In a later report, Yun and co-workers successfully extended their work towards cyclic enone substrates (Scheme 2-3a).[5] The catalytic system of CuCl and ligand **2-7** provided the *β*-borylated 6- and 7-membered cyclic carbonyl compounds **2-8** with excellent enantioselectivity. However, this catalytic system was less selective for the 5-membered analog. Moreover, in 2009, Shibasaki and co-workers reported the copper-catalyzed enantioselective conjugate borylation of *β*-substituted cyclic enones using ligand **2-9** (Scheme 2-3b).[6] While *β*-aryl substituted cyclohexanones and cyclopentanones provided borylated products **2-10** in high enantioselectivity, *β*-alkyl cyclohexanones and cyclopentenones gave lower enantioselectivity; interestingly, this catalytic system did not require an alcohol additive. Compared to the 5- and 6-membered ring analogues, the conjugate borylation of the 4-membered ring has been relatively unexplored. Recently, the Hall Group reported the asymmetric conjugate borylation of *α,β*-disubstituted cyclobutenones to give *β*-borylated cyclobutanones **2-12** in good to excellent enantioselectivity and diastereoselectivity (Scheme 2-3c).[7] The high-throughput screening of chiral ligands proved key to this advancement in identifying the appropriate chiral ligand **2-11**.

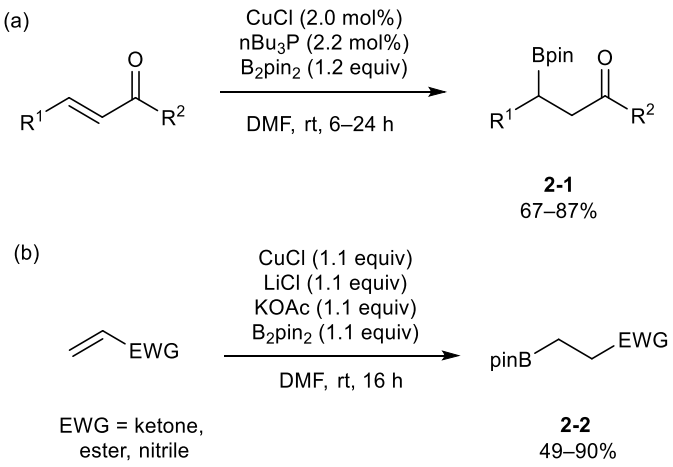

Scheme 2-1. First reports on copper-catalyzed and copper-mediated conjugate borylation reaction

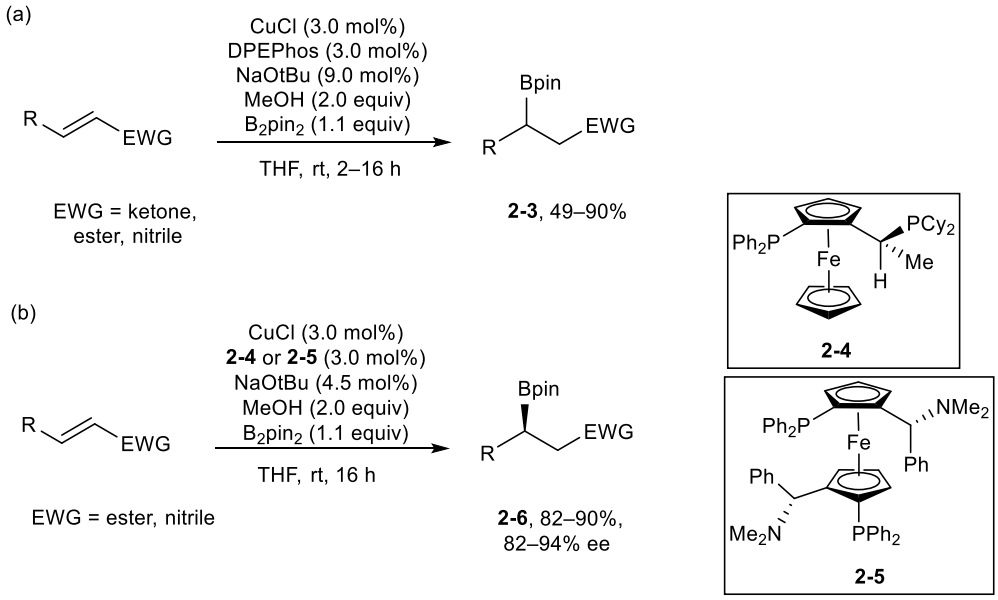

Scheme 2-2. (a) Copper-catalyzed conjugate borylation reaction with methanol as an additive and (b) enantioselective variant

The catalytic cycle (Figure 2-1) of the copper-catalyzed conjugate borylation reaction begins with a ligated copper-boryl species as the active catalyst, which is generated from the σ-bond metathesis between the copper pre-catalyst and bis(pinacolato)diboron. The copper-boryl

species undergoes a 3,4-addition onto an *α,β*-unsaturated carbonyl substrate to give the carbon-bound copper enolate intermediate. DFT calculations by Marder and co-workers found that the carbon-bound copper enolate can undergo subsequent isomerization to the oxygen-bound enolate in the case of *α,β*-unsaturated aldehydes.[8] This pathway provides a more facile σ-bond metathesis step with bis(pinacolato)diboron to regenerate the active catalyst species (Figure 2-1a). The effect of methanol as an additive was studied and an alternative catalytic cycle was proposed. In the presence of methanol, protodecupration of the carbon-bound copper enolate occurs (Figure 2-1b). In the case of methyl acrylate, isomerization is not favorable due to the less reactive ester group.[8] Protodecupration of the carbon-bound copper enolate is necessary to afford the desired product and the copper alkoxide species in which the latter can undergo σ-bond metathesis with bis(pinacolato)diboron to regenerate the active catalyst species (Figure 2-1c).

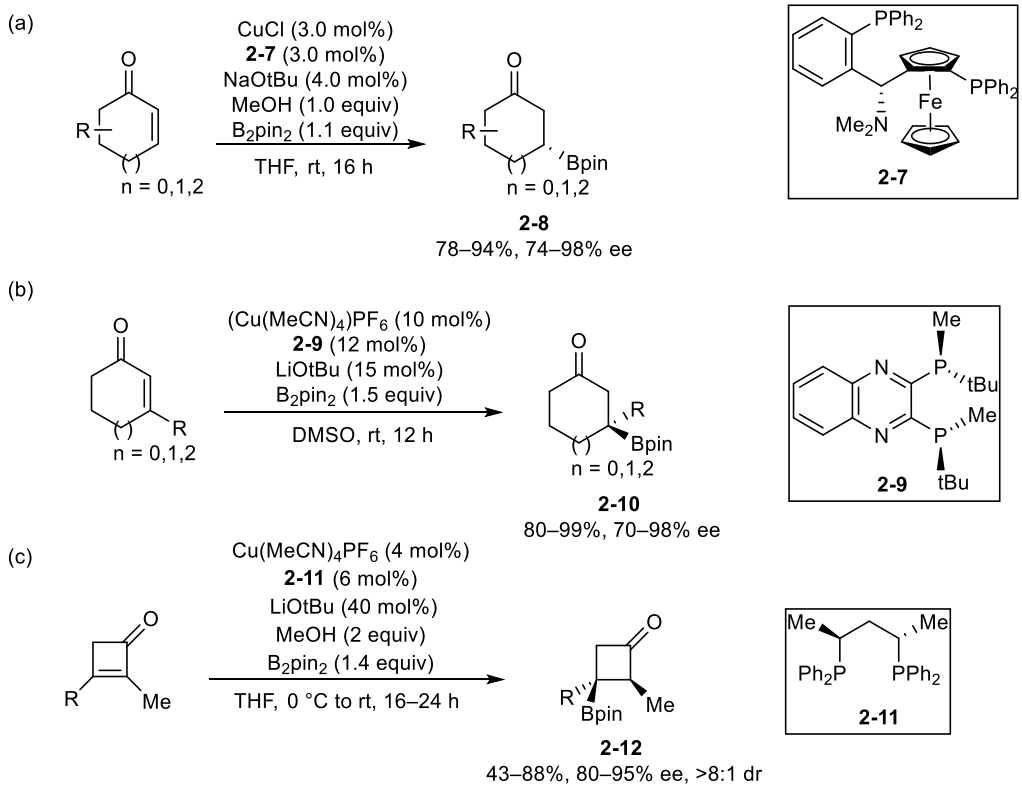

Scheme 2-3. Asymmetric copper-catalyzed conjugate borylation of cyclic enones

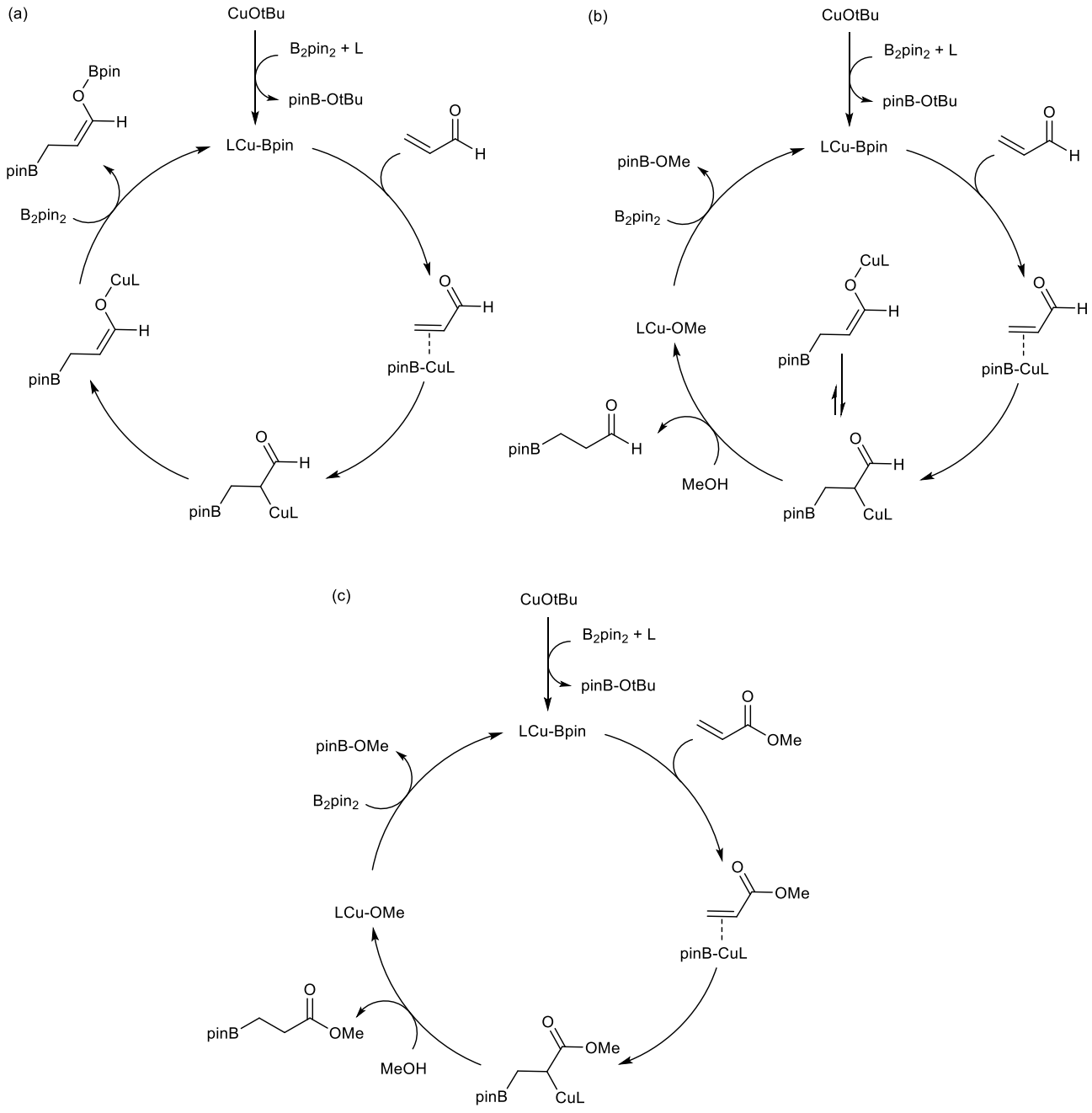

Figure 2-1. Proposed mechanism for copper-catalyzed conjugate borylation reaction of (a) acrolein, (b) acrolein in the presence of methanol, and (c) methyl acrylate in the presence of methanol

2.1.2 Objectives

As the number of bioactive cyclobutane-containing compounds is growing, as described in Chapter 1, accessing cyclobutanes with specific substitution patterns and configuration is highly desired. Furthermore, the presence of a boronic ester substituent in optically enriched boron-containing cyclobutane rings can serve as a versatile synthetic handle in the growing number of stereospecific transformations, such as in the famed Suzuki-Miyaura cross-coupling reaction. With this in mind, the goal of this project will involve the synthesis of an optically enriched *cis*-*β*-boronyl cyclobutylcarboxyester scaffold **2-14** in high enantio- and diastereoselectivity. The synthesis of this cyclobutylboronate intermediate could be achieved by way of an asymmetric copper-catalyzed conjugate borylation of cyclobutene 1-carboxyester **2-13** (Scheme 2-4).

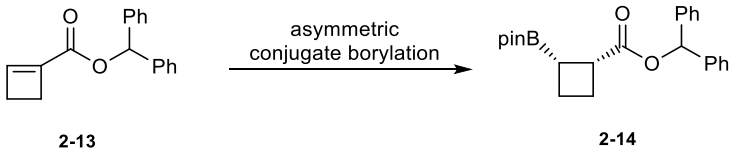

2-13 **2-14**

Scheme 2-4. Proposed route towards an optically enriched *cis*-*β*-boronyl cyclobutylcarboxyester

2.2 Synthesis of a suitable cyclobutene 1-carboxyester starting material (by Helen Clement)

It was reasoned that a cyclobutene 1-carboxyester could serve as a suitable precursor for the enantioselective synthesis of the 1,2-disubstituded cyclobutylboronate **2-14** via copper-catalyzed conjugate borylation. Lin and co-workers have reported the synthesis of cyclobutene 1-carboxyesters in three steps starting from commercially available ethyl cyclobutanecarboxylate (Scheme 2-5).[9] Using Lin's procedure, the synthetic route begins with bromination to give the

corresponding brominated product **2-15** in 39% yield. Next, treatment under basic and refluxing conditions affords the carboxylic acid **2-16** in 69% yield. Finally, conversion to the acid chloride and a subsequent reaction with an alcohol affords the desired cyclobutene 1-carboxyester. Initially the methyl and benzyl cyclobutene 1-carboxyesters derivatives **2-17** and **2-18** were synthesized. However, these derivatives were found to be volatile and unstable. Gratifyingly, cyclobutene 1-carboxyester **2-14** was synthesized and afforded a stable white solid that was easy to handle. The synthesis of cyclobutene 1-carboxyesters **2-13**, **2-17**, and **2-18** were performed by Dr. Helen Clement.

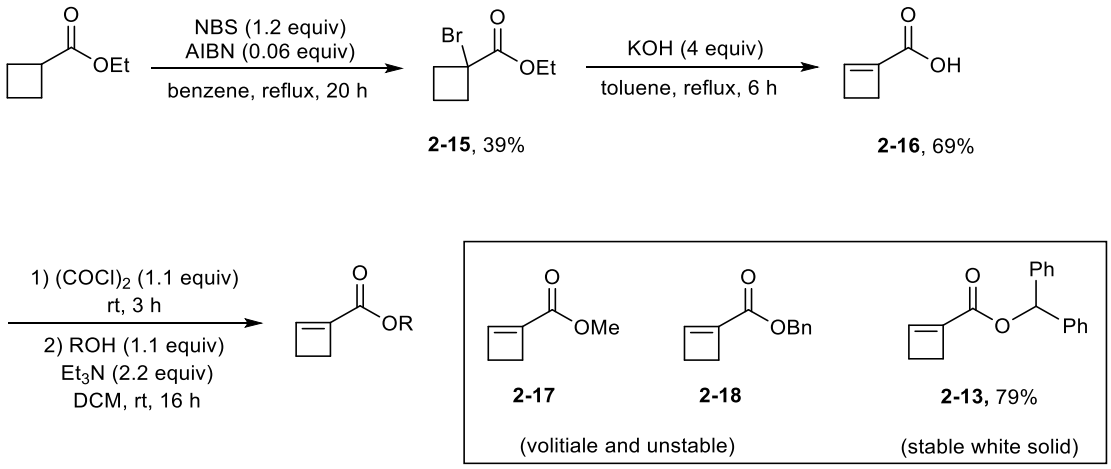

Scheme 2-5. Synthesis of cyclobutene 1-carboxyesters

2.3 Brief screening of chiral ligands and implementation of ligand high-throughput screening platform (in collaboration with Pfizer)

With the suitable benzhydrol cyclobutene 1-carboxyester **2-13** in hand, the focus was shifted towards identifying an effective chiral ligand for the asymmetric conjugate borylation of cyclobutene 1-carboxyester **2-13** to give the desired 1,2-disubstituted cyclobutylboronate **2-14** in high optical purity. Encouraged by the excellent results the Hall Group previously observed

when chiral ligand **2-19** was employed for the asymmetric conjugate borylation of *α,β*-disubstituted cyclobutenones as described in Chapter 1, this ligand was chosen to initiate our studies.[7] Unfortunately, using ligand **2-19** under pre-optimized conjugate borylation conditions in the presence of cyclobutene 1-carboxyester **2-13** did not provide satisfactory results (Table 2-1, entry 1). The difference in substitution pattern and the presence of an ester in contrast to a cyclic ketone made it nontrivial that similar results could be obtained with our model substrate. Switching to the Josiphos ligand **2-20**, which was reported to be an effective ligand for acyclic *β*-alkyl *α,β*-unsaturated esters, proved unfruitful as well (entry 2).[4] It should be mentioned that 11 mol% of the ligand was used to account for human error during the set-up of the reaction.

Table 2-1. Brief screening of potentially effective ligands for the preparation of cyclobutylboronate **2-14**

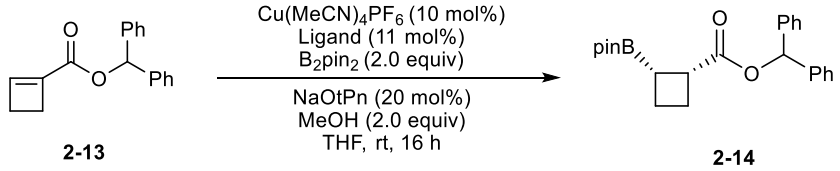

2-13 **2-14**

Entry	Ligand	Yield (%)[1]	dr (*cis:trans*)[2]	ee (%)[3]
1	**2-19**	70	1:2	–47
2	**2-20**	68	1:1	–56

[1] ^{1}H NMR yields using CH_2Br_2 as an internal standard. [2] dr determined by ^{1}H NMR analysis of the crude reaction mixture. [3] ee determined by chiral HPLC. NaOtPn = sodium *tert*-pentoxide.

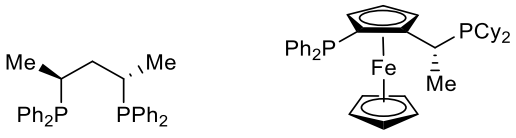

2-19 **2-20**

Considering the challenge of rational optimization pre-empted by these poor results, a chiral ligand high-throughput screening (HTS) strategy was planned with our collaborators at

Pfizer.[10] Reactions were performed on a nanomole-scale with direct supercritical fluid chromatography-mass spectroscopy analysis. From a library of 118 chiral ligands screened in nanomole-scale reactions under pre-optimized conditions, only the Naud family of phosphine-oxazoline ligands provided excellent enantioselectivities, while no other ligand provided greater than 80% ee, accounting for 95% of the ligands screened (Figure 2-2). Specifically, the Naud ligand **2-21** was identified as the optimal ligand, affording the desired product in 73% conversion, 94% ee and 4:1 dr. To the best of our knowledge, ligand **2-21** is an atypical ligand for the asymmetric conjugate borylation reaction. Reports of the ligand **2-21** include the asymmetric hydrogenation of ketones and imines as well as the Pd-catalyzed intramolecular desymmetrization of 1,3-diketones.[11]

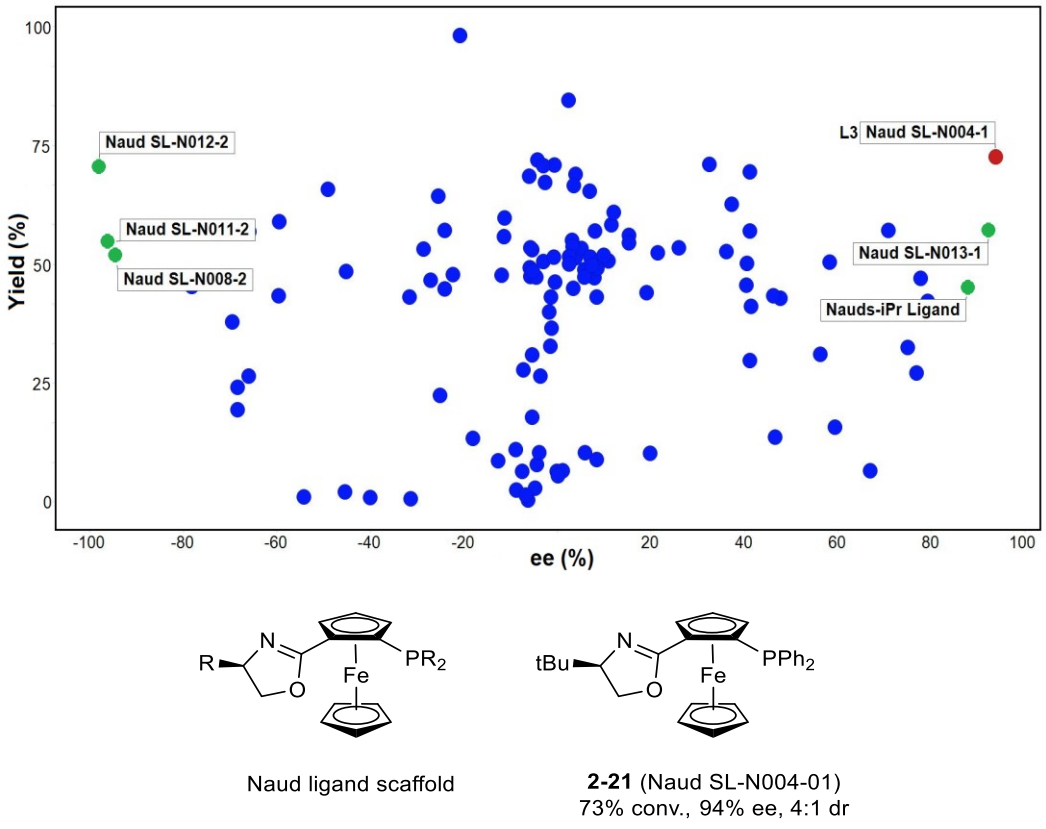

Figure 2-2. Summary of results from high-throughput screening of 118 chiral ligands

With the optimal ligand in hand, the reaction was reproduced in the lab (0.2 mmol scale), providing the desired borylated product **2-14** in a 69% yield, albeit with reduced enantio- and diastereoselectivity (90% ee, 1:1 dr) compared to the HTS results (Scheme 2-6).

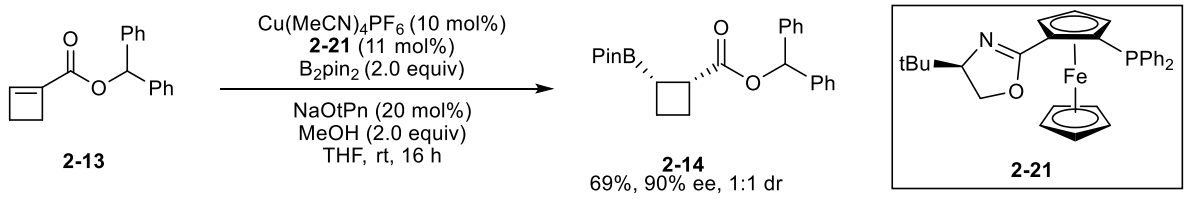

Scheme 2-6. Reproduction of HTS results on a benchtop (0.2 mmol scale)

2.4 Optimization of reaction parameters for the enantioselective copper-catalyzed conjugate borylation reaction (0.2 mmol scale)

2.4.1 Optimization of alcohol additive

In an attempt to improve the enantio- and diastereoselectivity of the reaction, various alcohol additives were screened. It was found that changing the alcohol from methanol to ethanol did not improve the dr or ee of the product (Table 2-2, entry 2). However, the dr and ee slightly improved when 2-propanol was employed (entry 3). It was surmised that increasing the steric bulk of the alcohol would promote protodecupration on the least hindered face of the cyclobutane ring to favor the formation of the *cis*-product. To our disappointment, *tert*-butanol did not improve the dr in comparison to 2-propanol (entry 4). Further screening of other sterically demanding alcohols such as 3-pentanol and 3-methyl-2-butanol proved unfruitful in further improving the reaction selectivity (entry 5-7).

Table 2-2. Optimization of alcohol additive

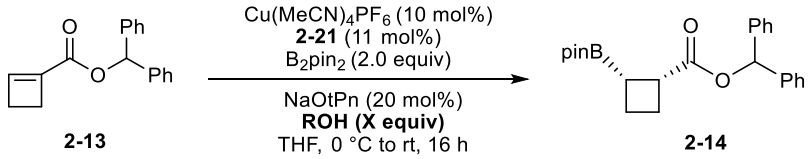

Entry	ROH (equiv)	Conversion of **2-13** (%)	dr (*cis*:trans)[1]	ee (%)[2]	Isolated yield (%)[3]
1	MeOH (2)	99%	1:1	90	69
2	EtOH (2)	99%	1:1	90	67
3	iPrOH (2)	99%	2:1	91	69
4	tBuOH (2)	99%	1:1	92	55
5	3-pentanol (2)	99%	2:1	90	65
6	3-methyl-2-butanol (2)	99%	2:1	92	69
7	3-methyl-2-butanol (4)	99%	2:1	86	58

[1]dr determined by ^{1}H NMR analysis of the crude reaction mixture using CH_2Br_2 as an internal standard. [2]ee determined for major diastereomer. [3]Isolated yield of both diastereomers.

2.4.2 Optimization of reaction temperature

Next, attention was directed towards screening the reaction temperature using 2-propanol (2 equiv) as the alcohol additive in order to enhance the enantio- and diastereoselectivity of the reaction. To begin, the reaction was run at 0 °C, which provided a negligible change in dr (Table 2-3, entry 2). Further decreasing the reaction temperature to –20 °C led to a slight increase in dr (3:1) and a significant improvement in ee (97%) (entry 3). When the reaction was performed at –55 °C, the dr and ee soared to 10:1 and 99%, respectively (entry 4). Chromatographic purification of the crude reaction mixture (10:1 dr) using silica gel neutralized with 30% weight deionized water allowed for the isolation of **2-14** in 16:1 dr. It should be mentioned that attempts to isolate the desired product by column chromatography using unaltered silica gel resulted in a decline in isolated yield (33%). An attempt to further decrease the reaction temperature to –60 °C

resulted in only 54% conversion in 22 h with no change in dr (entry 5). Overall, a strong temperature dependence was observed towards obtaining high enantio- and diastereoselectivity. It should be mentioned that the cryogenic temperatures were obtained using a cryocooler.

Table 2-3. Optimization of reaction temperature

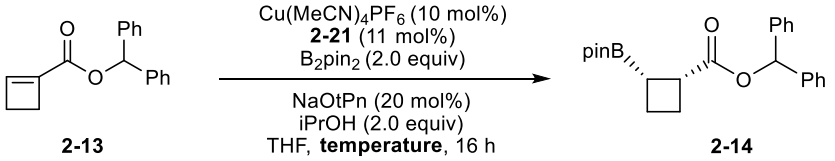

Entry	Temperature (°C)	Time (h)	Conversion of **2-13** (%)	dr (*cis*:trans)[1]	ee (%)[2]	Isolated yield (%)[3]
1	rt	16	99	2:1	91	69
2	0	16	99	2:1	ND	ND
3	–20	16	99	3:1	97	69
4	–55	16	99	10:1 (16:1)	99	72
5	–60	22	54	10:1	ND	ND

[1]dr determined by ^{1}H NMR analysis of the crude reaction mixture. Isolated dr in parentheses. [2]ee determined for major diastereomer. [3]Isolated yield of both diastereomers.

2.4.3 Optimization of solvent

To further improve the dr of the product, various solvents were screened that were suitable with a low reaction temperature of –55 °C. Dichloromethane dramatically decreased the dr to 2:1 (Table 2-4, entry 2). When toluene was employed as the solvent, the dr improved to 13:1 (entry 3). However, the reaction was found to be irreproducible due to solubility issues observed in the reaction mixture. As tetrahydrofuran was found to be an efficient solvent, other ethereal solvents were screened. Employing diethyl ether resulted in a 9:1 dr (entry 4). Both methyl *tert*-butyl ether and 2-methyltetrahydrofuran further improved the dr to 12:1, which

allowed for the isolation of cyclobutylboronate **2-14** in a 20:1 dr by silica column chromatography neutralized with 30% weight deionized water (entry 5 and 6). 2-Methyltetrahydrofuran was chosen as the preferred solvent as it is regarded as a green solvent.[12]

Table 2-4. Optimization of solvent

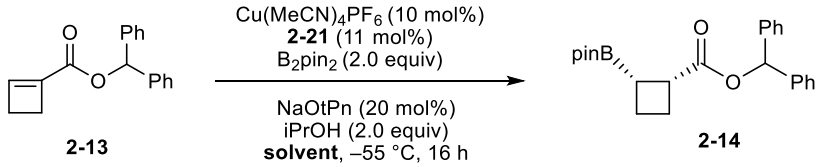

Entry	Solvent	Conversion of **2-13** (%)	dr (*cis*:trans)[1]	ee (%)[2]	Isolated yield (%)[3]
1	THF	99	10:1 (16:1)	99	72
2	DCM	99	2:1	ND	ND
3	Toluene	99	13:1	99	72
4	Diethyl Ether	99	9:1	ND	ND
5	MTBE	99	12:1 (20:1)	99	69
6	2-MeTHF	99	12:1 (20:1)	99	72

[1] dr determined by ^{1}H NMR analysis of the crude reaction mixture. Isolated dr from silica colum chromatography in parenthesis. [2] ee determined for major diastereomer. [3] Isolated yield of both diastereomers.

2.4.4 Optimization of base

With already excellent results in hand, alternative bases were briefly screened. While LiOtBu, NaOtBu and NaOMe proved detrimental to the reaction conversion (Table 2-5, entry 2, 4 and 5), KOtBu was found to be a compatible base (entry 3). Nonetheless, NaOtPn still provided the best selectivity (entry 1).

Table 2-5. Optimization of base

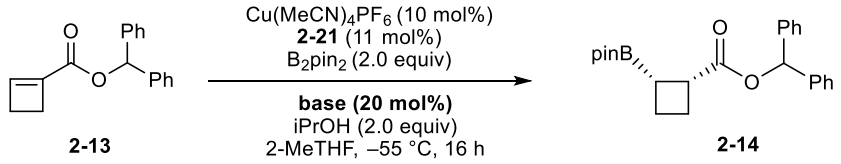

Entry	Base	Conversion of **2-13** (%)	dr (*cis*:trans)[1]	ee (%)[2]	Isolated yield (%)[3]
1	NaOtPn	99	12:1 (20:1)	99	72
2	LiOtBu	44	ND	ND	ND
3	KOtBu	99	10:1	ND	ND
4	NaOtBu	48	5:1	ND	ND
5	NaOMe	33	ND	ND	ND

[1]dr determined by ^{1}H NMR analysis of the crude reaction mixture. [2]ee determined for major diastereomer (d_1). [3]Isolated yield of both diastereomers. NaOtPn = sodium *tert*-pentoxide.

2.4.5. Optimized enantioselective conjugate borylation conditions (0.2 mmol scale)

Overall, under the optimized enantioselective copper-catalyzed conjugate borylation conditions using Naud ligand **2-21** (11 mol%), 2-propanol (2.0 equiv) as the alcohol additive, NaOtPn (20 mol%) as the base, and 2-MeTHF as the solvent at –55 °C, cyclobutylboronate **2-14** was isolated in 72% yield, 99% ee and 20:1 dr on a 0.2 mmol scale after silica column chromatography (Scheme 2-7).

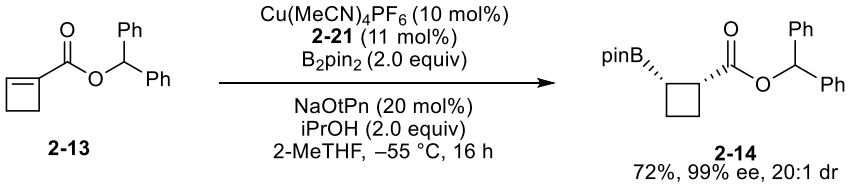

Scheme 2-7. Optimized enantioselective copper-catalyzed conjugate borylation condition (0.2 mmol scale)

2.5 Optimization of gram-scale enantioselective copper-catalyzed conjugate borylation reaction (3.8 mmol scale)

To demonstrate the practicality and scalability of this method, the asymmetric copper-catalyzed conjugate borylation was investigated on a gram-scale. Initial attempts to perform the reaction on a gram scale reaction under our optimized conditions resulted in no erosion in enantioselectivity, although the crude dr decreased to 8:1, and product **2-14** could only be isolated in 13:1 dr after silica column chromatography (Table 2-6, entry 1). As temperature was found to have a profound impact on the diastereoselectivity, the reaction temperature was re-examined on a gram-scale. Gratifyingly, the reaction was reproducibly successful at –65 °C with an extended reaction time of 40 h to give the cyclobutylboronate scaffold **2-14** in an improved isolated yield (1.2 g, 80%) and no decline in enantio- or diastereoselectivity (Table 2-6, entry 2, Scheme 2-8).

Table 2-6. Optimization of reaction temperature and time (1.0 gram, 3.8 mmol scale)

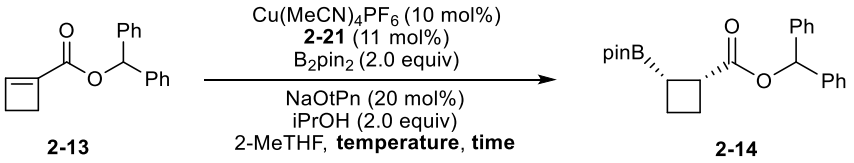

Entry	Temperature (°C)	Time (h)	Conversion of **2-13** (%)	dr (*cis*:trans)[1]	ee[2]	Isolated yield (%)[3]
1	–55	16	98%	8:1 (13:1)	99	78
2	**–65**	**40**	**98%**	**12:1 (>20:1)**	**99**	**80**

[1]dr determined by ^{1}H NMR of the crude reaction mixture. Isolated dr in parentheses. [2]ee determined for major diastereomer (d_1). [3]Isolated yield of both diastereomers.

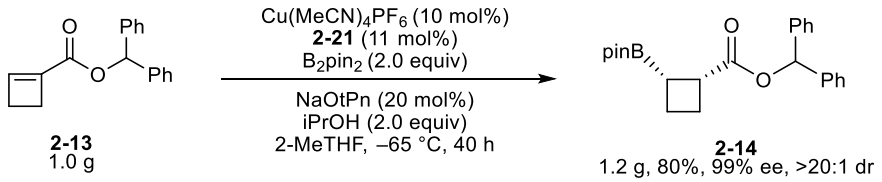

Scheme 2-8. Optimized enantioselective copper-catalyzed conjugate borylation conditions (1.0 gram, 3.8 mmol scale)

2.6 Attempts at the asymmetric conjugate borylation of cyclobutene 1-carboxyamide 2-22

An attractive synthetic application of the enantioenriched cyclobutylboronate scaffold would be in stereospecific Suzuki-Miyaura cross-coupling, in an effort to access *β*-aryl cyclobutylcarboxyesters of potential interest in drug discovery. In this regard, a Weinreb amide derivative would serve as an attractive precursor of ketones. An initial attempt was made to borylate cyclobutene 1-carboxyamide **2-22** with ligand **2-21**, however, only a low conversion was observed (Table 2-7, entry 1). Performing the reaction at room temperature afforded the borylated product **2-23** in 84% yield and good diastereoselectivity, however, the enantioselectivity of the reaction was unsatisfactory (47% ee) (entry 2). Lowering the reaction temperature to –20 °C provided modest enantioselectivity (entry 3). Further decreasing the reaction temperature to –30 and –40 °C led to a decrease in the reaction conversion and dr (entry 2 and 5). At this time, no further attempts were made to optimize the asymmetric conjugate borylation of cyclobutene 1-carboxyamide **2-22**. It should be mentioned that the stereochemistry of the major diastereomer for the borylated product **2-23** was not determined.

Table 2-7. Screening of reaction temperature with cyclobutene 1-carboxyamide **2-22**

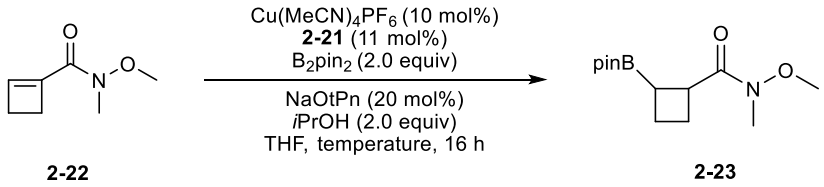

2-22 **2-23**

Entry	Temperature (°C)	Conversion of **2-22** (%)	dr[1]	ee[2]	Yield (%)[3]
1	–55	3	-	-	-
2	rt	96	7:1	47	72
3	–20	96	7:1	66	72
4	–30	86	3:1	-	63
5	–40	5	-	-	-

[1]dr determined by ^{1}H NMR of the crude reaction mixture. [2]ee determined for major diastereomer. [3] Isolated yield of both diastereomers.

2.7 Determination of relative and absolute stereochemistry of cyclobutylboronate 2-14

2.7.1 1D TROSEY NMR spectroscopic study

In order to determine the relative stereochemistry of cyclobutylboronate scaffold **2-14**, 1D TROSEY experiments were performed on both the major and minor diastereomers (Figure 2-3). Irradiation of H_a on the major diastereomer resulted in a 0.96% NOE enhancement with H_b. In order to make a firm conclusion on the relative stereochemistry, a 1D TROSEY experiment was also performed on the minor diastereomer for comparison. Irradiation of H_a on the minor diastereomer resulted in a decreased NOE enhancement of 0.47% with H_b. This outcome can be rationalized by the increased distance between the two protons when they are in a *trans*-configuration. Another key correlation in the minor diastereomer was observed between H_a and the methyl protons on the pinacol group resulting in a 0.13% NOE enhancement. Although this

enhancement is remarkably low, it is nonetheless absent in the major diastereomer. Overall, the 1D TROSEY experiments of both diastereomers put forward that the major diastereomer could be the *cis*-product. While the 1D TROSEY experiment of both diastereomers provided some valuable insight on the relative stereochemistry, the NOE enhancements observed were relatively inadequate as all enhancements were less than 1%. It should be mentioned that H_b was identified by gCOSY and HSQC analysis as the boron-bound carbon was not detected due to the quadrupolar relaxation of boron.

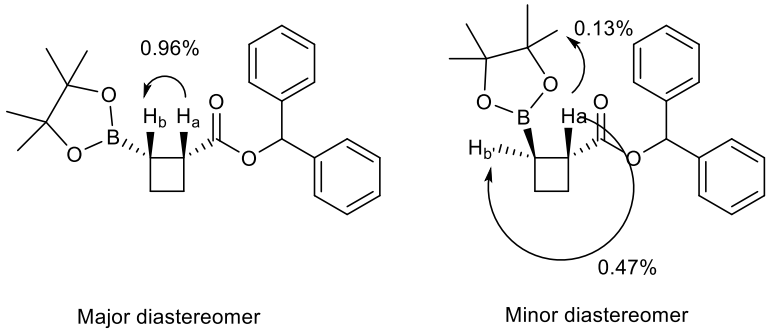

Figure 2-3. Key 1D TROSEY interactions in the major and minor diastereomer

2.7.2 Determination of relative and absolute stereochemistry

An alternative and unambiguous method to determine the relative and absolute stereochemistry of cyclobutylboronate **2-14** would be to obtain a quality crystal for an X-ray diffraction study. Incorporation of a heavy atom onto the molecule such as a bromine or iodine would allow for determination of the absolute stereochemistry by X-ray analysis as they have a larger contribution to the anomalous diffraction effect compared to lighter atoms, resulting in much stronger X-ray absorbance.[13] The derivatization of cyclobutylboronate **2-14** was required, in which, the chemical transformations for the incorporation of a heavy atom should retain the stereochemical integrity of the compound. It was surmised that a bromine atom can be

incorporated on the ester group of cyclobutylboronate **2-14** (Scheme 2-9). Deprotection of the benzhydrol ester provided the corresponding carboxylic acid **2-24**. Reaction with 4,4'-dibromobenzhydrol under Steglich esterification conditions gave the desired bromine-containing compound **2-25** as a clear oil. Transformation to the potassium trifluoroborate salt **2-26** resulted in a white solid that was successfully recrystallized by way of vapor diffusion (ethyl acetate:hexanes) to give thin blades of crystals for X-ray diffraction analysis. The relative configuration was determined to be *cis* with an absolute stereochemistry of (*S, R*) at C1A and C2A respectively, as depicted in Figure 2-4.

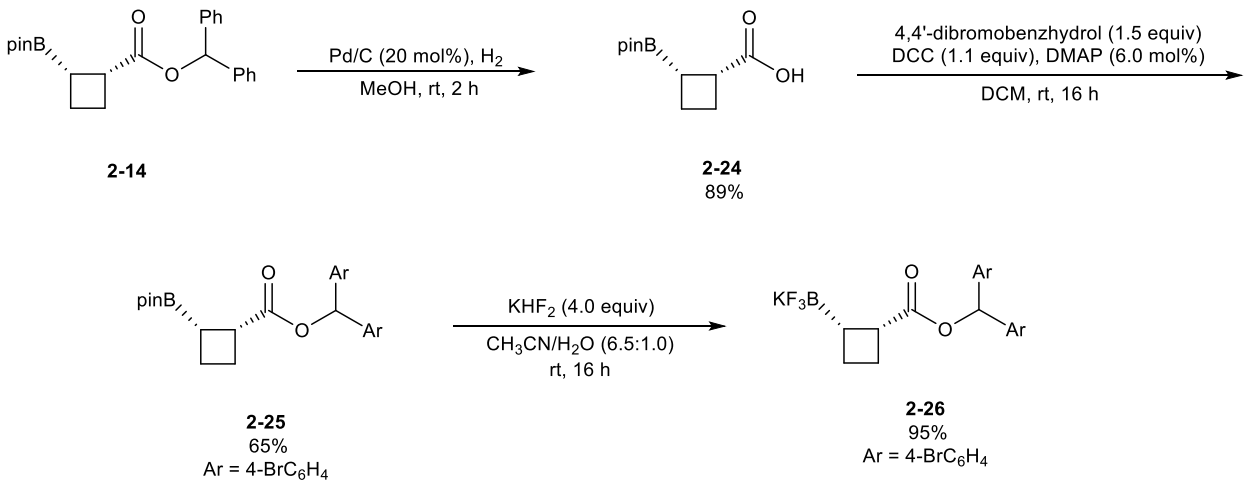

Scheme 2-9. Derivatization of cyclobutylboronate **2-14** for X-ray crystallographic analysis

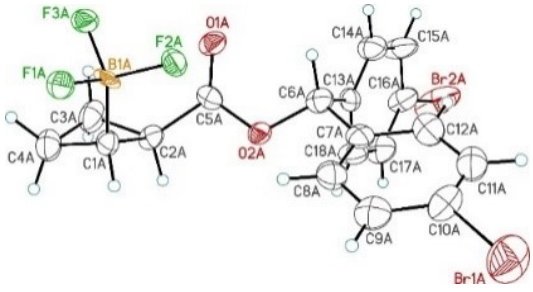

Figure 2-4. ORTEP of X-ray crystallographic structure of trifluoroborate salt **2-26**

2.8 Attempts to access the *trans-β*-boronyl cyclobutylcarboxyester scaffold

2.8.1 Epimerization of cyclobutylboronate 2-14

As the boronic ester substituent can undergo a number of stereospecific transformations, the *trans*-diastereomer would also serve as a versatile cyclobutylboronate building block in its own right. It was speculated that access to the *trans*-diastereomer could be obtained by the epimerization of the cyclobutylboronate **2-14** to afford the presumed thermodynamically more stable diastereomer. Thus, treatment of cyclobutylboronate **2-14** (2:1, *cis:trans* mixture) with DBU in THF at room temperature for 16 h only slightly improved the dr in favor of the *trans* diastereomer in 70% yield (Table 2-8, entry 1). Attempts to further drive the epimerization reaction by increasing the reaction temperature significantly improved the dr towards the *trans*-product, but also resulted in a diminished yield (entry 2). Changing the base to LiOtBu (0.5 equiv) and using a non-polar solvent did not result in an appreciable change in dr (entry 3 and 4). However, when 2 equiv of LiOtBu was employed, the dr soared in favor of the *trans* diastereomer, although in a low 43% yield (entry 5). Using an alcohol additive, changing the solvent to THF or using a *tert*-butoxide base with different counterions did not improve the yield (entry 6-9). In all cases, benzhydrol was observed as the only side product. It was surmised that transesterification may be a competing side reaction. However, epimerization using sodium diphenylmethoxide as the base, did not improve the yield (entry 10). It should be mentioned that other ester derivatives of cyclobutylboronate **2-14** were found to be volatile and unstable and thus other ester derivatives of cyclobutylboronate **2-14** were not utilized.

Table 2-8. Screening of reaction conditions for the epimerization of cyclobutylboronate **2-14**

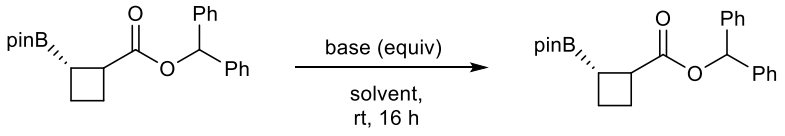

2-14
2:1 dr
(*cis:-trans)*

Entry	Base (equiv)	Solvent	Crude dr (*cis:trans*)[1]	Yield (%)[2]
1	DBU (3 equiv)	THF	1:2	70
2[3]	DBU (3 equiv)	THF	1:9	34
3	LiOtBu (0.5 equiv)	Toluene	2:1	83
4	LiOtBu (1 equiv)	Toluene	1:1	61
5	LiOtBu (2 equiv)	Toluene	1:10	43
6[4]	LiOtBu (2 equiv)	Toluene	1:10	37
7	LiOtBu (2 equiv)	THF	1:10	36
8	NaOtBu (2 equiv)	Toluene	0:1	38
9	KOtBu (2 equiv)	Toluene	1:10	36
10	Sodium diphenylmethoxide (2 equiv)	Toluene	1:10	30

[1] Determined from ^{1}H NMR analysis of the crude reaction mixture by peak height of the benzylic proton. [2] Determined by ^{1}H NMR analysis of the crude reaction mixture, using dibromomethane as an internal standard. [3] Reaction was performed at 50 °C. [4] *t*BuOH (2 equiv) added as an additive.

2.8.2 Epimerization control experiment

A series of control experiments employing starting material with different dr values suggested that selective decomposition of the *cis*-diastereomer may occur under the attempted epimerization conditions (Table 2-9). A strong correlation was observed with the relative amount of *trans*-diastereomer subjected to the epimerization condition and the ^{1}H NMR yield, which suggested the absence of epimerization but rather the selective decomposition of the *cis*-diastereomer and persistence of the *trans* diastereomer under these reaction conditions.

Furthermore, in all cases the only side product observed was benzhydrol. A strong correlation was observed between the yield of benzhydrol and the amount of *cis*-diastereomer subjected to the epimerization reaction, further supporting the notion of the selective decomposition of the *cis*-diastereomer, yielding benzhydrol as the by-product. It should be mentioned that the rest of the mass balance of the *cis*-diastereomer could not be accounted for.

Table 2-9. Control experiment for the selective decomposition of *cis*-diastereomer

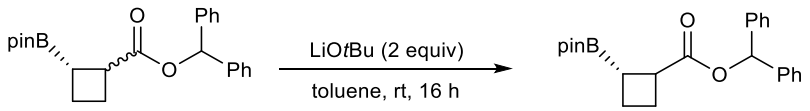

2-14

Entry	dr of starting material (*cis:trans*)	Crude dr (*cis:trans*)[1]	^{1}H NMR yield of benzhydrol (%)[2]	^{1}H NMR yield (%)[2]
1	2:1	1:10	56	37
2	1:1	1:15	32	48
3	18:1	4:1	63	31
4	1:3	0:1	25	69

[1]Determined from ^{1}H NMR analysis of the crude reaction mixture by peak height of the benzylic proton. [2] Determined by ^{1}H NMR analysis of the crude reaction mixture, using dibromomethane as an internal standard.

2.8.3 Epimerization of trifluoroborate salt 2-27

It was postulated that the Lewis acidic boronic ester could facilitate the selective decomposition of the *cis*-diastereomer **2-14** through coordination of the ester oxygen with the boron atom. Therefore, attempts to epimerize the non-Lewis acidic trifluoroborate salt **2-27** under milder conditions (20 mol% base) were conducted, however, these attempts were also unfruitful (Table 2-10, entry 1-3). KOtBu proved to be the most effective base resulting in a 1:8

dr (entry 2). However, the yield was still not satisfactory relative to the amount of *trans*-diastereomer in the starting material. It should be mentioned that THF was employed as the solvent due to solubility issues when toluene was employed with the trifluoroborate salt. Overall, attempts to epimerize the trifluoroborate salt **2-35** also proved unfruitful. At this time, no further attempts were made to epimerize cyclobutylboronate *cis*-**2-14** and the corresponding trifluoroborate salt **2-27** into the desired *trans*-diastereomer.

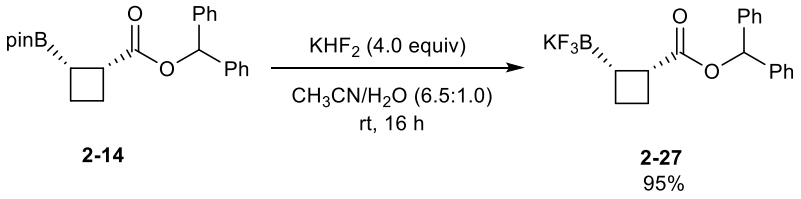

2-14 **2-27** 95%

Scheme 2-10. Synthesis of the trifluoroborate salt **2-27**

Table 2-10. Screening of bases for the epimerization of the trifluoroborate salt **2-27**

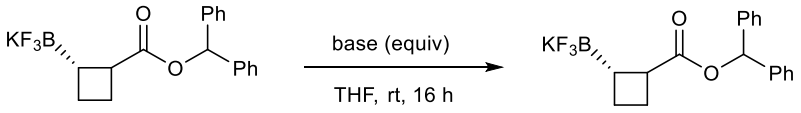

2-27 1:1 dr

Entry	Base (equiv)	d.r. (*cis:trans*)[1]	H NMR yield (%)[2]
1	LiOtBu (20 mol%)	1:1	89
2	KOtBu (20 mol%)	1:8	59
3	NaOtBu (20 mol%)	0:1	26

[1]Determined from ^{1}H NMR analysis of the crude reaction mixture by peak height of the benzylic proton. [2] Determined by ^{1}H NMR analysis of the crude reaction mixture, using dibromomethane as an internal standard.

2.9 Proposed catalytic cycle and stereochemical model (DFT modelling performed by Prof. Dennis G. Hall)

A mechanism was proposed for the copper-catalyzed conjugate borylation of cyclobutene 1-carboxyester **2-13** (Figure 2-5).[8] Copper(I) species **2-28** reacts with bis(pinacolato)diboron to form the active borylcopper(I) species **2-29**. Coordination of cyclobutene 1-carboxyester **2-14** with the copper center could result in the π-complex **2-30**. This intermediate could then undergo a 3,4-addition onto the alkene to give the carbon-bound copper(I) enolate, which would tautomerize to oxygen-bound copper(I) enolate **2-31**. The kinetically controlled and irreversible protodecupration would proceed on the opposite face of the boryl group to avoid an unfavorable

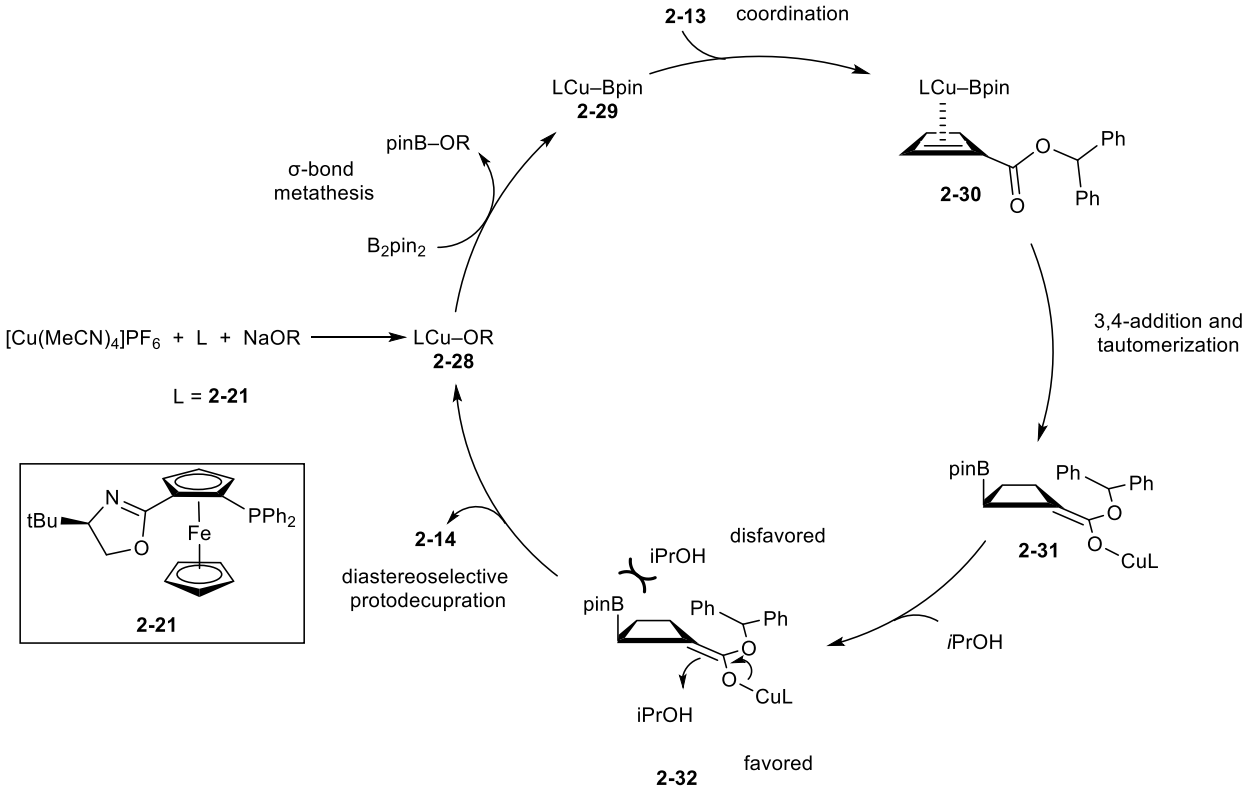

Figure 2-5. Proposed catalytic cycle for the copper-catalyzed conjugate borylation of cyclobutene 1-carboxyester **2-13**

steric interaction between the alcohol and pinacolate group as depicted in **2-32** to afford the desired product **2-14** and regenerate the copper(I) catalyst.

To determine if background epimerization occurred under the reaction conditions, cyclobutylboronate **2-14** with a specific dr value was subjected to the asymmetric conjugate borylation reaction conditions (Scheme 2-11). In the event, no significant change in dr was observed suggesting the lack of epimerization for both the *cis*- and *trans* diastereomer, in support of an irreversible protodecupration step.

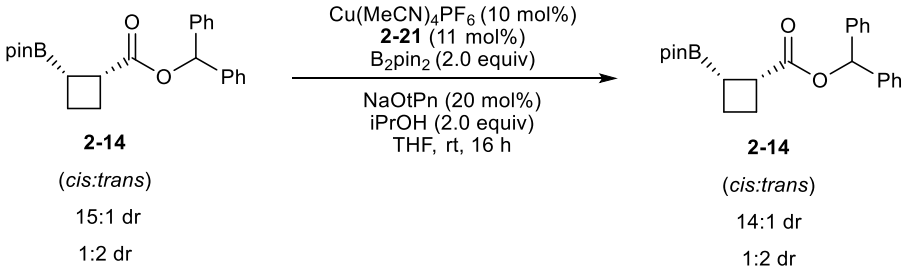

Scheme 2-11. Control experiment for the epimerization of the cyclobutylboronate **2-14** under the asymmetric copper-catalyzed conjugate borylation conditions

In an effort to rationalize the high level of enantioselectivity observed with Naud ligand **2-21**, the pre-insertion alkene π-complexes were considered. Taking into account the two possible configurations at the copper(I) center and the two prochiral faces of the cyclobutene ring of cyclobutylboronate **2-14**, four complexes **A-D** were modelled whereby the alkene π-bond is aligned with the copper-boron bond to maximize the stereoelectronics of the carbocupration step. All complexes were minimized using the semi-empirical PM3 program, followed by a more accurate, single-point energy calculation by DFT (B3LYP 6-31G*). The most favored complex leading to the observed enantiomer, **A**, was found to be 10.0 Kcal/mol more stable than the preferred complex **C** leading to the minor enantiomer. The high level of enantiofacial selectivity observed from Naud ligand **2-21** is best represented in a four-quadrant diagram. In the favored

complex, the diphenylphosphino group occupies both the right-hand quadrants, while the *tert*-butyl group occupies the bottom left-hand quadrant in its spatial environment (Figure 2-6). The top left quadrant remains unhindered, allowing for the larger ester group of the substrate to extend into and thus minimize steric repulsion. To investigate the substrate specificity the Naud ligand **2-21** provides with the cyclobutane substrate, the asymmetric copper-catalyzed conjugate borylation reaction was performed on the benzhydrol cyclopentenoate **2-33** (Scheme 2-12). The yields and selectivity obtained for compound **2-34** were poor, leading to the conclusion that the Naud ligand provides such a stringent spatial environment that it failed to accommodate the slightly larger cyclopentenoate ring. Calculations performed by Prof. Dennis G. Hall.

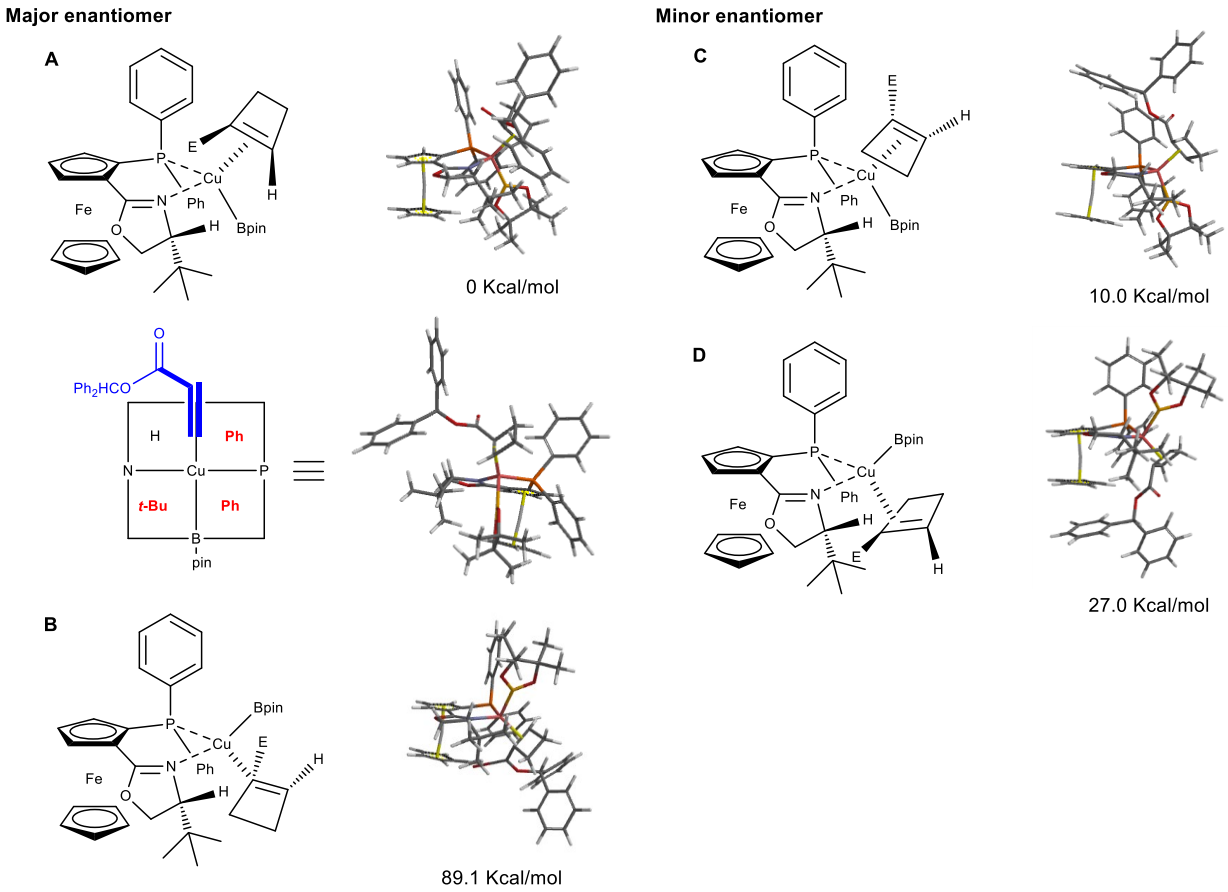

Figure 2-6. Proposed enantioselectivity model; E = CO_2CHPh_2

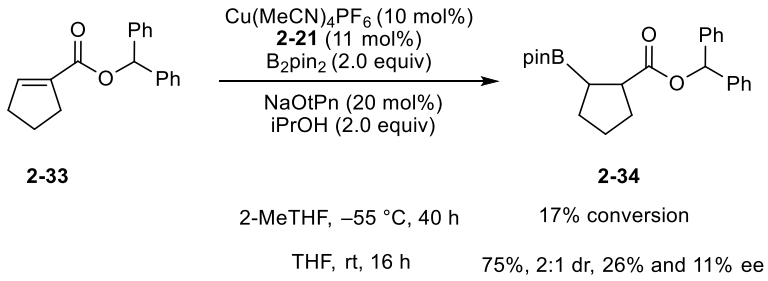

Scheme 2-12. Attempted enantioselective copper-catalyzed conjugate borylation of the benzhydrol cyclopentenoate **2-33**

2.10 Synthetic applications of cyclobutylboronate 2-13

2.10.1 Enantioselective copper-catalyzed tandem conjugate borylation-aldol reaction

A three-component, enantioselective copper-catalyzed tandem conjugate borylation-aldol reaction was investigated. The copper(I) enolate intermediate **2-31**, generated under a copper-catalyzed conjugate borylation reaction, can be efficiently trapped with an electrophile other than a proton, thus broadening the scope of the conjugate borylation reaction. In the presence of benzaldehyde, an enantioselective tandem conjugate borylation-aldol reaction proceeded with a high level of enantio- and diastereoselective control over three contiguous stereogenic centers, along with the formation of a challenging quaternary carbon center (Scheme 2-13).[6]

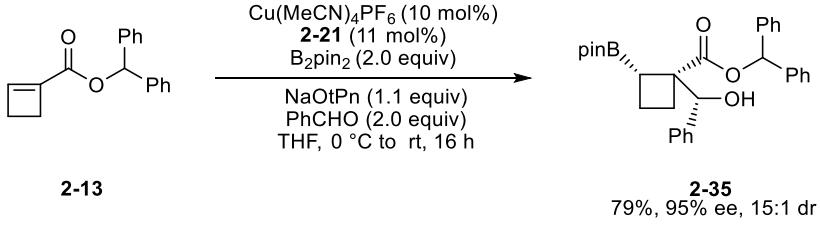

Scheme 2-13. Enantioselective copper-catalyzed tandem conjugate borylation-aldol reaction

The relative stereochemistry observed in the X-ray crystallographic structure of the major diastereomer **2-35** indicates that the aldol reaction occurs on the least hindered face of the cyclobutane ring, which can be explained by a six-membered chair-like transition state (Figure 2-7). Of note, attempts at trapping the copper(I) enolate intermediate with other electrophiles such as a ketone, allyl bromide or methyl mesylate proved unsatisfactory.

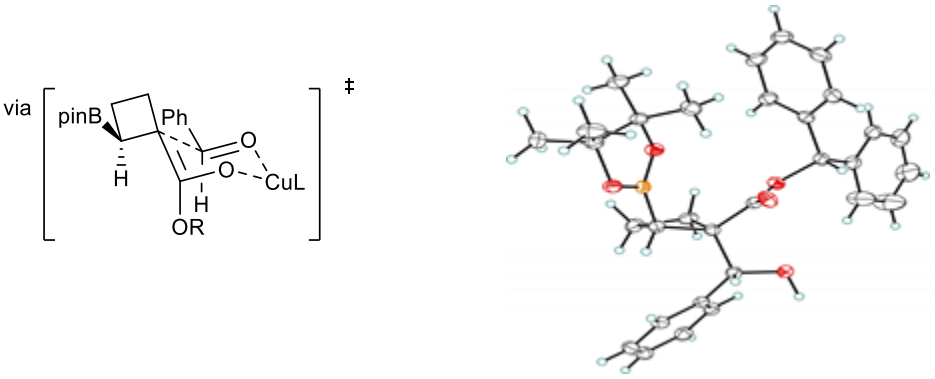

Figure 2-7. ORTEP of **2-35** and proposed 6-membered chair-like transition state

2.10.2 Oxidation of cyclobutylboronate 2-14

A preliminary effort was made to demonstrate the synthetic versatility of the enantioenriched cyclobutylboronate scaffold **2-14**. A mild and stereospecific oxidation of the carbon-boron bond in the presence of aqueous sodium dihydrogen phosphate and hydrogen

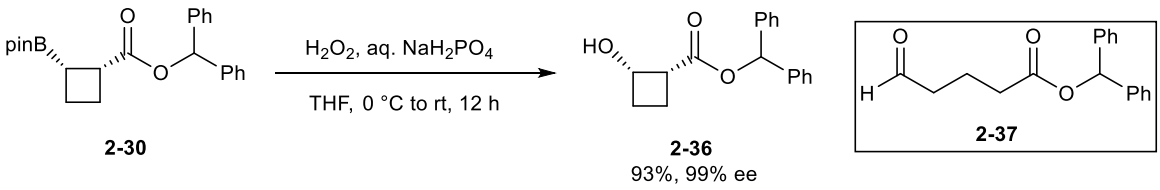

Scheme 2-14. Oxidation of the cyclobutylboronate **2-30**

peroxide afforded the *β*-hydroxy product **2-36** with complete retention of optical purity (Scheme 2-14). Of note, in the absence of monosodium phosphate, the corresponding oxidized ring-opened product **2-37** was observed.

2.11 Summary

In summary, the enantioselective copper-catalyzed conjugate borylation of cyclobutene 1-carboxyester **2-13** was demonstrated. Using a ligand HTS approach and the identification of cryogenic reaction conditions proved to be critical in affording the enantioenriched cyclobutylboronate scaffold **2-14** in 99% enantiomeric excess and excellent diastereoselectivity. The effectiveness of this approach was demonstrated with a reliable gram scale procedure. Computational modelling of the pre-insertion complexes shows that the large benzhydrol ester of the substrate occupies a relatively unhindered quadrant of the ligated copper complex in a spatially tight environment. Moreover, extension of the enantioselective copper-catalyzed conjugate borylation towards a three-component borylation/aldol tandem reaction provided a valuable synthetic intermediate containing a quaternary carbon center. With an optically enriched cyclobutylboronate scaffold in hand, the cross-coupling of the cyclobutylboronate **2-14** will be described in Chapter 3.

2.12 Experimental

2.12.1 General methods

Unless specified, all reactions were performed under nitrogen or argon atmosphere using glassware that was flame dried. Dichloromethane and tetrahydrofuran were used directly from an

MBraun Solvent Purification System. Benzene (ACS reagent grade) was used as received. 2-Methyltetrahydrofuran (anhydrous, inhibitor-free) and acetonitrile (HPLC grade) were purchased from Sigma Aldrich and used as received. 2-Propanol (reagent grade, 99%) was dried over 3Å molecular sieves overnight and stored under nitrogen. Bis(pinacolato)diboron (reagent grade, 99%) was purchased from Combi-Blocks and recrystallized from pentanes. Sodium *tert*-amylate (1.4 M solution in THF) was purchased from Sigma Aldrich and used as received (poor quality of sodium *tert*-amylate solution was found to have a negative impact on the reaction conversion). Triethylamine was distilled over CaH_2 and stored under nitrogen. (*R*)-4-*tert*-Butyl-2-[(S_P)-2-(diphenylphosphino)ferrocenyl]-2-oxazoline (Naud Ligand SL-N004-01)[14] was prepared according to a known literature procedure. All other reagents were purchased from Sigma Aldrich, Combi-Blocks or Strem Chemicals and used without further purification. Thin layer chromatography (TLC) was performed using Merck Silica Gel 60 F254 plates and visualized with UV light and PMA stain. NMR spectrum were recorded on INOVA-400, INOVA-500 or INOVA-700 MHz instruments. The residual solvent protons (^1H) of $CDCl_3$ (7.26 ppm) and the solvent carbons (^{13}C) of $CDCl_3$ (77.06 ppm) were used as internal standards. ^1H NMR data are presented as follows: chemical shift in ppm (δ) downfield from tetramethylsilane (multiplicity, coupling constant, integration). The following abbreviations are used in reporting the ^1H NMR data: s, singlet; br s, broad singlet; d, doublet; t, triplet; q, quartet; app q, apparent quartet; m, multiplet. High-resolution mass spectra were recorded by the University of Alberta Mass Spectrometry Services Laboratory using either electron impact (EI) or electrospray ionization (ESI) techniques. Infrared spectra were obtained on a Nicolet Magna-IR with frequencies expressed in cm^{-1}. Optical rotations were measured using a 1 mL cell with a 1 dm length on a P.E. 241 polarimeter. The enantiomeric excess and diastereomeric ratio for chiral compounds

were determined using a HPLC Agilent instrument with Chiralcel-OD, IC, IB, or Chiralpak-AS columns as specified in the following individual procedures. X-ray diffraction data were collected by the University of Alberta X-Ray Crystallography Laboratory. CCDC 2017200 (compound **2-40**) and CCDC 2017201 (compound **2-46**) contain the supplementary crystallographic data for this paper. These data can be obtained free of charge from The Cambridge Crystallographic Data Centre.

2.12.2 Preparation of benzhydrol cyclobutene 1-carboxyester 2-13

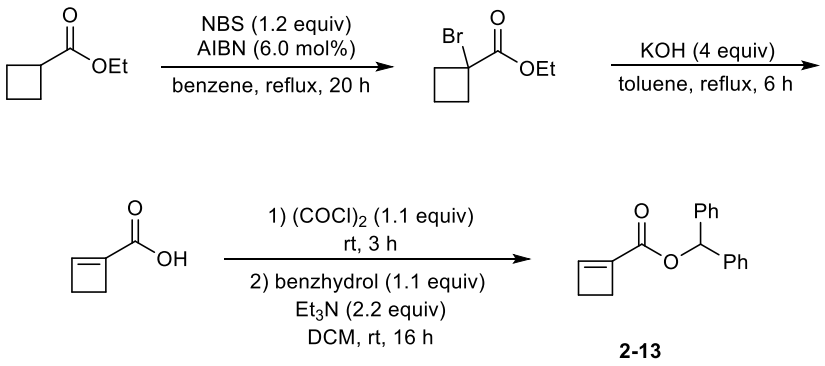

Ethyl 1-bromocyclobutanecarboxylate

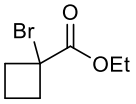

N-Bromosuccinimide (42.0 g, 242 mmol, 1.2 equiv) and 2,2′-azobis(2-methylpropionitrile) (1.8 g, 11 mmol, 6.0 mol%) were added to a solution of ethyl cyclobutanecarboxylate (25.0 g, 195 mmol, 1.0 equiv) in benzene (450 mL). The reaction mixture was heated to reflux for 16 h. The reaction mixture was allowed to cool to rt, water (500 mL) was added, and the mixture was extracted with ethyl acetate (×4). The combined organic phases were washed with brine, dried over anhydrous $MgSO_4$, filtered, then concentrated under reduced pressure. The crude mixture

was purified by fraction distillation under reduced pressure (thermometer temperature of product was recorded to be 55 °C) to give the desired product as a clear oil (15.7 g, 39%). **^{1}H NMR** (500 MHz, $CDCl_3$) δ 4.26 (q, *J* = 7.1 Hz, 2H), 2.96–2.85 (m, 2H), 2.69–2.58 (m, 2H), 2.22 (dtt, *J* = 11.5, 9.6, 5.9 Hz, 1H), 1.94–1.81 (m, 1H), 1.32 (t, *J* = 7.1 Hz, 3H). Characterization data was consistent with that reported in the literature.[9]

Cyclobutene-1-carboxylic acid

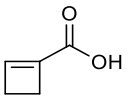

Potassium hydroxide (11.9 g, 0.200 mol, 4.5 equiv) in toluene (180 mL) was heated to reflux until the potassium hydroxide was dissolved (Note: potassium hydroxide was crushed to smaller size before use). The reaction vessel was removed from the oil bath and ethyl 1-bromocyclobutanecarboxylate (9.7 g, 47 mmol, 1.0 equiv) was added dropwise. The reaction mixture was heated to reflux for 1 h then allowed to cool to rt. Cold water (120 mL) was added and the aqueous phase was washed with pentane (×2). The pH of the aqueous phase was adjusted to 2.5 using 30% aqueous H_2SO_4. The product was extracted from the aqueous layer using diethyl ether (×4) and the combined organic layers were dried over anhydrous $MgSO_4$, filtered, and concentrated under reduced pressure. The crude mixture was purified by flash column chromatography (2:1 hexanes:ethyl acetate) to give the desired product as an off-white solid (3.2 g, 69%). **^{1}H NMR** (500 MHz, $CDCl_3$) δ 6.93 (t, *J* = 1.2 Hz, 1H), 2.80–2.65 (m, 2H), 2.61–2.38 (m, 2H). Characterization data was consistent with that reported in the literature.[9]

Benzhydrol cyclobutene 1-carboxyester **2-13**

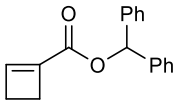

2-13

To a solution of cyclobutene-1-carboxylic acid (5.4 g, 55 mmol, 1.0 equiv) in dichloromethane (55 mL) cooled to 0 °C was added oxalyl chloride (5.1 mL, 61 mmol, 1.1 equiv) dropwise. The ice-bath was removed, and the reaction mixture was allowed to stir at rt for 3 h before being concentrated under reduced pressure in a water bath at rt to give a yellow oil (Note: the acid chloride is volatile). To a round bottom flask charged with benzhydrol (11.2 g, 61.0 mmol, 1.1 equiv) in dichloromethane (45 mL) was added triethylamine (15.3 mL, 110 mmol, 2.2 equiv). The reaction mixture was cooled to 0 °C, then the corresponding acid chloride in dichloromethane (10 mL) was added dropwise. The ice-bath was removed, and the reaction mixture was allowed to stir at rt for 16 h. The reaction mixture was quenched by the addition of 0.1 M HCl and extracted with dichloromethane (×3). The combined organic layers were washed with sat. $NaHCO_3$, dried over anhydrous $MgSO_4$, filtered, and concentrated under reduced pressure. The crude mixture was purified by flash column chromatography (9:1 hexanes:ethyl acetate) to give the desired product as a white solid (11.0 g, 79%). Stored at 0 °C. mp = 57.3–58.5 °C. **^{1}H NMR** (500 MHz, $CDCl_3$) δ 7.38–7.30 (m, 8H), 7.30–7.26 (m, 2H), 6.93 (s, 1H), 6.88 (t, J = 1.1 Hz, 1H), 2.80–2.76 (m, 2H), 2.52–2.47 (m, 2H). **^{13}C NMR** (176 MHz, $CDCl_3$) δ 161.2, 147.4, 140.5 (×2), 138.7 (×4), 128.6 (×2), 128.0 (×4), 127.3, 76.4, 29.3, 27.4. **IR** (cast film, CH_2Cl_2 cm^{-1}): 3032, 2984, 1718, 1600, 1586, 1495, 1454, 1188. **HRMS** (ESI) $[M+Na]^+$ calc. for $C_{18}H_{16}NaO_2$, 287.1043; observed, 287.1043.

2.12.3 High-throughput screening results

General procedure: Reactions were set-up in a glove box with <20 ppm O_2 and <20 ppm H_2O. $Cu(MeCN)_4PF_6$ (0.05 M solution in MeCN, 5.00 µL, 0.125 equiv) was first dispensed before evaporation to dryness. To the resulting residue was added Naud ligand **2-21** (0.05 M solution in toluene, 5.00 µL, 0.125 equiv) and THF (50 uL, 0.080 M). The reaction mixture was stirred for 1 h before the THF was evaporated. To the resulting residue was added bis(pinacolato)diboron (0.04 M solution in THF, 100 µL, 2 equiv). The reaction was stirred for 15 min before NaOtPn (0.08 M solution in THF, 5 µL, 0.2 equiv) was added. After stirring for another 15 min, the cyclobutene 1-carboxyester ester **1** (0.4 M solution in THF, 5 µL, 0.002 mmol) was added followed by MeOH (0.080 M solution in THF, 50 µL, 2.0 equiv). The reaction vial was crimp sealed to the glove-box environment before being stirred overnight. After 18 h the vials were diluted with MeCN (200 uL), mixed, centrifuged before being analyzed directly by SFC/MS. SFC/MS Analysis: Analysis by chiral SFC/MS. Peaks at 1.2 and 1.5 min (MW = 225+ve) and peaks at 2.3 and 2.5 min are enantiomers of cyclobutylboronate **2-30** (MW = 225+ve) as well as diastereomers of the first two eluted peaks. Peaks labelled as *trans*- and *cis*- for simplification.

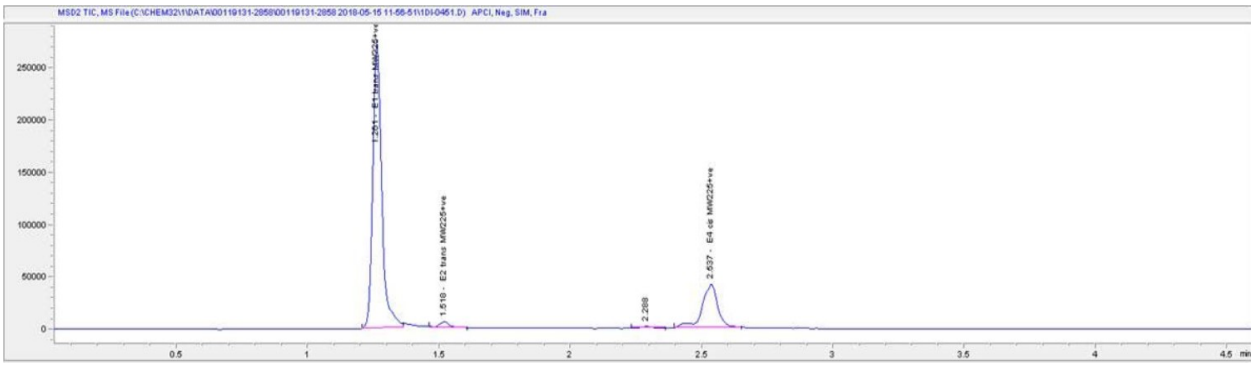

Table 2-11. Chiral ligand high-throughput screening results

Chiral Ligand	Product Yield Mass Ion Count (1200000.00)	% ee
(+)-TsCYDN	1178016.38	-20.87
(1)_(S)SEGPHOS	454501.57	-69.58
(2)_Xanthphos	583749.13	-5.24
(2R)-iPr-BPE	617569.63	-0.73
(3)_Blank	183875.08	8.3
(R,R,S,S)-DUANPHOS	686426.33	-24.06
(R,R)-Chiraphos	565946.86	7.91
(R,R)-DACH-naphthyl Trost ligand	751084.69	37.22
(R,R)-DIPAMP	639999.56	5.13
(R,R)-Et-DUPHOS	616499.97	3.94
(R,R)-i-Pr-DUPHOS	214328.59	-5.44
(R,R)-Me-BPE	799380.7	3.49
(R,R)-Me-DuPhos	77971.72	-7.5
(R,R)-NORPHOS	618691.46	6.97
(R,R)-QuinoxP*	528711.24	19.06
(R)-(+)-Cl-MeO-BIPHEP	372511.88	56.27
(R)-(+)-MeO-BIPHEP	565120.06	77.63
(R)-(+)-TolBINAP	325861.73	76.8
(R)-(+)-XylBINAP	642140.15	25.98
(R)-Binam-P	393755.45	-1.52
(R)-BINAP	517239.95	8.4
(R)-C3-Tunephos	506401.53	79.18
(R)-DIFLUORPHOS	389615.13	74.87
(R)-DM-SEGPHOS	686403.36	70.82
(R)-DTBM-SEGPHOS	600812.6	2.51
(R)-SDP	645340.45	3.32

(R)-SYNPHOS	520144.67	46.14
(R)-Tol-SDP	555420.49	-0.52
(R)-Xyl-SDP	124923.6	-3.95
(R)-Xylyl-P-Phos	357731.94	41.19
(Ra,S)-DTB-Bn-SIPHOX	539223.23	3.34
(Ra,S)-Ph-Bn-SIPHOX	641235.56	-5.76
(S,S,R,R)-TangPhos	581758.96	7.14
(S,S)-BDPP	582706.89	-45.24
(S,S)-DACH-pyridyl TROST	607169.08	-3.02
(S,S)-DIOP	654009.83	15.26
(S,S)-f-Binaphane	601804.37	40.6
(S,S)-Me-BPF	513820.56	47.71
(S,S)-N-Ms-1,2-DPEN	863704.14	-4.25
(S,S)-TsDPEN	517895.3	-1.33
(S)-BINAPINE	517366.02	-31.6
(S)-BINOL	103324.83	-12.72
(S)-Me-f-KetalPhos	684984.26	41.21
(S)-Methyl BoPhoz	493299.93	41.47
(S)-Phanephos	567661.2	5.76
2,2BNDMDiE	731278.84	11.99
Box Ligand 1	1015057.77	2.38
Box Ligand 10	4921.88	-6.25
Box Ligand 11	772435.03	-25.45
Box Ligand 12	123262.42	19.77
Box Ligand 13	163668.18	46.53
Box Ligand 14	716692.24	-11.25
Box Ligand 15	93991.73	-4.35
Box Ligand 16	124805.22	5.95
Box Ligand 2	849190.15	-3.02
Box Ligand 3	537514.23	-24.05

Box Ligand 4	78441.72	1.09
Box Ligand 5	672487.28	15.27
Box Ligand 6	636901.93	-5.41
Box Ligand 8	189675.94	59.31
Box Ligand 9	232350.89	-68.37
Buwen Ligand	850409.27	-0.67
catASium MNXylF(R)	822973.63	-6.05
catASium T1	12617.19	-54.2
ChenPhos	669814.25	-11.46
cis-Aindanol	826773.36	3.91
CTH-(R)-3,5-xylyl-PHANEPHOS	569710	-5.8
CTH-(R)-BINAM	806593.84	-2.62
CTH-(S)-P-Phos	11836.7	-40.05
Groton BINOL Ligand 1	7773.74	-31.36
Josiphos SL-J404-2	632891.09	36.14
JoSPOphos 1	587131.21	5.73
JoSPOphos 2	629324.71	21.47
Mandyphos SL-M002-1	833612.77	41.18
Mandyphos SL-M009-1	597069.05	7.47
N,N-DTsCHN	34464.54	-4.78
Naud SL-N004-1	**871369.52**	**93.75**
Naud SL-N008-2	620530.26	-94.64
Naud SL-N011-2	657780.18	-96.08
Naud SL-N012-2	846565.25	-98.01
Naud SL-N013-1	687041.02	92.28
Nauds-iPr Ligand	542137.41	88.05
P(Ph3)Chiral	573733.7	-22.35
Pfizer Ligand	371751.82	-5.43
PPM	269622.93	-25.09

R-Josiphos SL-J001-1	521262.19	-59.55
R-Josiphos SL-J002-1	66567.97	0.07
R-Josiphos SL-J003-1	547574.8	40.42
R-Josiphos SL-J004-1	605208.15	58.18
R-Josiphos SL-J006-1	131869.17	-8.85
R-Josiphos SL-J009-1	30625.78	-8.81
R-Josiphos SL-J011-1	290281.28	-68.4
R-Monophos	560573.54	-27.1
Salen	318199.59	-3.61
SaxS,S-BOBPHOS	17518.9	-6.77
SL-J005-2	638372.78	-28.58
SL-J007-1	684195.73	8.01
SL-J008-1	439327.4	-1.24
SL-J013-2	79390.73	66.89
SL-J014-1	317101.95	-66.04
SL-J015-1	609197.91	10.86
SL-J212-1	334354.2	-7.27
SL-J216-2	590838.99	-5.94
SL-J418-1	623182.17	9.96
SL-J425-2	708316.81	-59.47
SL-J452-2	544182.55	-78.25
SL-J502-1	659990.94	3.16
SL-J505-1	606983.38	8.88
SL-M003-2	572065.59	-11.89
t-BuDPPPO	789897.83	-49.06
Taniaphos SL-T002-1	589193.09	8.52
TCI1	681979.33	-65.92
TCI2	785020.39	6.88
Trifer	480457.63	-1.79
Walphos SL-W002-1	852649.35	32.52

Walphos SL-W003-1	699280.7	11.56
Walphos SL-W005-2	25042	-45.42
Walphos SL-W008-1	619006.11	2.52
Walphos SL-W022-2	568162.92	-4.55

Note: while other Naud ligands provided higher ee values, only Naud ligand SL-N004-01 was commercially available from Solvais.

Structures of Naud ligands in HTS screen:

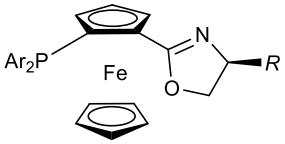

	Ar	R
Naud SL-N012-2	2-methoxyphenyl	iPr
Naud SL-N011-2	1-naphthyl	iPr
Naud SL-N008-2	3,5-dimethyl-4-methoxyphenyl	iPr

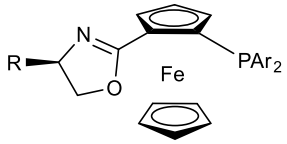

	Ar	R
Naud SL-N004-1	phenyl	tBu
Naud SL-N013-1	2-methylphenyl	iPr
Naud-*i*Pr ligand	phenyl	iPr

2.12.4 Procedure for the synthesis of cyclobutylboronate 2-14

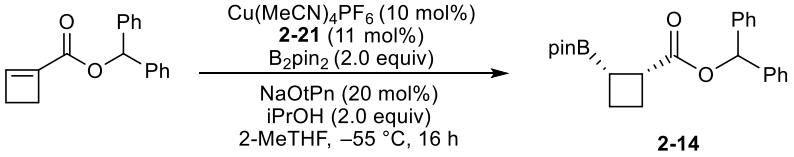

A microwave vial was charged with bis(pinacolato)diboron (102 mg, 0.400 mmol, 2.0 equiv), $[Cu(MeCN)_4]PF_6$ (7.5 mg, 0.020 mmol, 10 mol%) and Naud ligand **2-21** (10.9 mg, 0.0220 mmol, 11 mol%), capped, and purged with argon. 2-Methyltetrahydrofuran (0.6 mL) was added and the reaction mixture allowed to stir for 15 min at 0 °C. Sodium *tert*-amylate (1.4 M in THF, 29 µL, 0.040 mmol, 20 mol%) was added dropwise at 0 °C to give a dark orange-brown solution

which was allowed to stir for another 10 min at 0 °C. The reaction mixture was then removed from the ice-bath and transferred to an ethanol-bath that was pre-cooled at –55 °C using a cryocooler. The reaction mixture was allowed to stir for 10 min at –55 °C before the dropwise addition of a solution of cyclobutane 1-carboxyester **2-13** (52.9 mg, 0.200 mmol, 1.0 equiv) in 2-methyltetrahydrofuran (0.4 mL) followed by the dropwise addition of isopropanol (30.6 µL, 0.400 mmol, 2.0 equiv). The reaction mixture was allowed to stir at –55 °C for 16 h. The reaction mixture was quenched by the dropwise addition of sat. NH_4Cl (2 mL) at –55 °C and extracted with ethyl acetate (×3). The combined organic layers were washed with brine, dried over anhydrous $MgSO_4$, filtered, and concentrated under reduced pressure. The crude ^1H NMR yield was 98% using dibromomethane as the internal standard. The crude dr was 12:1 by peak height of the benzylic proton. The crude mixture was purified by flash column chromatography using 30 wt% deionized water deactivated silica (20:1 hexanes:ethyl acetate, TLC performed using 5:1 hexanes:ethyl acetate). The major diastereomer eluted first and appeared on the upper position on the TLC plate relative to the minor diastereomer. The desired product was isolated as a clear oil (55.8 mg, 71%, 20:1 dr). Stored at 0 °C. **^{1}H NMR** (700 MHz, $CDCl_3$) δ 7.39–7.21 (m, 10H), 6.89 (s, 1H), 3.40 (app q, *J* = 9.0 Hz, 1H), 2.43–2.34 (m, 1H), 2.34–2.27 (m, 1H), 2.21 (app q, *J* = 9.1 Hz, 1H), 2.12–2.01 (m, 2H), 1.13 (s, 6H), 1.12 (s, 6H). **^{13}C NMR** (176 MHz, $CDCl_3$) δ 174.7, 140.8, 140.6, 128.5 (×2), 128.4 (×2), 127.8, 127.7, 127.4 (×2), 127.2 (×2), 83.3 (×2), 76.5, 40.2, 25.2, 24.9 (×2), 24.8 (×2), 20.3 (the boron-bound carbon was not detected due to quadrupolar relaxation of boron). **^{11}B NMR** (128 MHz, $CDCl_3$) δ 33.6. **IR** (cast film, CH_2Cl_2 cm^{-1}): 3031, 2977, 1732, 1600, 1586, 1495, 1142. **HRMS** (ESI) $[M+Na]^+$ calc. for $C_{24}H_{29}BNaO_4$, 415.2051; observed, 415.2051. **$[\alpha]_D^{20}$**: 6.20 (*c* = 1.06, CH_2Cl_2). **HPLC**: Chiralpak IC: 1:99 isopropanol:hexanes, 0.5 mL/min, 5 °C, λ = 210 nm, Major diastereomer (*cis*) T_{minor} =

7.0 min, T_{major} = 7.7 min, ee = 99% Minor diastereomer (*trans*) T_{major} = 10.0 min, T_{minor} = 10.7 min, ee = 99%.

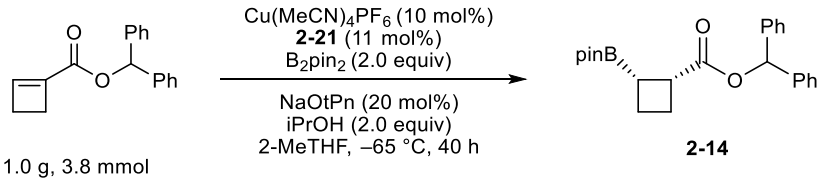

Gram-scale procedure: A cylindrical 30 mL Schlenk vessel was charged with bis(pinacolato)diboron (1.93 g, 7.60 mmol, 2.0 equiv), $[Cu(MeCN)_4]PF_6$ (141 mg, 0.380 mmol, 10 mol%) and Naud ligand SL-N004-01 (206 mg, 0.420 mmol, 11 mol%), covered with a septum and purged with argon. 2-Methyltetrahydrofuran (14 mL) was added and the reaction mixture allowed to stir for 15 min at 0 °C. Sodium *tert*-amylate (1.4 M in THF, 0.54 mL, 0.76 mmol, 20 mol%) was added dropwise at 0 °C to give a dark orange-brown solution which was allowed to stir for another 10 min at 0 °C. The reaction mixture was then removed from the ice-bath and transferred to an ethanol-bath that was pre-cooled at –65 °C using a cryocooler. The reaction mixture was allowed to stir for 15 min at –65 °C before the dropwise addition of a solution of cyclobutane 1-carboxyester **2-13** (1.0 g, 3.8 mmol, 1.0 equiv) in 2-methyltetrahydrofuran (4 mL) followed by the dropwise addition of isopropanol (0.58 mL, 7.6 mmol, 2.0 equiv). The reaction mixture was allowed to stir at –65 °C for 40 h. The reaction mixture was quenched by the dropwise addition of sat. NH_4Cl (20 mL) at –65 °C and extracted with ethyl acetate (×4). The combined organic layers were washed with brine, dried over anhydrous $MgSO_4$, filtered, and concentrated under reduced pressure. The crude ^1H NMR yield was 98% using dibromomethane as the internal standard. The crude dr was 12:1 by peak height of the benzylic proton. The crude reaction mixture was purified by flash column chromatography

using 30 wt% deionized water deactivated silica (20:1 hexanes:ethyl acetate, TLC performed using 5:1 hexanes:ethyl acetate). Note: cracking of the silica will persist while performing flash column chromatography. The major diastereomer eluted first and appeared on the upper position on the TLC plate relative to the minor diastereomer. The desired product was isolated as a clear oil (1.2 g, 80%, >20:1 dr). Stored at 0 °C.

2.12.5 1D TROSEY NMR spectroscopy study for the major and minor diastereomer of cyclobutylboronate 2-13

While the 1D TROSEY experiments of both diastereomers provided some valuable insight on the relative stereochemistry, the NOE interactions observed were relatively inadequate as all interaction were less than 1%. Note: Hb was identified by gCOSY and HSQC analysis as the boron-bound carbon was not detected due to quadrupolar relaxation of boron.

1D TROSEY of major diastereomer – selective excitation at 3.40 ppm (H_a)

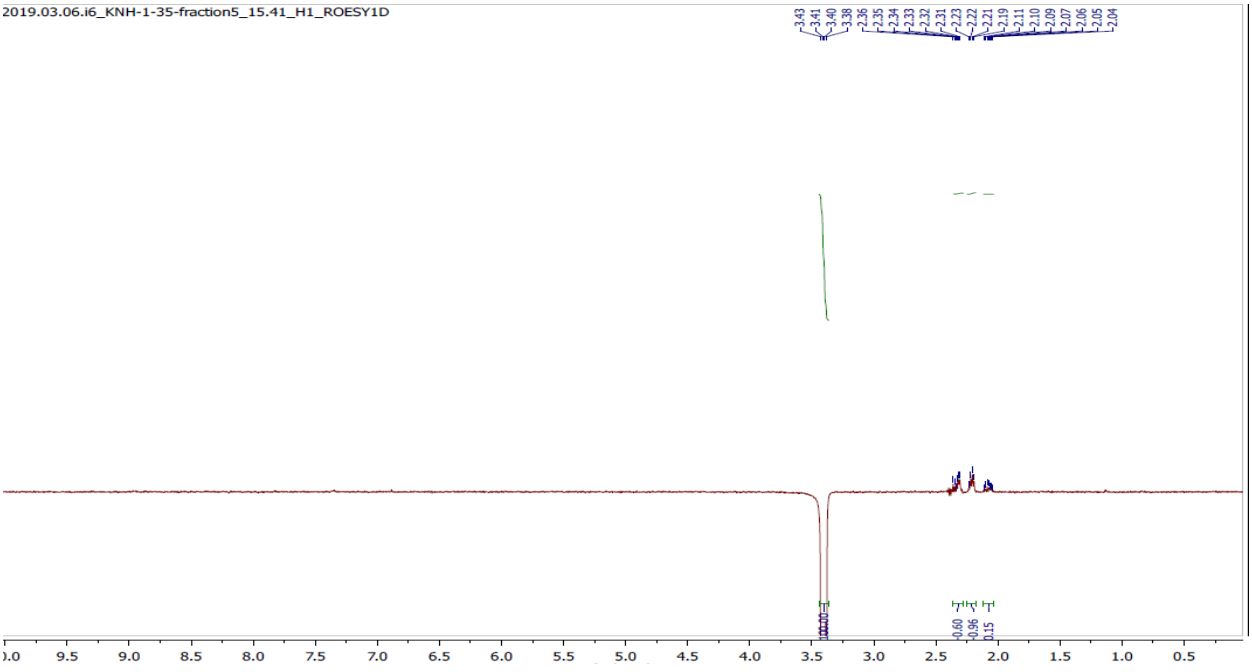

1D TROSEY of minor diastereomer – selective excitation at 3.29 ppm (H_a)

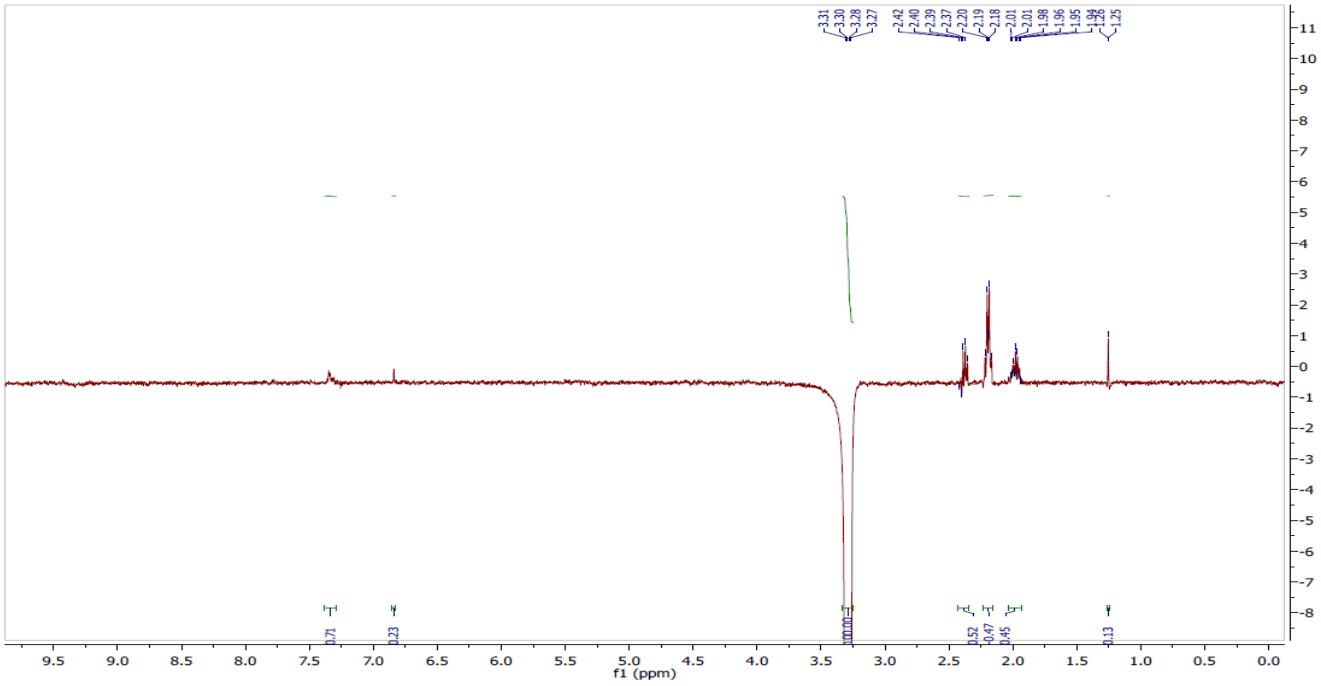

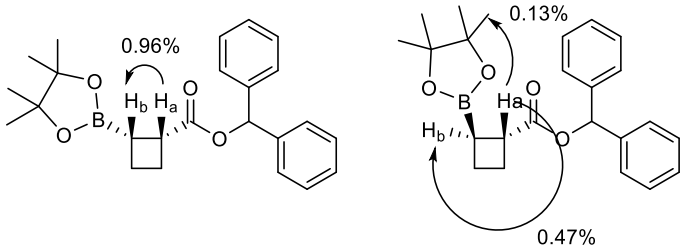

Major diastereomer Minor diastereomer

2.12.6 Preparation of *β*-boronyl cyclobutylcarboxyamide 2-23

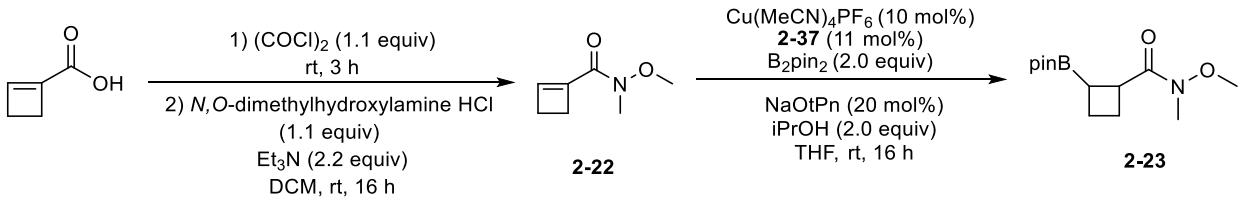

Following the procedure for the preparation of benzhydrol cyclobutene 1-carboxyester. Using cyclobutene 1-carboxylic acid (1.0 equiv), oxalyl chloride (1.1 equiv), *N,O*-

dimethylhydroxylamine hydrochloride (1.1 equiv) and triethylamine (2.2 equiv). Compound **2-22** was obtained as a yellow oil (74%). **^{1}H NMR** (400 MHz, $CDCl_3$) δ 6.66 (s, 1H), 3.70 (s, 3H), 3.24 (s, 3H), 2.83–2.78 (m, 2H), 2.51–2.46 (m, 2H). **^{13}C NMR** (101 MHz, $CDCl_3$) δ 162.9, 144.9, 139.5, 61.5, 53.6, 30.6, 27.7. **IR** (cast film, CH_2Cl_2 cm^{-1}): 2958, 1660, 1600. **HRMS** (ESI) $[M+Na]^+$ calc. for $C_7H_{11}NNaO_2$, 164.0682; observed, 164.0682.

A microwave vial was charged with bis(pinacolato)diboron (102 mg, 0.400 mmol, 2 equiv), $[Cu(MeCN)_4]PF_6$ (7.5 mg, 10 mol%, 0.020 mmol) and 4,5-bis(diphenylphosphino)-9,9-dimethylxanthene (19.1 mg, 11 mol%, 0.0220 mmol), capped, and purged with argon. Tetrahydrofuran (0.6 mL) was added and the reaction mixture allowed to stir for 15 min at 0 °C. Sodium *tert*-pentoxide (1.4 M in THF, 29 µL, 0.040 mmol, 20 mol%) was added dropwise at 0 °C and allowed to stir for another 10 min at 0 °C. A solution of cyclobutane 1-carboxyamide **2-23** (50 mg, 0.20 mmol, 1 equiv) in tetrahydrofuran (0.4 mL) was added dropwise followed by the dropwise addition of isopropanol (30.6 µL, 0.400 mmol, 2 equiv) at 0 °C. The ice-bath was removed and the reaction mixture was allowed to stir at rt for 16 h. The reaction mixture was quenched by the addition of sat. NH_4Cl (2 mL) and extracted with ethyl acetate (×3). The combined organic layers were washed with brine, dried over anhydrous $MgSO_4$, filtered, and concentrated under reduced pressure. The crude mixture was purified by flash column chromatography using 30 wt% deionized water deactivated silica (20:1 hexanes:ethyl acetate, TLC performed using 5:1 hexanes:ethyl acetate). The desired product was isolated as a yellow oil (33.8 mg, 62%, 7:1 dr). **^{1}H NMR** (400 MHz, $CDCl_3$) δ 3.63 (s, 3H), 3.57 (m, 1H), 3.14 (s, 3H), 2.40–2.28 (m, 1H), 2.27–2.15 (m, 1H), 2.14–1.93 (m, 4H), 1.25 (d, J = 5.5 Hz, 12H). **^{13}C NMR** (126 MHz, $CDCl_3$) δ 171.1, 83.1, 83.0 (×2), 61.2, 39.0, 25.1 (×2), 24.9 (×2), 24.8, 20.1.

^{11}B NMR (128 MHz, $CDCl_3$) δ 33.6. **IR** (cast film, CH_2Cl_2 cm^{-1}): 2976, 1660, 1146. **HRMS**: (ESI) $[M+H]^+$ calc. for $C_{13}H_{24}BNO_4$, 270.1871; observed, 270.1871.

2.12.7 Synthesis of trifluoroborate salts

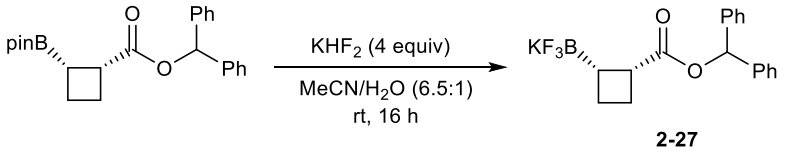

2-27

To a round bottom flask charged with cyclobutylboronate **2-13** (1.0 g, 2.5 mmol, 1 equiv) and potassium hydrogen difluoride (796 mg, 10.0 mmol, 4 equiv) was added distilled water (2.8 mL) and acetonitrile (18 mL). The reaction was allowed to stir at rt for 16 h. The solvents were removed under reduced pressure and the crude reaction mixture was dried under high vacuum. The resulting crude solid was suspended in diethyl ether (20 mL), filtered and further washed with diethyl ether (20 mL × 4). The remaining solid was extracted with acetonitrile (35 mL × 4). The solvent from the resulting filtrate was removed under reduced pressure to give the desired product as a white solid (913 mg, 97%). **^{1}H NMR** (700 MHz, $(D_3C)_2CO$) δ 7.41–7.20 (m, 10H), 6.83 (s, 1H), 3.20 (app q, J = 9.3 Hz, 1H), 2.57–2.39 (m, 1H), 1.82–1.75 (m, 4H). **^{13}C NMR** (176 MHz, $(D_3C)_2CO$) δ 177.3, 142.5, 142.2, 129.1 (×2), 128.9 (×2), 128.3, 128.24, 128.20 (×2), 128.0 (×2), 77.0, 40.7, 24.1, 21.4 (the boron-bound carbon was not detected due to quadrupolar relaxation of boron). **^{11}B NMR** (128 MHz, $(D_3C)_2CO$) δ 4.0. **^{19}F NMR** (376 MHz, $(D_3C)_2CO$) δ -144.5. **HRMS** (ESI) $[M]^{*-}$ calc. for $C_{18}H_{17}BF_3O_2$, 333.1279; observed, 333.1277. **$[\alpha]_D^{20}$**: 26.8 (*c* = 1.09, $(CH_3)_2CO$).

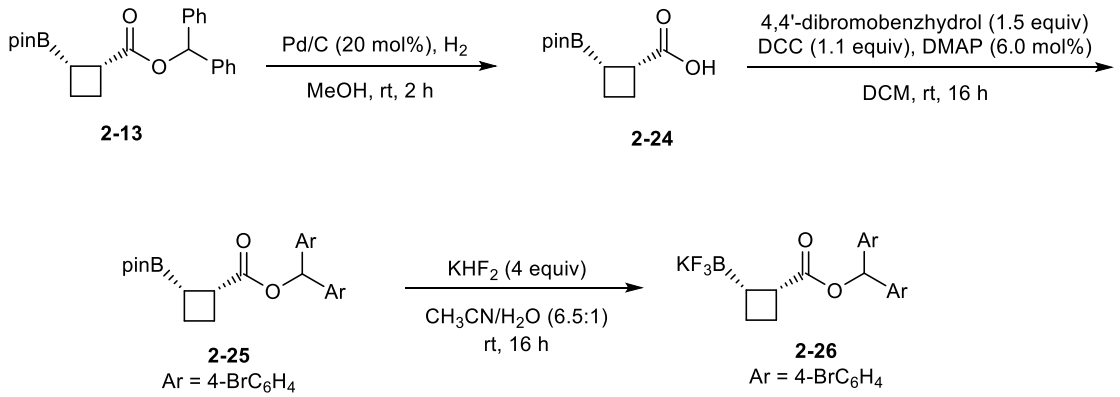

To a round bottom flask charged with cyclobutylboronate **2-13** (500 mg, 1.30 mmol, 1.0 equiv) was added methanol (7 mL). Pd/C (30 mg, 0.25 mmol, 20 mol%) was added and the reaction mixture was purged with a hydrogen gas-filled balloon for 10 min. The reaction was then allowed to stir at rt for 2 h under hydrogen gas. The reaction mixture was filtered through Celite and washed with ethyl acetate. The filtrate was concentrated under reduced pressure and the crude mixture was purified by flash column chromatography using 30 wt% deionized water deactivated silica (5:1 hexanes:ethyl acetate, TLC performed using 1:1 hexanes:ethyl acetate) to give the desired product **2-24** as a clear oil (287 mg, 89%). **^{1}H NMR** (700 MHz, $CDCl_3$) δ 3.30 (app q, *J* = 9.3 Hz, 1H), 2.38–2.25 (m, 2H), 2.16 (app q, *J* = 9.1 Hz, 1H), 2.03 (m, 2H), 1.21 (s, 6H), 1.19 (s, 6H). **^{13}C NMR** (126 MHz, $CDCl_3$) δ 181.9, 83.4 (×2), 39.9, 25.3, 25.0 (×2), 24.9 (×2), 20.2 (the boron-bound carbon was not detected due to quadrupolar relaxation of boron). **^{11}B NMR** (128 MHz, $CDCl_3$) δ 33.2. **IR** (cast film, CH_2Cl_2 cm^{-1}): 3010, 2979, 1702, 1165. **HRMS** (ESI) $[M-H]^-$ calc. for $C_{11}H_{18}BO_4$, 225.1303; observed, 225.1303. **$[\alpha]_D^{20}$**: 6.60 (*c* = 1.20, CH_2Cl_2).

Carboxylic acid **2-24** (100 mg, 0.260 mmol, 1.0 equiv), 4-dimethylaminopyridine (2.0 mg, 0.015 mmol, 6.0 mol%) and 4,4'-dibromobenzhydrol (131 mg, 0.380 mmol, 1.5 equiv) were dissolved in dichloromethane (3 mL) and stirred at rt for 5 min. N,N'-dicyclohexylcarbodiimide (58 mg,

0.28 mmol, 1.1 equiv) was added resulting in a suspension. The reaction mixture was allowed to stir at rt for 16 h, then filtered and washed with dichloromethane. The resulting filtrate was concentrated under reduced pressure and the crude mixture was purified by flash column chromatography (5:1 hexanes:ethyl acetate) to give the desired product **2-25** as a clear oil (118 mg, 65%). **^{1}H NMR** (500 MHz, $CDCl_3$) δ 7.76–7.33 (m, 4H), 7.18 (m, 4H), 6.74 (s, 1H), 3.36 (app q, *J* = 9.0 Hz, 1H), 2.40–2.24 (m, 2H), 2.20 (m, 1H), 2.13–1.97 (m, 2H), 1.14 (s, 6H), 1.12 (s, 6H). **^{13}C NMR** (126 MHz, $CDCl_3$) δ 174.5, 139.3, 139.1, 131.7 (×2), 131.6 (×2), 129.0 (×2), 128.9 (×2), 122.1, 122.0, 83.3 (×2), 75.2, 39.9, 25.0, 24.8 (×2), 24.7 (×2), 20.3 (the boron-bound carbon was not detected due to quadrupolar relaxation of boron). **^{11}B NMR** (128 MHz, $CDCl_3$) δ 35.6. **IR** (cast film, CH_2Cl_2 cm^{-1}): 3031, 2977, 1735, 1592, 1488, 1467, 1142. **HRMS** (ESI) $[M]^{*-}$ calc. for $C_{24}H_{27}BBr_2O_4$, 548.0375; observed, 548.0371. **$[\alpha]_D^{20}$**: 0.70 (*c* = 0.35, CH_2Cl_2).

To a round bottom flask charged with cyclobutylboronate **2-25** (80 mg, 0.11 mmol, 1 equiv) and potassium hydrogen difluoride (35 mg, 0.44 mmol, 4 equiv) was added distilled water (0.11 mL) and acetonitrile (0.75 mL). The reaction mixture was allowed to stir at rt for 16 h. The solvents were removed under reduced pressure and the crude mixture was dried under high vacuum. The resulting crude solid was suspended in diethyl ether (3 mL) then filtered and washed with diethyl ether (5 mL × 4). The product was extracted with acetonitrile (5 mL × 4) and filtered. The solvent from the resulting filtrate was removed under reduced pressure to give the desired product **2-26** as a white solid (75 mg, 95%). Recrystallized by way of vapour diffusion (ethyl acetate:hexanes) to give thin blades of crystals. **^{1}H NMR** (500 MHz, CD_3CN) δ 7.48 (m, 4H), 7.35–7.26 (m, 4H), 6.61 (s, 1H), 3.09 (br q, *J* = 8.7 Hz, 1H), 2.35 (m, 1H), 1.89–1.63 (m, 4H). **^{13}C NMR** (126 MHz, CD_3CN) δ 177.1, 141.5, 141.1, 132.4 (×2), 132.3 (×2), 130.3 (×2), 130.0 (×2), 122.13, 122.05, 75.8, 40.6, 23.8, 21.5 (the boron-bound carbon was not detected due to

quadrupolar relaxation of boron). **^{11}B NMR** (128 MHz, CD_3CN) δ 4.7. **^{19}F NMR** (376 MHz, (CD_3CN) δ -144.5. **IR** (cast film, CH_3CN cm^{-1}): 3028, 1979, 1717, 1592, 1488, 1174. **HRMS** (ESI) $[M]^{*-}$ calc. for $C_{18}H_{15}BBr_2F_3O_2$, 488.9482; observed, 488.9482. **$[\alpha]_D^{20}$**: 14.9 (*c* = 0.800, CH_3CN).

2.12.8 Molecular modeling of the copper-catalyzed conjugate borylation

Methodology

Package: MacSpartan 18

Y.Shao et al., Mol. Phys. 113, 184 - 215 (2015), DOI : 10.1080/00268976.2014.952696

Method: The equilibrium geometry of the four pre-insertion complexes was computed using the PM3 semi-empirical model. The PM3 model is parameterized for transition metals and is known to generally provide a reasonable account of equilibrium geometries. In a second round of calculations, the alkene pi bond of each complex was aligned (periplanar) with the Cu–B bond of the complex to approximate the pre-insertion conformation. The geometry was minimized, and in a final operation, more reliable energy values were obtained using single-point calculation using DFT with the B3LYP 6-31G* basis set.

Additional views of conformer **A**

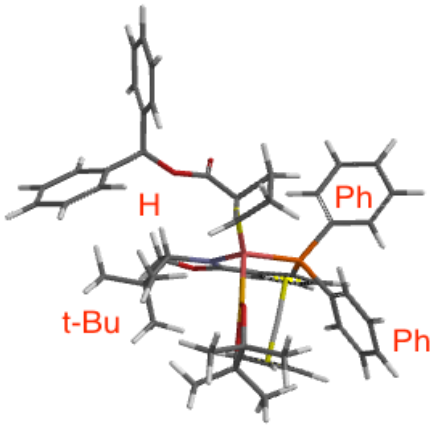

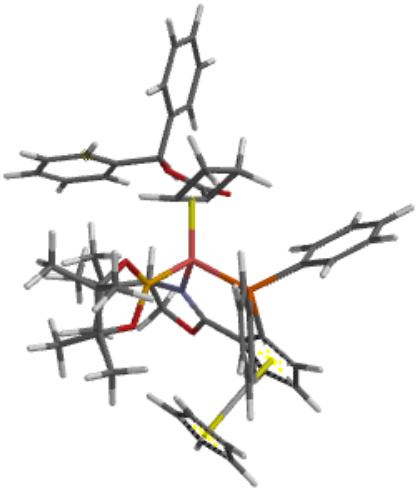

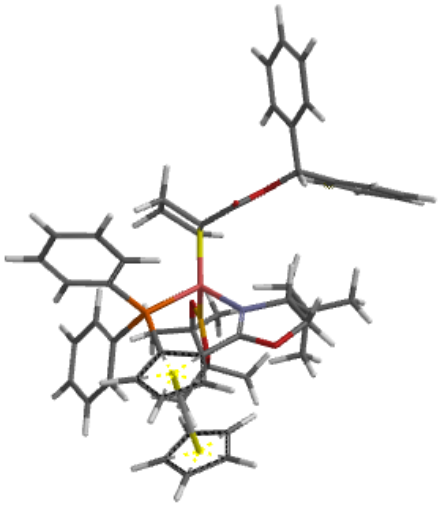

2.12.9 Rationale for the diastereoselectivity observed for the conjugate borylation reaction

The observed diastereoselectivity can arise from a kinetically controlled and irreversible protodecupration step on the least hindered face of the cyclobutane ring, away from the large Bpin group leading to the major diastereomer. The alternative protodecupration step is disfavored as it would occur on the same face as the sterically demanding Bpin group resulting in the minor diastereomer.

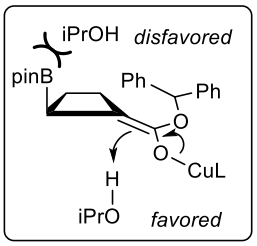

Control experiment for epimerization post-protodecupration

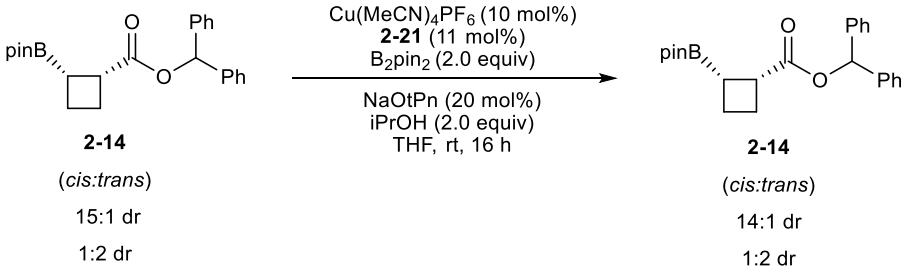

When cyclobutylboronate **2** (15:1 and 1:2 dr, *cis:trans*) was subjected to the asymmetric conjugate borylation reaction conditions at rt, no significant amount of epimerization was observed which suggest the absence of the epimerization of cyclobutylboronate **2-13** and an irreversible protodecupration step. The dr of the resulting product was determined by ^{1}H NMR analysis of the crude reaction mixture by peak height of the benzylic proton.

2.12.10 Procedure for the synthesis of *β*-boronyl cyclopentylcarboxyester 2-34

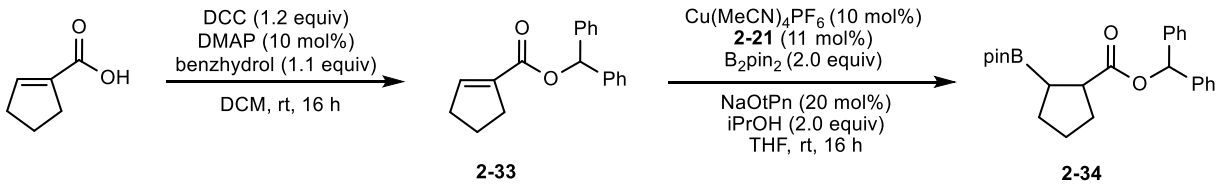

To a round bottom flask charged with 1-cyclopentenecarboxylic acid (100 mg, 0.900 mmol, 1.0 equiv.), 4-dimethylaminopyridine (11 mg, 0.090 mmol, 10 mol%), and benzhydrol (180 mg, 0.980 mmol, 1.1 equiv) in dichloromethane (4.5 mL) was added N,N′-dicyclohexylcarbodiimide (220 mg, 1.10 mmol, 1.2 equiv) at 0 °C. After 16 h, the reaction mixture was filtered, then concentrated under reduced pressure. The resulting filtrate was concentrated under reduced pressure and the crude mixture was purified by flash column chromatography (9:1 hexanes:ethyl acetate) to give the desired product **2-33** as a white solid (187 mg, 97%). **^{1}H NMR** (500 MHz, $CDCl_3$) δ 7.32 (m, 10H), 6.95 (s, 1H), 6.93 (s, 1H), 2.65 (br s, 2H), 2.53 (br s, 2H), 2.05–1.92 (m, 2H). **^{13}C NMR** (126 MHz, $CDCl_3$) δ 164.2, 140.6 (×3), 136.6, 128.5 (×4), 127.8 (×2), 127.1 (×4), 76.4, 33.5, 31.4, 23.1. **IR** (cast film, CH_2Cl_2 cm^{-1}): 3031, 2932, 1707, 1086. **HRMS** (ESI) $[M+Na]^+$ calc. for $C_{19}H_{18}NaO_2$, 301.1199; observed, 301.1214.

A microwave vial was charged with bis(pinacolato)diboron (102 mg, 0.400 mmol, 2.0 equiv), $[Cu(MeCN)_4]PF_6$ (7.5 mg, 0.020 mmol, 10 mol%) and Naud ligand **2-21** (10.9 mg, 0.0220 mmol, 11 mol%), capped, and purged with argon. Tetrahydrofuran (0.6 mL) was added and the reaction mixture allowed to stir for 15 min at 0 °C. Sodium *tert*-amylate (1.4 M in THF, 29 µL, 0.040 mmol, 20 mol%) was added dropwise at 0 °C to give a dark orange-brown solution which was allowed to stir for another 10 min at 0 °C before the dropwise addition of a solution of cyclopentenoate **2-33** (55.6 mg , 0.20 mmol, 1.0 equiv) in tetrahydrofuran (0.4 mL) followed by

the dropwise addition of isopropanol (30.6 μL, 0.400 mmol, 2.0 equiv). The ice-bath was removed, and reaction mixture was allowed to stir at rt for 16 h. The reaction mixture was quenched by the addition of sat. NH_4Cl (2 mL) and extracted with ethyl acetate (×3). The combined organic layers were washed with brine, dried over anhydrous $MgSO_4$, filtered, and concentrated under reduced pressure. The crude ^1H NMR yield was 82% using dibromomethane as the internal standard. The crude mixture was purified by flash column chromatography using 30 wt% deionized water deactivated silica (30:1 hexanes:ethyl acetate, TLC performed using 7:1 hexanes:ethyl acetate). The desired product **2-35** was isolated as a white solid (61.0 mg, 75%, 2:1 dr). **^{1}H NMR** (500 MHz, $CDCl_3$) δ 7.37–7.30 (m, 12H), 7.26 (m, 3H), 6.87 (s, 0.5H, minor diastereomer), 6.83 (s, 1H, major diastereomer), 3.15 (m, 1H, major diastereomer), 2.96 (app q, *J* = 8.2 Hz, 0.5H, minor diastereomer), 2.06–1.48 (m, 11H), 1.18 (s, 6H), 1.14 (s, 6H), 1.08 (s, 6H). Major diastereomer **^{13}C NMR** (126 MHz, $CDCl_3$) δ 175.9, 140.6 (×2), 128.44 (×2), 128.36 (×2), 127.7 (×2), 127.3 (×2), 127.1 (×2), 83.1 (×2), 76.6, 46.7, 31.2, 27.5, 25.7, 24.8 (×2), 24.6 (×2). Minor diastereomer **^{13}C NMR** (126 MHz, $CDCl_3$) δ 175.4, 140.7 (×2), 128.4 (×4), 127.7 (×2), 127.18 (×2), 127.15 (×2), 83.2 (×2), 76.6, 30.7, 28.9, 26.7, 24.8 (×2), 24.7 (×2). **^{11}B NMR** (128 MHz, CDCl3) δ 33.9. **IR** (cast film, CH_2Cl_2 cm^{-1}): 3032, 2976, 1734, 1144. **HRMS** (ESI) $[M+Na]^+$ calc. for $C_{25}H_{31}BNaO_4$, 429.2208; observed, 429.2214. **HPLC**: Major diastereomer, Chiralpak OD: 0.3:99.7 isopropanol:hexanes, 0.5 mL/min, 20 °C, λ = 220 nm, Tmajor = 10.7 min, Tminor = 12.0 min, ee = 26%. Minor diastereomer, Chiralpak IC: 0.3:99.7 isopropanol:hexanes, 0.5 mL/min, 5 °C, λ = 220 nm, T_{major} = 8.2 min, T_{minor} = 8.9 min, ee = 11%.

2.12.11 Procedure for the copper-catalyzed enantioselective tandem conjugate borylation-aldol reaction

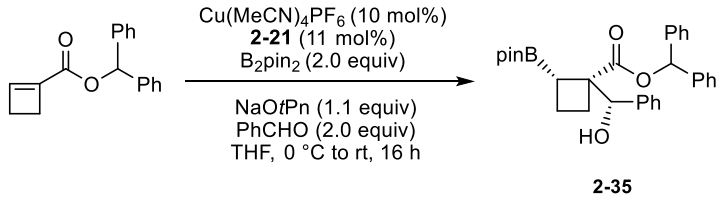

2-35

A microwave vial was charged with bis(pinacolato)diboron (102 mg, 0.400 mmol, 2.0 equiv), $[Cu(MeCN)_4]PF_6$ (7.5 mg, 0.020 mmol, 10 mol%) and Naud ligand **2-21** (10.9 mg, 0.0220 mmol, 11 mol%), capped, then purged with argon. Tetrahydrofuran (0.6 mL) was added and the reaction mixture and allowed to stir for 15 min at 0 °C. Sodium *tert*-amylate (1.4 M in THF, 143 µL, 0.200 mmol, 1.0 equiv) was added dropwise at 0 °C to give a dark orange-brown solution which was allowed to stir for another 10 min at 0 °C. A solution of cyclobutene 1-carboxyester **2-13** (52.9 mg, 0.200 mmol, 1.0 equiv) in tetrahydrofuran (0.4 mL) was added dropwise, followed by the dropwise addition of benzaldehyde (41 µL, 0.40 mmol, 2.0 equiv) at 0 °C. The ice-bath was removed, and the reaction mixture was allowed to stir at rt for 16 h. The reaction mixture was quenched by the addition of sat. NH_4Cl (2 mL) and extracted with ethyl acetate (×3). The combined organic layers were washed with brine, dried over anhydrous $MgSO_4$, filtered, and concentrated under reduced pressure. The crude ^1H NMR yield of cyclobutylboronate **7** was 82% using dibromomethane as the internal standard. 15% ^1H NMR yield of cyclobutylboronate **2** was observed. The crude dr was determined to be 12:1 by peak height of the benzylic proton. The crude mixture was purified by flash column chromatography using 30 wt% deionized water deactivated silica (20:1 hexanes: ethyl acetate, TLC performed using 4:1 hexanes:ethyl acetate) to give the desired product as a clear oil (76.3 mg, 79%, 15:1

dr). The isolated dr was determined to be 15:1 by peak height of the benzylic proton. Recrystallized in hexanes and stored at –20 °C. **^{1}H NMR** (500 MHz, $CDCl_3$) δ 7.28–7.12 (m, 13H), 7.03 (m, 2H), 6.82 (s, 1H), 4.94 (d, *J* = 7.0 Hz, 1H), 3.58 (d, *J* = 7.0 Hz, 1H), 2.58 (ddd, *J* = 11.9, 8.9, 5.4 Hz, 1H), 2.31 (m, 2H), 2.00–1.92 (m, 1H), 1.87 (m, 1H), 1.12 (s, 6H), 1.09 (s, 6H). **^{13}C NMR** (126 MHz, $CDCl_3$) δ 175.2, 140.5, 140.1, 139.8, 128.34 (×2), 128.30 (×2), 128.0 (×2), 127.71, 127.67, 127.32 (×2), 127.30, 127.2 (×2), 126.6 (×2), 83.5 (×2), 79.1, 77.4, 55.2, 27.7, 24.8 (×2), 24.7 (×2), 18.0 (the boron-bound carbon was not detected due to quadrupolar relaxation of boron). **^{11}B NMR** (128 MHz, $CDCl_3$) δ 32.0. **IR** (cast film, CH_2Cl_2 cm^{-1}): 3483 (br s), 3031, 2977, 1721, 1586, 1496, 1379, 1180. **HRMS** (ESI) $[M+Na]^+$ calc. for $C_{31}H_{35}BNaO_5$, 521.247; observed, 521.2469. **$[\alpha]_D^{20}$**: –3.50 (*c* = 1.34, CH_2Cl_2). **HPLC**: Chiralpak IB: 1:99 isopropanol:hexanes, 0.5 mL/min, 20 °C, λ = 210 nm, T_{major} = 13.6 min, T_{minor} = 14.9 min, ee = 95%.

2.12.12 Procedure for the oxidation of cyclobutylboronate 2-13

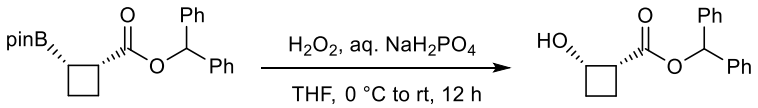

2-36

To a round bottom flask charged with cyclobutylboronate **2** (50 mg, 0.12 mmol, 1.0 equiv) was added THF (0.6 mL) followed by aq. NaH_2PO_4 (0.3 mL, 0.5 M). The reaction mixture was cooled to 0 °C then 30% w/w H_2O_2 (0.6 mL) was added dropwise resulting in a suspension. The ice-bath was removed, and the reaction was allowed to stir at rt for 12 h. H_2O was added (5 mL) and the aqueous phase was extracted with ethyl acetate (×3). The combined organic layers were washed with brine, dried over anhydrous $MgSO_4$, filtered then concentrated under reduced pressure. The crude reaction mixture was purified by flash column chromatography (4:1

hexanes:ethyl acetate) to give the desire product as a clear oil (31.5 mg, 93%). **^{1}H NMR** (500 MHz, $CDCl_3$) δ 7.34 (m, 8H), 7.32–7.27 (m, 2H), 6.95 (s, 1H), 4.44 (app q, *J* = 7.7 Hz, 1H), 3.49–3.42 (m, 1H), 3.22 (d, *J* = 9.4 Hz, 1H), 2.41–2.32 (m, 1H), 2.27–2.16 (m, 1H), 2.07–2.00 (m, 1H), 1.90 (ddd, *J* = 18.3, 11.7, 8.8 Hz, 1H). **^{13}C NMR** (126 MHz, $CDCl_3$) δ 173.7, 140.0, 139.9, 128.64(×2), 128.60 (×2), 128.1 (×2), 127.2 (×2), 127.1 (×2), 77.2, 67.1, 46.0, 32.4, 17.2. **IR** (cast film, CH_2Cl_2 cm^{-1}): 3477, 3031, 2950, 1728, 1586, 1495, 1453, 1210. **HRMS** (ESI) $[M+Na]^+$ calc. for $C_{18}H_{18}O_3$, 305.1148; observed, 305.1148. **$[\alpha]_D^{20}$**: –19.6 (*c* = 0.960, CH_2Cl_2). **HPLC**: Chiralpak IC: 2:98 isopropanol:hexanes, 0.5 mL/min, 20 °C, λ = 210 nm, T_{major} = 30.3 min, ee = 99%.

2.13 References

[1] Ito, H.; Yamanaka, H.; Tateiwa, J.; Hosomi, A. *Tetrahedron Lett.* **2000***, 41*, 6821–6285.

[2] Takahashi, K.; Ishiyama, T.; Miyaura, N. *Chem. Lett*. **2000**, 982–983.

[3] Mun, S.; Lee, J. E.; Yun, J. *Org. Lett.* **2006**, *8*, 4887–4889.

[4] Lee. J. E.; Yun, J. *Angew. Chem. Int. Ed*. **2008**, *47*, 145–147.

[5] Feng, X.; Yun, J. *Chem. Commun*. **2009**, 6577–6579.

[6] Chen, I. H.; Yin, L.; Itano, W.; Kanai, M.; Shibasaki, M. *J. Am. Chem. Soc.* **2009**, *131*, 11664–11665.

[7] Clement, H. A.; Boghi, M.; Mcdonald, R. M.; Bernier, L.; Coe, J. W.; Farrell, W.; Helal, C. J.; Reese, M. R.; Sach, N. W.; Lee, J. C.; Hall, D. G. *Angew. Chem. Int. Ed*. **2019**, *131*, 18576–18580.

[8] Dang, L.; Lin, Z.; Marder, T. B. *Organometallics*, **2008**, *27*, 4443–4454.

[9] Chen, Y-J.; Hu, T-J.; Feng, C-G.; Lin, G-Q. *Chem. Commun.* **2015**, *51*, 8773—8776.

[10] Perera, D.; Tucker J. W.; Brahmbhatt, S.; Helal, C. J.; Chong, A.; Farrell, W.; Richardson, P.; Sach, N. W. *Science* **2018**, *359*, 429–434.

[11] Reports of Naud ligand SL-N-004-01 in asymmetric hydrogenation: a) Naud, F.; Malan, C.; Spindler, F.; Rüggeberg, C.; Schmidt, A. T.; Blaser, H.-U. *Adv. Synth. Catal.* **2016**, *348*, 47–50. b) Tellers, D. M.; Bio, M.; Song, Z. J.; McWilliams, J. C.; Sun, Y. *Tetrahedron: Asymmetry* **2006**, *17*, 550–553. Pd-catalyzed intramolecular arylative desymmetrization of 1,3-diketones: c) Zhu, C.; Wang, D.; Zhao, Y.; Sun, W.-Y.; Shi, Z. *J. Am. Chem. Soc*. **2017**, *139*, 16486–16489.

[12] Slater, C. S.; Savelski, M. J.; Hitchcock, D.; Cavanagh, E. J. *J. Environ. Sci. Heal. Part A* **2016***, 51*, 487–494.

[13] Rhodes, G. *Crystallography made crystal clear (2nd ed.),* **2000***,* San Diego: Academic Press.

[14] Zhu, C.; Wang, D.; Zhao, Y.; Sun, W.-Y.; Shi, Z. *J. Am. Chem. Soc*, **2017**, *139*, 16486–16489.

Chapter 3. Highly Diastereoselective Nickel/Photoredox Dual-Catalyzed C(sp^3)–C(sp^2) Cross-Coupling of an Optically Enriched *cis*-*β*-Boronyl Cyclobutylcarboxyester Scaffold

3.1 Introduction

3.1.1 Suzuki-Miyaura cross-coupling of optically enriched secondary alkylboronates

The Suzuki-Miyaura cross-coupling reaction is a popular method for the construction of C–C bonds from organoboron compounds.[1] While the Suzuki-Miyaura C(sp^2)–C(sp^2) cross-coupling has been thoroughly investigated, C(sp^3)–C(sp^2) coupling reactions have been less developed. The mechanistic challenges associated with the coupling of C(sp^3) alkylboronates lie in various steps of the catalytic cycle (Figure 3-1). The transmetallation step is typically slow due to steric hindrance of C(sp^3) alkylboronates.[2] In this regard, protodeboronation becomes a competing side-reaction and therefore an excess of boron reagent is typically employed in the reaction. Once the transmetallation is successful, the transmetallated species is prone to irreversible *β*-hydride elimination if the reductive elimination step is slow.

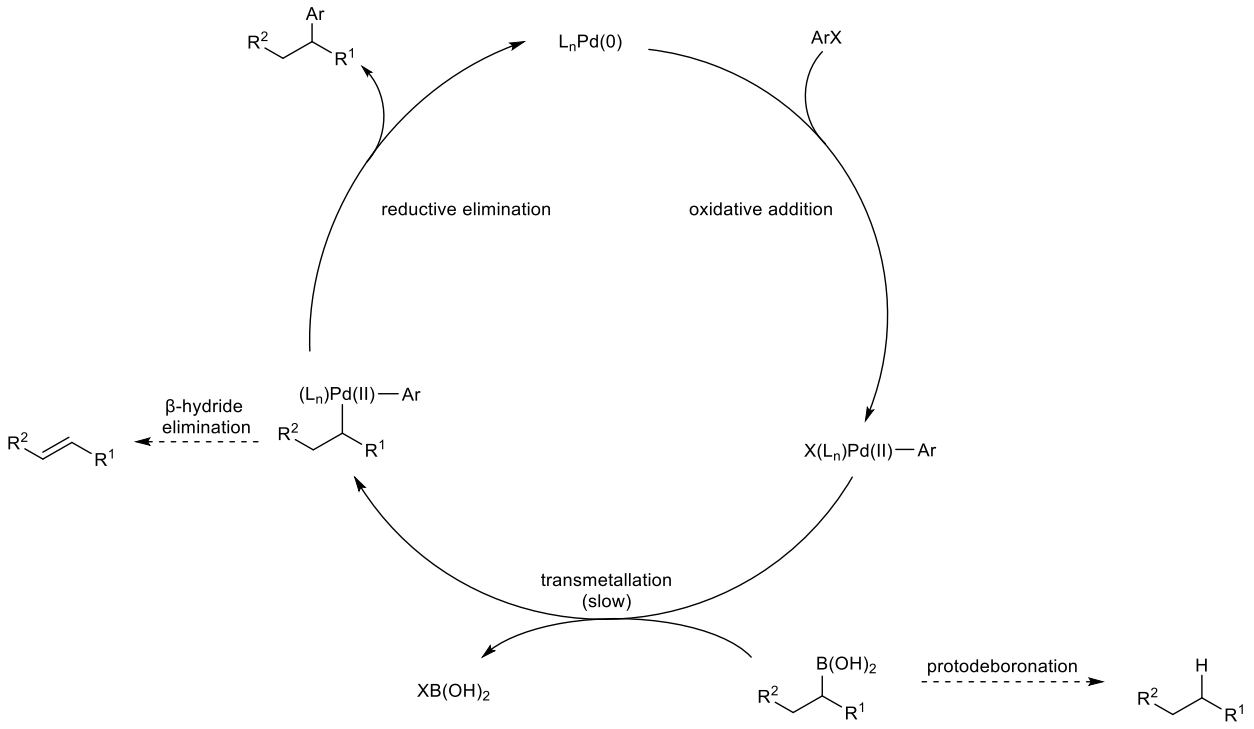

Figure 3-1. Mechanistic challenges in Suzuki-Miyaura cross-coupling of alkylboronates

Despite the aforementioned challenges, in 2009, Crudden and co-workers reported the cross-coupling of enantioenriched secondary benzylic boronates with aryl iodides to provide products **3-1** with retention of stereochemistry (Scheme 3-1a).[3] The authors found that silver oxide was crucial for the success of the reaction, as Kishi and co-workers previously found that silver oxide was responsible for accelerating the rate of transmetallation.[4] The observed retention in stereochemistry was likely a result of the transmetallation step proceeding via a 4-membered cyclic transition state which was originally proposed by Soderquist and co-workers.[5] In 2011, Suginome and co-workers reported the Suzuki-Miyaura cross-coupling of cyclic boronate **3-2** proceeded with retention of stereochemistry to afford compounds **3-3** in moderate to good yield (Scheme 3-1b).[6] The authors found that attempts to cross-couple the Bpin derivative were

unfruitful and therefore they proposed that the enhanced reactivity of the cyclic boronate **3-2** may be due to an intramolecular bond between the oxygen and boron atoms.

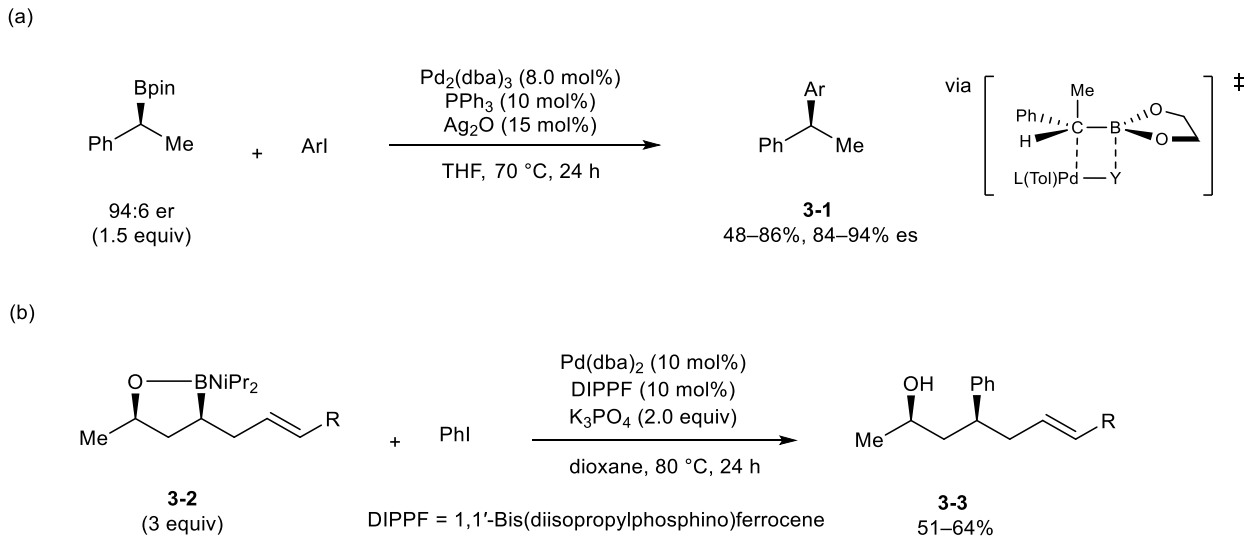

Scheme 3-1. Stereoselective Suzuki-Miyaura cross-coupling of secondary alkylboronates with retention of stereochemistry

In 2010, the Suginome group reported the stereoselective Suzuki-Miyaura cross-coupling of optically enriched *α*-(acylamino)benzylboronic esters with aryl bromides and chlorides proceeding with inversion of stereochemistry (Scheme 3-2a).[7] A dramatic acyl group effect was observed, as only the *tert*-butyl derivative **3-4** was successfully cross-coupled to provide the corresponding product **3-5** in high enantioselectivity. In a later report, the authors described the stereoselective cross-coupling of optically enriched *α*-(acylamino)benzylboronic esters **3-6** with a remarkable additive effect on the stereochemical outcome of the reaction (Scheme 3-2b).[8] Employing phenol as the additive provided the product **3-7** with stereoinversion. On the other hand, $Zr(OiPr)_4$·iPrOH as the additive resulted in stereoretention to afford product **3-8**. Based on these observations the authors proposed that the presence of the amide group can facilitate

transmetallation by way of intramolecular coordination of the amide oxygen atom to the boron center, leading to an S_N2-like open-chain transition state, in which the palladium species attacks the boron-bound carbon atom from the opposite side of the boron group. The role of the phenol additive would be to increase the Lewis acidity of the boron center by protonating the oxygen atom of the pinacol ligand and thus enhance the intramolecular coordination**.** On the other hand, performing the reaction in the presence of $Zr(OiPr)_4$•iPrOH as the additive would result in cleavage of the intramolecular coordination by competitively coordinating to the amide oxygen atom, resulting in the formation of the expected four-membered transition state.

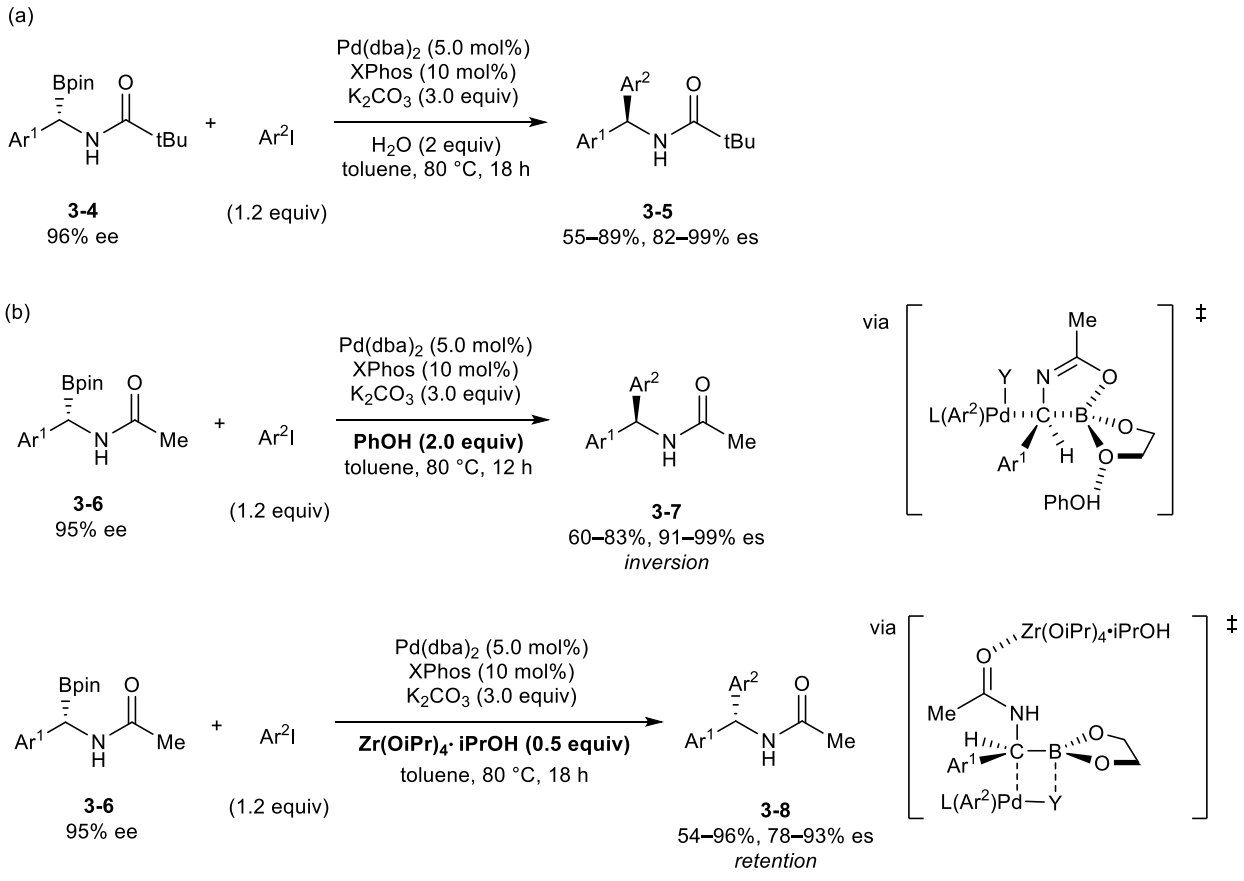

Scheme 3-2. Stereoselective cross-coupling of *α*-(acylamino)benzylboronates

In 2010, Molander and co-workers reported the stereospecific cross-coupling of optically enriched non-benzylic alkyl trifluoroborates. (Scheme 3-3).[9] As observed in the work of Suginome and co-workers, the trifluoroborate salt benefited from the intramolecular coordination from the amide oxygen atom, thus facilitating transmetallation to provide the product **3-9** with complete stereoinversion.

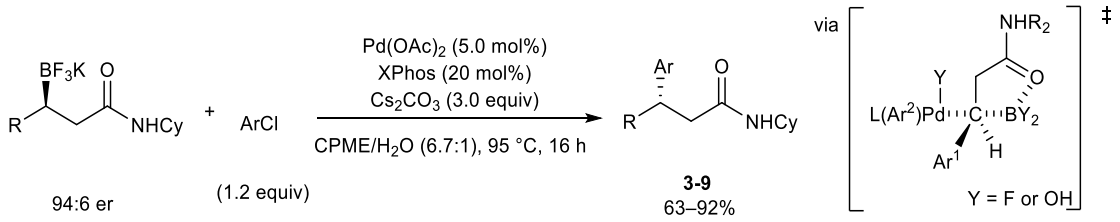

Scheme 3-3. Stereoselective cross-coupling of β-trifluoroboratoamides

In 2011, Hall and co-workers reported the chemoselective and stereospecific cross-coupling of optically enriched 3,3-diboronyl carboxyesters **3-10** (Scheme 3-4a).[10] The 3,3-diboronyl carboxyester substrates benefited from the stabilization of the second boronyl group, and internal coordination of the oxygen from the nearby ester group, in which both facilitated the transmetallation step. As in the Suginome and Molander reports, the cross-coupled product **3-11** were obtained with inversion of stereochemistry. In a later report, the Hall Group reported the direct stereoinvertive cross-coupling of the Bpin derivative **3-12**, which was achieved by replacing the ester group with a more Lewis basic amide group. The use of a Weinreb or morpholine amide proved most effective for stereoinvertive cross-coupling due to the α-effect of the amide nitrogen (Scheme 3-4b).[11]

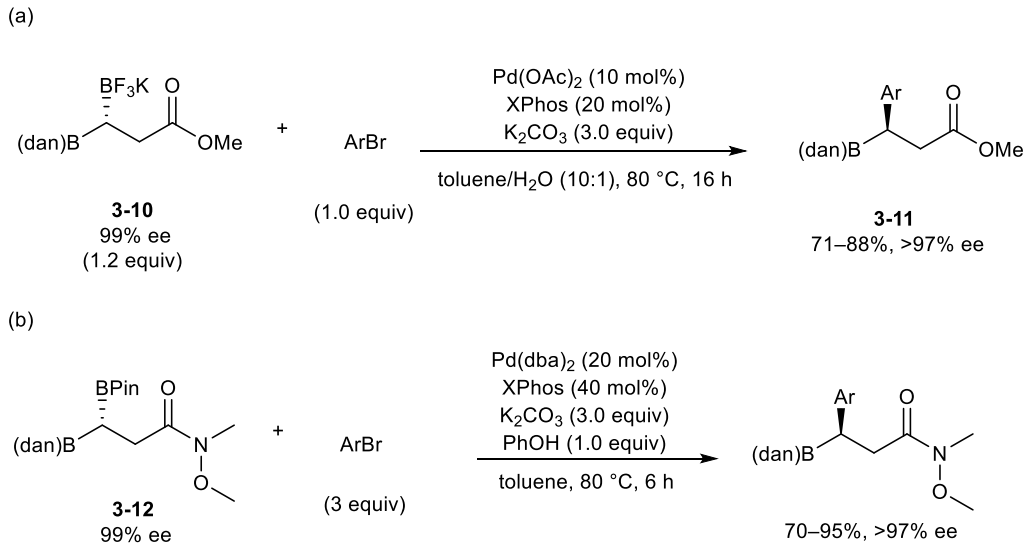

Scheme 3-4. Chemo- and stereoselective cross-coupling of a 3,3-diboronylcarboxyester

3.1.2 Nickel/photoredox dual-catalyzed cross-coupling of alkylboronates

The challenges associated with the Suzuki-Miyaura cross-coupling of C(sp^3) alkylboronates arise from the nature of the transmetallation step, which results in a negative charge build up on the transferring carbon in the transition state. Therefore, reagents that stabilize the negative charge best such as C(sp) and C(sp^2) boronates perform best. Rather than attempting to overcome the mechanistic limitations associated with transmetallation, a seminal report by Molander and co-workers described the nickel/photoredox dual-catalyzed cross-coupling of racemic benzyl trifluoroboronate salts to give the corresponding products **3-13** in moderate to excellent yield (Scheme 3-5a).[12] Furthermore, Molander and co-workers successfully applied their method towards the cross-coupling of optically enriched *N*-trifluoroboratomethyl salts to afford compound **3-15** with complete retention in optical purity (Scheme 3-5b).[13] However, limitations remain in the cross-coupling of optically enriched substrates with a stereogenic center at the boron-bound carbon atom, due to the formation of a

radical intermediate at that carbon center.[14] Interestingly, modest enantioselectivity could be achieved by cross-coupling a benzyltrifluoroborate salt using chiral ligand **3-16** to obtain the product **3-17**. (Scheme 3-5c).

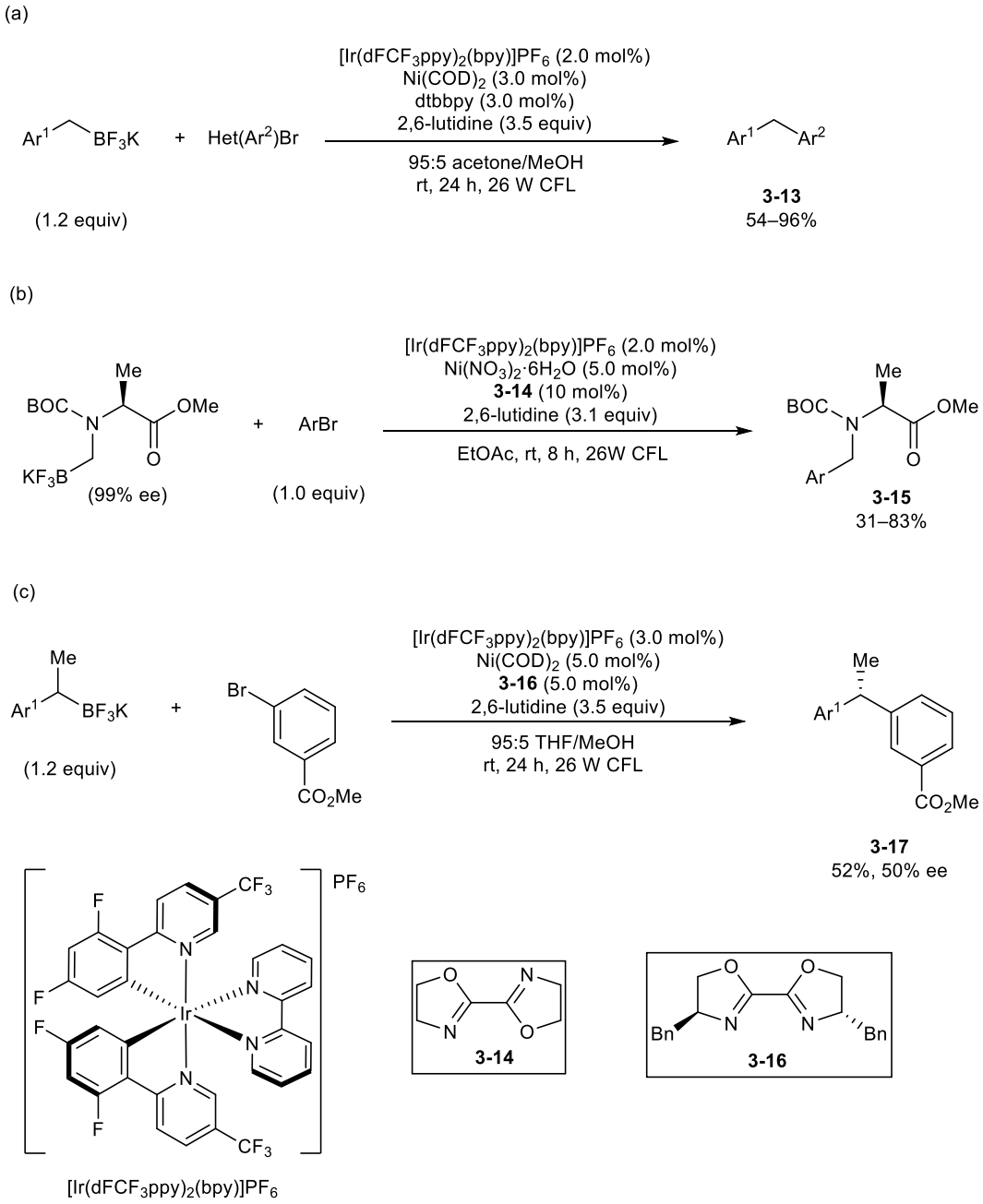

Scheme 3-5. (a,b) Nickel/photoredox dual-catalyzed cross-coupling of trifluoroborate salts and (c) preliminary results for stereoconvergent cross-coupling

In the catalytic cycle, activation of racemic benzyltrifluoroboronate salt can proceed by way of a formal transmetallation single-electron transfer event (Figure 3-2). The photoexcited iridium species can oxidize the trifluroborate salt to generate the corresponding carbon-centered radical which can subsequently combine with the nickel catalyst in an energetically barrierless single electron transmetallation event. Mechanistic details for the nickel/photoredox dual-catalyzed cross-coupling of the racemic benzylic trifluoroborate salt show that the radical can converge onto either the Ni(0) or Ni(II) intermediate.[15] Both pathways arrive at the Ni(III) intermediate where stereoinduction arises from a dynamic kinetic resolution under Curtin-Hammett principle. Reductive elimination follows to afford the cross-coupled product and Ni(I) species, which is subsequently reduced by Ir(II) to regenerate Ni(0) and the iridium catalyst. Overall, this method complements the trend associated with Suzuki-Miyaura cross-coupling where trends in radical stability and single electron transfer rates ($C(sp^3) > C(sp^2) > C(sp)$) are contrary to the stabilization of a negative charge on the nucleophile and the transmetallation rate ($C(sp) > C(sp^2) > C(sp^3)$).

3.1.3 Objectives

With an optically enriched cyclobutylboronate scaffold in hand, the potential of intermediate **3-18** or the corresponding trifluoroborate salt **3-19** in cross-coupling will be explored. It should be mentioned that compounds **3-18** and **3-19** in this Chapter correspond to compounds **2-14** and **2-27** in Chapter 2, respectively. Previous studies have shown that *β*-boryl amides and esters can serve as an attractive substrate in stereoselective Suzuki-Miyaura cross-coupling. Furthermore, the Molander Group have developed a novel method for the cross-coupling of alkyl trifluoroborate salts. The stereoselective cross-coupling of the optically

enriched cyclobutylboronate scaffold would provide access towards *trans-β*-aryl and/or hetereoaryl cyclobutylcarboxyesters with potential applications in medicinal chemistry and drug discovery (Scheme 3-6).

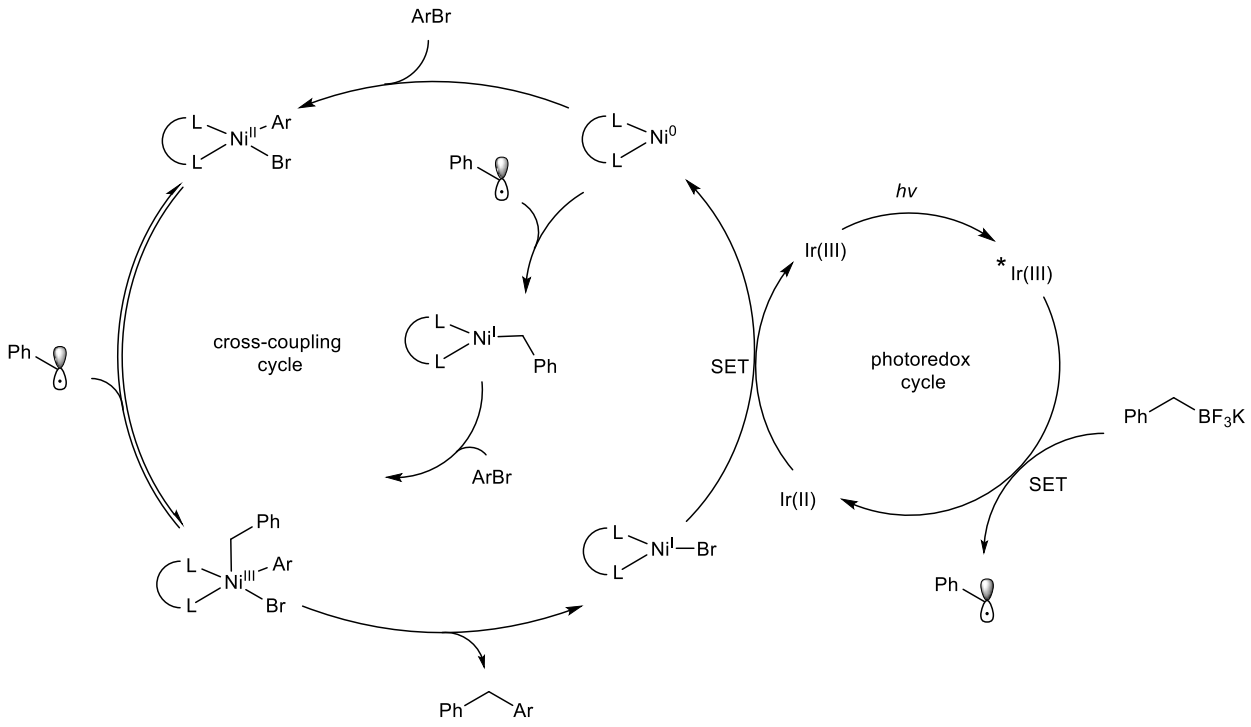

Figure 3-2. Catalytic cycle of the nickel/photoredox dual-catalyzed cross-coupling reaction

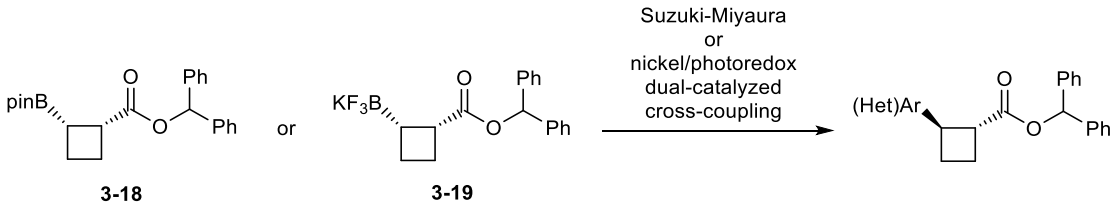

Scheme 3-6. Stereoselective cross-coupling of cyclobutylboronate scaffold

3.2. Suzuki-Miyaura cross-coupling of *cis-β*-boronyl cyclobutylcarboxyester scaffold

3.2.1 Attempted Suzuki-Miyaura cross-coupling of cyclobutylboronate 3-18

It was envisioned that this scaffold could be a valuable intermediate for the stereoselective Suzuki-Miyaura cross-coupling reaction to afford the corresponding *β*-aryl and/or heteroaryl products. Attempts at the direct cross-coupling of cyclobutylboronate **3-18** under Crudden and Suginome conditions proved unfruitful, leading to complex product mixtures (Scheme 3-7).[2, 6] In all cases, the desired cross-coupled product was not observed. Interestingly, benzhydrol was observed in trace amounts by ^{1}H NMR analysis of the crude reaction mixture.

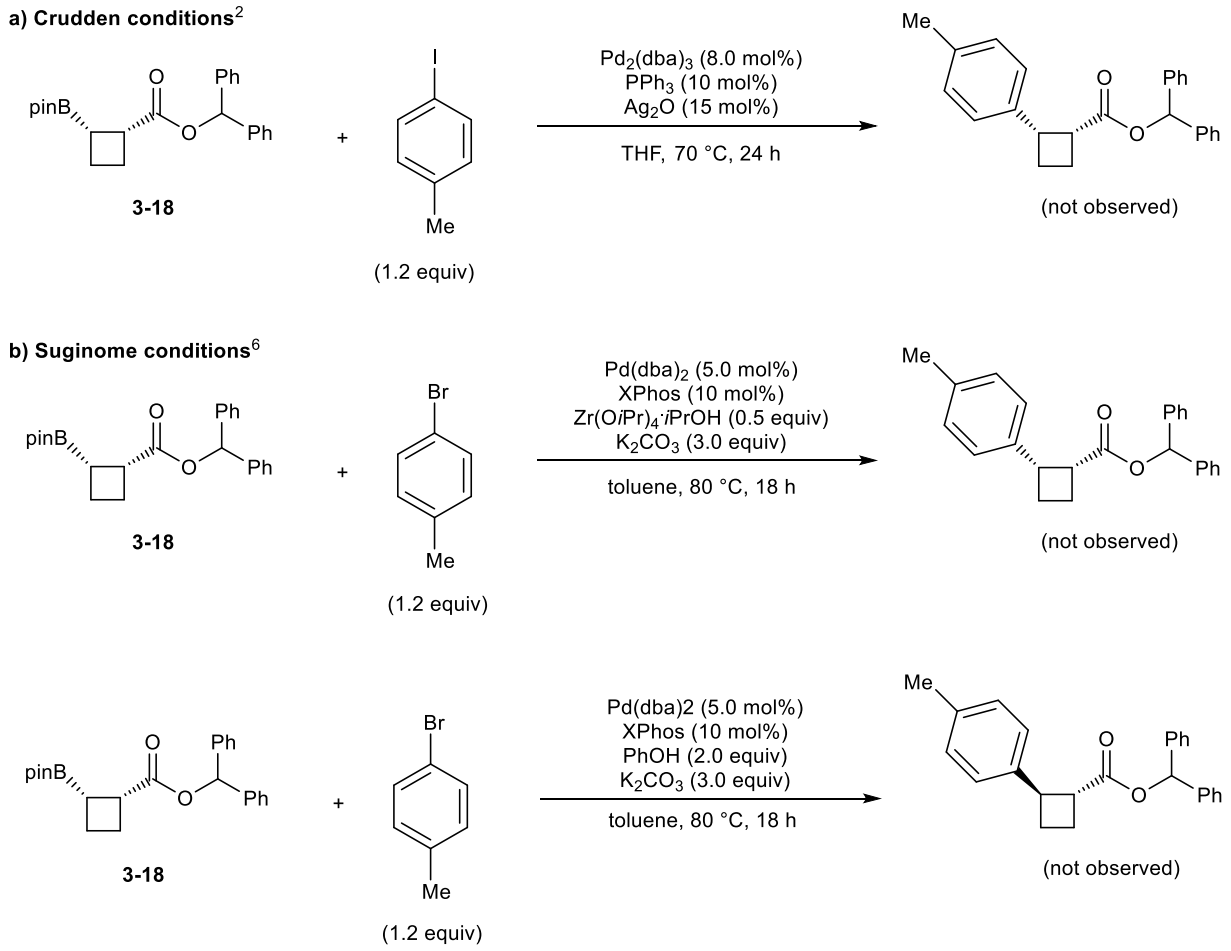

Scheme 3-7. Literature conditions attempted for the cross-coupling of cyclobutylboronate **3-18**

3.2.2 Suzuki-Miyaura cross-coupling of trifluoroborate salt 3-19

Next, attention was directed towards the cross-coupling of the cyclobutylboronate scaffold, as the trifluoroborate salt **3-19**. Trifluoroborate salts have been proven to be more potent cross-coupling partners with distinct advantages. Trifluoroborate salts are typically easy to handle, stable white solids. They have also shown higher stability under cross-coupling conditions, which mitigates side reactions such as protodeboronation. Due to the promising properties of trifluoroborate salts, there have been a number of reports for the stereoselective Suzuki-Miyaura cross-coupling of secondary alkyl trifluoroborate salts as mentioned in the introduction of this Chapter. Unfortunately, all literature conditions attempted failed to deliver the desired product in our hands and complex mixtures were obtained (Scheme 3-8).[9,10,16,17,18] Again, trace amounts of benzhydrol were isolated and observed by ^{1}H NMR analysis of the crude reaction mixture. It was surmised that the harsh aqueous and basic palladium-catalyzed cross-coupling conditions resulted in hydrolysis of the benzhydrol ester.

3.2.3 Synthesis and Suzuki-Miyaura cross-coupling of morpholino trifluoroborate salt 3-22

As described in the introduction of this Chapter, the inversion of configuration observed during the Suzuki-Miyaura cross-coupling of *β*-boronyl carboxyesters and amides was attributed to intramolecular coordination of the carbonyl oxygen to the boron center. By enhancing the Lewis basicity of the coordinating group from an ester to an amide, it was surmised that the cross-coupling of the cyclobutylboronate scaffold could benefit from this strengthened internal coordination. With this in mind, the morpholino trifluoroborate salt **3-22** was synthesized from cyclobutylboronate **3-18** in three steps (Scheme 3-9). Of note, attempts to cross-couple

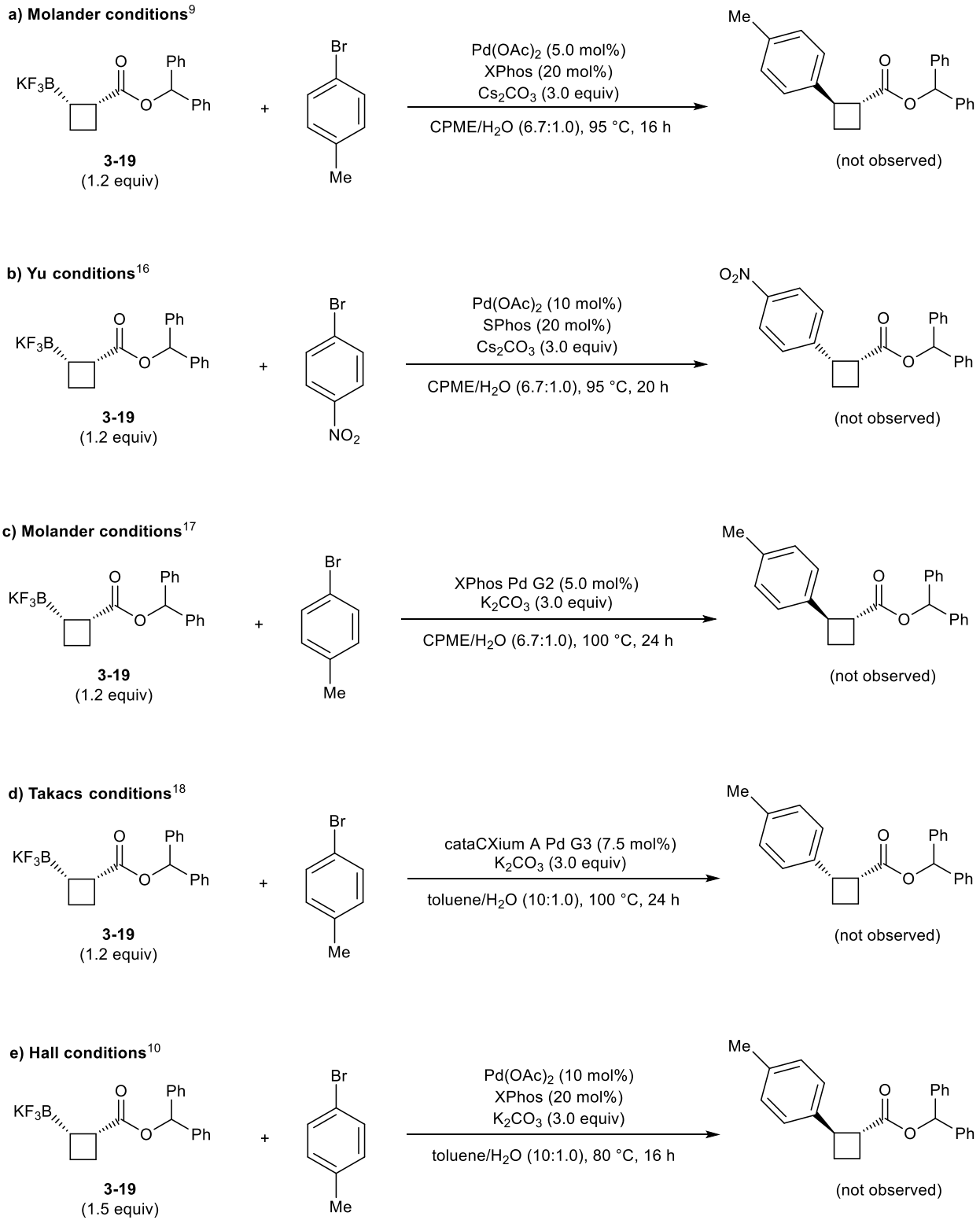

Scheme 3-8. Literature conditions attempted for the cross-coupling of trifluoroborate salt **3-19**

morpholine amide **3-21** were not performed as the trifluoroborate salt **3-22** was viewed as a more promising substrate for cross-coupling. With the morpholino trifluoroborate salt **3-22** in hand, attempts to cross-coupling under Molander's and Yu's conditions were conducted.[17,18] However, the desired product was not observed. In both cases, the *N*-aryl morpholine side product **3-23** was isolated by silica column chromatography as the major product (Scheme 3-10). In order to rationalize the formation of this side product, it is surmised that under the harsh aqueous and basic palladium-catalyzed cross-coupling conditions, the morpholine amine could be liberated and subsequently undergo Buchwald-Hartwig amination.

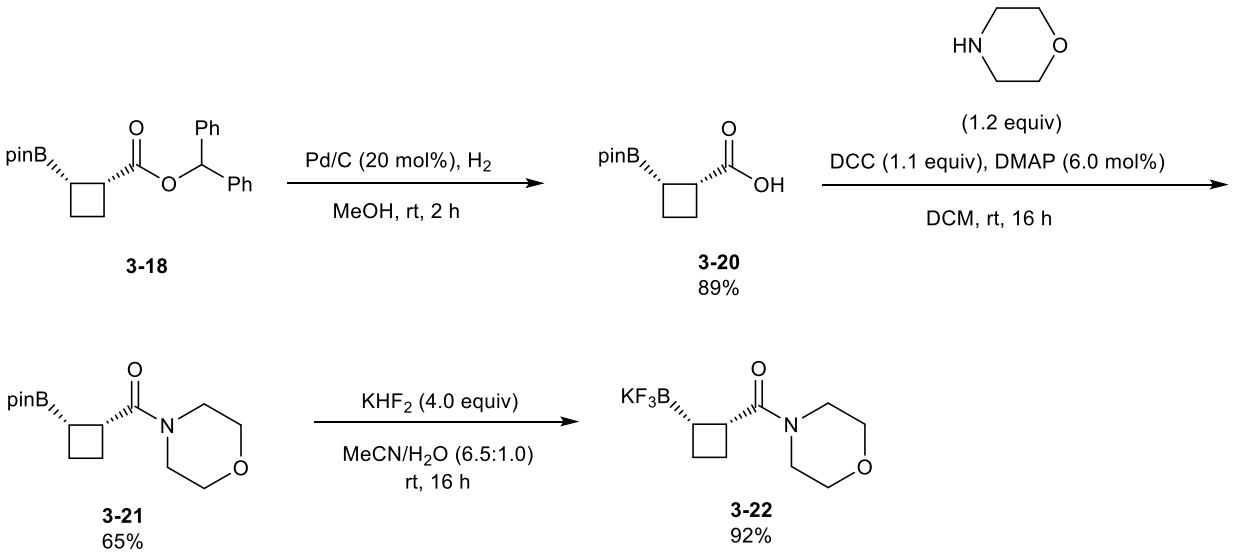

Scheme 3-9. Synthesis of the morpholine trifluoroborate salt **2-22**

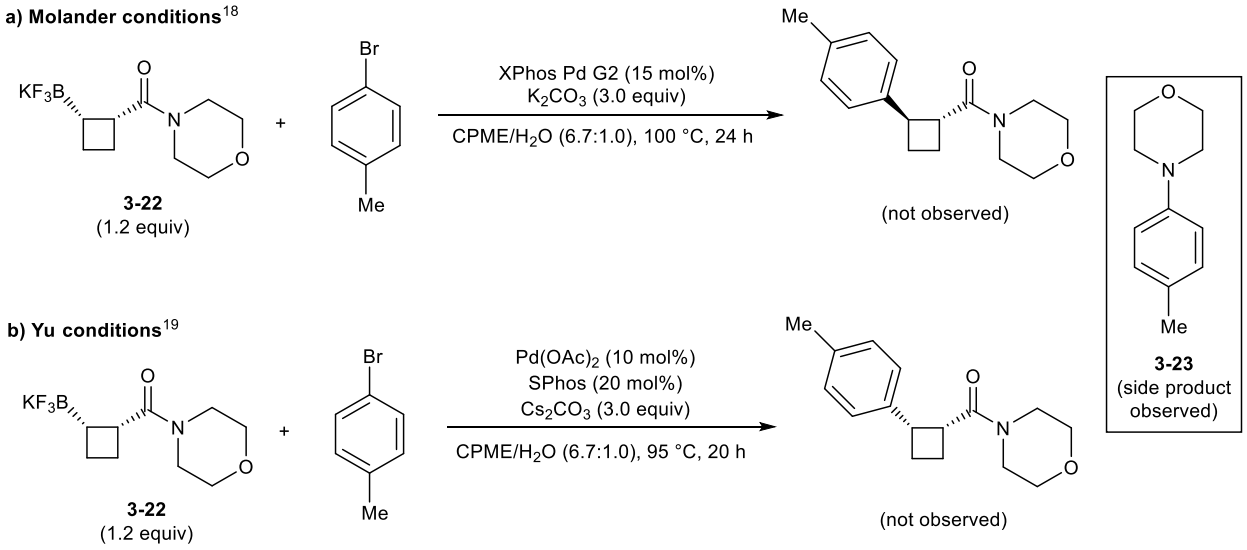

Scheme 3-10. Literature conditions attempted for the cross-coupling of the morpholine amide derivative **3-21**

3.2.4 Synthesis of boronolactone derivatives for Suzuki-Miyaura cross-coupling

Since the ester and amide groups were found to be labile under the cross-coupling conditions, the ester group was removed from cyclobutylboronate **3-18** to afford the carboxylic acid **3-20**. Subsequent treatment with potassium hydrogen difluoride was carried out and surprisingly, the expected trifluoroborate salt was not observed. Characterization of the product revealed the formation of the difluoroboronolactone **3-24** (Scheme 3-11a). ^{11}B NMR supports the presence of a B–O bond between the carboxylic acid oxygen atom and the boron atom by the presence of a signal at 9.2 ppm, indictive of a tetrahedral boron species. Furthermore, the signal was of a triplet splitting pattern which suggest the presence of only two B−F bonds. In line with the ^{11}B NMR results, ^{19}F NMR revealed the presence of two signals, indicative of two diastereotopic fluorine atoms. The HRMS of the compound revealed that the O−B interaction from the carboxylic acid oxygen atom could be in fact a dative bond due to the absence of a

proton in the molecular formula which would be consistent with the carboxylate form. The absence of a carboxylic acid OH stretch in the IR sprectra also supports this notion. It should be mentioned that attempts to obtain an X-ray crystal structure were unfruitful. Moreover, a second boronolactone derivative was synthesized from carboxylic acid **3-20.** By way of a transesterification approach with phenylboronic acid, deprotection of the boronic ester gave a crude mixture of the boronolactone **3-25** and boronic acid **3-26** in an undetermined ratio by HRMS analysis (Scheme 3-11b). The presence of both the open and closed forms suggest that there may be ring strain and steric restriction for the formation of an internal O–B bond with the carboxylic acid oxygen atom. Due to the presence of the internal carboxylic acid O–B bond, these boronolactone intermediates could serve as attractive precursors for stereoinvertive Suzuki-Miyaura cross-coupling. Attempts at cross-coupling both boronolactone intermediates under Molander's conditions did not give the desired product, but instead resulted in complex product mixtures (Scheme 3-12).[9, 18] There have been two literature reports of C(sp^2) difluoroborates and their application in Suzuki-Miyaura cross-coupling (Scheme 3-13).[19, 20]

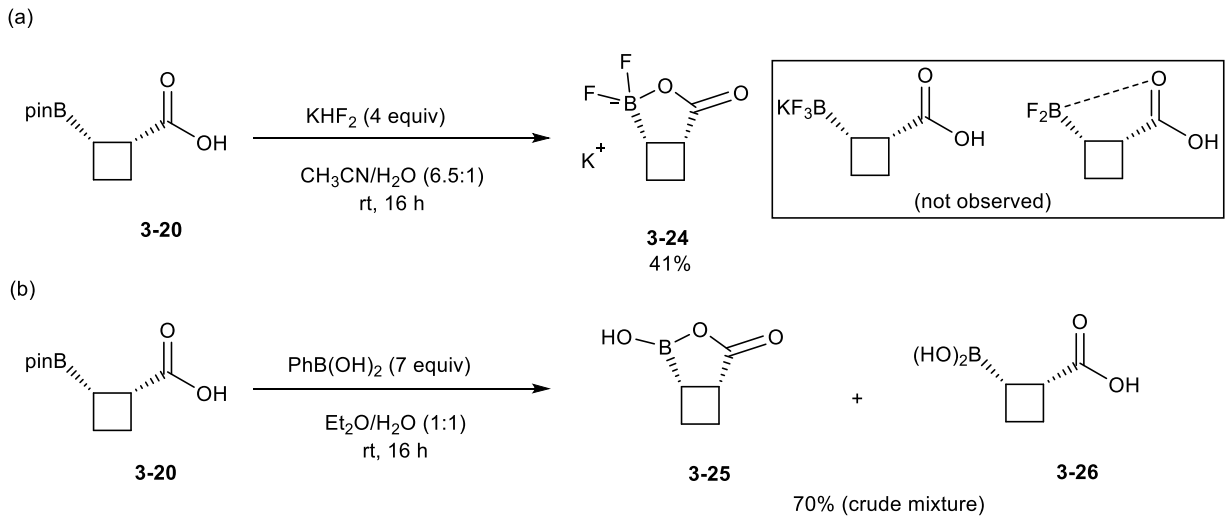

Scheme 3-11. Synthesis of boronolactone derivatives

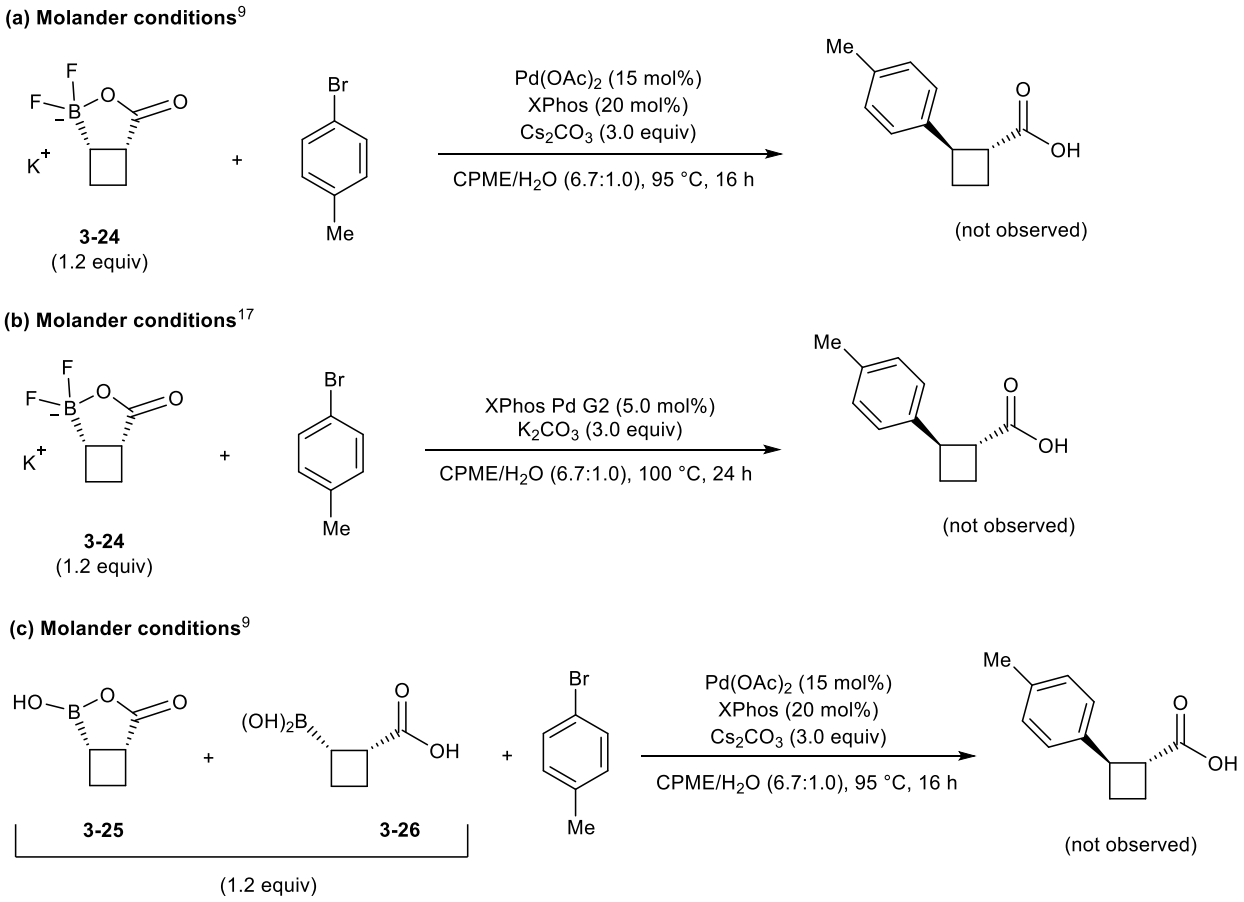

Scheme 3-12. Literature conditions attempted for the cross-coupling of boronolactone derivative

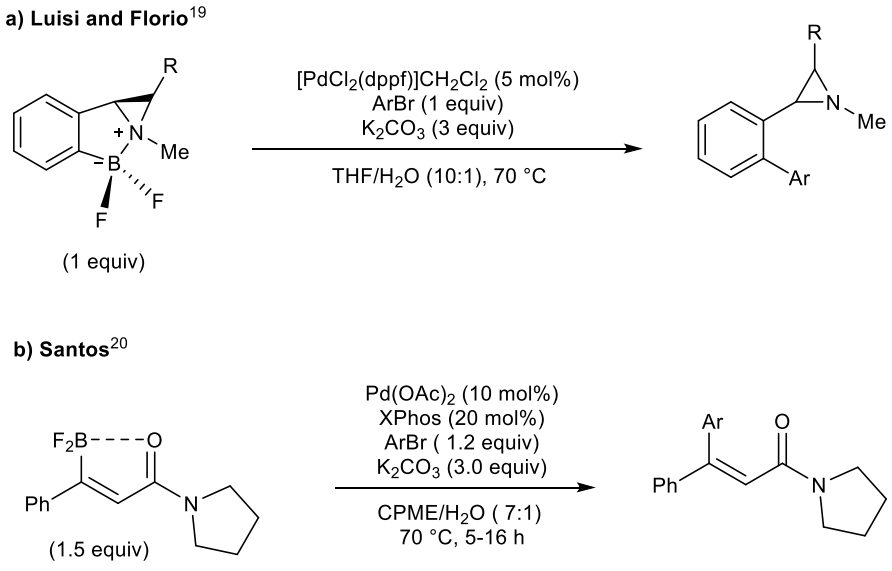

Scheme 3-13. Previous reports on the Suzuki-Miyaura cross-coupling of C(sp^2) difluoroborates

3.3 Nickel/photoredox dual-catalyzed cross-coupling of *cis*-*β*-boronyl cyclobutylcarboxyester scaffold

In our hands, the Pd-catalyzed cross-coupling methods did not provide the desired cross-coupled products. Thus, attention was directed towards the nickel/photoredox dual-catalyzed cross-coupling of alkyl trifluoroborates developed by Molander and co-workers.[12] It was surmised that the coupling can occur in a *trans*-diastereoselective manner without the complete loss of stereochemical information from the formation of an alkyl radical intermediate. The existing stereogenic *α*-carbon could translate chirality to the newly formed sp^2–sp^3 carbon–carbon bond through a chiral relay and to control the diastereoselectivity by way of steric effects.

3.3.1 Screening of reaction conditions

After a brief stint of screening nickel/photoredox dual-catalyzed cross-coupling reaction conditions appropriate for alkyl *β*-trifluoroboratoesters[21] (Table 3-1, entry 1 and 2), the conditions optimized by Liu and co-workers for their amido trifluoroborate salt **3-27** afforded the desired cross-coupled product in good yield with excellent enantio- and diastereoselectivity (Scheme 3-14, Table 3-1, entry 3).[22] It should be mentioned that when Liu and co-workers cross-coupled their amido trifluoroborate salt, they obtained *trans* diastereomers in 82:18 to 98:2 dr.[22] They proposed that the minor *cis* diastereomer was obtained as a result of a weak coordinating effect of the amide group to the nickel catalyst to result in cross-coupling with stereoretention. However, in the case of trifluoroborate salt **3-19**, the presence of a weaker coordinating ester group provided exclusively the *trans* diastereomer. Changing the iridium photocatalyst from $[Ir(dFCF_3ppy)_2(bpy)]PF_6$ to $[Ir(dFCF_3ppy)_2(dtbpy)]PF_6$ resulted in a significant decrease in yield (entry 4). Degassing of the 1,4-dioxane solvent by freeze-pump-thaw in contrast to sparring with

nitrogen gas for one hour slightly improved the enantioselectivity (Table 3-1, entry 5). Overall, the optimal conditions of entry 5 provided the desired product in good yield and excellent enantio- and diastereoselectivity. Advantageously, the pre-formed nickel complex $[Ni(dtbbpy)(H_2O)_4]Cl_2$ developed by Molander and coworkers was used and assessed as being benchtop stable, which allowed for a convenient reaction set-up without the need for a glovebox.[23] Of note, the kessil lamp used in the reaction is the irradiation source of ultra-violet (UV) light. UV light excitation of the photoeredox catalyst, $[Ir(dFCF_3ppy)_2(bpy)]PF_6$ (λ_{max} = 379 nm) generates the corresponding photoexcited species that can serve as a strong oxidant of the trifluoroborate salt in the reaction ($E_{1/2}$ *Ir/$^-$Ir = +1.32 V vs SCE).[24]

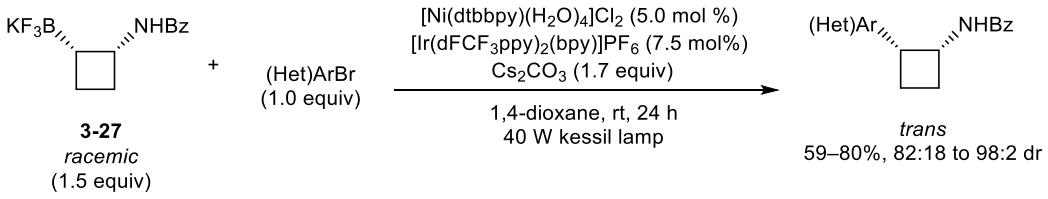

Scheme 3-14. Nickel/photoredox dual-catalyzed cross-coupling of amido trifluoroborate salt reported by Liu and co-workers

Table 3-1. Small screening of nickel/photoredox dual catalyzed cross-coupling conditions

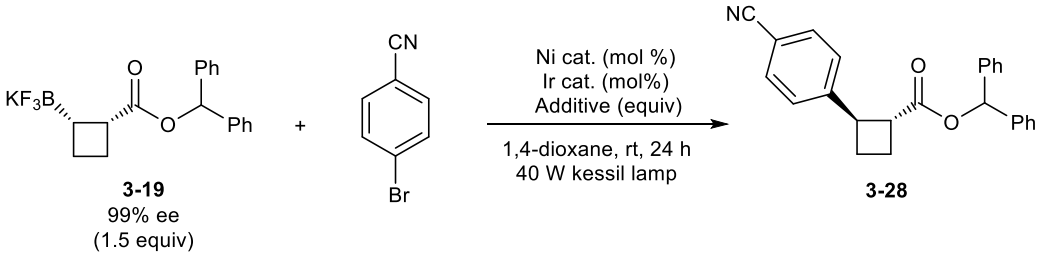

Entry	Ni cat. (mol%)	Ir cat. (mol%)	Additive (equiv)	Yield (%)[1]	dr (*trans:cis*)[2]	ee (%)[3]
1[4]	$NiCl_2$·DME (2.5 mol%)	$[Ir(dFCF_3ppy)_2(bpy)]PF_6$ (2.5 mol%)	Cs_2CO_3 (0.5 equiv) 2,6-lutidine (0.5 equiv)	27	>20:1	79
2[4]	$NiCl_2$·DME (2.5 mol%)	$[Ir(dFCF_3ppy)_2(bpy)]PF_6$ (2.5 mol%)	Cs_2CO_3 (1.5 equiv)	32	>20:1	83
3	$[Ni(dtbbpy)(H_2O)_4]Cl_2$ (5 mol%)	$[Ir(dFCF_3ppy)_2(bpy)]PF_6$ (7.5 mol%)	Cs_2CO_3 (1.7 equiv)	70	>20:1	95
4	$[Ni(dtbbpy)(H_2O)_4]Cl_2$ (5 mol%)	$[Ir(dFCF_3ppy)_2(dtbpy)]PF_6$ (7.5 mol%)	Cs_2CO_3 (1.7 equiv)	20	>20:1	90
5[5]	$[Ni(dtbbpy)(H_2O)_4]Cl_2$ (5 mol%)	$[Ir(dFCF_3ppy)_2(bpy)]PF_6$ (7.5 mol%)	Cs_2CO_3 (1.7 equiv)	67	>20:1	97

1,4-Dioxane was degassed sparring with N_2 for 1 h. [1] Isolated Yield. [2] Determined from ^1H NMR analysis of the isolated product from peak height of the benzylic proton. [3] ee determined by chiral HPLC. [4] 26 W CFL instead of 40 W kessil lamp. [5] 1,4-Dioxane degassed by three cycles of freeze-pump-thaw.

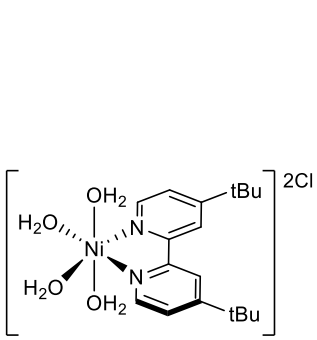

$[Ni(dtbbpy)(H_2O)_4]Cl_2$

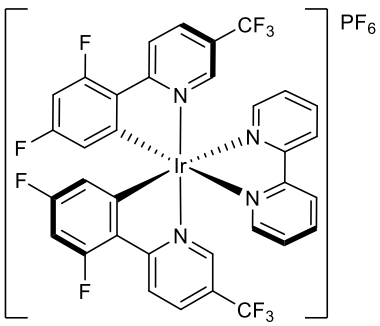

$[Ir(dFCF_3ppy)_2(bpy)]PF_6$

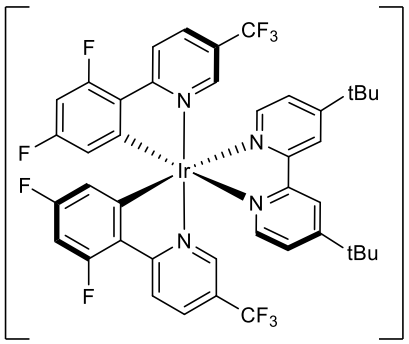

$[Ir(dFCF_3ppy)_2(dtbpy)]PF_6$

3.3.2 Scope of aryl and heteroaryl bromides

With suitable nickel/photoredox dual-catalyzed cross-coupling conditions in hand, the scope of aryl and heteroaryl bromides as well as alkenyl pseudohalides were examined (Table 3-2). An impressive range of functional groups could be tolerated. *Para*-tolyl bromide was cross-coupled in very good yield (**3-29**). Reactions of electron-poor aryl bromides functionalized with nitrile and carbonyl substituents proceeded smoothly in good yields (**3-28**, **3-30** to **3-32)**. The synthetically useful chloride in **3-33** can serve as a handle for subsequent cross-coupling. Aryl bromides containing *ortho* fluoro- and *para* trifluoromethyl group of the sort relevant to drug discovery afforded **3-34** and **3-35** in good yields. It should be mentioned that the cross-coupling of a few electrophiles, such as the *para*-methoxy and *para*-nitro aryl bromides, proved more difficult which resulted in poor reaction conversion (**3-36** and **3-37**). A variety of more challenging and medicinally relevant heterocyclic bromides were examined.[25] In some cases in the literature, nitrogenous containing heterocycles were found to be incompatible in catalytic cross-coupling due to possible binding of the metal center disabling the catalyst.[26] Here, however, these cross-coupling conditions proved compatible with a diverse range of functionalized and unfunctionalized pyridines and pyrimidines to provide the corresponding products in moderate to excellent yields

Table 3-2. Substrate scope for the cross-coupling of the trifluoroborate salt **3-19** with aryl and heteroaryl bromides

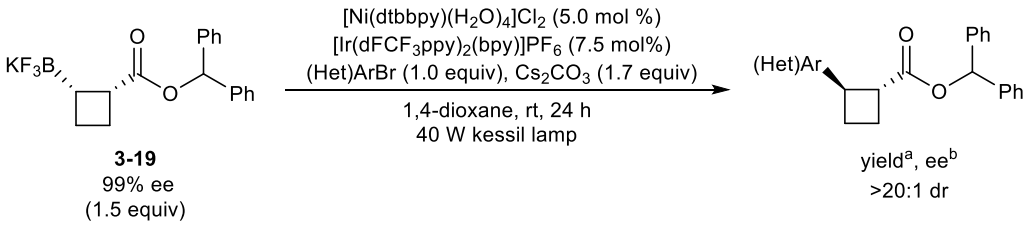

3-19
99% ee
(1.5 equiv)

yield[a], ee[b]
>20:1 dr

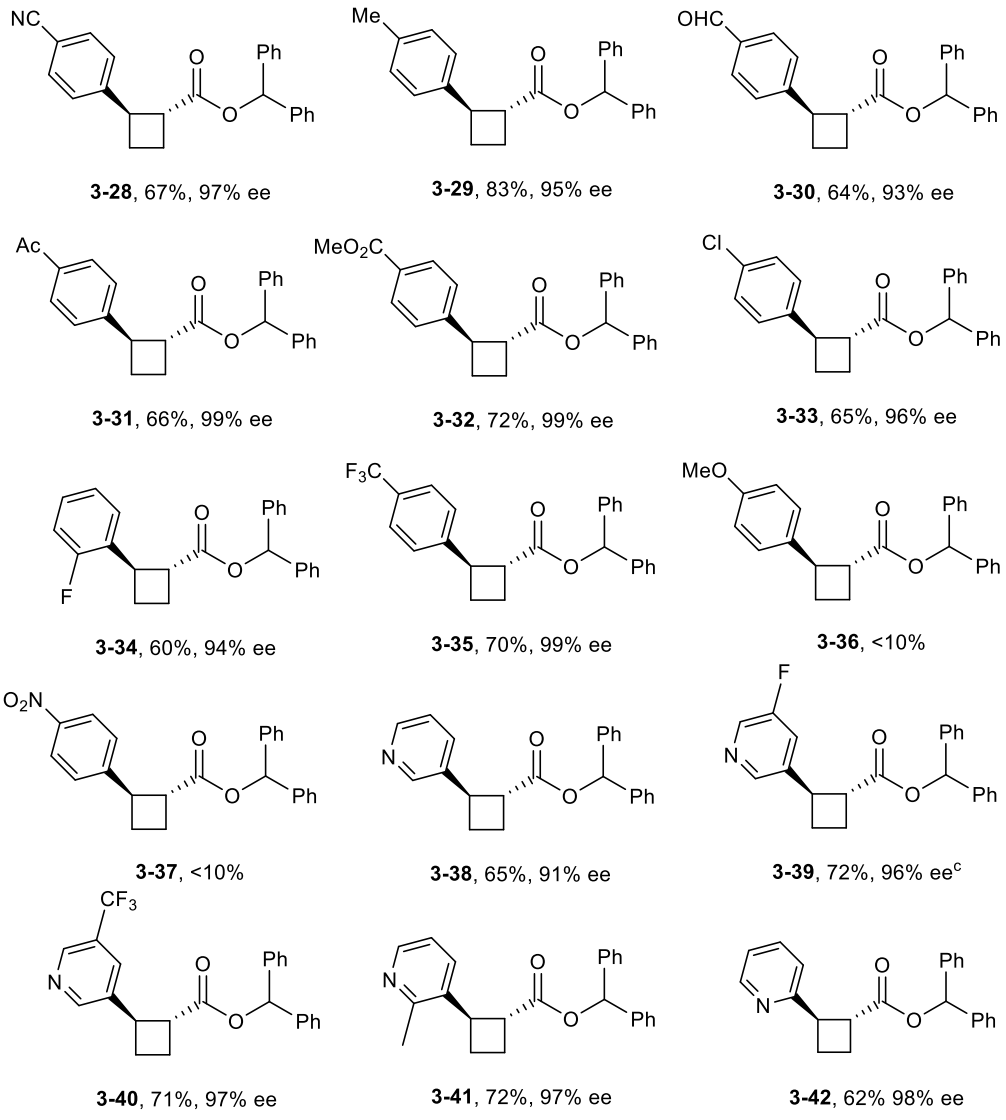

3-28, 67%, 97% ee

3-29, 83%, 95% ee

3-30, 64%, 93% ee

3-31, 66%, 99% ee

3-32, 72%, 99% ee

3-33, 65%, 96% ee

3-34, 60%, 94% ee

3-35, 70%, 99% ee

3-36, <10%

3-37, <10%

3-38, 65%, 91% ee

3-39, 72%, 96% ee[c]

3-40, 71%, 97% ee

3-41, 72%, 97% ee

3-42, 62% 98% ee

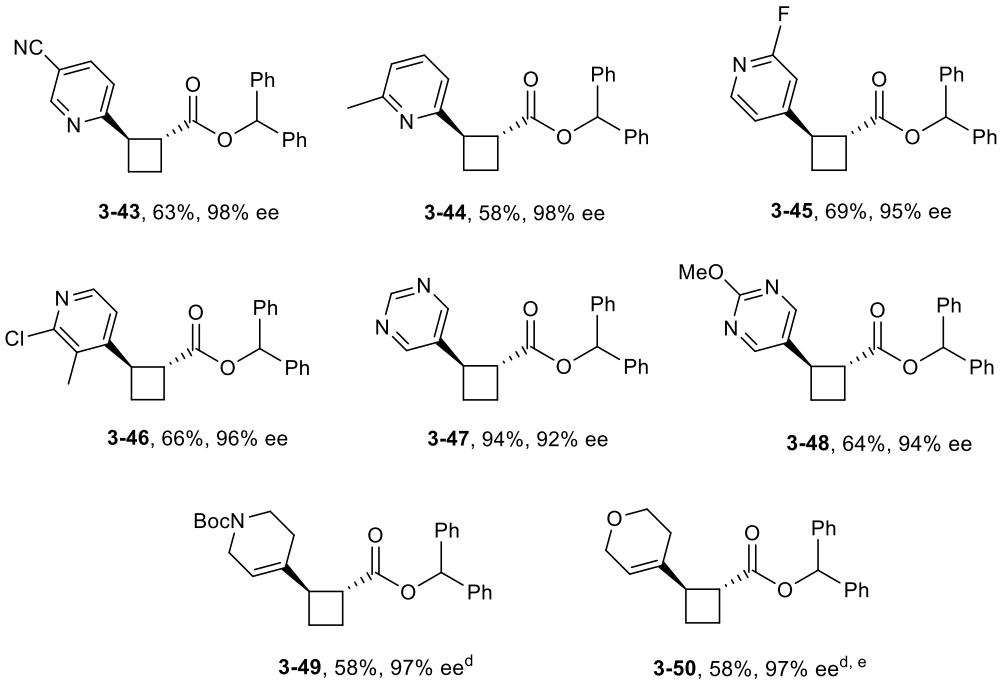

[a] Isolated yield. [b] Determined by chiral HPLC analysis. [c] Reaction was performed three times: yield and ee reported as an average. [d] Using alkenyl nonaflate. [e] Reaction time of 48 h. All products were isolated in >20:1 dr by ^{1}H NMR and HPLC analysis All products were isolated in >20:1 dr by ^{1}H NMR and HPLC analysis.

and high optical purities (**3-38** to **3-48**). Products **3-41** and **3-44** demonstrated the reaction is tolerant toward *ortho* substitution, indicating that steric effects may not be a major factor in cross-coupling. In all cases, the optical purity was retained at a high level and excellent diastereoselectivity was observed.

The stereochemical course of the reaction was determined to occur with inversion of the C–B bond to give the corresponding *β*-aryl and heteroaryl products with *trans* stereochemistry. The relative stereochemistry was assigned based on the X-ray crystallographic analysis of **(*rac*)-3-51** (Figure 3-15), which was synthesized from the ester deprotection of compound **(*rac*)-3-29** (Scheme 2-24).

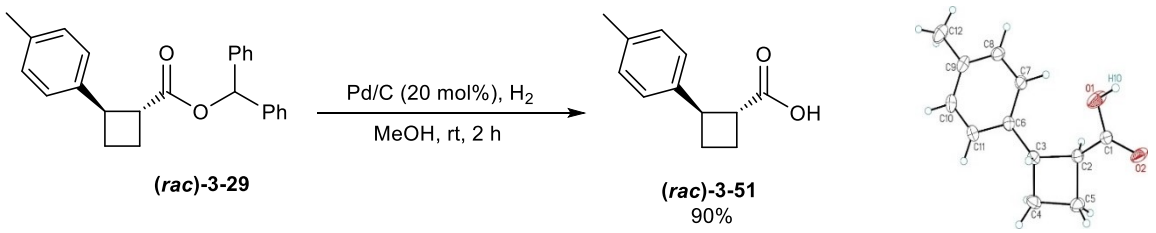

Scheme 3-15. Ester deprotection of **(*rac*)-3-29** and ORTEP of **(*rac*)-3-51**

3.3.3 Mechanistic proposal and stereoselectivity model

The reaction mechanism is presumed to follow the pathway proposed by Molander and co-workers (Figure 3-3).[15] UV light excitation of the Ir^{III} complex would generate the long-lived photoexcited $^{*}Ir^{III}$ species which could oxidize trifluoroborate salt **2-34** to the corresponding secondary alkyl radical and provide the reduced photocatalyst. The resulting alkyl radical can combine with the ligated Ni^{0} complex to generate the alkyl–Ni^{I} complex, which could subsequently undergo oxidative addition with the aryl and/or hetereoaryl bromide to afford the Ni^{III} complex. Reductive elimination would provide the cross-coupled product and reform the Ni^{I} species which is subsequently reduced by the photocatalyst to regenerate Ni^{0} and Ir^{III} catalyst. An alternative pathway was recognized where oxidative addition precedes addition of the alkyl radical onto the Ni^{0} complex.[15] Nonetheless, both cycles converge onto the same Ni^{III} intermediate. In this catalytic cycle where Ni^{II} is employed, reduction of the $Ni^{II}Cl_2$ complex is required to access the active Ni^{0} catalyst. This is likely facilitated by the iridium photocatalyst through sacrificial oxidation of the trifluoroborate salt and subsequent reduction of $Ni^{II}Cl$ to generate the active Ni^{0} catalyst.

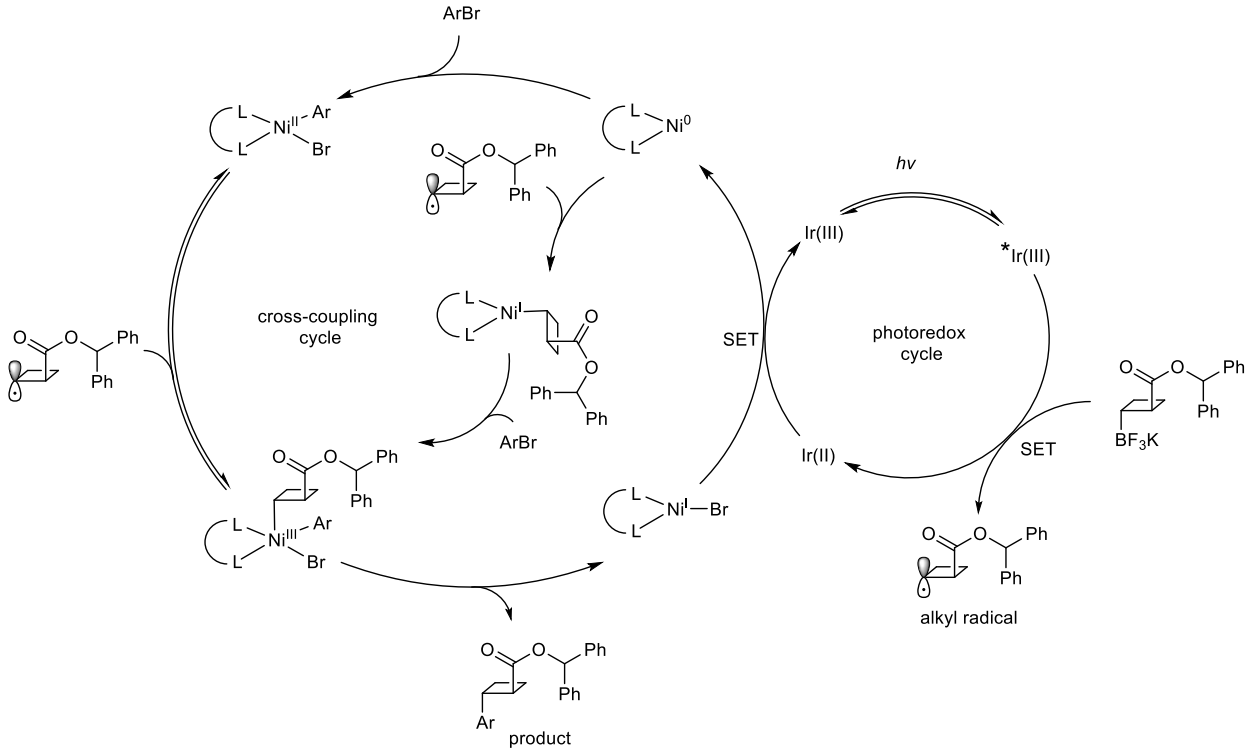

Figure 3-3. Proposed catalytic cycle for the nickel/photoredox dual-catalyzed reaction

Based on the *trans*-diastereoselectivity outcome of the product, it is presumed that the conformationally labile alkyl radical generated from trifluoroborate salt **2-34** converges onto the nickel intermediate on the least hindered face of the cyclobutane ring, away from the sterically encumbered ester group to achieve excellent control of diastereoselectivity (Figure 3-4).

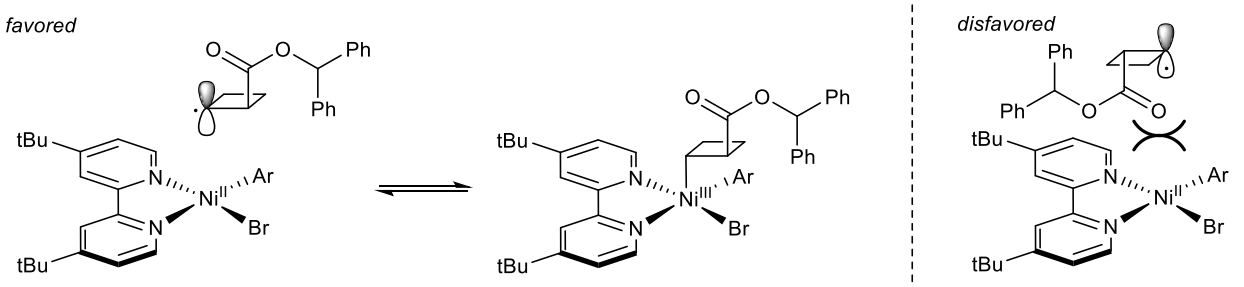

Figure 3-4. Proposed diastereoselective model

Despite the formation of the corresponding alkyl radical from the trifluoroborate salt that relinquishes the stereochemistry of the carbon bound to the boron, it is proposed that the flanking carboxy ester could effectively relay its chiral information towards the newly from carbon-carbon bond. In this regard, the use of the *cis*-trifluoroborate salt in high diastereoselectivity is required in order to obtain the cross-coupled products in high optical purity. As depicted in Figure 3-5, the presence and cross-coupling of the minor diastereomer (*trans*-trifluoroborate salt) would lead to enantiomers and diminish the optical purity of the product. As a control experiment, the trifluoroborate salt was prepared in 1.0:1.2 and 97, 91% dr and ee, respectively, and subjected to the nickel/photoredox dual-catalyzed cross-coupling reaction (Scheme 3-16). In the event, the cross-coupled product was obtained on –34% ee, which confirms that a high dr of trifluoroborate salt **3-19** is crucial to obtain the cross-coupled products in excellent enantioselectivities.

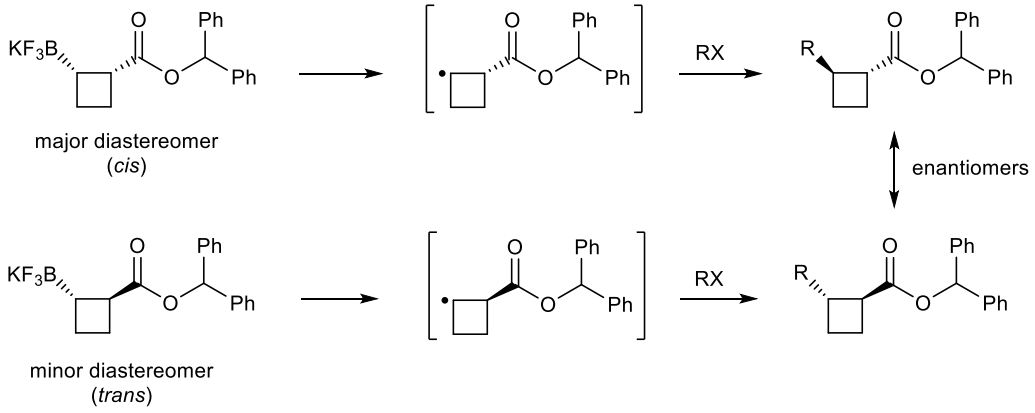

Figure 3-5. Dependence of the optical purity of the cross-coupled products and the diastereomeric ratio of the trifluoroborate salt **3-19**

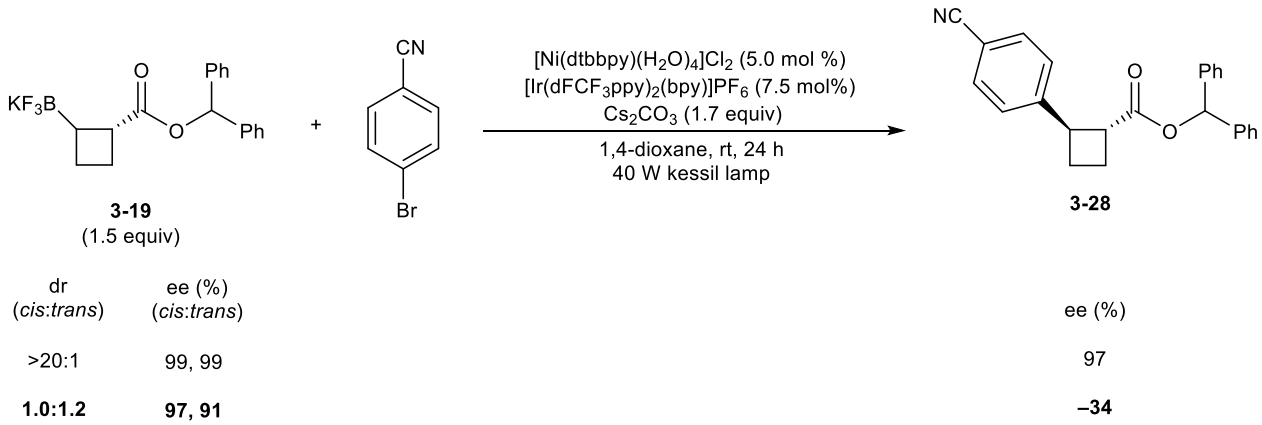

Scheme 3-16. Control experiment for nickel/photoredox dual-catalyzed cross-coupling reaction

3.4 Summary

The application of cyclobutylboronate **3-18** and the corresponding trifluoroborate salt **3-19** was investigated in the stereoselective Suzuki-Miyaura cross-coupling. However, in our hands, these Pd-catalyzed methods were unsuccessful. Attention was directed towards the nickel/photoredox dual-catalyzed cross-coupling reaction of trifluoroborate salt **3-19** which afforded the cross-coupled products. A wide range of aryl and hetereoaryl bromides were shown to couple effectively in moderate to excellent yields with high levels of optical purity and diastereoselectivity to afford the corresponding *trans*-*β*-aryl and heteroaryl cyclobutylcarboxyester of potential interest in medicinal chemistry. This methodology provides a robust and complementary alternative towards optically enriched 1,2-disubstituted cyclobutanes.

3.5 Experimental

3.5.1 General methods

Unless specified, all reactions were performed under nitrogen or argon atmosphere using glassware that was flame dried. Dichloromethane and tetrahydrofuran were used directly from a MBraun Solvent Purification System. Acetonitrile (HPLC grade) were purchased from Sigma Aldrich and used as received. 1,4-Dioxane was purchased from Fisher Scientific, distilled from sodium, subjected to three cycles of freeze-pump-thaw and stored in a Schlenk vessel under nitrogen. $[Ni(dtbbpy)(H_2O)_4]Cl_2$,[23] 2-(2,4-Difluorophenyl)-5-(trifluoromethyl)pyridine,[27] and $[Ir(dFCF_3ppy)_2(bpy)]PF_6$,[12] were prepared according to known literature procedures. All other reagents were purchased from Sigma Aldrich, Combi-Blocks or Strem Chemicals and used without further purification. Thin layer chromatography (TLC) was performed using Merck Silica Gel 60 F254 plates and visualized with UV light and PMA stain. NMR spectrum were recorded on INOVA-400, INOVA-500 or INOVA-700 MHz instruments. The residual solvent protons (^1H) of $CDCl_3$ (7.26 ppm) and the solvent carbons (^{13}C) of $CDCl_3$ (77.06 ppm) were used as internal standards. ^1H NMR data are presented as follows: chemical shift in ppm (δ) downfield from tetramethylsilane (multiplicity, coupling constant, integration). The following abbreviations are used in reporting the ^1H NMR data: s, singlet; br s, broad singlet; d, doublet; t, triplet; q, quartet; app q, apparent quartet; m, multiplet. High-resolution mass spectra were recorded by the University of Alberta Mass Spectrometry Services Laboratory using either electron impact (EI) or electrospray ionization (ESI) techniques. Infrared spectra were obtained on a Nicolet Magna-IR with frequencies expressed in cm^{-1}. Optical rotations were measured using a 1 mL cell with a 1 dm length on a P.E. 241 polarimeter. The enantiomeric excess and

diastereomeric ratio for chiral compounds were determined using a HPLC Agilent instrument with Chiralcel-OD, IC, IB, or Chiralpak-AS columns as specified in the following individual procedures. X-ray diffraction data were collected by the University of Alberta X-Ray Crystallography Laboratory. CCDC 2017339 (compound **(rac)-3-29**) contain the supplementary crystallographic data for this paper. These data can be obtained free of charge from The Cambridge Crystallographic Data Centre.

3.5.2 Preparation of trifluoroborate salt 3-22

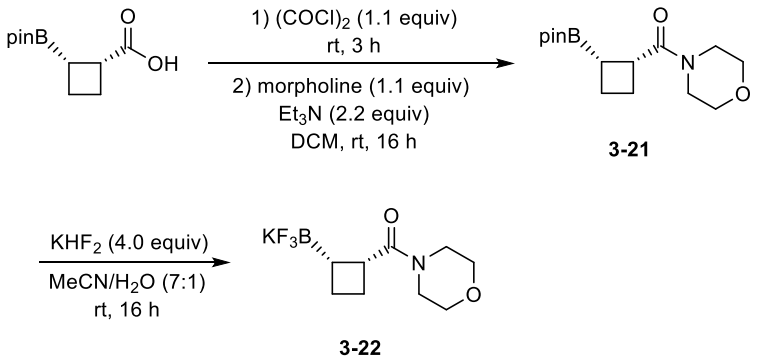

Cyclobutylboronate carboxylic acid **2-38** (200 mg, 0.520 mmol, 1.0 equiv), 4-dimethylaminopyridine (4.0 mg, 0.030 mmol, 6.0 mol%) and morpholine (66 mg, 0.76 mmol, 1.5 equiv) were dissolved in dichloromethane (6 mL) and stirred at rt for 5 min. *N,N′*-dicyclohexylcarbodiimide (116 mg, 0.560 mmol, 1.1 equiv) was added resulting in a suspension. The reaction mixture was allowed to stir at rt for 16 h, then filtered and washed with dichloromethane. The resulting filtrate was concentrated under reduced pressure and the crude mixture was purified by flash column chromatography (5:1 hexanes:ethyl acetate) to give the desired product **3-21** as a clear oil (99 mg, 64%). **^{1}H NMR** (400 MHz, $CDCl_3$) δ 3.74–3.18 (m, 8H), 2.51 (m, 1H), 2.24 (app q, J = 9.2 Hz, 1H), 2.18–2.00 (m, 2H), 1.98–1.86 (m, 1H), 1.25 (s, 6H), 1.23 (s, 6H). **^{13}C NMR** (126 MHz, $CDCl_3$) δ 173.5, 83.4 (×2), 67.0, 66.9, 45.6, 45.5, 42.3,

42.2, 37.3, 24.9 (×2), 24.6 (×2), 19.8. **^{11}B NMR** (128 MHz, $CDCl_3$) δ 33.8. **IR** (cast film, CH_2Cl_2, cm^{-1}): 2978, 1629, 1144. **HRMS** (ESI) $[M+H]^+$ calc. for $C_{15}H_{26}BNO_4$, 296.2028; observed, 296.2026.

To a round bottom flask charged with cyclobutylboronate **2-53** (99 mg, 0.33 mmol, 1.0 equiv), potassium hydrogen difluoride (105 mg, 1.33 mmol, 4.0 equiv) was added deionized water (0.33 mL) and acetonitrile (2.3 mL). The reaction mixture was allowed to stir at rt for 16 h. The solvents were removed under reduced pressure and the crude mixture was dried under high vacuum. The resulting crude solid was suspended in diethyl ether (3 mL) then filtered and washed with diethyl ether (5 mL × 4). The product was extracted with acetonitrile (5 mL × 4) and filtered. The solvent from the resulting filtrate was removed under reduced pressure to give the desired product **3-22** as a white solid (95%). **^{1}H NMR** (500 MHz, $((D_3C)_2CO)$ δ 3.77–3.33 (m, 8H), 3.19 (app q, J = 9.2 Hz, 1H), 2.64–2.54 (m, 1H), 1.61 (m, 4H). **^{13}C NMR** (126 MHz, $(D_3C)_2CO$) δ 175.5, 66.2, 65.9, 45.3, 41.6, 38.9, 22.1, 20.2. (the boron-bound carbon was not detected due to quadrupolar relaxation of boron). **^{11}B NMR** (128 MHz, $(D_3C)_2CO$) δ 4.6. **^{19}F NMR** (376 MHz, $(D_3C)_2CO$) δ -144.6. **IR** (cast film, acetonitrile, cm^{-1}): 2927, 1629. **HRMS** (ESI) $[M]^{*-}$ calc. for $C_9H_{14}BF_3NO_2$, 236.1075; observed, 236.1077.

3.5.3 Preparation of boronolactones

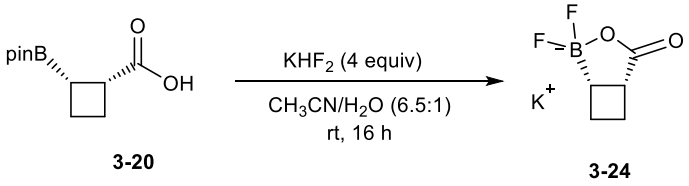

3-20 3-24

To a round bottom flask charged with cyclobutylboronate carboxylic acid **3-20** (220 mg, 1.00 mmol, 1 equiv) and potassium hydrogen difluoride (304 mg, 3.90 mmol, 4 equiv) was added

distilled water (1.0 mL) and acetonitrile (6.7 mL). The reaction was allowed to stir at rt for 16 h. The solvents were removed under reduced pressure and the crude reaction mixture was dried under high vacuum. The resulting crude solid was suspended in diethyl ether (20 mL) then filtered and washed with diethyl ether (20 mL × 4). The product was extracted with warm acetone (100 mL × 4) and filtered. The solvent from the resulting filtrate was removed under reduced pressure to give the desired product **3-24** as a beige solid (79 mg, 41%). **^{1}H NMR** (700 MHz, acetone) δ 2.84 (br s, 1H), 2.42–2.38 (m, 1H), 2.01–2.00 (m, 3H), 1.57 (br s, 1H).**^{13}C NMR** (126 MHz, $(D_3C)_2CO$) δ 184.0, 43.3, 25.6, 20.1 (the boron-bound carbon was not detected due to quadrupolar relaxation of boron). **IR** (cast film, CH_2Cl_2, cm^{-1}): 2945, 1704, 1284. **HRMS:** (ESI) $[M]^{*-}$ calc. for $C_5H_6BF_2O_2$, 147.0434; observed, 147.0434. **^{11}B NMR** (128 MHz, $(D_3C)_2CO$) δ 9.2. **^{19}F NMR** (376 MHz, $(D_3C)_2CO$) δ -154.3 (m) and -144.0 (m). **[α]D_20**: –52 (*c* = 0.76, CH_2Cl_2).

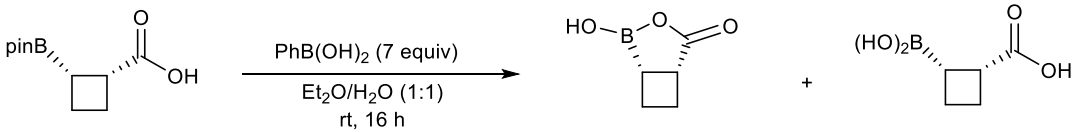

3-20 **3-25** **3-26**

To a round bottom flask with cyclobutylboronate carboxylic acid **2-30** (50 mg, 0.22 mmol, 1 equiv), phenylboronic acid (108 mg, 0.880 mmol, 4 equiv) as added diethyl ether (1.5 mL) and distilled water (1.5 mL). The reaction mixture was allowed to stir at rt for 16 h. The aqueous layer was extracted with diethyl ether to give the desired product as a clear oil. The crude reaction mixture was used without further purification. **^{13}C NMR** (176MHz, $(D_3C)_2CO$) δ 180.2, 41.0, 25.5, 25.0 (the boron-bound carbon was not detected due to quadrupolar relaxation of boron). **^{11}B NMR** (128 MHz, $(D_3C)_2CO$) δ 37.2, 32.4, 20.4. **HRMS** (ESI) $[M-H]^-$ calc. for

$C_5H_8BO_4$, 143.0521; observed, 143.0522. (ESI) $[M-H]^-$ calc. for $C_5H_8BO_4$, 125.0415; observed, 125.0416.

3.5.4 General procedure for nickel/photoredox dual-catalyzed cross-coupling reaction

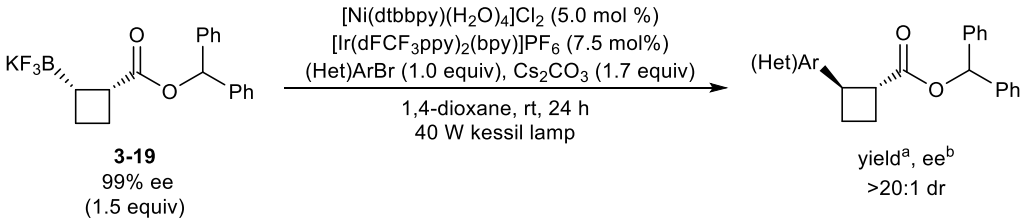

Following a slightly modified procedure.[6] To a microwave vial was added the bromide or pseudohalide electrophile (0.12 mmol, 1.0 equiv), trifluoroborate salt **3-19** (67 mg, 0.18 mmol, 1.5 equiv), $[Ni(dtbbpy)(H_2O)_4]Cl_2$ (2.8 mg, 0.0060 mmol, 5.0 mol%), $[Ir\{dFCF_3ppy\}_2(bpy)]PF_6$ (9.1 mg, 0.0090 mmol, 7.5 mol%) and cesium carbonate (66 mg, 0.20 mmol, 1.7 equiv), capped and purged with argon. 1,4-Dioxane (4.8 mL) was added followed by the bromide or pseudohalide electrophile (0.12 mmol, 1.0 equiv) if it was a liquid. The cap of the microwave vial was thoroughly wrapped with Parafilm and placed 4 cm away from a A160WE Kessil lamp (40 W) which was set to maximum brightness and maximum whitening. The reaction mixture was allowed to stir at rt for 20 h with external cooling from a 6-inch fan placed 7 cm away from the microwave vial. The reaction was filtered over Celite and washed with ethyl acetate. The filtrate was concentrated under reduced pressure and the crude reaction mixture was purified by flash column chromatography using the eluent described below for each compound to give the desired product.

3.5.5 Characterization of *β*-aryl, heteroaryl and alkenyl cyclobutanoates 3-28 to 3-50

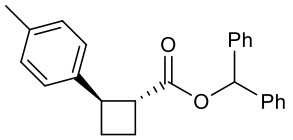

3-29

Purified by flash column chromatography (11:1 hexanes:ethyl acetate) to give the desired product as a clear oil (35.4 mg, 83%, >20:1 dr). **^{1}H NMR** (500 MHz, $CDCl_3$) δ 7.31 (m, 10H), 7.11 (m, 4H), 6.89 (s, 1H), 3.74 (app q, *J* = 8.7 Hz, 1H), 3.27 (app q, *J* = 8.9 Hz, 1H), 2.33 (s, 3H), 2.30–2.23 (m, 2H), 2.20–2.11 (m, 2H). **^{13}C NMR** (126 MHz, $CDCl_3$) δ 173.4, 140.6, 140.5, 140.4, 136.1, 129.1 (×2), 128.6 (×2), 128.6 (×2), 128.0, 127.9, 127.20 (×2), 127.19 (×2), 126.6 (×2), 76.5, 46.1, 43.4, 25.5, 21.5, 21.2. **IR** (cast film, CH_2Cl_2, cm^{-1}): 3031, 2948, 1732, 1600, 1515, 1495, 1155. **HRMS** (ESI) $[M+Na]^+$ calc. for $C_{25}H_{24}NaO_2$, 379.1669; observed, 379.1666. **[α]$_D^{20}$**: –86.5 (*c* = 0.990, CH_2Cl_2). **HPLC**: Chiralpak IC: 0.5:99.5 isopropanol:hexanes, 0.5 mL/min, 20 °C, λ = 210 nm, T_{minor} = 12.0 min, T_{major} = 14.9 min, ee = 95%.

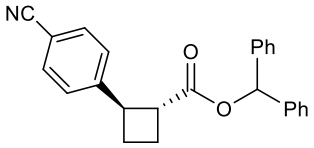

3-28

Purified by flash column chromatography (4:1 hexanes:ethyl acetate) to give the desired product as a clear oil (29.7 mg, 67%, >20:1 dr). **^{1}H NMR** (500 MHz, $CDCl_3$) δ 7.56 (m, 2H), 7.37–7.26 (m, 12H), 6.91 (s, 1H), 3.81 (app q, *J* = 9.3 Hz, 1H), 3.28 (app q, *J* = 8.9 Hz, 1H), 2.41–2.28 (m, 2H), 2.27–2.08 (m, 2H). **^{13}C NMR** (176 MHz, $CDCl_3$) δ 172.8, 148.8, 140.1, 140.1, 132.3 (×2), 128.7 (×2), 128.7 (×2), 128.2, 128.1, 127.4 (×2), 127.2 (×2), 127.1 (×2), 119.1, 110.4, 77.0, 45.6,

43.3, 24.9, 21.7. **IR** (cast film, CH_2Cl_2, cm^{-1}): 3032, 2987, 2227, 1730, 1608, 1586, 1496, 1161. **HRMS** (ESI) $[M+Na]^+$ calc. for $C_{25}H_{21}NNaO_2$, 390.1465; observed, 390.1462. **$[\alpha]_D^{20}$**: –99.0 (*c* = 1.55, CH_2Cl_2). **HPLC**: Chiralpak IC: 25:75 isopropanol:hexanes, 0.5 mL/min, 20 °C, λ = 210 nm, T_{major} = 11.9 min, T_{minor} = 13.9 min, ee = 97%.

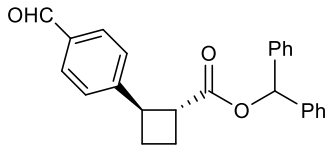

3-30

Purified by flash column chromatography (4:1 hexanes:ethyl acetate) to give the desired product as a clear oil (28.3 mg, 64%, >20:1 dr). **^{1}H NMR** (500 MHz, $CDCl_3$) δ 9.99 (s, 1H), 7.80 (m, 2H), 7.37 (m, 2H), 7.30 (m, 10H), 6.91 (s, 1H), 3.85 (app q, *J* = 9.3 Hz, 1H), 3.33 (app q, *J* = 9.2 Hz, 1H), 2.43–2.29 (m, 2H), 2.28–2.13 (m, 2H). **^{13}C NMR** (176 MHz, $CDCl_3$) δ 191.9, 172.8, 150.5, 140.1, 140.1, 134.9, 130.0 (×2), 128.58 (×2), 128.57 (×2), 128.04, 128.01, 127.2 (×2), 127.1 (×2), 127.0 (×2), 77.1, 45.5, 43.4, 25.0, 21.6. **IR** (cast film, CH_2Cl_2, cm^{-1}): 2021, 2951, 2870, 2735, 1606, 1586, 1574, 1230, 1701, 1168. **HRMS** (ESI) $[M+Na]^+$ calc. for $C_{25}H_{22}NaO_3$, 393.1461; observed, 393.1461. **$[\alpha]_D^{20}$**: –103.9 (*c* = 0.7000, CH_2Cl_2). **HPLC**: Chiralpak IC: 10:90 isopropanol:hexanes, 0.5 mL/min, 20 °C, λ = 210 nm, T_{major} = 18.8 min, T_{minor} = 22.7 min, ee = 93%.

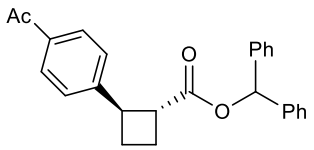

3-31

Purified by flash column chromatography (7:1 hexanes:ethyl acetate) to give the desired product as a clear oil (30.2 mg, 66%, >20:1 dr). **^{1}H NMR** (600 MHz, $CDCl_3$) δ 7.89 (m, 2H), 7.36–7.26 (m, 12H), 6.91 (s, 1H), 3.83 (app q, *J* = 9.3 Hz, 1H), 3.32 (app q, *J* = 8.8 Hz, 1H), 2.59 (s, 3H), 2.44–2.28 (m, 2H), 2.27–2.10 (m, 2H). **^{13}C NMR** (176 MHz, $CDCl_3$) δ 197.8, 172.9, 148.9, 140.2, 140.1, 135.5, 128.57 (×2), 128.55 (×2), 127.99 (×2), 127.98 (×2), 127.1 (×2), 127.0 (×2), 126.7 (×2), 77.0, 45.5, 43.3, 26.6, 25.1, 21.6. **IR** (cast film, CH_2Cl_2, cm^{-1}): 3032, 2951, 1732, 1682, 1606, 1568, 1495, 1269. **HRMS** (ESI) $[M+Na]^+$ calc. for $C_{26}H_{24}NaO_3$, 407.1618; observed, 407.1617. **$[\alpha]_D^{20}$**: –126.9 (*c* = 1.150, CH_2Cl_2). **HPLC**: Chiralpak IC: 5:95 isopropanol:hexanes, 0.5 mL/min, 20 °C, λ = 210 nm, T_{major} = 37.0 min, T_{minor} = 43.4 min, ee = 99%.

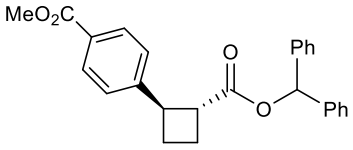

3-32

Purified by flash column chromatography (7:1 hexanes:ethyl acetate) to give the desired product as a clear oil (33.6 mg, 72%, >20:1 dr). **^{1}H NMR** (500 MHz, $CDCl_3$) δ 7.96 (m, 2H), 7.29 (m, 12H), 6.91 (s, 1H), 3.91 (s, 3H), 3.82 (app q, *J* = 10.0 Hz, 1H), 3.32 (app q, *J* = 10.0 Hz, 1H), 2.39–2.28 (m, 2H), 2.25–2.13 (m, 2H). **^{13}C NMR** (126 MHz, $CDCl_3$) δ 172.9, 167.1, 148.7, 140.19, 140.15, 129.7 (×2), 128.57 (×2), 128.55 (×2), 128.4, 127.99, 127.97, 127.1 (×2), 127.0

(×2), 126.6 (×2), 76.8, 52.1, 45.6, 43.3, 25.1, 21.5. **IR** (cast film, CH_2Cl_2, cm^{-1}): 3032, 2951, 1722, 1610, 1586, 1572, 1279, 1241. **HRMS** (ESI) $[M+Na]^+$ calc. for $C_{26}H_{24}NaO_4$, 423.1567; observed, 423.1566. **$[\alpha]_D^{20}$**: –111.8 (*c* = 1.000, CH_2Cl_2). **HPLC**: Chiralpak IA: 2:98 isopropanol:hexanes, 0.5 mL/min, 20 °C, λ = 210 nm, T_{majorr} = 22.2 min, T_{minor} = 24.4 min, ee = 99%.

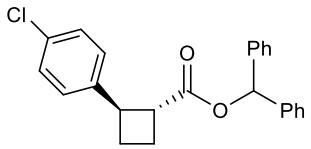

3-33

Purified by flash column chromatography (10:1 hexanes:ethyl acetate) to give the desired product as a clear oil (29.5 mg, 65%, >20:1 dr). **^{1}H NMR** (700 MHz, $CDCl_3$) δ 7.34–7.25 (m, 12H), 7.15 (m, 2H), 6.92 (s, 1H), 3.75 (app q, *J* = 9.3 Hz, 1H), 3.27 (app q, *J* = 8.9 Hz, 1H), 2.36–2.26 (m, 2H), 2.23–2.17 (m, 1H), 2.17–2.10 (m, 1H). **^{13}C NMR** (176 MHz, $CDCl_3$) δ 173.0, 141.9, 140.2, 140.1, 132.1, 128.6 (×2), 128.54 (×2), 128.47 (×2), 127.97 (×2), 127.96 (×2), 127.1 (×2), 127.0 (×2), 77.0, 45.9, 43.0, 25.2, 21.4. **IR** (cast film, CH_2Cl_2, cm^{-1}): 3032, 2987, 1731, 1586, 1493, 1454, 1157. **HRMS** (ESI) $[M+Na]^+$ calc. for $C_{24}H_{21}ClNaO_2$, 399.1122; observed, 399.1123. **$[\alpha]_D^{20}$**: –106.5 (*c* = 0.8600, CH_2Cl_2). **HPLC**: Chiralcel OD IC: 0.3:99.7 isopropanol:hexanes, 0.5 mL/min, 20 °C, λ = 210 nm, T_{minor} = 56.2 min, T_{major} = 61.9 min, ee = 96%.

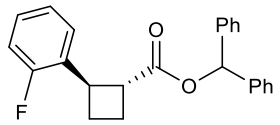

3-34

Purified by flash column chromatography (10:1 hexanes:ethyl acetate) to give the desired product as a clear oil (26.0 mg, 60%, >20:1 dr). **^{1}H NMR** (700 MHz, $CDCl_3$) δ 7.27–7.20 (m, 11H), 7.15 (tdd, *J* = 7.2, 5.2, 1.7 Hz, 1H), 7.05 (td, *J* = 7.5, 1.0 Hz, 1H), 6.94 (ddd, *J* = 10.3, 8.2, 1.0 Hz, 1H), 6.84 (s, 1H), 3.93 (app q, *J* = 9.3 Hz, 1H), 3.40 (app q, *J* = 8.7 Hz, 1H), 2.33–2.23 (m, 2H), 2.22–2.09 (m, 2H). **^{13}C NMR** (126 MHz, $CDCl_3$) δ 172.9, 161.9, 160.0, 140.3 (d, *J* = 10.4 Hz), 130.0 (d, *J* = 15.0 Hz), 128.5 (×2), 128.5 (×2), 128.2 (d, *J* = 4.9 Hz), 128.1 (d, *J* = 8.1 Hz), 127.9, 127.8, 127.1 (×2), 127.0 (×2), 124.0 (d, *J* = 3.4 Hz), 115.4 (d, *J* = 21.9 Hz), 76.9, 44.4, 38.1, 25.4 (d, *J* = 1.9 Hz), 22.0. **^{19}F NMR** (376 MHz, $CDCl_3$) δ -116.7. **IR** (cast film, CH_2Cl_2, cm^{-1}): 3032, 2989, 1733, 1600, 1585, 1492, 1158. **HRMS** (ESI) $[M+Na]^+$ calc. for $C_{24}H_{21}FNaO_2$, 383.1418; observed, 383.1418. **[α]$_D^{20}$**: –82.5 (*c* = 1.05, CH_2Cl_2). **HPLC**: Chiralpak IA: 2:98 isopropanol:hexanes, 0.5 mL/min, 20 °C, λ = 210 nm, T_{major} = 10.6 min, T_{minor} = 12.9 min, ee = 95%.

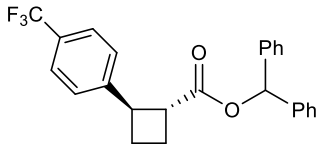

3-35

Purified by flash column chromatography (10:1 hexanes:ethyl acetate) to give the desired product as a clear oil (34.3 mg, 70%, >20:1 dr). **^{1}H NMR** (700 MHz, $CDCl_3$) δ 7.54 (m, 2H), 7.35–7.26 (m, 12H), 6.92 (s, 1H), 3.83 (app q, *J* = 9.1 Hz, 1H), 3.31 (app q, *J* = 9.2 Hz, 1H),

2.41–2.28 (m, 2H), 2.26–2.13 (m, 2H). **^{13}C NMR** (176 MHz, $CDCl_3$) δ 172.8, 147.3, 140.1, 140.1, 128.7 (q, *J* = 32.3 Hz), 128.5 (×2), 128.5 (×2), 128.0, 127.9, 127.1 (×2), 127.0 (×2), 126.8 (×2), 125.3 (q, *J* = 3.7 Hz, ×2), 124.3 (q, *J* = 271.9 Hz), 77.0, 45.6, 43.1, 25.0, 21.5. **^{19}F NMR** (376 MHz, $CDCl_3$) δ -62.3. **IR** (cast film, CH_2Cl_2, cm^{-1}): 3032, 2952, 1732, 1618, 1495, 1455, 1326, 1163. **HRMS** (ESI) $[M+Na]^+$ calc. for $C_{25}H_{21}F_3NaO_2$, 433.1386; observed, 433.1385. **[α]$_D^{20}$**: –81.6 (*c* = 1.00, CH_2Cl_2). **HPLC:** Chiralpak IA: 0.5:99.5 isopropanol:hexanes, 0.5 mL/min, 20 °C, λ = 210 nm, T_{minor} = 12.4 min, T_{major} = 13.7 min, ee = 99%.

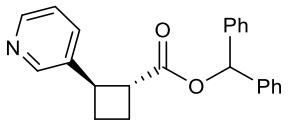

3-38

Purified by flash column chromatography (1:1 hexanes:ethyl acetate) to give the desired product as a clear oil (26.7 mg, 65%, > 20:1 dr). **^{1}H NMR** (700 MHz, $CDCl_3$) δ 8.50 (br s, 1H), 8.48 (br d, *J* = 3.0 Hz, 1H), 7.57 (dt, *J* = 7.9, 1.6 Hz, 1H), 7.36–7.24 (m, 10H), 7.22 (dd, *J* = 7.7, 4.8 Hz, 1H), 6.90 (s, 1H), 3.78 (app q, *J* = 9.3 Hz, 1H), 3.32 (app q, *J* = 9.0 Hz, 1H), 2.42–2.28 (m, 2H), 2.29–2.13 (m, 2H). **^{13}C NMR** (126 MHz, $CDCl_3$) δ 172.7, 148.33, 147.9, 140.12, 140.07, 138.6, 134.2, 128.6 (×4), 128.02, 127.99, 127.1 (×2), 127.0 (×2), 123.4, 77.0, 45.5, 41.0, 25.0, 21.8. **IR** (cast film, CH_2Cl_2, cm^{-1}): 3031, 1952, 1731, 1599, 1495, 1470, 1160. **HRMS** (ESI) $[M+H]^+$ calc. for $C_{23}H_{22}NO_2$, 344.1645; observed, 344.1644. **[α]$_D^{20}$**: –59.8 (*c* = 1.04, CH_2Cl_2). **HPLC**: Chiralpak IC: 15:85 isopropanol:hexanes, 0.5 mL/min, 20 °C, λ = 210 nm, T_{minor} = 26.8 min, T_{major} = 29.3 min, ee = 91%.

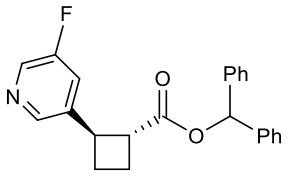

3-39

Purified by flash column chromatography (2:1 hexanes:ethyl acetate) to give the desired product as a clear oil (32.4 mg, 72%, >20:1 dr). **^{1}H NMR** (500 MHz, $CDCl_3$) δ 8.33 (d, *J* = 2.7 Hz, 1H), 8.30 (br s, 1H), 7.36–7.27 (m, 11H), 6.91 (s, 1H), 3.80 (app q, *J* = 9.5 Hz, 1H), 3.30 (app q, *J* = 9.3 Hz, 1H), 2.42–2.30 (m, 2H), 2.30–2.21 (m, 1H), 2.21–2.12 (m, 1H). **^{13}C NMR** (126 MHz, $CDCl_3$) δ 172.5, 160.6, 158.6, 144.2 (d, *J* = 3.7 Hz), 140.5 (d, *J* = 2.7 Hz), 140.0 (d, *J* = 6.7 Hz),), 136.3 (d, *J* = 23.1 Hz), 128.62 (×2), 128.60 (×2), 128.1, 128.0, 127.1 (×2), 127.0 (×2), 121.0 (d, *J* = 17.9 Hz), 77.3, 45.5, 40.4, 24.9, 21.7. **^{19}F NMR** (376 MHz, $CDCl_3$) δ -127.2. **IR** (cast film, CH_2Cl_2, cm^{-1}): 3033, 2988, 1732, 1600, 1577, 1495, 1241, 1163. **HRMS** (ESI) $[M+H]^+$ calc. for $C_{23}H_{21}FNO_2$, 362.1551; observed, 362.1550. **$[\alpha]_D^{20}$**: –69.8 (*c* = 1.84, CH_2Cl_2). **HPLC**: Chiralpak IC: 15:85 isopropanol:hexanes, 0.5 mL/min, 20 °C, λ = 210 nm, T_{minor} = 12.2 min, T_{major} = 14.2 min, ee = 96%.

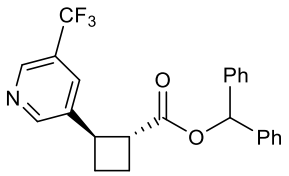

2-40

Purified by flash column chromatography (5:1 hexanes:ethyl acetate) to give the desired product as a clear oil (35.1 mg, 71%, >20:1 dr). **^{1}H NMR** (700 MHz, $CDCl_3$) δ 8.73 (s, 1H), 8.65 (s, 1H), 7.78 (s, 1H), 7.29 (m, 10H), 6.89 (s, 1H), 3.82 (app q, *J* = 9.1 Hz, 1H), 3.32 (app q, *J* = 9.1 Hz,

1H), 2.42–2.30 (m, 2H), 2.30–2.23 (m, 1H), 2.23–2.13 (m, 1H). **^{13}C NMR** (176 MHz, $CDCl_3$) δ 172.4, 151.8, 144.7 (q, *J* = 4.0 Hz), 139.93, 139.89, 138.85, 131.0 (q, *J* = 3.5 Hz), 128.63 (×2), 128.62 (×2), 128.12, 128.07, 127.04 (×2), 126.97 (×2), 126.5 (q, *J* = 32.9 Hz), 123.5 (q, *J* = 272.6 Hz), 77.4, 45.3, 40.5, 24.8, 21.8. **^{19}F NMR** (376 MHz, $CDCl_3$) δ -62.3. **IR** (cast film, CH_2Cl_2, cm^{-1}): 3032, 1952, 1733, 1605, 1582, 1495, 1145, 1132. **HRMS** (ESI) $[M+H]^+$ calc. for $C_{24}H_{21}F_3NO_2$, 412.1519; observed, 412.1516. **$[\alpha]_D^{20}$**: –72.3 (*c* = 0.980, CH_2Cl_2). **HPLC:** Chiralpak IC: 1:99 isopropanol:hexanes, 0.5 mL/min, 20 °C, λ = 210 nm, T_{minor} = 27.6 min, T_{major} = 31.8 min, ee = 97%.

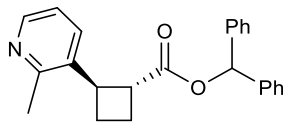

2-41

Purified by flash column chromatography (1:1 hexanes:ethyl acetate) to give the desired product as a clear oil (32.6.0 mg, 72%, >20:1 dr). **^{1}H NMR** (700 MHz, $CDCl_3$) δ 8.33 (dd, *J* = 4.8, 1.5 Hz, 1H), 7.60 (d, *J* = 7.7 Hz, 1H), 7.30–7.19 (m, 10H), 7.09 (dd, *J* = 7.7, 4.8 Hz, 1H), 6.86 (s, 1H), 3.85 (app q, *J* = 9.1 Hz, 1H), 3.41 (app q, *J* = 9.0 Hz, 1H), 2.39–2.28 (m, 5H), 2.21–2.15 (m, 1H), 1.99–1.90 (m, 1H). **^{13}C NMR** (176 MHz, $CDCl_3$) δ 172.8, 156.5, 146.9, 140.1, 140.0, 136.0, 133.3, 128.54 (×2), 128.52 (×2), 128.0 (×2), 127.01 (×2), 126.97 (×2), 121.2, 77.1, 43.3, 40.4, 25.9, 22.6, 21.6. **IR** (cast film, CH_2Cl_2, cm^{-1}): 3031, 2989, 1730, 1599, 1571, 1454, 1156. **HRMS** (ESI) $[M+H]^+$ calc. for $C_{24}H_{24}NO_2$, 358.1802; observed, 358.1800. **$[\alpha]_D^{20}$**: –117.0 (*c* = 1.160, CH_2Cl_2). **HPLC:** Chiralpak IA: 10:90 isopropanol:hexanes, 0.5 mL/min, 20 °C, λ = 210 nm, T_{minor} = 11.5 min, T_{major} = 13.0 min, ee = 97%.

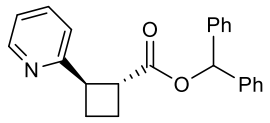

2-42

Purified by flash column chromatography (2:1 hexanes:ethyl acetate) to give the desired product as a clear oil (25.5 mg, 62%, >20:1 dr). **^{1}H NMR** (500 MHz, $CDCl_3$) δ 8.61 (d, *J* = 4.3 Hz, 1H), 7.59–7.53 (m, 1H), 7.37–7.22 (m, 10H), 7.16–7.08 (m, 2H), 6.88 (s, 1H), 3.85 (app q, *J* = 8.7 Hz, 1H), 3.62 (app q, *J* = 8.7 Hz, 1H), 2.45–2.20 (m, 4H). **^{13}C NMR** (126 MHz, $CDCl_3$) δ 173.3, 161.7, 149.6, 140.40, 140.37, 136.2, 128.50 (×2), 128.46 (×2), 127.8 (×2), 127.1 (×2), 127.0 (×2), 122.0, 121.6, 76.7, 45.0, 43.9, 24.3, 21.5. **IR** (cast film, CH_2Cl_2, cm^{-1}): 3031, 2991, 1732, 1590, 1568, 1495, 1154. **HRMS** (ESI) $[M+H]^+$ calc. for $C_{23}H_{22}NO$, 344.1645; observed, 344.1645. **$[\alpha]_D^{20}$**: –107.0 (*c* = 0.9000, CH_2Cl_2). **HPLC**: Chiralpak IB: 7:93 isopropanol:hexanes, 0.5 mL/min, 20 °C, λ = 210 nm, T_{major} = 6.5 min, T_{minor} = 7.0 min, ee = 98%.

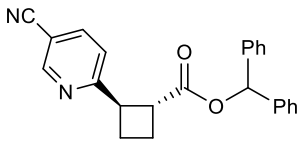

2-43

Purified by flash column chromatography (5:1 hexanes:ethyl acetate) to give the desired product as a clear oil (27.7 mg, 63%, >20:1 dr). **^{1}H NMR** (500 MHz, $CDCl_3$) δ 8.85 (d, *J* = 1.5 Hz, 1H), 7.81 (dd, *J* = 8.1, 2.0 Hz, 1H), 7.34–7.27 (m, 10H), 7.21 (d, *J* = 8.1 Hz, 1H), 6.89 (s, 1H), 3.91 (app q, *J* = 8.6 Hz, 1H), 3.60 (app q, *J* = 8.6 Hz, 1H), 2.44–2.23 (m, 4H). **^{13}C NMR** (126 MHz, $CDCl_3$) δ 172.8, 166.1, 152.4, 140.10, 140.09, 139.3, 128.54 (×2), 128.51 (×2), 128.0, 123.0, 127.1 (×2), 126.9 (×2), 122.0, 116.9, 107.7,77.03, 44.8, 43.6, 24.0, 21.6. **IR** (cast film, CH_2Cl_2,

cm^{-1}): 3033, 2986, 2232, 1731, 1594, 1554, 1495, 1161. **HRMS** (ESI) $[M+Na]^+$ calc. for $C_{24}H_{20}N_2NaO_3$, 391.1414; observed, 391.1417. **$[\alpha]_D^{20}$**: –104.3 (*c* = 1.110, CH_2Cl_2). **HPLC**: Chiralpak IC: 10:90 isopropanol:hexanes, 0.5 mL/min, 20 °C, λ = 210 nm, T_{major} = 20.8 min, T_{minor} = 29.7 min, ee = 98%.

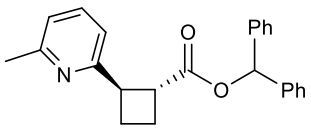

2-44

Purified by flash column chromatography (7:1 hexanes:ethyl acetate) to give the desired product as a clear oil (24.9 mg, 58%, >20:1 dr). **^{1}H NMR** (500 MHz, $CDCl_3$) δ 7.48 (t, *J* = 7.7 Hz, 1H), 7.36–7.27 (m, 10H), 7.00 (d, *J* = 7.6 Hz, 1H), 6.95 (d, *J* = 7.6 Hz, 1H), 6.89 (s, 1H), 3.85 (app q, *J* = 8.7 Hz, 1H), 3.63 (app q, *J* = 8.7 Hz, 1H), 2.57 (s, 3H), 2.45–2.19 (m, 4H). **^{13}C NMR** (126 MHz, $CDCl_3$) δ 173.4, 161.1, 158.1, 140.48, 140.45, 136.3, 128.48 (×2), 128.45(×2), 127.82 (×2), 127.79 (×2), 127.1 (×2), 121.1, 118.6, 76.7, 45.2, 43.8, 24.7, 24.4, 21.5. **IR** (cast film, CH_2Cl_2, cm^{-1}): 3031, 2985, 1731, 1590, 1575, 1495, 1160. **HRMS** (ESI) $[M+Na]^+$ calc. for $C_{24}H_{23}NNaO_2$, 380.1621; observed, 380.1627. **$[\alpha]_D^{20}$**: –126.9 (*c* = 0.9600, CH_2Cl_2). **HPLC:** Chiralpak IA: 0.5:99.5 isopropanol:hexanes, 0.5 mL/min, 20 °C, λ = 210 nm, T_{major} = 21.6 min, T_{minor} = 25.4 min, ee = 98%.

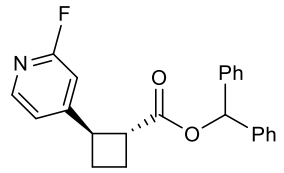

2-45

Purified by flash column chromatography (4:1 hexanes:ethyl acetate) to give the desired product as a clear oil (30.1 mg, 69%, >20:1 dr). **^{1}H NMR** (400 MHz, $CDCl_3$) δ 8.10 (d, *J* = 5.2 Hz, 1H), 7.39–7.27 (m, 10H), 7.02–6.97 (m, 1H), 6.92 (s, 1H), 6.77 (br s, 1H), 3.78 (app q, *J* = 9.1 Hz, 1H), 3.30 (app q, *J* = 9.0 Hz, 1H), 2.43–2.08 (m, 4H). **^{13}C NMR** (126 MHz, $CDCl_3$) δ 172.4, 165.1, 163.2, 158.1 (d, *J* = 7.6 Hz), 147.6 (d, *J* = 15.2 Hz), 139.9 (d, *J* = 4.5 Hz), 128.61 (×2), 128.60 (×2), 128.12, 128.05, 127.1 (×2), 127.0 (×2), 119.6 (d, *J* = 3.9 Hz), 107.3 (d, *J* = 37.2 Hz), 77.00, 44.9, 42.1 (d, *J* = 2.9 Hz), 24.4, 21.6. **^{19}F NMR** (376 MHz, $CDCl_3$) δ -68.3. **IR** (cast film, CH_2Cl_2, cm^{-1}): 3032, 2990, 1733, 1611, 1587, 1565, 1159. **HRMS** (ESI) $[M+H]^+$ calc. for $C_{23}H_{21}FNO_2$, 362.1551; observed, 362.1548. **$[\alpha]_D^{20}$:** –72.9 (*c* = 1.86, CH_2Cl_2). **HPLC:** Chiralpak IA: 2:98 isopropanol:hexanes, 0.5 mL/min, 20 °C, λ = 210 nm, T_{minor} = 16.4 min, T_{major} = 18.4 min, ee = 95%.

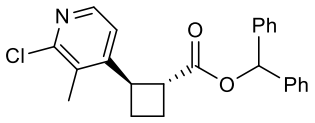

2-46

Purified by flash column chromatography (5:1 hexanes:ethyl acetate) to give the desired product as a clear oil (30.8 mg, 66%, >20:1 dr). **^{1}H NMR** (500 MHz, $CDCl_3$) δ 8.20 (d, *J* = 5.1 Hz, 1H), 7.34–7.25 (m, 10H), 7.20 (d, *J* = 5.1 Hz, 1H), 6.89 (s, 1H), 3.90 (app q, *J* = 9.3 Hz, 1H), 3.45 (app q, *J* = 9.1 Hz, 1H), 2.44–2.30 (m, 2H), 2.27–2.21 (m, 1H), 2.20 (s, 3H), 2.01 (m, 1H). **^{13}C**

NMR (126 MHz, $CDCl_3$) δ 172.5, 152.8, 152.4, 146.8, 140.0, 139.9, 130.2, 128.60 (×2), 128.59 (×2), 128.08, 128.06, 127.00(×4), 120.00, 77.27, 43.35, 41.12, 26.00, 21.57, 15.66. **IR** (cast film, CH_2Cl_2, cm^{-1}): 3033, 2987, 1733, 1584, 1544, 1495, 1166. **HRMS** (ESI) $[M+H]^+$ calc. for $C_{24}H_{23}ClNO_2$, 392.1412; observed, 392.1418. **$[\alpha]_D^{20}$**: –92.2 (*c* = 0.840, CH_2Cl_2). **HPLC**: Chiralpak IC: 15:85 isopropanol:hexanes, 0.5 mL/min, 20 °C, λ = 210 nm, T_{minor} = 21.5 min, T_{major} = 25.5 min, ee = 96%.

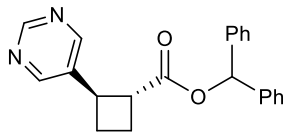

2-47

Purified by flash column chromatography (1:2 hexanes:ethyl acetate) to give the desired product as a clear oil (38.9 mg, 94%, >20:1 dr). **^{1}H NMR** (700 MHz, $CDCl_3$) δ 9.10 (s, 1H), 8.62 (s, 2H), 7.36–7.25 (m, 10H), 6.91 (s, 1H), 3.76 (app q, *J* = 9.3 Hz, 1H), 3.34 (app q, *J* = 9.1 Hz, 1H), 2.43–2.26 (m, 3H), 2.22 (m, 1H). **^{13}C NMR** (126 MHz, $CDCl_3$) δ 172.3, 157.2, 155.4 (×2), 139.89, 139.85, 136.0, 128.63 (×2),128.61 (×2), 128.14, 128.06, 127.1 (×2), 127.0 (×2), 77.3, 45.2, 38.6, 24.5, 22.0. **IR** (cast film, CH_2Cl_2, cm^{-1}): 3031, 2981, 1730, 1583, 1560, 1413, 1165. **HRMS** (ESI) $[M+Na]^+$ calc. for $C_{22}H_{20}N_2NaO_2$, 367.1417; observed, 367.1415. **$[\alpha]_D^{20}$:** –69.5 (*c* = 1.01, CH_2Cl_2). **HPLC:** Chiralpak AS: 2:98 isopropanol:hexanes, 0.5 mL/min, 20 °C, λ = 210 nm, T_{major} = 60.7 min, T_{minor} = 66.4 min, ee = 92%.

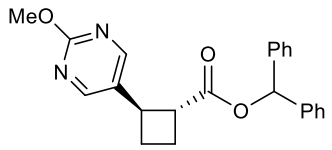

2-48

Purified by flash column chromatography (2:1 hexanes:ethyl acetate) to give the desired product as a clear oil (28.5 mg, 64%, >20:1 dr). **^{1}H NMR** (500 MHz, $CDCl_3$) δ 8.39 (s, 2H), 7.34–7.25 (m, 10H), 6.90 (s, 1H), 4.00 (s, 3H), 3.67 (app q, J = 9.4 Hz, 1H), 3.27 (app q, J = 9.1 Hz, 1H), 2.41–2.21 (m, 3H), 2.15 (m, 1H). **^{13}C NMR** (126 MHz, $CDCl_3$) δ 172.5, 164.8, 157.8 (×2), 139.99, 139.96, 129.3, 128.63 (×2), 128.61 (×2), 128.1, 128.0, 127.1 (×2), 127.0 (×2), 77.2, 54.9, 45.7, 38.2, 24.9, 21.8. **IR** (cast film, CH_2Cl_2, cm^{-1}): 3031, 2987, 1731, 1599, 1557, 1495. **HRMS** (ESI) $[M+H]^+$ calc. for $C_{23}H_{22}N_2O_3$, 375.1703; observed, 375.1701. **$[\alpha]_D^{20}$**: –93.5 (*c* = 0.850, CH_2Cl_2). **HPLC**: Chiralpak IC: 25:75 isopropanol:hexanes, 0.5 mL/min, 20 °C, λ = 210 nm, T_{minor} = 22.6 min, T_{major} = 27.7 min, ee = 94%.

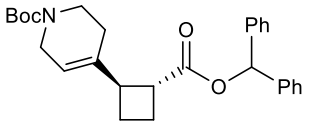

2-49

Purified by flash column chromatography (5:1 hexanes:ethyl acetate) to give the desired product as a clear oil (31.9 mg, 58%, >20:1 dr). **^{1}H NMR** (500 MHz, $CDCl_3$) δ 7.34–7.27 (m, 10H), 6.88 (s, 1H), 5.40 (br s, 1H), 3.88 (br s, 2H), 3.44 (br s, 2H), 3.14–3.04 (m, 2H), 2.19 (m, 1H), 2.07–1.84 (m, 5H), 1.47 (s, 9H). **^{13}C NMR** (126 MHz, $CDCl_3$) δ 173.2, 154.9, 140.30, 140.27, 137.6 (br s), 128.54 (×2), 128.50 (×2), 127.93, 127.91, 127.1 (×2), 127.0 (×2), 117.5 (br s), 79.5, 76.8, 44.6 (×2), 43.0, 28.5(×3), 26.0 (br s), 22.9, 21.1 (×2). **IR** (cast film, CH_2Cl_2, cm^{-1}): 3443 (br),

3091, 2977, 1731, 1700, 1496, 1454, 1162. **HRMS** (ESI) $[M+Na]^+$ calc. for $C_{28}H_{33}NNaO_4$, 470.2302; observed, 470.2299. **$[\alpha]_D^{20}$**: –42.9 (*c* = 0.590, CH_2Cl_2). **HPLC**: Chiralpak IC: 5:95 isopropanol:hexanes, 0.5 mL/min, 20 °C, λ = 210 nm, T_{minor} = 18.8 min, T_{major} = 23.3 min, ee = 97%.

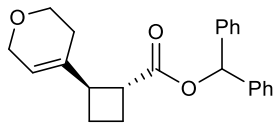

2-50

Reaction time of 48 h. Purified by flash column chromatography (7:1 hexanes:ethyl acetate) to give the desired product as a clear oil (23.8 mg, 58%, >20:1 dr). **^{1}H NMR** (500 MHz, $CDCl_3$) δ 7.35–7.26 (m, 10H), 6.88 (s, 1H), 5.47 (br s, 1H), 4.17–4.08 (m, 2H), 3.74 (br s, 2H), 3.10 (t, *J* = 6.3 Hz, 2H), 2.24–2.16 (m, 1H), 2.09–1.85 (m, 5H). **^{13}C NMR** (126 MHz, $CDCl_3$) δ 173.3, 140.32, 140.30, 136.8, 128.54 (×2), 128.49 (×2), 127.9 (×2), 127.1 (×2), 127.0 (×2), 119.2, 76.81, 65.5, 64.2, 44.5, 42.9, 26.2, 22.7, 21.2. **IR** (cast film, CH_2Cl_2, cm^{-1}): 3031, 2950, 1732, 1495, 1454, 1154. **HRMS** (ESI) $[M+Na]^+$ calc. for $C_{23}H_{24}NaO_3$, 371.1618; observed, 371.1618. **$[\alpha]_D^{20}$**: –63.0 (*c* = 0.760, CH_2Cl_2). **HPLC**: Chiralpak IC: 5:95 isopropanol:hexanes, 0.5 mL/min, 20 °C, λ = 210 nm, T_{minor} = 13.3 min, T_{major} = 15.7 min, ee = 97%.

3.5.6 Procedure for ester deprotection of compound (*rac*)-3-29

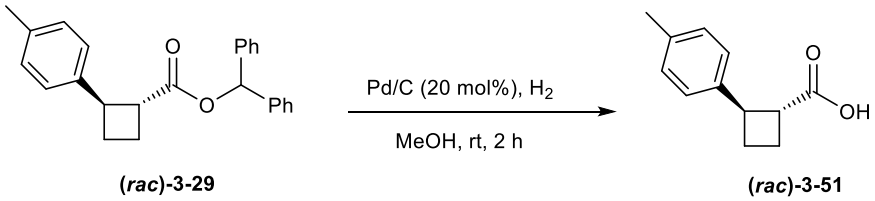

(*rac*)-3-29 (*rac*)-3-51

To a round bottom flask charged with compound **(*rac*)-3-29** (360 mg, 1.00 mmol, 1 equiv) was added methanol (5 mL). Wet 10% Pd/C (21 mg, 0.20 mmol, 20 mol%) was added and the reaction was purged with a hydrogen gas-filled balloon for 10 min. The reaction was then allowed to stir at rt for 2 h under hydrogen gas. The reaction mixture was filtered over Celite and washed with ethyl acetate. The filtrate was concentrated under reduced pressure and the crude mixture was purified by flash column chromatography (1:1 hexanes:ethyl acetate) to give the desired product as a clear oil (171 mg, 90%). Recrystallized in hexanes and storing at –20 °C. **^{1}H NMR** (700 MHz, $CDCl_3$) δ 7.16 (m, 2H), 7.13 (m, 2H), 3.77 (app q, *J* = 8.8 Hz, 1H), 3.20 (app q, *J* = 8.9 Hz, 1H), 2.33 (s, 3H), 2.29 (m, 2H), 2.21–2.11 (m, 2H). **^{13}C NMR** (176 MHz, $CDCl_3$) δ 179.7, 140.3, 136.1, 126.4 (×2), 126.3 (×2), 45.2, 43.0, 25.5, 21.6, 21.1. **IR** (cast film, CH_2Cl_2, cm^{-1}): 3025 (br s), 3051, 2972, 1701, 1515, 1425. **HRMS** (ESI) $[M-H]^-$ calc. for $C_{12}H_{13}O_2$, 189.0921; observed, 189.0921.

3.6 References

[1] Carey, J. S.; Laffan, D.; Thomson, C.; Williams, M. T. *Org. Biomol. Chem.* **2006**, *4*, 2337−2347.

[2] Jana, R.; Pathak, T. P.; Sigman, M. S. *Chem. Rev*. **2011***, 111*, 1417–1492.

[3] Imao, D.; Glasspoole, B. W.; Laberge, V. S.; Crudden, C. M. *J. Am. Chem. Soc.* **2009**, *131*, 5024−5025.

[4] Uenishi, J.; Beau, J. M.; Armstrong, R. W.; Kishi, Y. *J. Am. Chem. Soc.* **1987**, *109*, 4756−4758.

[5] Matos, K.; Soderquist, J. A. *J. Org. Chem.* **1998**, *63*, 461−470.

[6] Daini, M.; Suginome, M. *J. Am. Chem. Soc.* **2011**, *133*, 4758−4761.

[7] Ohmura, T.; Awano, T.; Suginome, M. *J. Am. Chem. Soc.* **2010**, *132*, 13191−13193.

[8] Awano, T.; Ohmura, T.; Suginome, M. *J. Am. Chem. Soc.* **2011**, *133*, 20738−20741.

[9] Sandrock, D. L.; Jean-Gérard, L.; Chen, C.-Y.; Dreher, S. D.; Molander, G. A. *J. Am. Chem. Soc.* **2010**, *132*, 17108−17110.

[10] Lee, J. C. H.; Mcdonald, R.; Hall, D. G. *Nat. Chem.* **2011**, *3,* 894–899.

[11] Lee, J. C. H.; Sun, H.-Y.; Hall, D. G. *J. Org. Chem.* **2015**, *80*, 7134–7143.

[12] Tellis, J. C.; Primer, D. N.; Molander, G. A. *Science* **2014**, *345*, 433–436.

[13] Khatib, M. E.; Augusto, R.; Serafim, M.; Molander, G. A. *Angew. Chem. Int. Ed*. **2016**, *55*, 254 –258.

[14] Review of trifluoroborate substrates in nickel/photoredox dual-catalyzed cross-coupling: Milligan, J. A.; Phelan, J. P.; Badir, S. O.; Molander, G. A. *Angew. Chem. Int. Ed*. **2019**, *58,* 6152–6163.

[15] Gutierrez, O.; Tellis, J. C.; Primer, D. N.; Molander, G. A.; Kozlowski, M. C. *J. Am. Chem. Soc.* **2015**, *137*, 4896–4899.

[16] He, J.; Shao, Q.; Wu, Q.; Yu, J.-Q. *J. Am. Chem. Soc.* **2017**, *139*, 3344–3347.

[17] Molander, G. A.; Wisniewski, S. R.; Hosseini-Sarvari, M. *Adv. Synth. Catal.* **2013**, *355*, 3037–3057.

[18] Hoang, G. L.; Takacs, J. M. *Chem. Sci.* **2017**, *8*, 4511–4516.

[19] Luisi, R.; Giovine, A.; Florio, S. *Chem. Eur. J*. **2010**, *16*, 2683−2687.

[20] Fritzemeier R. G.; Medici, E. J.; Szwetkowski, C.; Wonilowicz, L. G.; Sibley, C. D.; Slebodnick, C.; Santos, W. L. *Org. Lett.* **2019**, *21*, 8053−8057.

[21] Tellis, J. C.; Amani, J.; Molander, G. A. *Org. Lett.* **2016**, *18*, 2994−2997.

[22] Giustra, Z. X.; Yang, X.; Chen, M.; Bettinger, H. F.; Liu, S. Y. *Angew. Chem. Int. Ed*. **2019**, *58*, 18918–18922.

[23] Gutiérrez-Bonet, Á.; Tellis, J. C.; Matsui, J. K.; Vara, B. A.; Molander, G. A. *ACS Catal.* **2016**, *6*, 8004–8008.

[24] Hanss, D.; Freys, J. C.; Bernardinelli, G.; Blanhard, N. *Eur. J. Inorg. Chem*. **2009**, 4850–4859.

[25] Welsch, M. E.; Snyder, S. A.; Stockwell, B. R. *Curr. Opin. Chem. Biol.* **2010**, *14*, 347–361.

[26] Primer, D. N.; Molander, G. A. *J. Am. Chem. Soc*. **2017**, *139*, 9847−9850.

[27] Skubi, K. L.; Kidd, J. B.; Jung, H.; Guzei, I. A.; Baik, M-H.; Yoon, T. P. *J. Am. Chem. Soc*. **2017***, 139*, 17186−17192.

Chapter 4. Preparation of Allylic Cyclobutylboronates by Way of a Copper-Catalyzed Boryl Substitution

4.1 Introduction

4.1.1 Applications of allylboronates in organic synthesis

Allylboronates serve as attractive synthetic intermediates in a number of carbon-carbon bond formation reactions.[1] The allylboronate group is a relatively simple synthetic precursors that can be transformed into a diverse range of more complex products. Optically enriched compounds can be accessed from allylboronates using two general approaches: (a) chiral allylboronates can be prepared in an asymmetric manner, in which, chirality transfer is conveyed to the product (b) use of an asymmetric catalyst to couple an achiral allylboronate with its prochiral reaction partner. The most popular reaction of allylboronates is the allylboration of aldehydes to provide the corresponding homoallylic alcohol products. The reaction involves a closed, Zimmerman-Traxler chair-like transition state with the carbonyl group, in which, activation of the carbonyl group is achieved by coordination to the boron atom (Figure 4-1). Due to this close transition state, crotylboronation of aldehydes could be performed in high diastereoselectivity. In 2008, the Hall Group described the catalytic enantioselective allylboration of aldehydes using a chiral diol complex with tin tetrachloride to induce high levels of selectivity (Scheme 4-1a).[2] In 2016, the same group optimized the aldehyde allylboration of

an optically enriched piperidinyl allylic boronate to provide the corresponding homoallylic alcohol products as a single diastereomer and in high enantioselectivity (Scheme 4-1b).[3] Moreover, allylboronates can participate in other carbon-carbon bond formation reactions such

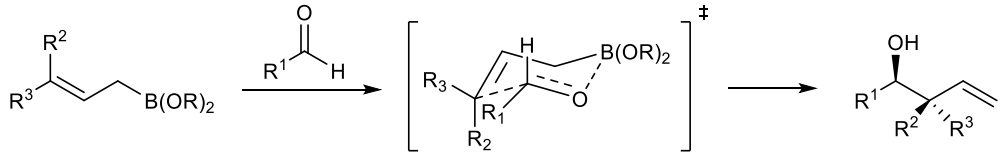

Figure 4-1. Allylboration reaction and Zimmerman-Traxler transition state

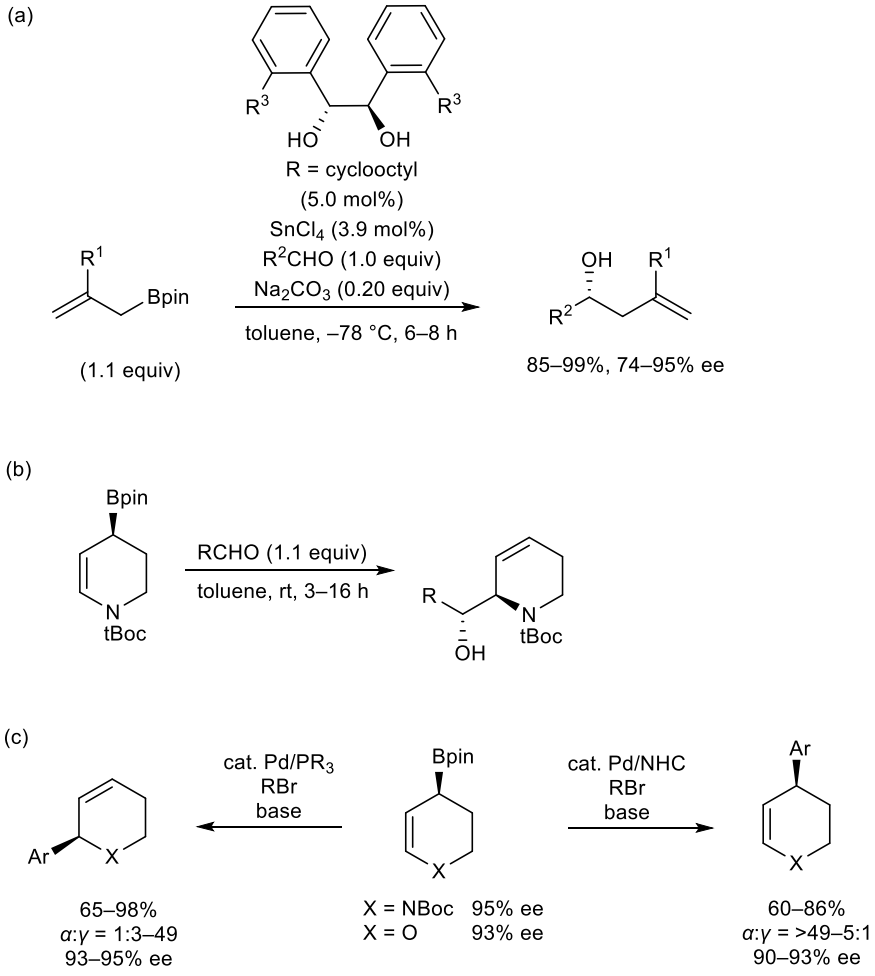

Scheme 4-1. Applications of acyclic and cyclic allylboronates in carbon-carbon bond formation

as the famed Suzuki-Miyaura cross-coupling. In 2014, the Hall Group reported the ligand-controlled regiodivergent cross-coupling of an optically enriched heterocyclic allylic boronate with high retention of optical purity to afford either the α-or γ-arylated isomers in high selectivity (Scheme 4-1c).[4]

4.1.2 Copper-catalyzed allylic borylation

While the first reports of copper-catalyzed conjugate borylation were independently reported by Hosomi[5] and Miyaura[6] in 2000, as described in Chapter 2, subsequent reports have emerged that expanded the reaction scope of the copper-boryl species. In 2005, Sawamura and Ito reported the copper-catalyzed boryl substitution reaction of acyclic allylic carbonates to afford the corresponding allylboronates with excellent regioselectivity and control of alkene geometry (Scheme 4-2a).[7] In 2007, Sawamura and Ito expanded their work towards an enantioselective variant by employing chiral phosphine ligand **4-1** to obtain α-substituted allylboronates in high enantioselectivity (Scheme 4-2b).[8] Furthermore, they found that their optimized catalyst system can be employed for the desymmetrization of *meso* compound **4-2** as depicted in Scheme 4-2c.[9] The enantioselective copper-catalyzed boryl substitution of the *meso* compound provided the optically enriched allylboronate intermediate, which subsequently underwent an allylboration reaction with an aldehyde, followed by alcohol protection. Interestingly, a second boryl substitution reaction was performed in a sterically controlled manner affording a second allylboronate intermediate, which was subjected to another allylboration reaction with an aldehyde to yield the 1,6-diol **4-3** in high enantio- and diastereoselectivity. Moreover, Sawamura has reported a number of examples of copper-catalyzed alkyl substitution reactions between alkylboranes and/or alkylboronates with allylic chlorides and/or phosphates (Scheme 4-2d).[10]

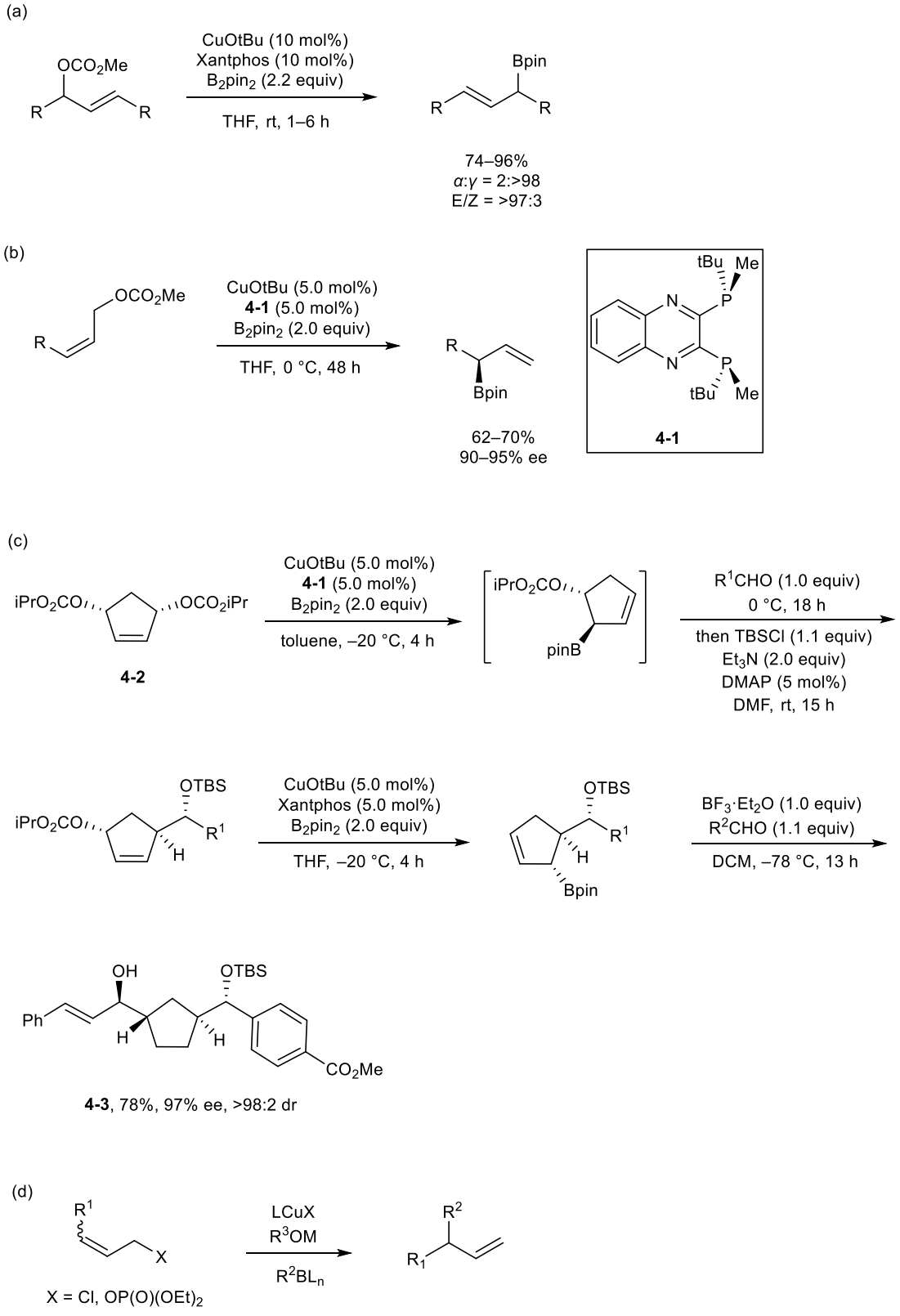

Scheme 4-2. Examples of (a, b, c) copper-catalyzed boryl and (d) alkyl substitution reactions

The authors proposed a mechanism for the copper-catalyzed boryl substitution reaction, beginning with the reaction of copper alkoxide **4-4** and the diboron reagent to generate the copper-boryl species **4-5** (Figure 4-2).[8] A copper-alkene π-interaction forms to give complex **4-6**, which results in the addition of the copper-boron bond onto the alkene to afford intermediate **4-7**. The regioselectivity arises from stereoelectronic effects that stabilize the copper-carbon σ-bond by interacting with the carbon-oxygen σ* orbital. Lastly, the alkylcopper intermediate can undergo *β*-elimination to give the desired borylated product and generate a copper carbonate species that can subsequently undergo decarboxylation to regenerate copper alkoxide **4-4**.

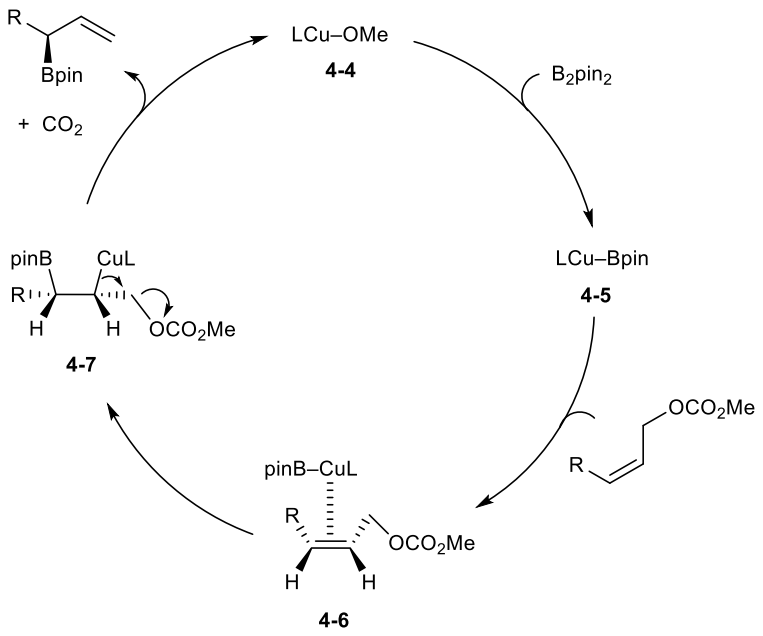

Figure 4-2. Proposed mechanism for the copper-catalyzed allylic borylation reaction

4.1.3 Objectives

Allylboronate intermediates serve as an attractive synthetic handle in several carbon-carbon bond formation reactions such as the aldehyde allylboration reaction and Suzuki-Miyaura

cross-coupling. In an effort to prepare a highly versatile allylic cyclobutylboronate intermediate, the goal of this project is to synthesize allylic cyclobutylboronates **4-8** and **4-9** by way of the copper-catalyzed boryl substitution reaction from the corresponding allylic cyclobutylphosphates (Scheme 4-3). It should be mentioned that Didier and co-workers have reported the preparation of an enantioenriched cyclobutenylmethylboronate and its application in aldehyde allylboration and Suzuki-Miyaura cross-coupling as described in Chapter 1.[11]

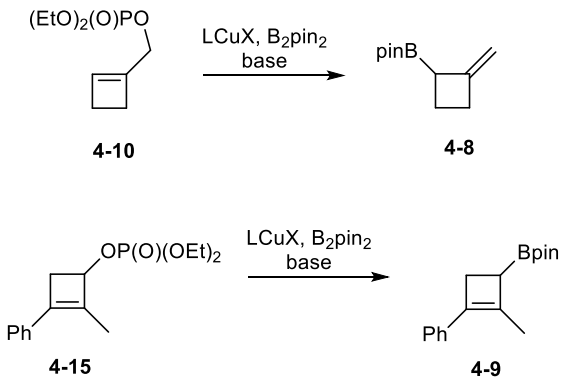

Scheme 4-3. Proposed route towards allylic cyclobutylboronates

4.2 Synthesis of the allylic cyclobutylboronate 4-8

The synthesis of starting material cyclobutenylmethylphosphate **4-11** began with the reduction of a cyclobutene 1-carboxyester to give the corresponding alcohol **4-10** in 72% yield, which was then transformed into phosphate **4-11** in 89% yield (Scheme 4-4a). With the starting material in hand, the copper-catalyzed boryl substitution reaction was investigated (Scheme 4-4b). Under the allylic substitution conditions reported by Sawamura and co-workers,[12] the racemic reaction provided the desired allylic cyclobutylboronate **4-8** in a 94% ^{1}H NMR yield. After silica column chromatography, the product was isolated in only a 36% yield. It was surmised that the product was air-sensitive and unstable towards silica gel. Thus, attempts were

made to improve the isolated yield by performing a short pad silica column chromatography and using silica deactivated with 30% wt H_2O, which was found to have improved the isolated yield of organoboronate compounds.[12] However, these efforts proved unfruitful, providing the product in similar yields. In this regard, a brief attempt was made to use the crude reaction mixture directly and transform the unstable intermediate to the corresponding trifluoroborate salt **4-12** (Scheme 4-4c). However, the trifluoroborate salt was obtained in moderate (41%) yield. Future work would involve investigating the allylic cyclobutylboronate intermediate in the allylboration reaction. In an effort to minimize exposure of the allylic cyclobutylboronates to air, a solvent exchange followed by the addition of the aldehyde can be conducted air-free to perform the allylboration reaction. Furthermore, a three-component copper-catalyzed boryl substitution/allylboration reaction may be viable.

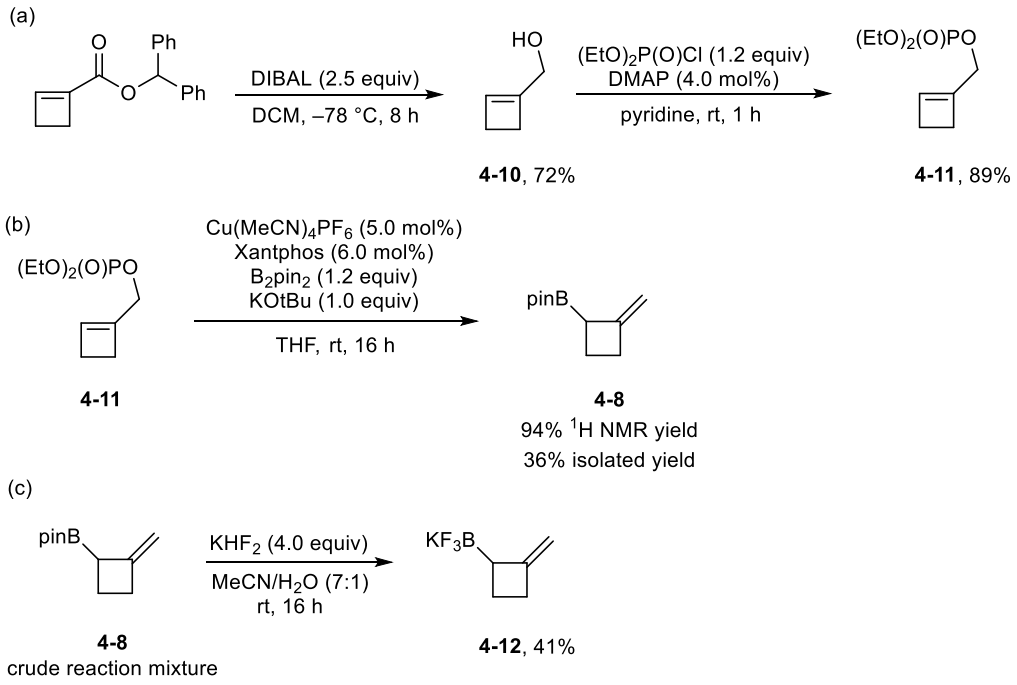

Scheme 4-4. Synthesis of a cyclobutylmethylphosphate and its copper-catalyzed boryl substitution

4.3 Synthesis of the allylic cyclobutylboronate 4-9

Due to the air-sensitivity and low stability of compound **4-8**, an alternative allylic cyclobutylboronate scaffold (**4-9**) was envisioned. The synthesis of starting material, allylic cyclobutylphosphate **4-15** began with the preparation of cyclobutenone **4-13** that was previously reported by the Hall Group (Scheme 4-5a).[12] The [2 + 2] cycloaddition between an amide-derived keteniminium intermediate and phenylacetylene, followed by isomerization of the regioisomeric mixture gave the thermodynamic cyclobutenone **4-13** in 40% yield over two steps. Luche reduction[13] of the cyclobutenone provided the corresponding alcohol **4-14** in 92% yield. Finally, transformation of the alcohol to the phosphate afforded the desired allylic cyclobutylphosphate **4-15** in 20% yield. With the starting material in hand, the copper-catalyzed boryl substitution was investigated on this substrate (Scheme 4-5b). Under pre-optimized conditions,[12] allylic cyclobutylboronate **4-9** was obtained in a 50% ^{1}H NMR yield and 50% isolated yield after a short column chromatography using silica deactivated with 30% wt H_2O. Future work would involve improving the yield of phosphate **4-15**. Moreover, the SN_2 product **4-9** could be made optically pure by preparing alcohol **4-14** enantioselectively. Furthermore, a thorough examination of ligands may be appropriate in an effort to gain access to both the SN_2 and SN_2' products in a regiodivergent ligand-controlled manner, in which, the SN_2' product can be potentially obtained enantioconvergently.

4.4 Summary

In summary, the copper-catalyzed boryl substitution of allylic cyclobutylphosphates **4-11** and **4-15** provided access to the corresponding allylic cyclobutylboronates **4-8** and **4-9**, respectively. Allylic cyclobutylboronate **4-8** was found to be air-sensitive and unstable towards silica gel.

Future work would involve investigate the application of this scaffold in allylboration chemistry using techniques that minimize exposure to air. Moreover, allylic cyclobutylboronate **4-9** was found to be a stable allylboronate compound. Future work would include screening chiral ligands in an effort to prepare an allylic cyclobutylboronate in optically enriched form.

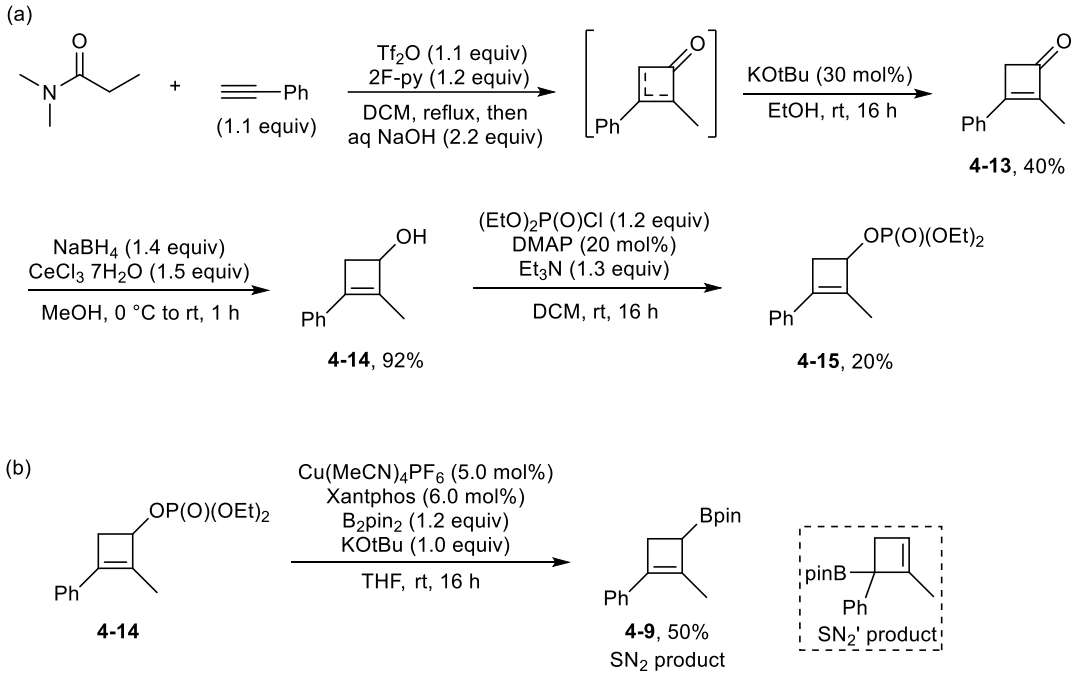

Scheme 4-5. Synthesis of an allylic cyclobutylphosphate and its copper-catalyzed allylic borylation

4.5 Experimental

4.5.1 General methods

Unless specified, all reactions were performed under nitrogen or argon atmosphere using glassware that was flame dried. Dichloromethane was used directly from a MBraun Solvent Purification System. Tetrahydrofuran was obtained from a MBraun Solvent Purification System

and subjected to three cycles of freeze-pump-thaw and stored in a Schlenk vessel under nitrogen. Bis(pinacolato)diboron (reagent grade, 99%) was purchased from Combi-Blocks and recrystallized from pentanes. Triethylamine was distilled over CaH_2 and stored under nitrogen. All other reagents were purchased from Sigma Aldrich, Combi-Blocks or Strem Chemicals and used without further purification. Thin layer chromatography (TLC) was performed using Merck Silica Gel 60 F254 plates and visualized with UV light and Phosphomolybdic Acid (PMA) stain. NMR spectrum were recorded on INOVA-400, INOVA-500 or INOVA-700 MHz instruments. The residual solvent protons (^{1}H) of $CDCl_3$ (7.26 ppm) and the solvent carbons (^{13}C) of $CDCl_3$ (77.06 ppm) were used as internal standards. ^{1}H NMR data are presented as follows: chemical shift in ppm (δ) downfield from tetramethylsilane (multiplicity, coupling constant, integration). The following abbreviations are used in reporting the ^{1}H NMR data: s, singlet; br s, broad singlet; d, doublet; t, triplet; q, quartet; app q, apparent quartet; m, multiplet. High-resolution mass spectra were recorded by the University of Alberta Mass Spectrometry Services Laboratory using either electron impact (EI) or electrospray ionization (ESI) techniques. Infrared spectra were obtained on a Nicolet Magna-IR with frequencies expressed in cm^{-1}.

4.5.2 Preparation of allylic cyclobutylphosphates 4-11 and 4-15

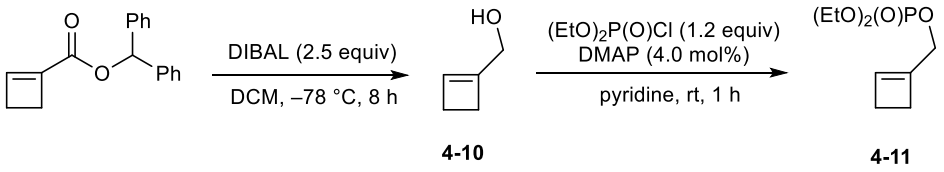

4-10 **4-11**

Following a literature procedure.[14] DIBAL-H (1.0M solution in THF, 45 mL, 45 mmol, 2.5 equiv) was added droppwise to a solution of benzhydrol cyclobutene 1-carboxyester (4.5 g, 18 mmol) in dry dichloromethane (45 mL) that was cooled to –78 °C. After stirring at –78 °C for 8

h, the reaction mixture was allowed to warm up to 0 °C and stopped with the addition of a saturated aqueous solution of potassium sodium tartrate (250 mL). The reaction mixture was allowed to stir vigorously for 1 h before separating organic layer. The aqueous layer was extracted with dichloromethane (3×25 mL) and the combined organic layers were dried over $MgSO_4$, filtered, and concentrated under reduced pressure. The crude mixture was purified by column chromatography (3:1 hexanes:ethyl acetate) to give the desired product **4-10** as a clear oil (72%, 1.1 g). **^{1}H NMR** (500 MHz, $CDCl_3$) δ 5.94 (s, 1H), 4.17–4.02 (m, 2H), 2.65–2.49 (m, 2H), 2.45–2.42 (m, 2H). Characterization data is consistent with that reported in literature.[14]

To a solution of alcohol **4-10** (580 mg, 6.90 mmol. 1.00 equiv), 4-dimethylaminopyridine (35 mg, 4.0 mol%) in pyridine (8.0 mL) was added dropwise diethyl chlorophosphite (1.2 mL, 8.3 mmol, 1.2 equiv) at 0 °C. The ice-bath was removed, and the reaction mixture was allowed to stir at rt for 1 h, resulting in a white precipitate. The reaction mixture was diluted with ethyl acetate (20 mL), then water (20 mL). The organic layer was extracted and washed with saturated aqueous copper sulfate (3×10 mL), brine, dried over $MgSO_4$, filtered, and concentrated under reduced pressure. The crude mixture was purified by column chromatography (1:2 hexanes:ethyl acetate) to give the desired product **4-11** as a clear oil (1.2 g, 80%). **^{1}H NMR** (500 MHz, $CDCl_3$) δ 6.00 (s, 1H), 4.45 (br d, J = 8.0 Hz, 2H), 4.14–4.09 (m, 5H), 2.54 (br s, 2H), 2.41 (br s, 2H), 1.33 (t, J = 7.0 Hz, 7H). **^{13}C NMR** (126 MHz, $CDCl_3$) δ 143.5 (d, J = 7.1 Hz), 131.9, 64.8 (d, J = 5.5 Hz), 63.8 (d, J = 5.8 Hz), 29.7, 27.2, 16.1 (d, J = 6.5 Hz). **^{31}P NMR** (162 MHz, $CDCl_3$) δ -0.61. **IR** (cast film, neat, cm^{-1}): 3056, 2982, 1030. **HRMS** (ESI) $[M+Na]^+$ calc. for $C_9H_{17}NaO_4P$, 243.0757; observed, 243.0754.

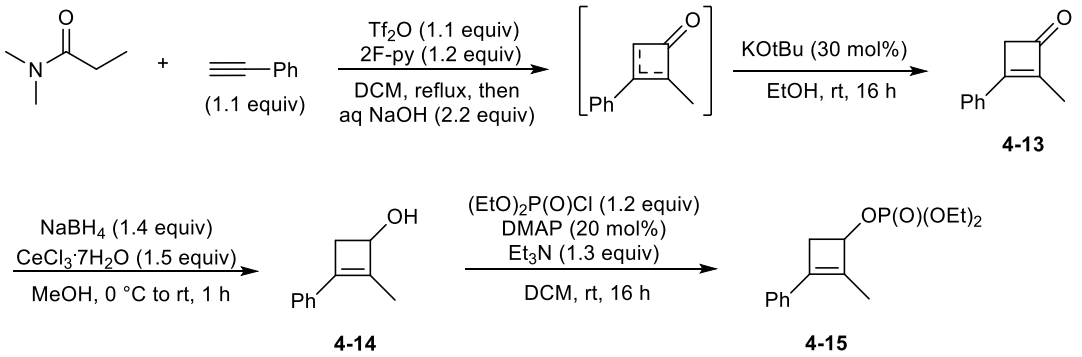

Cyclobutenone **4-13** was prepared according to a literature procedure.[12] (44% over two steps). **^{1}H NMR** (500 MHz, $CDCl_3$) δ 7.64–7.56 (m, 2H), 7.55–7.45 (m, 3H), 3.46 (q, J = 2.3 Hz, 2H), 2.01 (t, J = 2.4 Hz, 3H). Characterization data is consistent with that reported in literature.[12]

$NaBH_4$ (167 mg, 4.40 mmol, 1.4 equiv) was added in three portions over 15 min to a solution of cyclobutenone **4-13** (500 mg, 3.20 mmol, 1.00 equiv), $CeCl_3{\cdot}7H_2O$ (1.80 mg, 4.80 mmol, 1.5 equiv) in MeOH (16 mL) at 0 °C. The ice-bath was removed, and the reaction was allowed to stir at rt for 1 h, after which time the mixture was filtered over celite and concentrating the filtrate under reduced pressure. Water (15 mL) was added and the aqueous layer was extracted with ethyl acetate (3×15 mL), washed with brine, dried over $MgSO_4$, filtered, and concentrated under reduced pressure. The crude mixture was purified by column chromatography (1:1 hexanes:ethyl acetate) to give the desired product **4-14** as a yellow oil (460 mg, 92%). **^{1}H NMR** (500 MHz, $CDCl_3$) δ 7.40–7.32 (m, 4H), 4.57 (s, 1H), 3.06 (d, J = 12.2 Hz, 1H), 2.46 (d, J = 12.1 Hz, 1H), 2.02 (s, 3H), 1.67 (br s, 1H). **^{13}C NMR** (126 MHz, $CDCl_3$) δ 140.4, 138.1, 135.2, 128.4 (×2), 127.6, 126.4 (×2), 69.5, 39.0, 12.7. **HRMS** (ESI) $[M\text{-}H]^+$ calc. for $C_{11}H_{11}O$, 159.0810; observed, 159.0810. **IR** (cast film, CH_2Cl_2, cm^{-1}): 3319, 3027, 2912, 1446, 1065.

To a solution of alcohol **4-14** (300 mg, 1.90 mmol. 1.00 equiv), 4-dimethylaminopyridine (48 mg, 0.38 mmol, 20 mol%), triethylamine (0.34 mL, 0.24 mmol, 1.3 equiv) in dichloromethane (4 mL) was added dropwise diethyl chlorophosphite (0.35 mL, 0.24 mmol, 1.3 equiv) at 0 °C. The ice-bath was removed, and the reaction mixture was allowed to stir at rt for 16 h, resulting in a white precipitate. The reaction mixture was stopped with the addition of sat. $NaHCO_3$ (15 mL) and the aqueous layer was extracted with dichloromethane (3×15 mL). The combined organic layers were washed with brine, dried over $MgSO_4$, filtered, and concentrated under reduced pressure. The crude mixture was purified by column chromatography (1:1 hexanes:ethyl acetate) to give the desired product **4-15** as a clear oil (104 mg, 20%). **^{1}H NMR** (700 MHz, $CDCl_3$) δ 7.39–7.35 (m, 4H), 7.33–7.28 (m, 1H), 5.12–5.09 (m, 1H), 4.16 (app dqd, *J* = 14.2, 7.1, 5.0 Hz, 4H), 3.09 (app doublet of sextet, *J* = 12.2, 1.8 Hz, 1H), 2.78 (app doublet of sextet, *J* = 12.2, 1.1 Hz, 1H), 2.07–2.03 (m, *J* = 2.9 Hz, 3H), 1.37 (app tq, *J* = 7.0, 1.0 Hz, 6H). **^{13}C NMR** (126 MHz, $CDCl_3$) δ 139.2, 137.2 (d, *J* = 6.8 Hz), 134.4, 128.5 (×2), 128.1, 126.6 (×2), 73.0 (d, *J* = 7.2 Hz), 63.8 (d, *J* = 5.1 Hz) (×2), 36.6 (d, *J* = 3.6 Hz), 16.2 (d, *J* = 6.7 Hz) (×2), 12.9. **^{31}P NMR** (162 MHz, $CDCl_3$) δ -1.5. **IR** (cast film, CH_2Cl_2, cm^{-1}): 3051, 2983, 1446, 1037. **HRMS** (ESI) $[M+Na]^+$ calc. for $C_{15}H_{21}NaO_4P$, 319.1070; observed, 319.1055.

4.5.3 Preparation of allylic cyclobutylboronates 4-8 and 4-9

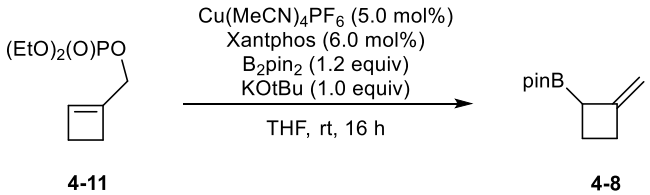

4-11 **4-8**

A microwave vial was charged with bis(pinacolato)diboron (79 mg, 0.31 mmol, 1.2 equiv), $[Cu(MeCN)_4]PF_6$ (5.0 mg, 0.013 mmol, 5.0 mol%) and Xantphos (8.0 mg, 0.014 mmol, 6.0

mol%), capped, and purged with argon. Tetrahydrofuran (0.7 mL) was added, and the reaction mixture was cooled 0 °C. Potassium *tert*-butoxide (1.0M solution in THF, 0.23 mL, 0.23 mmol, 1.0 equiv) was added dropwise followed by the dropwise addition of phosphate **4-11** (50 mg, 0.23 mmol, 1.0 equiv) at 0 °C. The ice-bath was removed, and the reaction was allowed to stir at rt for 16 h. The reaction mixture was stopped by the addition of sat. NH_4Cl (2 mL) and extracted with ethyl acetate (3×5 mL). The combined organic layers were washed with brine, dried over $MgSO_4$, filtered, and concentrated under reduced pressure. The crude mixture was purified by flash column chromatography using 30 wt% deionized water deactivated silica (20:1 hexanes:ethyl acetate, TLC performed using 5:1 hexanes:ethyl acetate) to give the desired product **4-8** as a clear oil (15.1 mg, 36%). **^{1}H NMR** (498 MHz, $CDCl_3$) δ 4.69 (app dq, J = 7.3, 2.5 Hz, 2H), 2.81–2.67 (m, 3H), 2.09–1.95 (m, 2H), 1.26 (s, 12H). **^{13}C NMR** (126 MHz, $CDCl_3$) δ 151.2, 104.3, 83.2 (×2), 32.3, 24.8, 24.7, 24.6 (×2), 18.2 (the boron-bound carbon was not detected due to quadrupolar relaxation of boron). **^{11}B NMR** (128 MHz, $CDCl_3$) δ 33.4. **IR** (cast film, CH_2Cl_2 cm^{-1}): 3027, 2977, 1447, 1179. **HRMS** (EI) calc. for $C_{11}H_{19}O_2B$, 194.1478; observed, 194.1473.

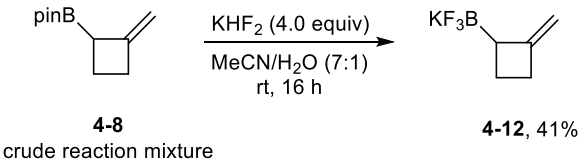

To a round bottom flask charged with allylic cyclobutylboronate **4-8** (1.0 g, 2.5 mmol, 1.0 equiv) and potassium hydrogen difluoride (796 mg, 10.0 mmol, 4.0 equiv) was added distilled water (2.8 mL) and acetonitrile (18 ml). The reaction was allowed to stir at rt for 16 h. The solvents were removed under reduced pressure and the crude reaction mixture was dried under high vacuum. The resulting crude solid was suspended in diethyl ether (20 ml) then filtered and

washed with diethyl ether (4×20 mL). The product was extracted with acetonitrile (4×35 mL) and filtered. The solvent from the resulting filtrate was removed under reduced pressure to give the desired product as a white solid (913 mg, 97%). **^{1}H NMR** (500 MHz, CD_3CN) δ 4.40 (s, 1H), 4.35 (s, 1H), 2.60–2.57 (m, 1H), 2.53–2.42 (m, 1H), 2.09–1.98 (m, 1H), 1.81–1.77 (m, 1H), 1.71–1.62 (m, 1H). **^{13}C NMR** (126 MHz, CD_3CN) δ 160.3, 118.3, 32.1, 19.5 (the boron-bound carbon was not detected due to quadrupolar relaxation of boron). **^{11}B NMR** (128 MHz, $(D_3C)_2CO$) δ 4.2. **^{19}F NMR** (376 MHz, $(D_3C)_2CO$) δ -147.3. **IR** (cast film, acetonitrile, cm^{-1}): 3068, 2970, 1658. **HRMS** (ESI) $[M]^{*-}$ calc. for $C_5H_7BF_3$, 135.0598; observed, 135.0592.

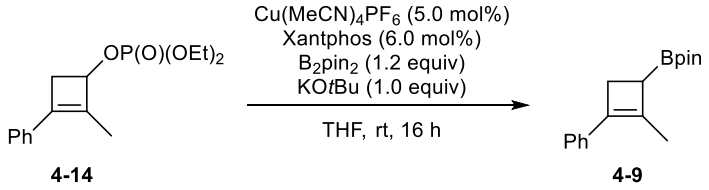

4-14 **4-9**

A microwave vial was charged with bis(pinacolato)diboron (61 mg, 0.24 mmol, 1.2 equiv), $[Cu(MeCN)_4]PF_6$ (4.0 mg, 0.010 mmol, 5.0 mol%) and Xantphos (7.0 mg, 0.012 mmol, 6.0 mol%), capped, and purged with argon. Tetrahydrofuran (0.7 mL) was added, and the reaction mixture was cooled 0 °C. Potassium *tert*-butoxide (1.0M solution in THF, 0.20 mL, 0.20 mmol, 1.0 equiv) was added dropwise followed by the dropwise addition of phosphate **4-14** (59 mg, 0.2 mmol, 1.0 equiv) at 0 °C. The ice-bath was removed, and the reaction was allowed to stir at rt for 16 h. The reaction mixture was stopped by the addition of sat. NH_4Cl (2 mL) and extracted with ethyl acetate (3×7 mL). The combined organic layers were washed with brine, dried over $MgSO_4$, filtered, and concentrated under reduced pressure. The crude mixture was purified by flash column chromatography using 30 wt% deionized water deactivated silica (20:1 hexanes:ethyl acetate, TLC performed using 5:1 hexanes:ethyl acetate) to give the desired

product **4-9** as a clear oil (15.1 mg, 36%). **^{1}H NMR** (500 MHz, $CDCl_3$) δ 7.33–7.29 (m, 4H), 7.18–7.14 (m, 1H), 2.77–2.70 (m, 1H), 2.70–2.62 (m, 1H), 2.38 (br s, 1H), 2.03 (m, 3H), 1.25 (s, 9H). **^{13}C NMR** (126 MHz, $CDCl_3$) δ 140.2, 136.8, 136.5, 128.3 (×2), 126.1, 125.2 (×2), 83.1 (×2), 27.9, 24.9 (×2), 24.8 (×2), 16.4 (the boron-bound carbon was not detected due to quadrupolar relaxation of boron). **^{11}B NMR** (128 MHz, $CDCl_3$) δ 33.6. **IR** (cast film, CH_2Cl_2 cm^{-1}): 3059, 2978, 1492, 1472, 1166. **HRMS** (EI) calc. for $C_{17}H_{23}O_2B$, 270.2791; observed, 270.1795.

4.6 References

[1] Diner, C.; Szabo, K. J. *J. Am. Chem. Soc.* **2017**, *139*, 2−14.

[2] Rauniyar, V.; Zhai, H.; Hall, D. G. *J. Am. Chem. Soc.* **2008**, *130*, 8481−8490.

[3] Kim, Y-R.; Hall, D. G. *Org. Biomol. Chem.* **2016**, *14*, 4739−4748.

[4] Ding, J.; Rybak, T.; Hall, D. G. *Nature Commun.* **2014**, *5*, 5474.

[5] Ito, H.; Yamanaka, H.; Tateiwa, J.; Hosomi, A. *Tetrahedron Lett.* **2000***, 41*, 6821–6285.

[6] Takahashi, K.; Ishiyama, T.; Miyaura, N. *Chem. Lett*. **2000**, 982–983.

[7] Ito, H.; Kawakami, C.; Sawamura, M. *J. Am. Chem. Soc.* **2005**, *127*, 16034−16035.

[8] Ito, H.; Ito, S.; Sasaki, Y.; Matsuura, K.; Sawamura, M. *J. Am. Chem. Soc.* **2007**, *129*, 14856−14857.

[9] Ito, H.; Okura, T.; Matsuura, K.; Sawamura, M. *Angew. Chem. Int. Ed.* **2010**, *49*, 560−563.

[10] Select examples of copper-catalyzed alkyl substitution between alkylborans and/or alkylboronates and allylic chloride and/or phosphates. (a) Yasuda, Y.; Ohmiya, H.; Sawamura, M. *Angew. Chem*. *Int. Ed.* **2016**, *55*, 10816−10820. (b) Hojoh, K.; Shido, Y.; Ohmiya, H.;

Sawamura, M. *Angew. Chem*. *Int. Ed.* **2014**, *53*, 4954−4958. (c) Yasuda, Y.; Ohmiya, H.; Sawamura, M. *Synthesis* **2018**, *50*, 2235−2246.

[11] (a) Eisold, M.; Kiefl, G. M.; Didier, D. *Org. Lett.* **2016**, *18*, 3022−3025. (b) Eisold, M.; Didier, D. *Org. Lett.* **2017**, *19*, 4046−4049.

[12] Ito, H.; Hortia, Y.; Sawamura, M. *Adv. Synth. Catal*. **2012**, *354*, 813–817.

[13] Clement, H. A.; Boghi, M.; Mcdonald, R. M.; Bernier, L.; Coe, J. W.; Farrell, W.; Helal, C. J.; Reese, M. R.; Sach, N. W.; Lee, J. C.; Hall, D. G. *Angew. Chem. Int. Ed*. **2019**, *131*, 18576–18580.

[14] Luche, J. L. *J. Am. Chem. Soc.* **1978**, *100*, 2226–2227.

[15] Song, A.; Lee, J. C.; Parker, K. A.; Sampson, N. S. *J. Am. Chem. Soc.* **2010**, *132*, 10513–10520.

Chapter 5. Conclusions and Future Perspectives

Cyclobutanes represent an important structural motif found in numerous natural products and pharmaceutical agents. Polysubstituted analogs have gained continuous interest in drug discovery for their applications as conformationally rigid scaffolds and as a non-classical bioisostere for arenes. Accessing cyclobutanes with a specific substitution pattern and configuration remains a notorious challenge in modern organic synthesis. Over the past two decades, there has been a surge of literature reports on the preparation of optically enriched polysubstituted cyclobutanes as described in Chapter 1. However, reports on the preparation of optically enriched cyclobutylboronates remain limited (Chapter 1). Cyclobutylboronates can serve as a highly versatile synthetic intermediate because the boronic ester group can undergo several stereospecific transformations, including the famed Suzuki-Miyaura cross-coupling.

In Chapter 2, the successful preparation of an optically enriched *cis*-1,2-disubstituted cyclobutylboronate scaffold was described. Since the cyclobutylboronate scaffold can serve as a versatile intermediate, efforts should be made to investigate the preparation of this scaffold beyond a gram scale. As the boronic ester substituent can undergo a number of stereospecific transformations, the *trans*-1,2-disubstituted cyclobutylboronate scaffold would serve as a versatile building block in its own right. While preliminary efforts were made to epimerize the cyclobutylboronate to the corresponding trans-diastereomer, attempts to derivatize the

cyclobutylboronate scaffold for epimerization should be conducted. This includes attempting to epimerize the less liable amide derivative of the scaffold and looking into different boron protecting groups. In order to further expand the scope of this project, the enantioselective copper-catalyzed conjugate borylation of β-substituted cyclobutanoates can be investigated. Furthermore, the three-component enantioselective copper-catalyzed conjugate borylation-aldol reaction was successfully demonstrated in a single example. Efforts should be made to investigate the scope of this reaction with different aryl and heteroaryl aldehydes.

In Chapter 3, the optically enriched cyclobutylboronate scaffold was successfully applied towards a highly diastereoselective nickel/photoredox dual-catalyzed cross-coupling reaction with excellent retention of optical purity. This method provided access towards trans aryl, heteroaryl and cycloalkenyl cyclobutylcarboxyesters that are relevant in drug discovery. Efforts can be made to both improve the efficiency of the route and attain access toward the *cis*-heteroaryl cyclobutylcarboxyesters using the transition metal-free cross-coupling methods developed by Aggarwal and co-workers.[1]

Chapter 4 described the preparation of allylic cyclobutylboronates by way of the copper-catalyzed boryl substitution of allylic cyclobutylphosphates. Future work would include investigating an enantioselective protocol for the preparation of the allylic cyclobutylboronates and its application in carbonyl allylboration and regiocontrolled cross-coupling chemistry.

5.1 References

[1] A. Bonet, M. Odachowski, D. Leonori, S. Essafi, V. K. Aggarwal, *Nat. Chem.* **2014**, *6*, 584–589.

Bibliography

[1] Dembitsky, V. M. *Phytomedicine*, **2014**, *21*, 1559–1581.

[2] Tsai, I-L.; Lee, F-P.; Wu, C-C; Duh, C-Y.; Ishikawa, T.; Chen, J-J.; Chen, Y. C.; Seki H.; Chen, I. S. *Planta Med.* **2005**, *71*, 535–542.

[3] Jiao, W. H.; Ga,o H.; Li, C. Y.; Zhao, F.; Jiang, R.W.; Wang, Y.; Zhou, G. X.; Yao, X. S. *J. Nat. Prod*. **2010**, *73*, 167-171.

[4] Piao, S-J.; Song, Y-L.; Jiao, W-H.; Yang, F.; Liu, X-F.; Chen, W-S.; Han, B. N.; Lin, W-H. *Org. Lett*. **2013**, *15*, 3526–3529.

[5] a) Field, A.; Tuomari, A.; Mcgeever-Rubin, B.; Terry, B.; Mazina, K.; Haffey, M.; Hagen, M. E.; Clark, J. M.; Braitman, A.; Slusarchyk, W. A.; Young, M. G.; Zahler, R. *Antiviral Research*, **1990**, *13*, 41–52. b) Yamanaka, G.; Wilson, T.; Innaimo, S.; Bisacchi, G. S.; Egli, P.; Rinehart, J. K.; Zahler, R.; Colonno, R. J. *Antimicrobial Agents and Chemotherapy*, **1999**, *43*, 190–193. c) Hoffman, V. F.; Skiest, D. J. *Expert Opinion on Investigational Drugs*, **2000**, *9*, 207–220.

[6] Wager, T. T.; Pettersen, B. A.; Schmidt, A. W.; Spracklin, D. K.; Mente, S.; Butler, T. W.; Howard, H.; Lettiere, D. J.; Rubitski, D. M.; Wong, D. F.; Nedza, F. M.; Nelson, F. R.; Rollema, H.; Raggon, J. W.; Aubrecht, J.; Freeman, J. K.; Marcek, J. M.; Cianfrogna, J.; Cook, K. W.; James, L. C.; Chatman, L. A.; Iredale, P. A.; Banker, M. J.; Homiski, M. L.; Munzner, J. B.; Chandrasekaran, R. Y. *J. Med. Chem*. **2011**, *54*, 7602−7620.

[7] Wrobleski, M. L.; Reichard, G. A.; Paliwal, S.; Shah, S.; Tsui, H. C.; Duffy, R. A.; Lachowicz, J. E.; Morgan, C. A.; Varty, C. B.; Shiha, Y. N. *Bioorg. Med. Chem. Lett.* **2006,** *16*, 3859–3863.

[8] Stepan, A. F.; Subramanyam, C.; Efremov, I. V.; Dutra, J. K.; O'Sullivan, T. J.; DiRico, K. J.; McDonald, W. S.; Won, A.; Dorff, P. H., Nolan, C. E.; Becker, S. L.; Pustilnik, L. R.; Riddel, D. R.; Kauffman, G. W.; Kormos, B. L.; Zhang, L.; Lu, Y.; Capetta, S. H.; Green, M. E.; Karki, K.; Sibley, E.; Atchison, K. P.; Hallgren, A. J.; Oborski, C. E.; Robshaw, A. E.; Sneed, B.; O'Donnell, C. J. *J. Med. Chem.* **2012**, *55*, 3414–3424.

[9] Hu, J.-L.; Feng, L.-W.; Wang, L.; Xie, Z.; Tang, Y.; Li, X. *J. Am. Chem. Soc.* **2016**, *138*, 13151–13154.

[10] Duan, G.-J.; Ling, J.-B.; Wang, W.-P.; Luo, Y.-C.; Xu, P.-F. *Chem. Commun.* **2013**, *49*, 4625–4627.

[11] Albrecht, L.; Dickmeiss, G.; Acosta, F. C.; Rodriguez-Escrich, C.; Davis, R. L.; Jørgensen, K. A. *J. Am. Chem. Soc*. **2012**, *134*, 2543–2546.

[12] Du, J.; Skubi, K. L.; Schultz, D. M.; Yoon, T. P. *Science* **2014**, *344*, 392–396.

[13] Miller, Z. D.; Lee, B. J.; Yoon, T. P. *Angew. Chem. Int. Ed.* **2017**, *56*, 11891–11895.

[14] Daub, M. E.; Jung, H.; Lee, B. J.; Won, J.; Baik, M.-H.; Yoon, T. P. *J. Am. Chem. Soc.* **2019**, *141*, 9543–9547.

[15] Huang, X.; Quinn, T. R.; Harms, K.; Webster, R. D.; Zhang, L.; Wiest, O.; Meggers, E. *J. Am. Chem. Soc.* **2017**, *139*, 9120–9123.

[16] Rigotti, T.; Mas-Balleste, R.; Aleman, J. *ACS Catal*. **2020**, *10*, 5335−5346.

[17] García-Morales, C.; Ranieri, B.; Escofet, I.; López-Suarez, L.; Obradors, C.; Konovalov, A. I.; Echavarren, A. M. *J. Am. Chem. Soc.* **2017,** *139*, 13628–13631.

[18] Parsutkar, M. M.; Pagar, V. V.; Rajanbabu, T. V. *J. Am. Chem. Soc.* **2019**, *141*, 15367–15377.

[19] Xiao, K.-J.; Lin, D. W.; Miura, M.; Zhu, R.-Y.; Gong, W.; Wasa, M.; Yu, J.-Q. *J. Am. Chem. Soc*. **2014**, *136*, 8138–8142.

[20] Wu, Q.-F.; Wang, X.-B.; Shen, P.-X.; Yu, J.-Q. *ACS Catal.*, **2018,** *8*, 2577–2581.

[21] Yu, J.-Q.; Xiao, L.-J.; Hong, K.; Luo, F.; Hu, L.; Ewing, W. R.; Yeung, K.-S. *Angew. Chem*. In. Ed. **2020**, *59*, 2–9.

[22] Beck, J. C.; Lacker, C. R.; Chapman, L. M.; Reisman, S. E. *Chem. Sci.*, **2019**, *10*, 2315–2319.

[23] Chen, Y-J.; Hu, T-J.; Feng, C-G.; Lin, G-Q. *Chem. Commun.* **2015**, *51*, 8773–8776.

[24] Zhong, C.; Huang, Y.; Zhang, H.; Zhou, Q.; Liu, Y.; Lu, P. *Angew. Chem. Int. Ed*. **2020**, *59*, 2750 –2754.

[25] Panish, R.; Chintala, S. R.; Boruta, D. T.; Fang, Y.; Taylor, M. T.; Fox, J. M. *J. Am. Chem. Soc*. **2013**, *135*, 9283–9286.

[26] Wang, Y.-M.; Bruno, N. C.; Placeres, Á. L.; Zhu, S.; Buchwald, S. L. *J. Am. Chem. Soc.*, **2015**, *137*, 10524–10527.

[27] Lorton, C.; Castanheiro, T.; Voituriez, A. *J. Am. Chem. Soc.* **2019**, *141*, 10142−10147.

[28] Sandford, C.; Aggarwal, V. K. *Chem. Commun.* **2017**, *53*, 5481–5494.

[29] Man, H-W.; Hiscox, W. S.; Matteson, D. S. *Org. Lett.* **1999**, *1*, 379–381.

[30] Coote, S. C.; Bach, T. *J. Am. Chem. Soc.* **2013**, *135*, 14948–14951.

[31] Guisán-Ceinos, M.; Parra, A.; Martín-Heras, V.; Tortosa, M. *Angew. Chem. Int. Ed.* **2016**, *128*, 7038–7086.

[32] Clement, H. A.; Boghi, M.; Mcdonald, R. M.; Bernier, L.; Coe, J. W.; Farrell, W.; Helal, C. J.; Reese, M. R.; Sach, N. W.; Lee, J. C.; Hall, D. G. *Angew. Chem. Int. Ed*. **2019**, *131*, 18576–18580.

[33] Shen, P.-X.; Hu, L.; Shao, Q.; Hong, K.; Yu, J.-Q. *J. Am. Chem. Soc.* **2018**, *140*, 6545–6549.

[34] Eisold, M.; Kiefl, G. M.; Didier, D. *Org. Lett.* **2016**, *18*, 3022−3025.

[35] Matteson, D. S.; Ray, R. *J. Am. Chem. Soc.* **1980**, *102*, 7590–7591.

[36] Matteson, D. S.; Sadhu, K. M. *J. Am. Chem. Soc.* **1983**, *105*, 2077–2078.

[37] Eisold, M.; Didier, D. *Org. Lett.* **2017**, *19*, 4046−4049.

[38] Whyte, A.; Mirabi, B.; Torelli, A.; Prieto, L.; Bajohr, J.; Lautens, M. *ACS Catal.* **2019**, *9*, 9253–9258.

[39] Ito, H.; Yamanaka, H.; Tateiwa, J.; Hosomi, A. *Tetrahedron Lett.* **2000***, 41*, 6821–6285.

[40] Takahashi, K.; Ishiyama, T.; Miyaura, N. *Chem. Lett*. **2000**, 982–983.

[41] Mun, S.; Lee, J. E.; Yun, J. *Org. Lett.* **2006**, *8*, 4887–4889.

[42] Lee. J. E.; Yun, J. *Angew. Chem. Int. Ed*. **2008**, *47*, 145–147.

[43] Feng, X.; Yun, J. *Chem. Commun*. **2009**, 6577–6579.

[44] Chen, I. H.; Yin, L.; Itano, W.; Kanai, M.; Shibasaki, M. *J. Am. Chem. Soc.* **2009**, *131*, 11664–11665.

[45] Dang, L.; Lin, Z.; Marder, T. B. *Organometallics*, **2008**, *27*, 4443–4454.

[46] Chen, Y-J.; Hu, T-J.; Feng, C-G.; Lin, G-Q. *Chem. Commun.* **2015**, *51*, 8773—8776.

[47] Perera, D.; Tucker J. W.; Brahmbhatt, S.; Helal, C. J.; Chong, A.; Farrell, W.; Richardson, P.; Sach, N. W. *Science* **2018**, *359*, 429–434.

[48] a) Naud, F.; Malan, C.; Spindler, F.; Rüggeberg, C.; Schmidt, A. T.; Blaser, H.-U. *Adv. Synth. Catal.* **2016**, *348*, 47–50. b) Tellers, D. M.; Bio, M.; Song, Z. J.; McWilliams, J. C.; Sun, Y. *Tetrahedron: Asymmetry* **2006**, *17*, 550–553. Pd-catalyzed intramolecular arylative

desymmetrization of 1,3-diketones: c) Zhu, C.; Wang, D.; Zhao, Y.; Sun, W.-Y.; Shi, Z. *J. Am. Chem. Soc*. **2017**, *139*, 16486–16489.

[49] Slater, C. S.; Savelski, M. J.; Hitchcock, D.; Cavanagh, E. J. *J Environ Sci Heal Part A,* **2016***, 51*, 487–494.

[50] Rhodes, G. *Crystallography made crystal clear (2nd ed.),* **2000***,* San Diego: Academic Press.

[51] Zhu, C.; Wang, D.; Zhao, Y.; Sun, W.-Y.; Shi, Z. *J. Am. Chem. Soc*, **2017**, *139*, 16486–16489.

[52] Carey, J. S.; Laffan, D.; Thomson, C.; Williams, M. T. *Org. Biomol. Chem.* **2006**, *4*, 2337−2347.

[53] Jana, R.; Pathak, T. P.; Sigman, M. S. *Chem. Rev*. **2011***, 111*, 1417–1492.

[54] Imao, D.; Glasspoole, B. W.; Laberge, V. S.; Crudden, C. M. *J. Am. Chem. Soc.* **2009**, *131*, 5024−5025.

[55] Uenishi, J.; Beau, J. M.; Armstrong, R. W.; Kishi, Y. *J. Am. Chem. Soc.* **1987**, *109*, 4756−4758.

[56] Matos, K.; Soderquist, J. A. *J. Org. Chem.* **1998**, *63*, 461−470.

[57] Daini, M.; Suginome, M. *J. Am. Chem. Soc.* **2011**, *133*, 4758−4761.

[58] Ohmura, T.; Awano, T.; Suginome, M. *J. Am. Chem. Soc.* **2010**, *132*, 13191−13193.

[59] Awano, T.; Ohmura, T.; Suginome, M. *J. Am. Chem. Soc.* **2011**, *133*, 20738−20741.

[60] Sandrock, D. L.; Jean-Gérard, L.; Chen, C.-Y.; Dreher, S. D.; Molander, G. A. 26

J. Am. Chem. Soc. **2010**, *132*, 17108−17110.

[61] Lee, J. C. H.; Mcdonald, R.; Hall, D. G. *Nat. Chem.* **2011**, *3,* 894–899.

[62] Lee, J. C. H.; Sun, H.-Y.; Hall, D. G. *J. Org. Chem.* **2015**, *80*, 7134–7143.

[63] Tellis, J. C.; Primer, D. N.; Molander, G. A. *Science* **2014**, *345*, 433–436.

[64] Khatib, M. E.; Augusto, R.; Serafim, M.; Molander, G. A. *Angew. Chem. Int. Ed*. **2016**, *55*, 254 –258.

[65] Milligan, J. A.; Phelan, J. P.; Badir, S. O.; Molander, G. A. *Angew. Chem. Int. Ed*. **2019**, *58,* 6152–6163.

[66] Gutierrez, O.; Tellis, J. C.; Primer, D. N.; Molander, G. A.; Kozlowski, M. C. *J. Am. Chem. Soc.* **2015**, *137*, 4896–4899.

[67] He, J.; Shao, Q.; Wu, Q.; Yu, J.-Q. *J. Am. Chem. Soc.* **2017**, *139*, 3344–3347.

[68] Molander, G. A.; Wisniewski, S. R.; Hosseini-Sarvari, M. *Adv. Synth. Catal.* **2013**, *355*, 3037–3057.

[69] Hoang, G. L.; Takacs, J. M. *Chem. Sci.* **2017**, *8*, 4511–4516.

[70] Luisi, R.; Giovine, A.; Florio, S. *Chem. Eur. J*. **2010**, *16*, 2683−2687.

[71] Fritzemeier R. G.; Medici, E. J.; Szwetkowski, C.; Wonilowicz, L. G.; Sibley, C. D.; Slebodnick, C.; Santos, W. L. *Org. Lett.* **2019**, *21*, 8053−8057.

[72] Tellis, J. C.; Amani, J.; Molander, G. A. *Org. Lett.* **2016**, *18*, 2994−2997.

[73] Giustra, Z. X.; Yang, X.; Chen, M.; Bettinger, H. F.; Liu, S. Y. *Angew. Chem. Int. Ed*. **2019**, *58*, 18918–18922.

[74] Gutiérrez-Bonet, Á.; Tellis, J. C.; Matsui, J. K.; Vara, B. A.; Molander, G. A. *ACS Catal.* **2016**, *6*, 8004–8008.

[75] Hanss, D.; Freys, J. C.; Bernardinelli, G.; Blanhard, N. *Eur. J. Inorg. Chem*. **2009**, *2009*, 4850–4859.

[76] Welsch, M. E.; Snyder, S. A.; Stockwell, B. R. *Curr. Opin. Chem. Biol.* **2010**, *14*, 347–361.

[77] Primer, D. N.; Molander, G. A. *J. Am. Chem. Soc*. **2017**, *139*, 9847−9850.

[78] Skubi, K. L.; Kidd, J. B.; Jung, H.; Guzei, I. A.; Baik, M-H.; Yoon, T. P. *J. Am. Chem. Soc*. **2017***, 139*, 17186−17192.

[79] Diner, C.; Szabo, K. J. *J. Am. Chem. Soc.* **2017**, *139*, 2−14.

[80] Rauniyar, V.; Zhai, H.; Hall, D. G. *J. Am. Chem. Soc.* **2008**, *130*, 8481−8490.

[81] Kim, Y-R.; Hall, D. G. *Org. Biomol. Chem.* **2016**, *14*, 4739−4748.

[82] Ding, J.; Rybak, T.; Hall, D. G. *Nature Communications* **2014**, *5*, 5474.

[83] Ito, H.; Kawakami, C.; Sawamura, M. *J. Am. Chem. Soc.* **2005**, *127*, 16034−16035.

[84] Ito, H.; Ito, S.; Sasaki, Y.; Matsuura, K.; Sawamura, M. *J. Am. Chem. Soc.* **2007**, *129*, 14856−14857.

[85] Ito, H.; Okura, T.; Matsuura, K.; Sawamura, M. *Angew. Chem*. **2010**, *122*, 570−573.

[86] (a) Yasuda, Y.; Ohmiya, H.; sawamura, M. *Angew. Chem*. **2016**, *55*, 10816−10820. (b) Hojoh, K.; Shido, Y.; Ohmiya, H.; Sawamura, M. *Angew. Chem*. **2014**, *53*, 4954−4958. (c) Yasuda, Y.; Ohmiya, H.; sawamura, M. *Synthesis* **2018**, *50*, 2235−2246.

[87] Ito, H.; Hortia, Y.; Sawamura, M. *Adv. Synth. Catal*. **2012**, *354*, 813–817.

[88] Luche, J. L. *J. Am. Chem. Soc.* **1978**, *100*, 2226–2227.

[89] Song, A.; Lee, J. C.; Parker, K. A.; Sampson, N. S. *J. Am. Chem. Soc.* **2010**, *132*, 10513–10520.

Appendices

Appendix 1. Selected NMR spectral reproductions

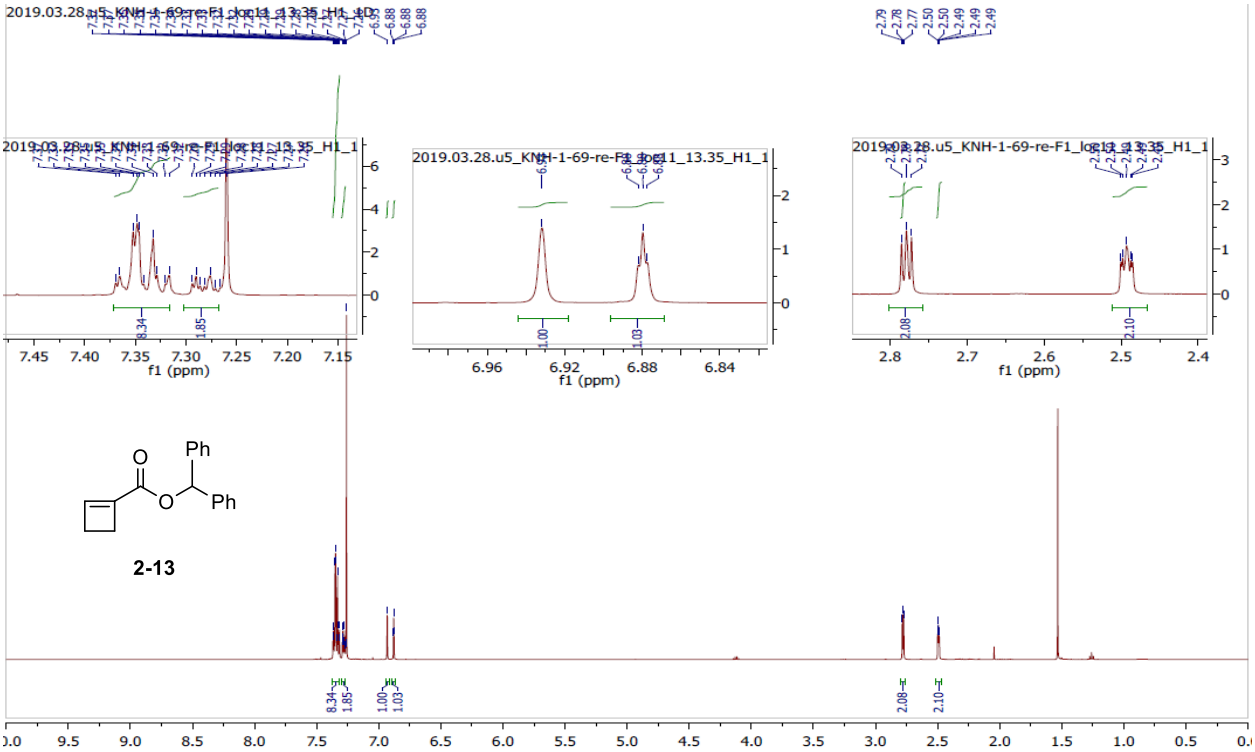

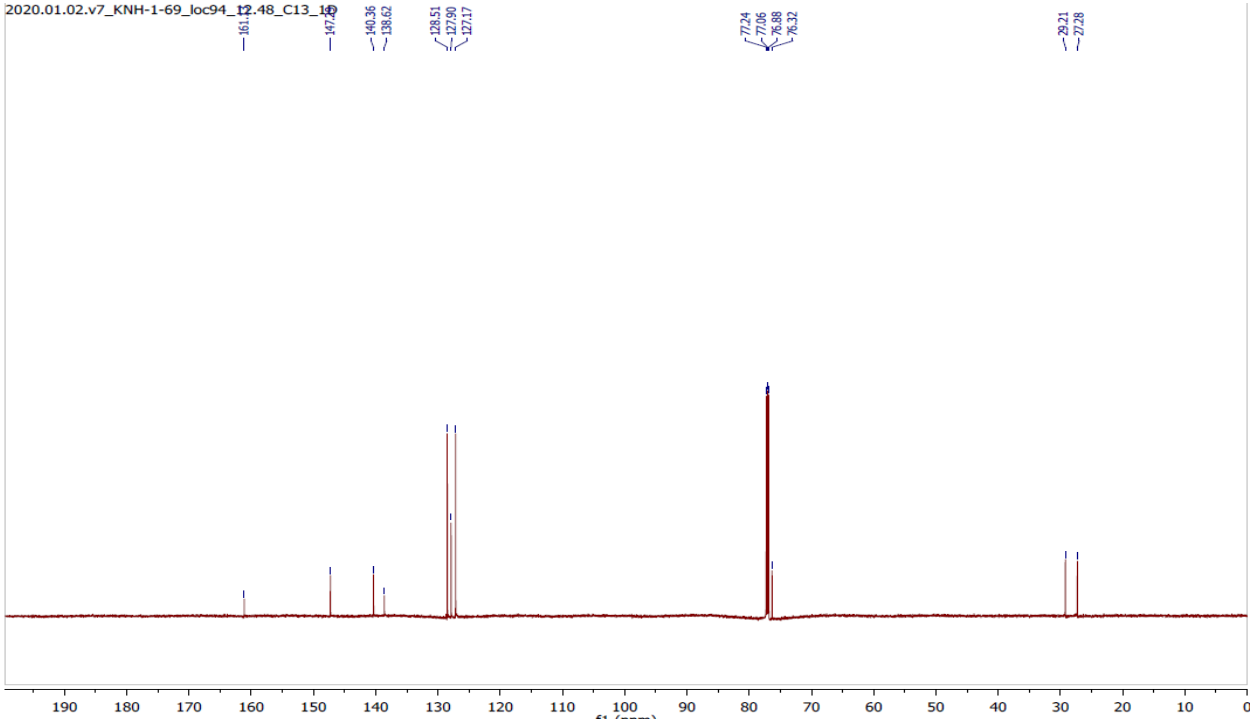

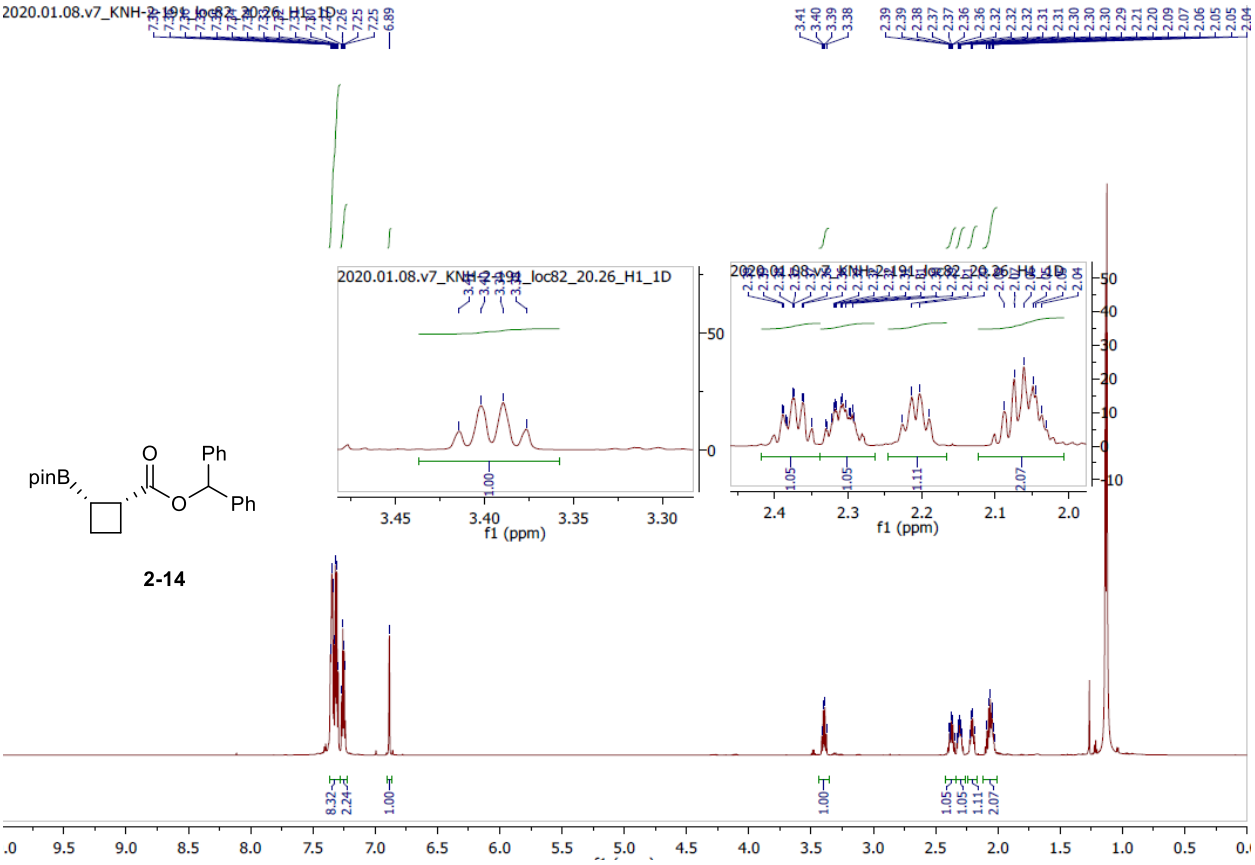
2020.01.08.v7_KNH-2-191_loc82_20.26_H1_1D
pinB
O
Ph
O
Ph
2-14
f1 (ppm)

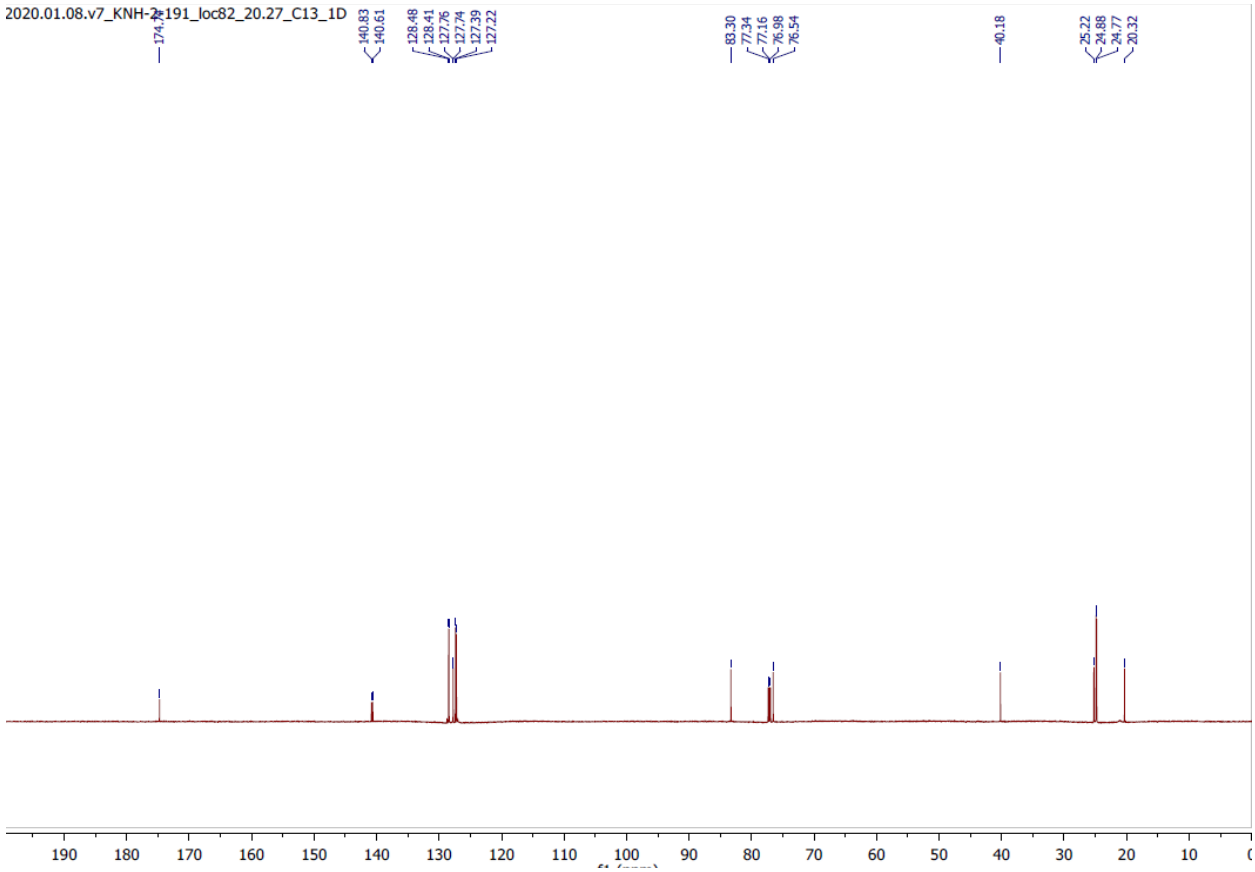
2020.01.08.v7_KNH-2-191_loc82_20.27_C13_1D
f1 (ppm)

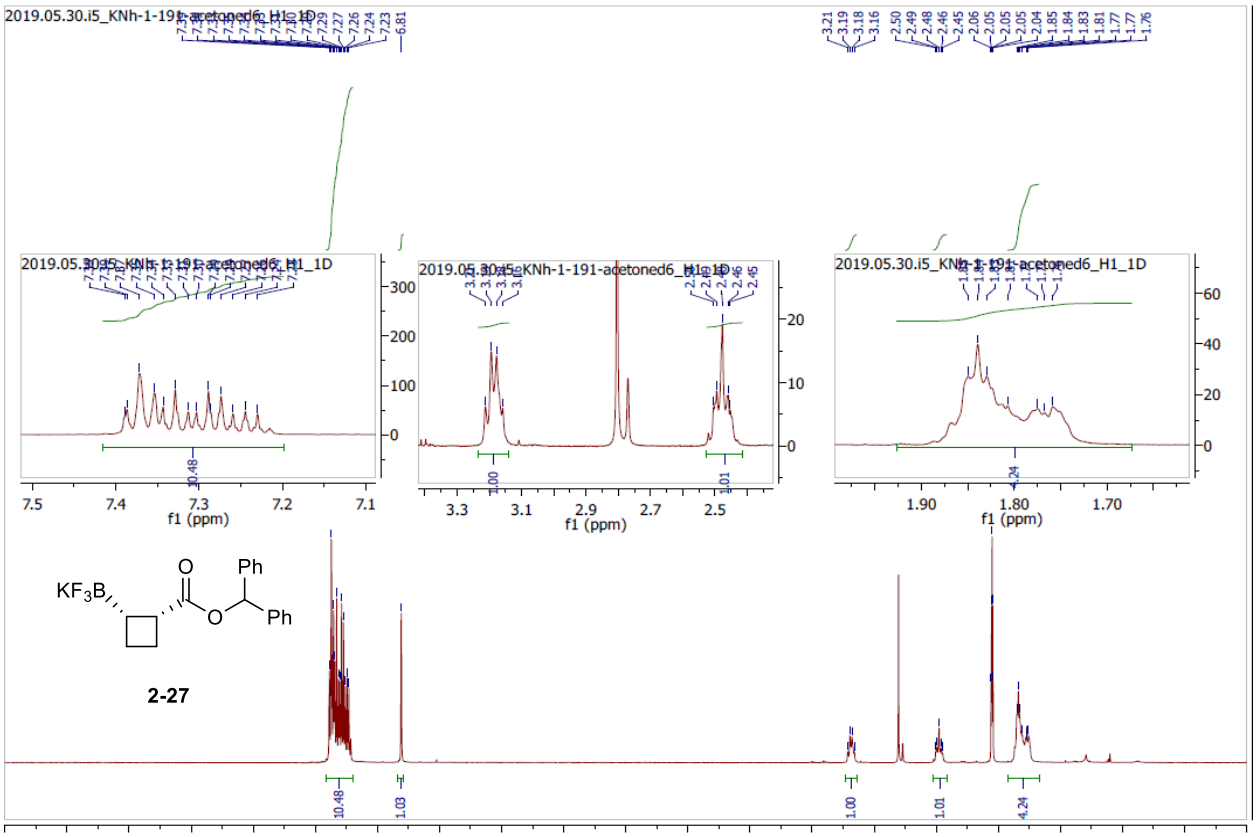
2019.05.30.i5_KNh-1-191-acetoned6_H1_1D
f1 (ppm)
KF3B
O
Ph
O
Ph
2-27

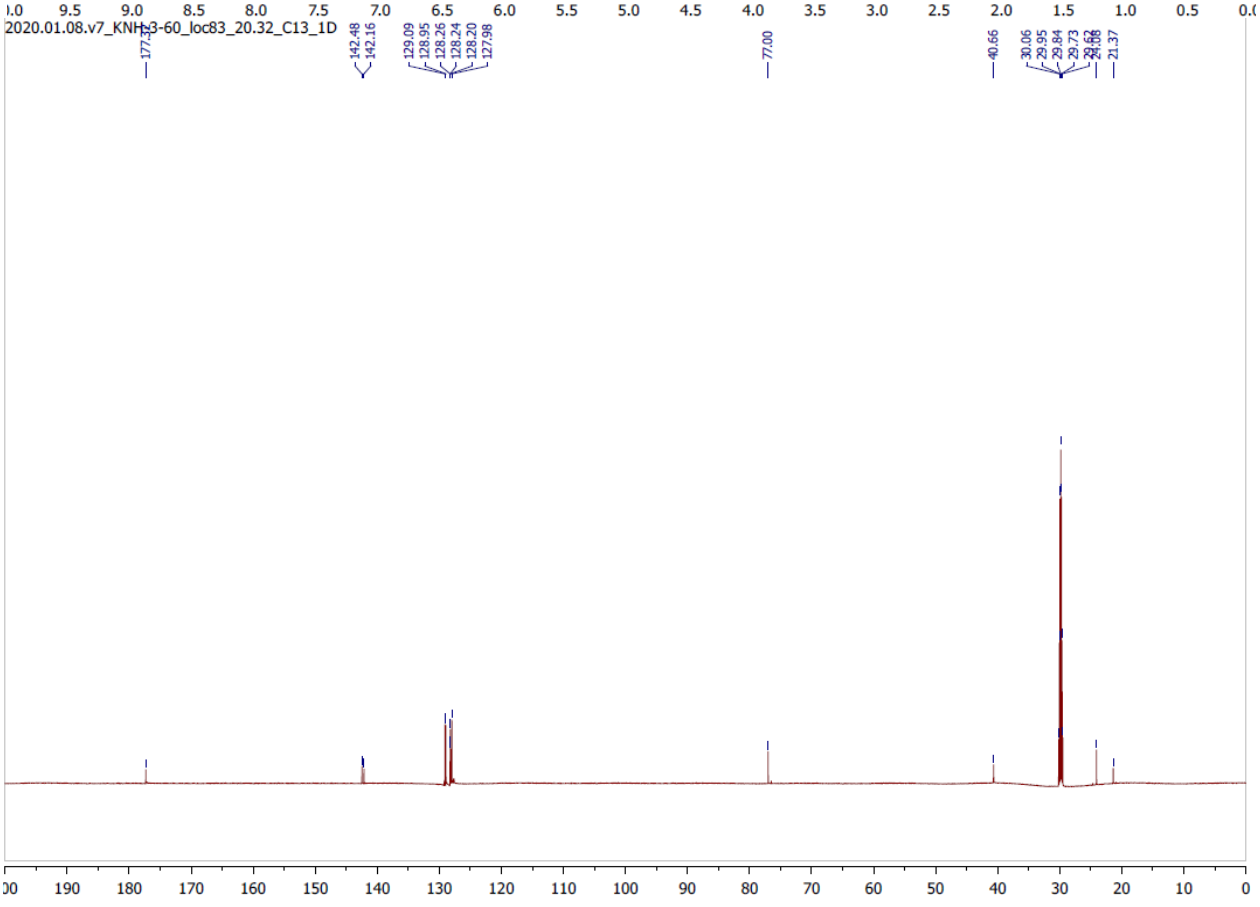
2020.01.08.v7_KNH-3-60_loc83_20.32_C13_1D

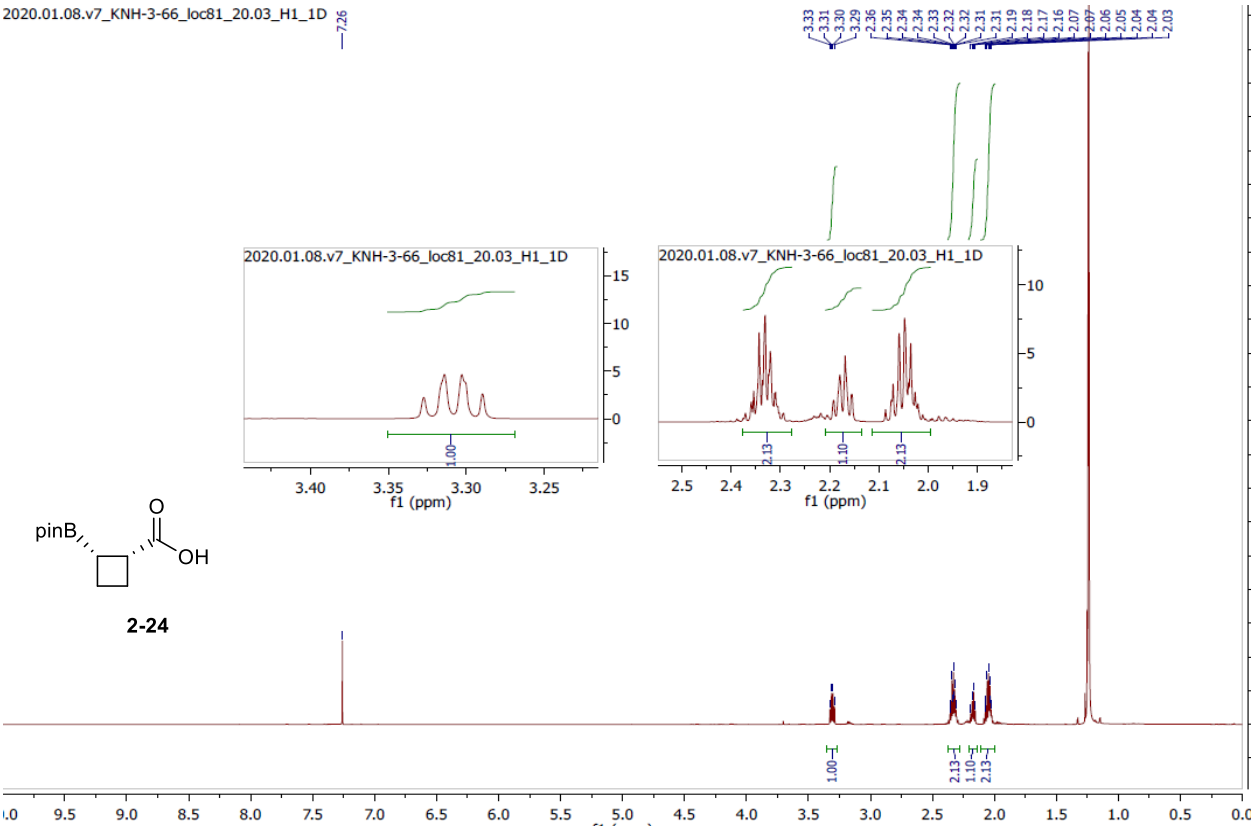
2020.01.08.v7_KNH-3-66_loc81_20.03_H1_1D
2020.01.08.v7_KNH-3-66_loc81_20.03_H1_1D
2020.01.08.v7_KNH-3-66_loc81_20.03_H1_1D
f1 (ppm)
f1 (ppm)
pinB
O
OH

2-24

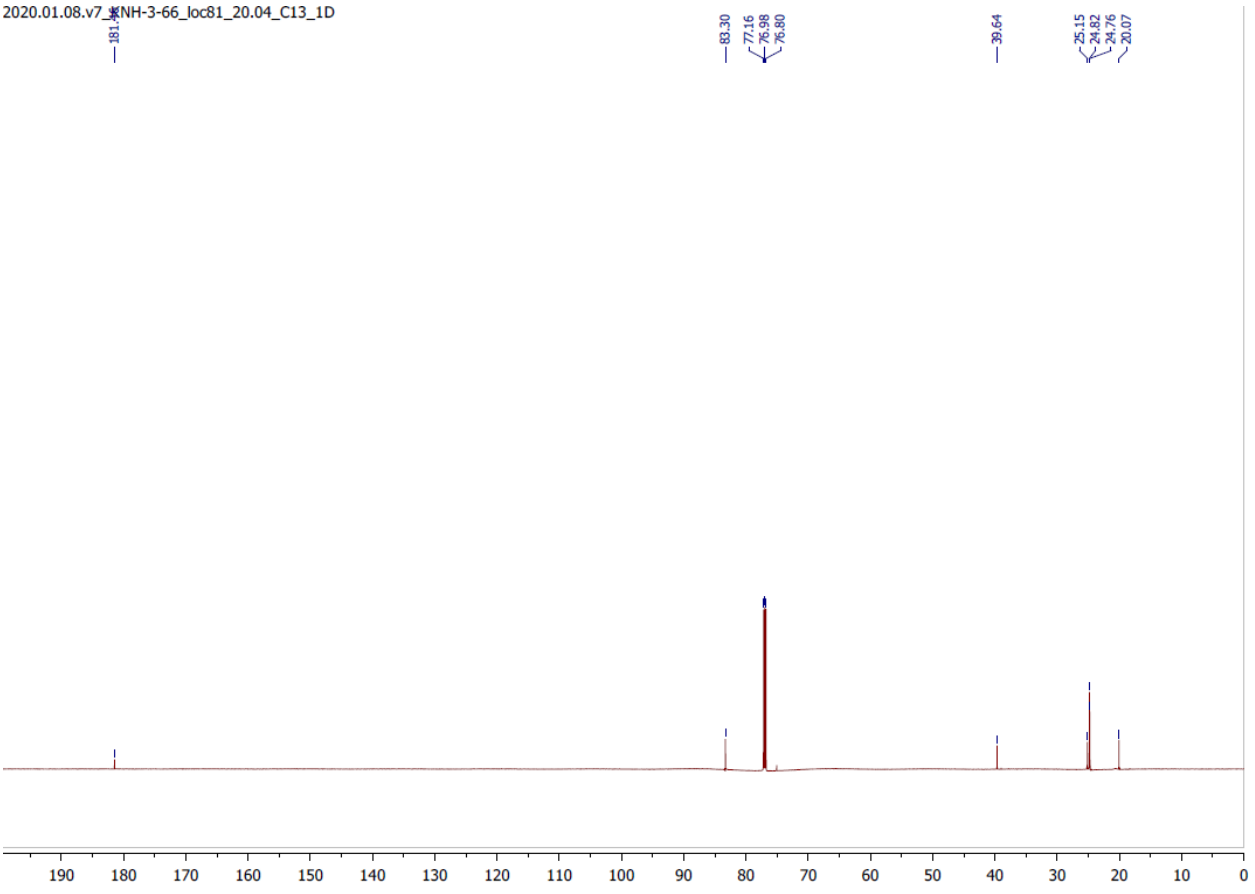
2020.01.08.v7_KNH-3-66_loc81_20.04_C13_1D

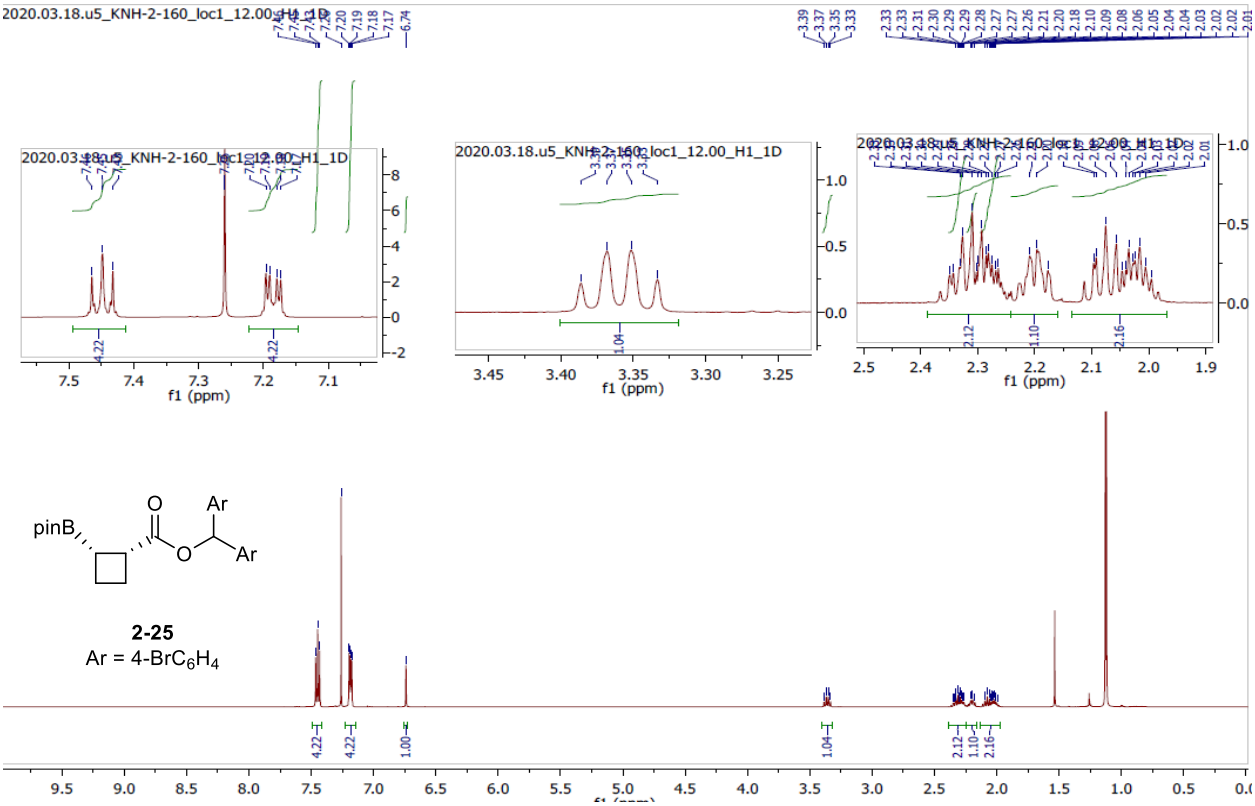
2020.03.18.u5_KNH-2-160_loc1_12.00_H1_1D
f1 (ppm)
pinB
O
Ar
O
Ar
2-25
Ar = 4-BrC6H4

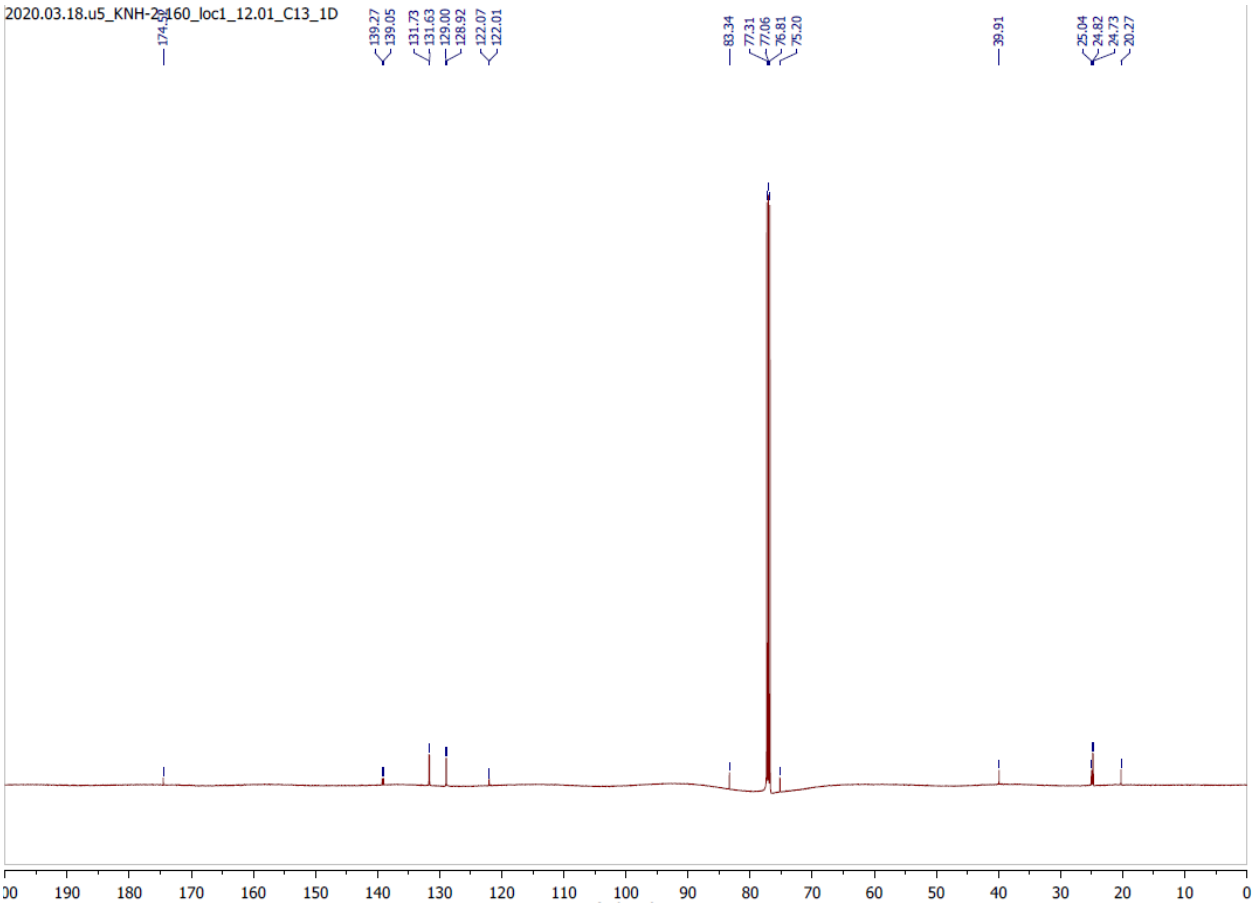
2020.03.18.u5_KNH-2-160_loc1_12.01_C13_1D
f1 (ppm)

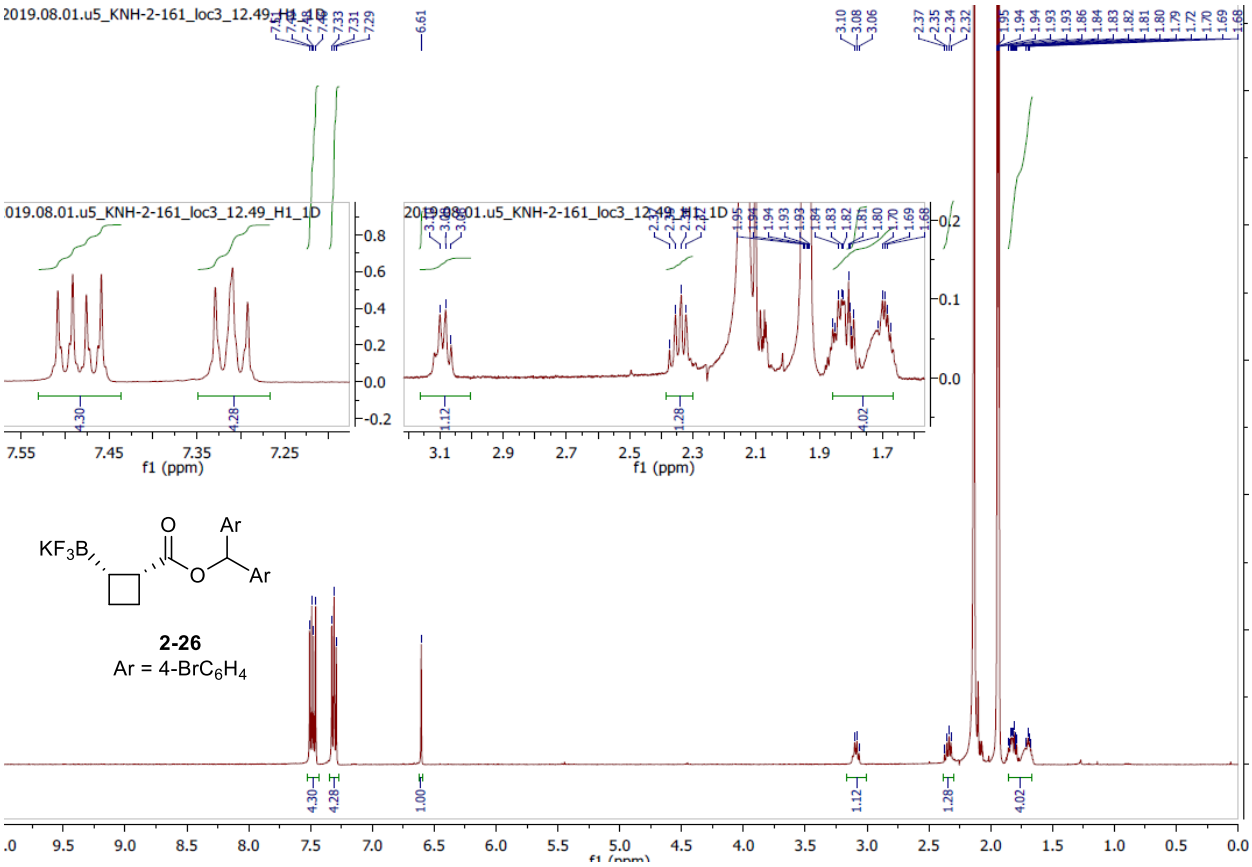
2019.08.01.u5_KNH-2-161_loc3_12.49_H1_1D
f1 (ppm)
KF3B
O
Ar
O
Ar
2-26
Ar = 4-BrC6H4

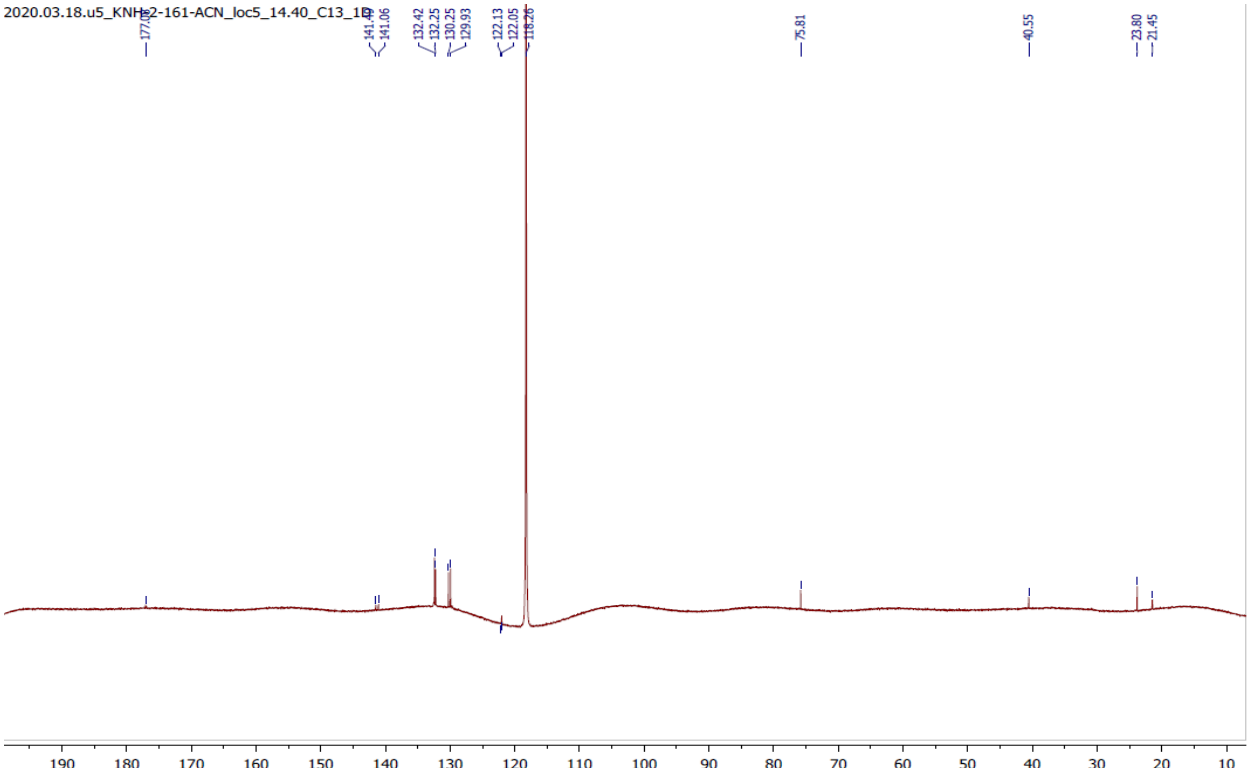
2020.03.18.u5_KNH-2-161-ACN_loc5_14.40_C13_1D

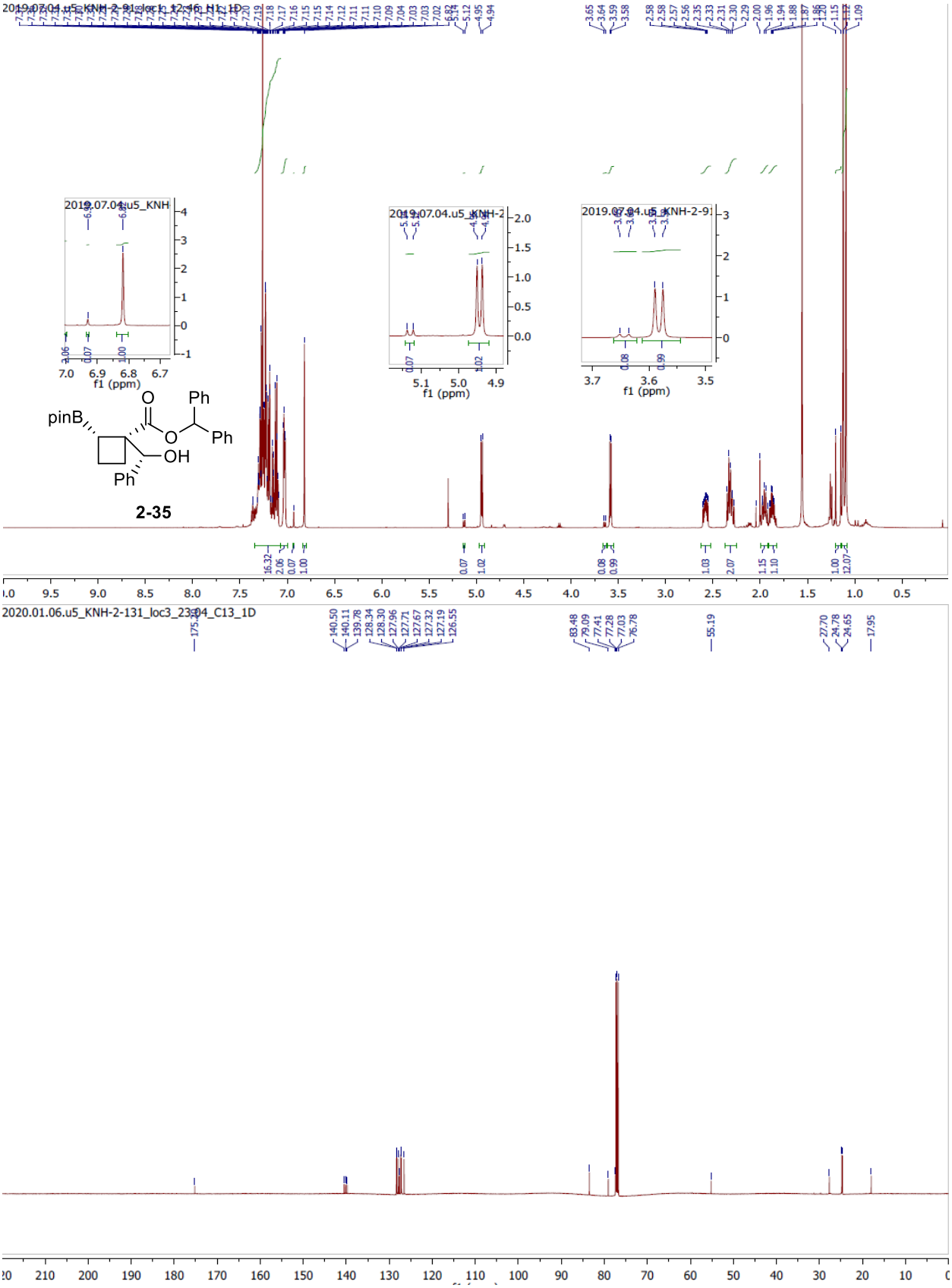
pinB
O
Ph
O
Ph
OH
Ph
2-35
f1 (ppm)

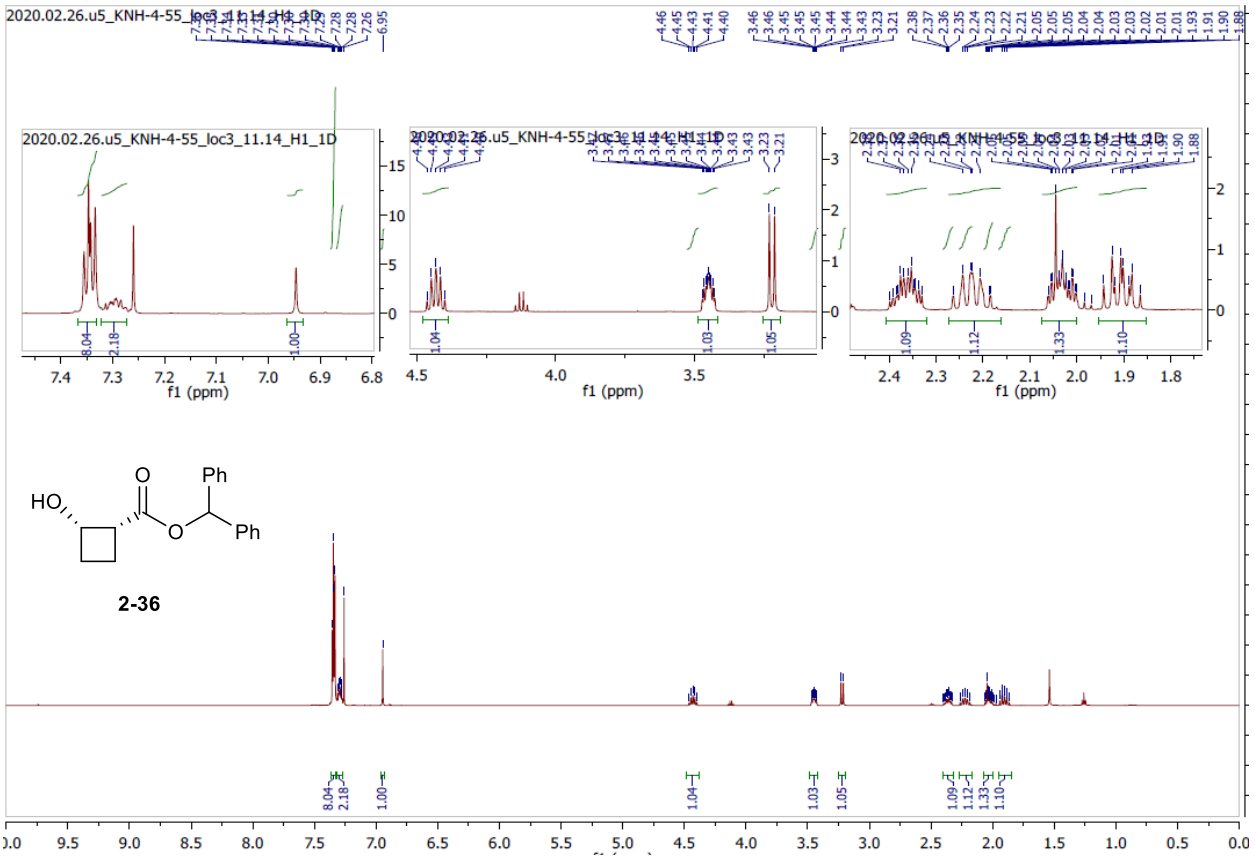
2020.02.26.u5_KNH-4-55_loc3_11.14_H1_1D
f1 (ppm)
HO
O
O
Ph
Ph
2-36

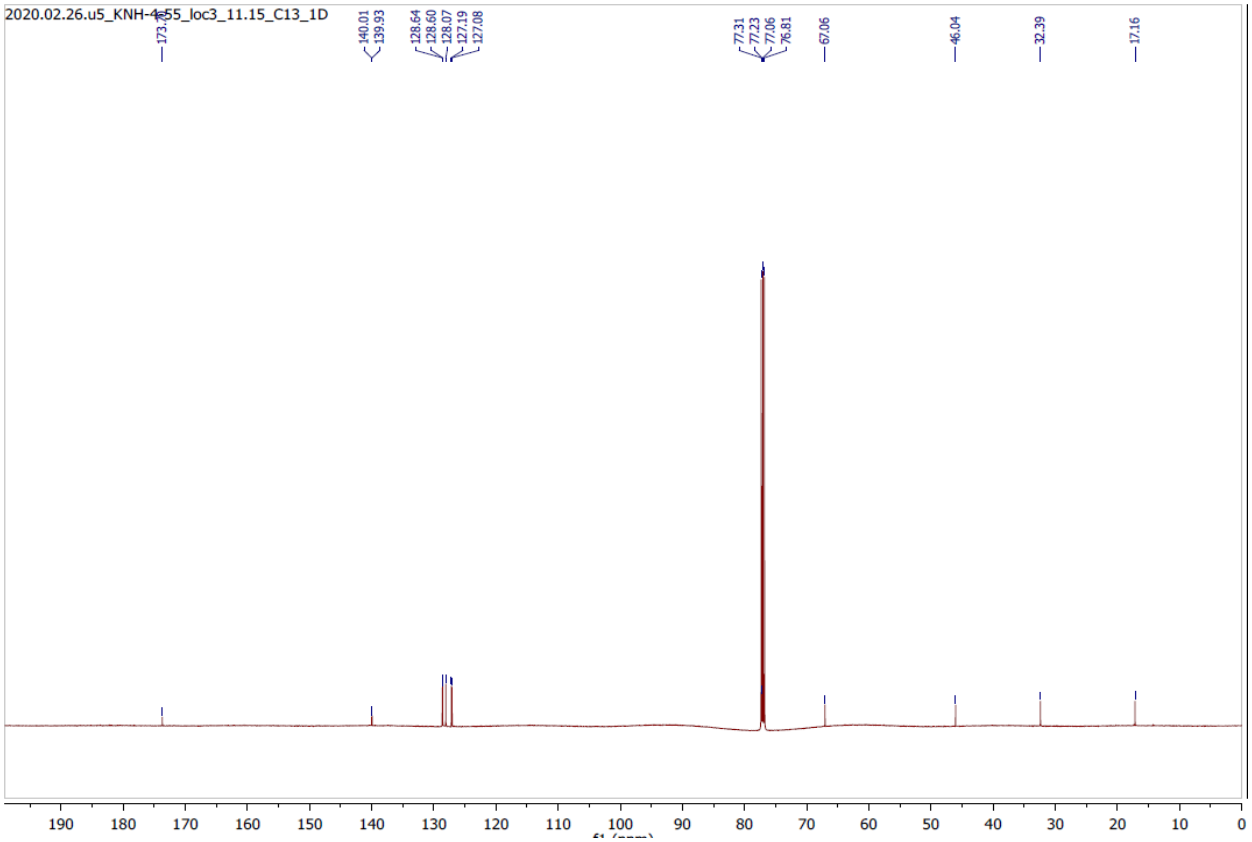
2020.02.26.u5_KNH-4-55_loc3_11.15_C13_1D

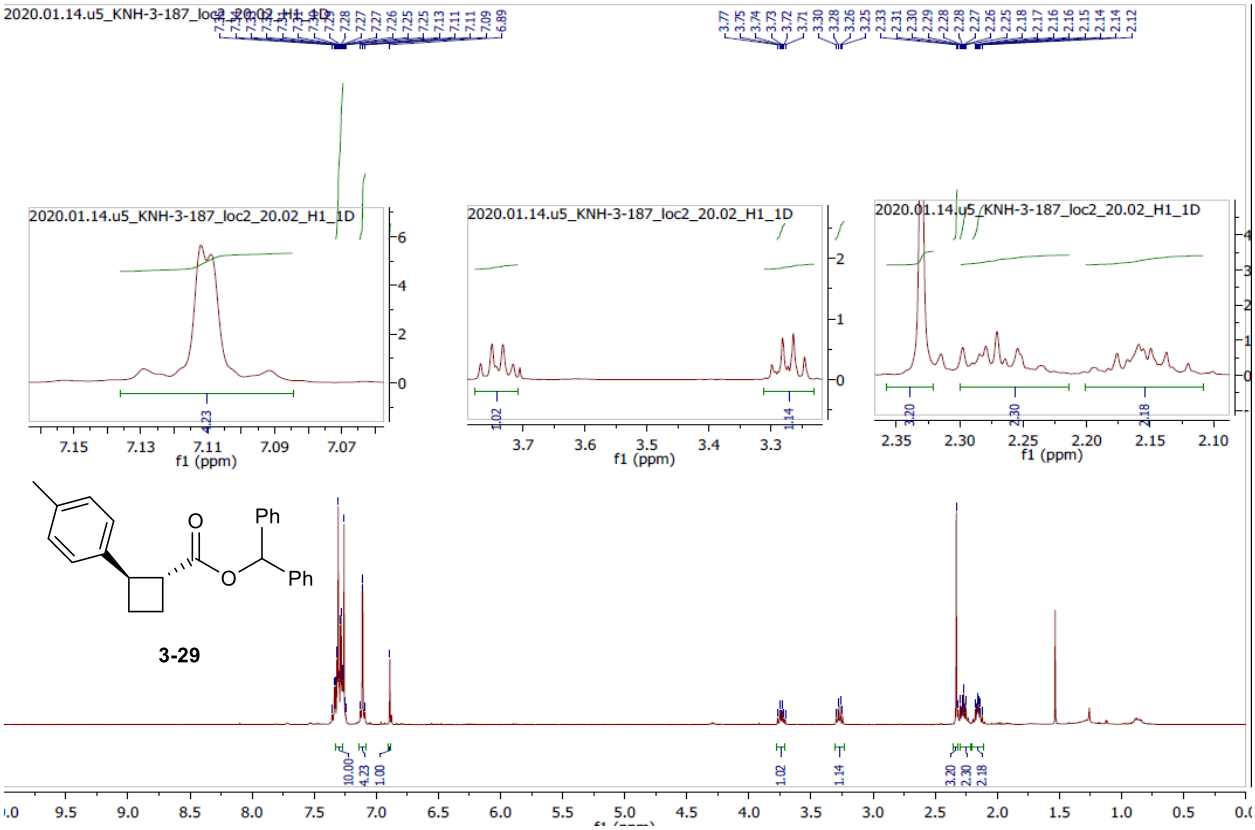
2020.01.14.u5_KNH-3-187_loc2_20.02_H1_1D
f1 (ppm)
O
Ph
O
Ph

3-29

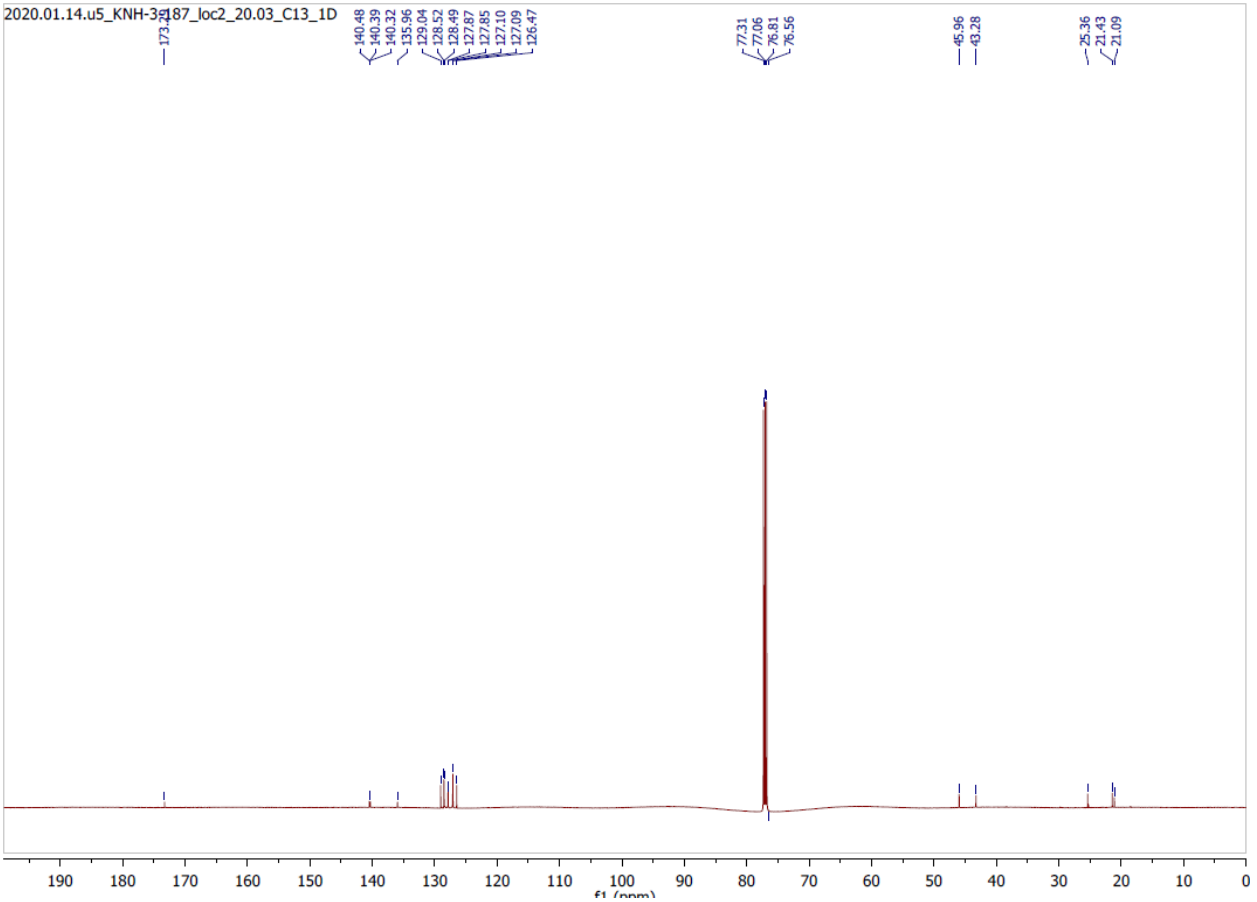
2020.01.14.u5_KNH-3-187_loc2_20.03_C13_1D
f1 (ppm)

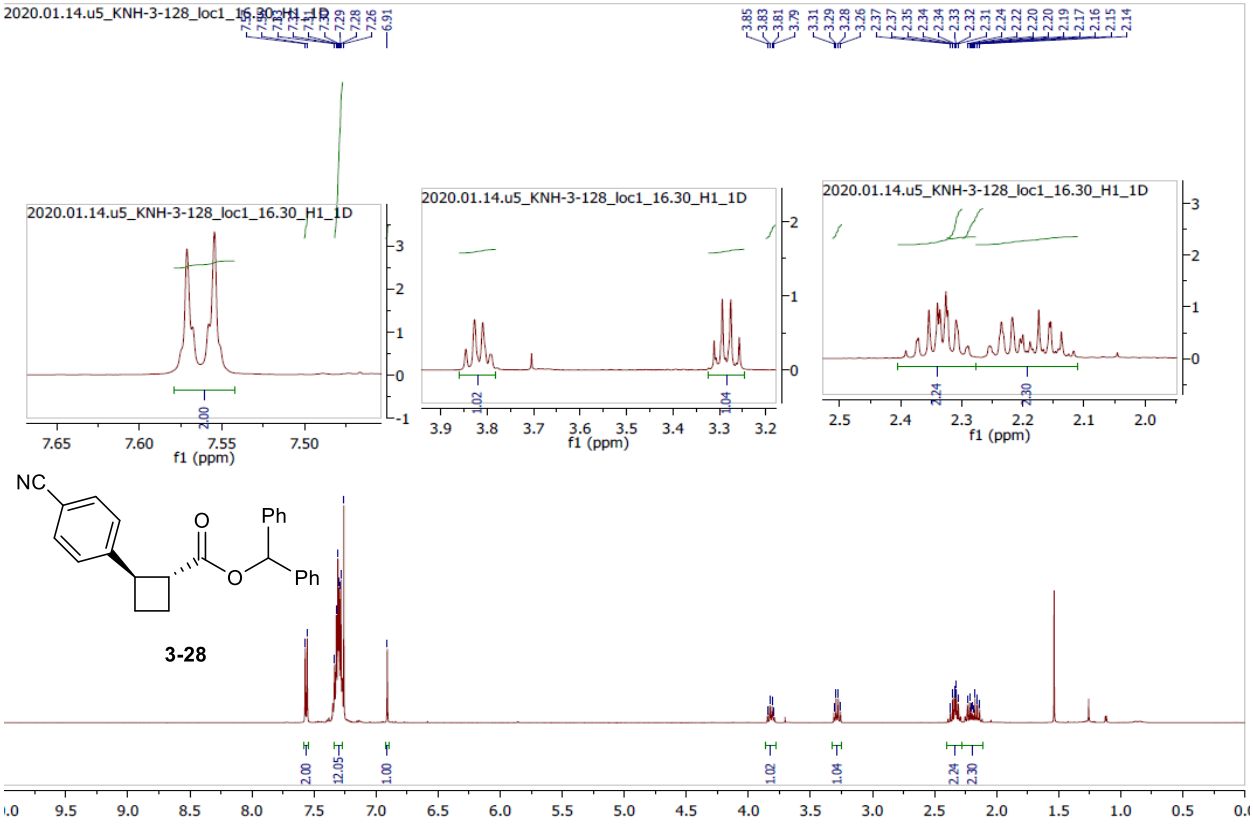
2020.01.14.u5_KNH-3-128_loc1_16.30_H1_1D
NC
O
O
Ph
Ph
3-28
f1 (ppm)

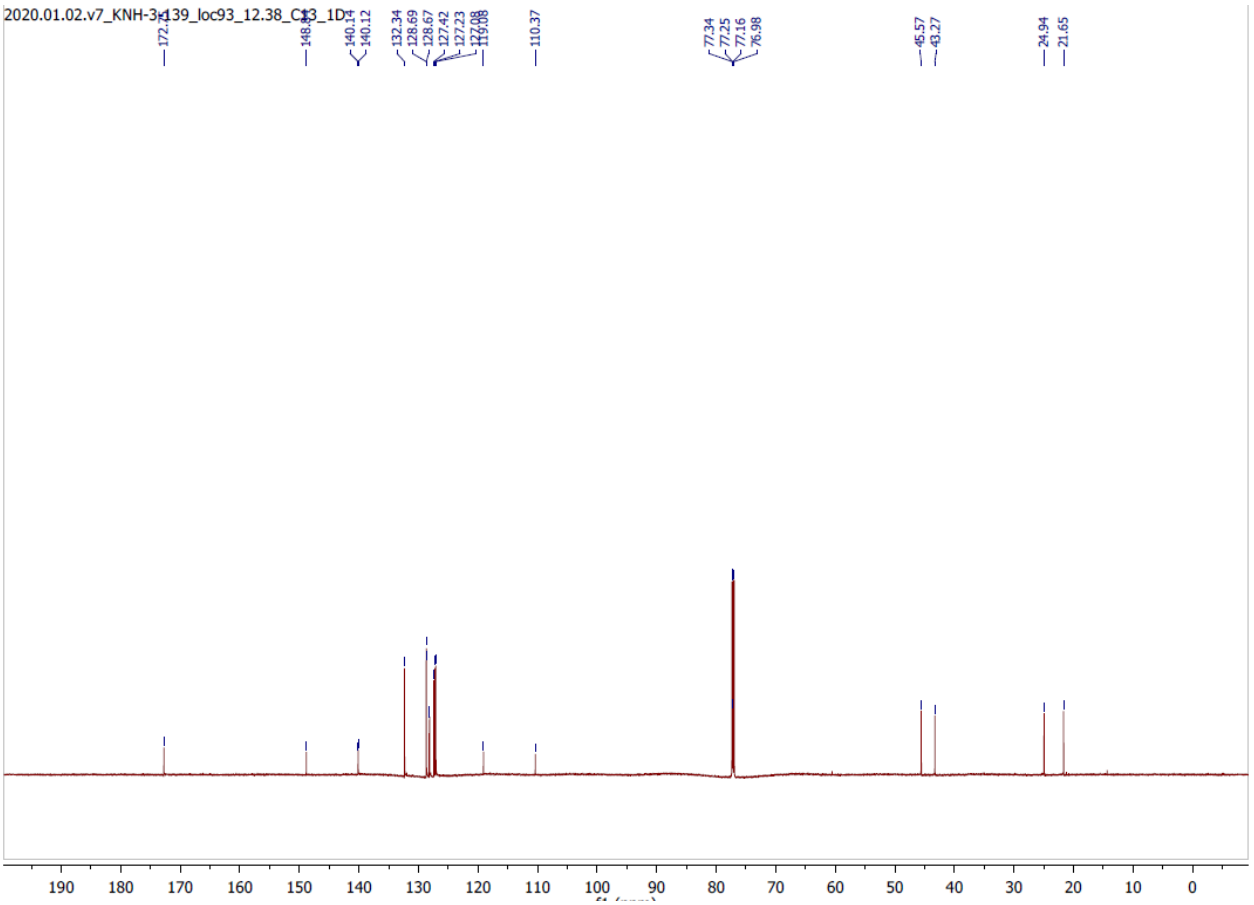
2020.01.02.v7_KNH-3-139_loc93_12.38_C13_1D

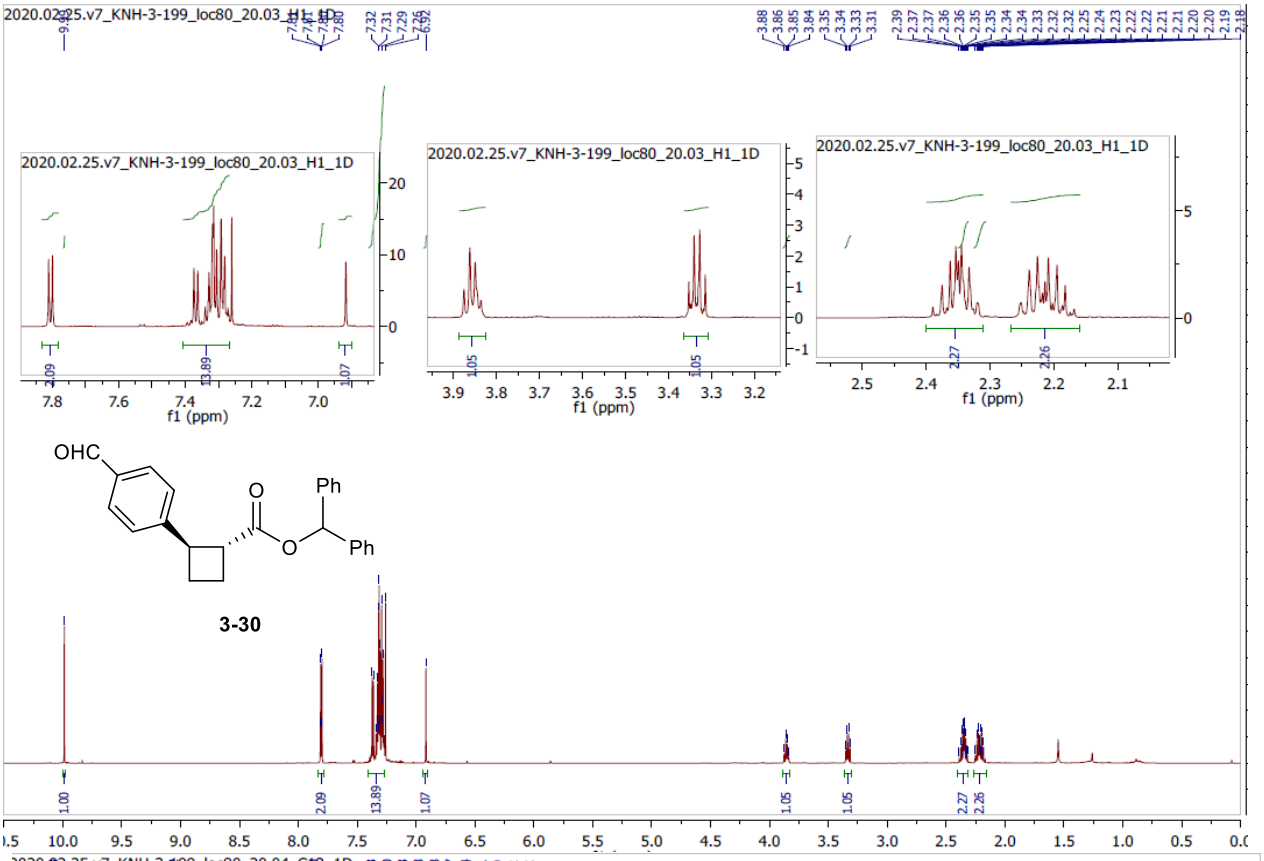
2020.02.25.v7_KNH-3-199_loc80_20.03_H1_1D
OHC
O
O
Ph
Ph
3-30
f1 (ppm)

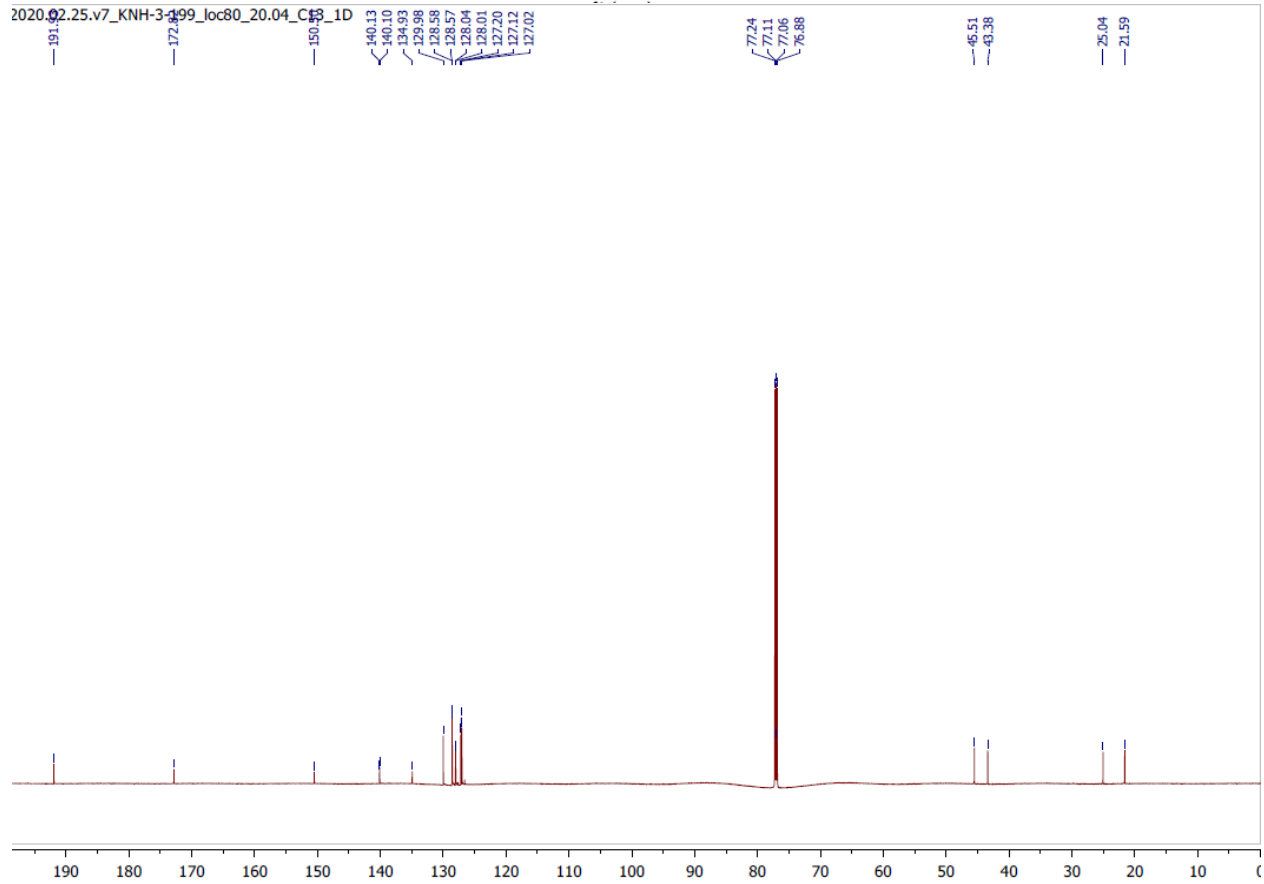
2020.02.25.v7_KNH-3-199_loc80_20.04_C13_1D
f1 (ppm)

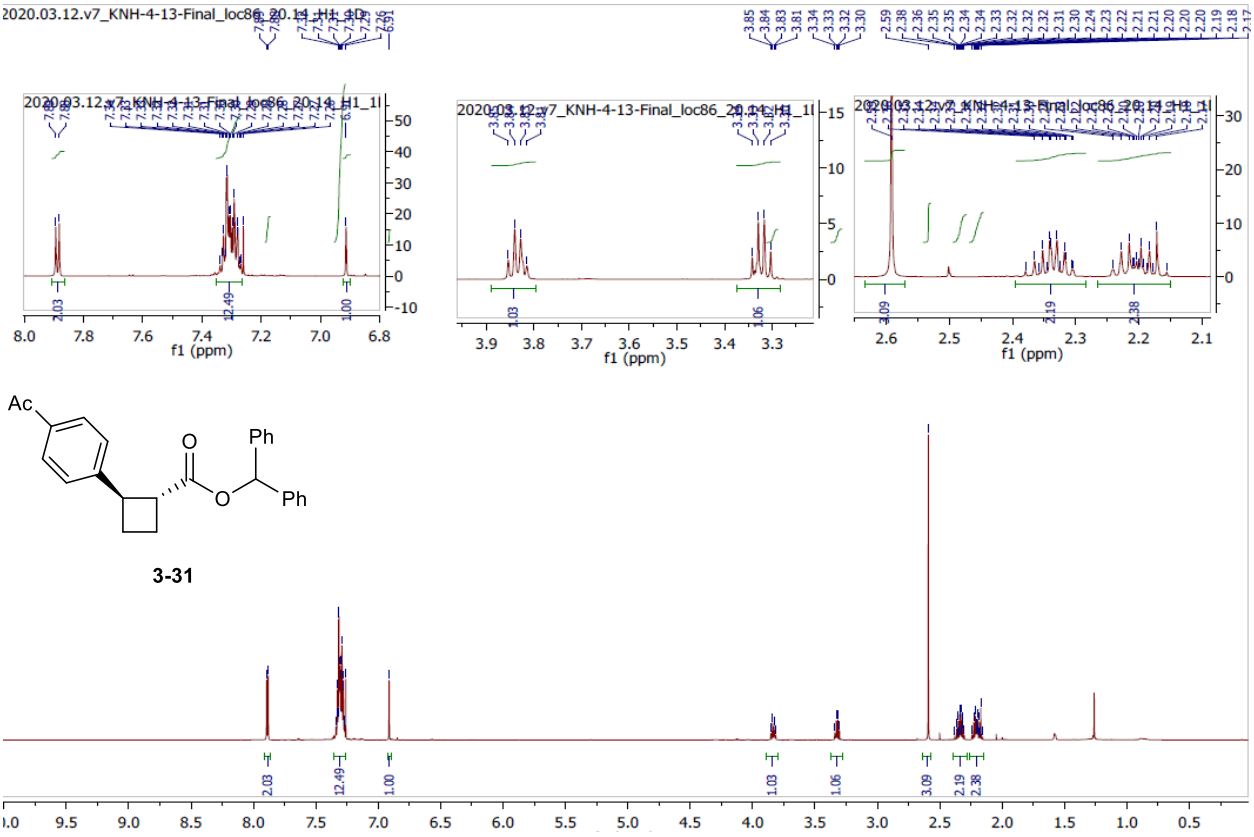

3-31

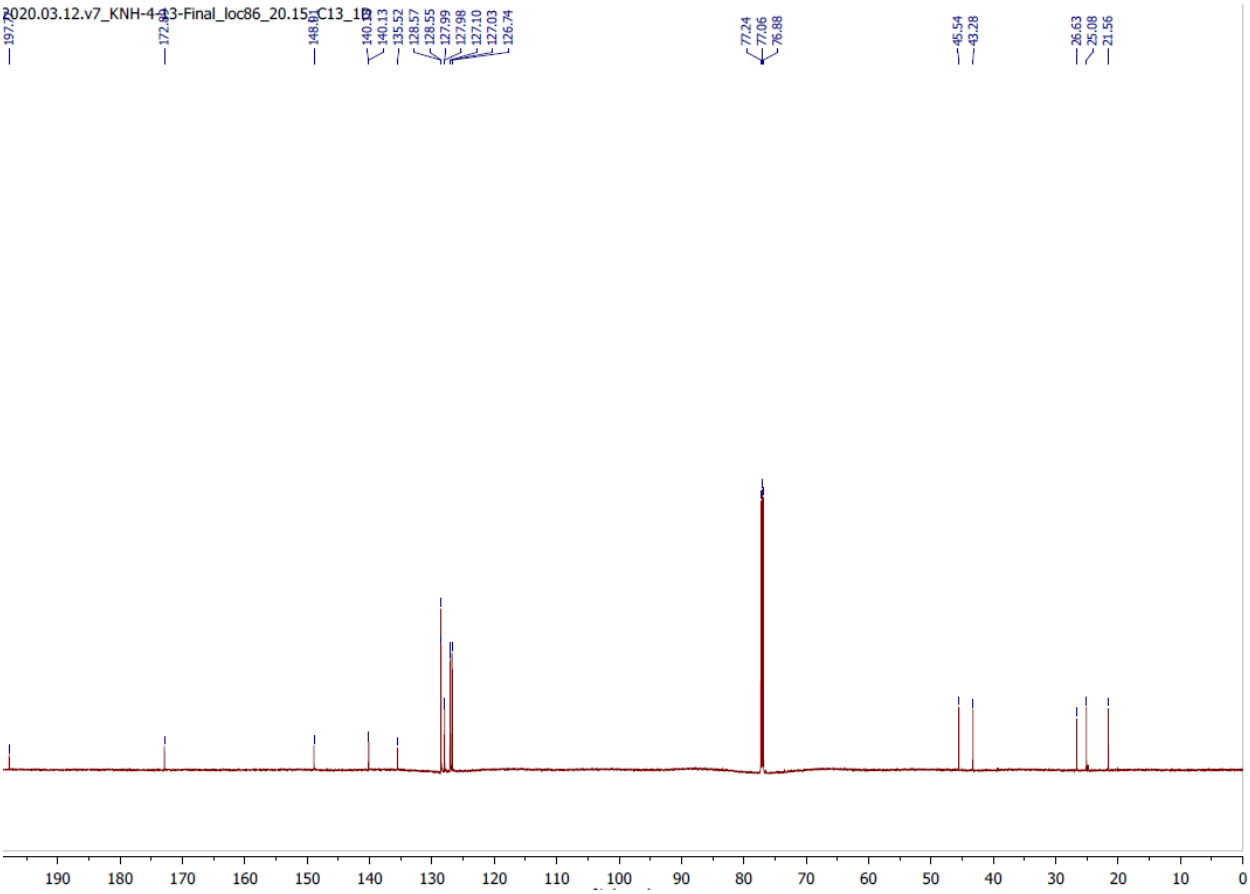

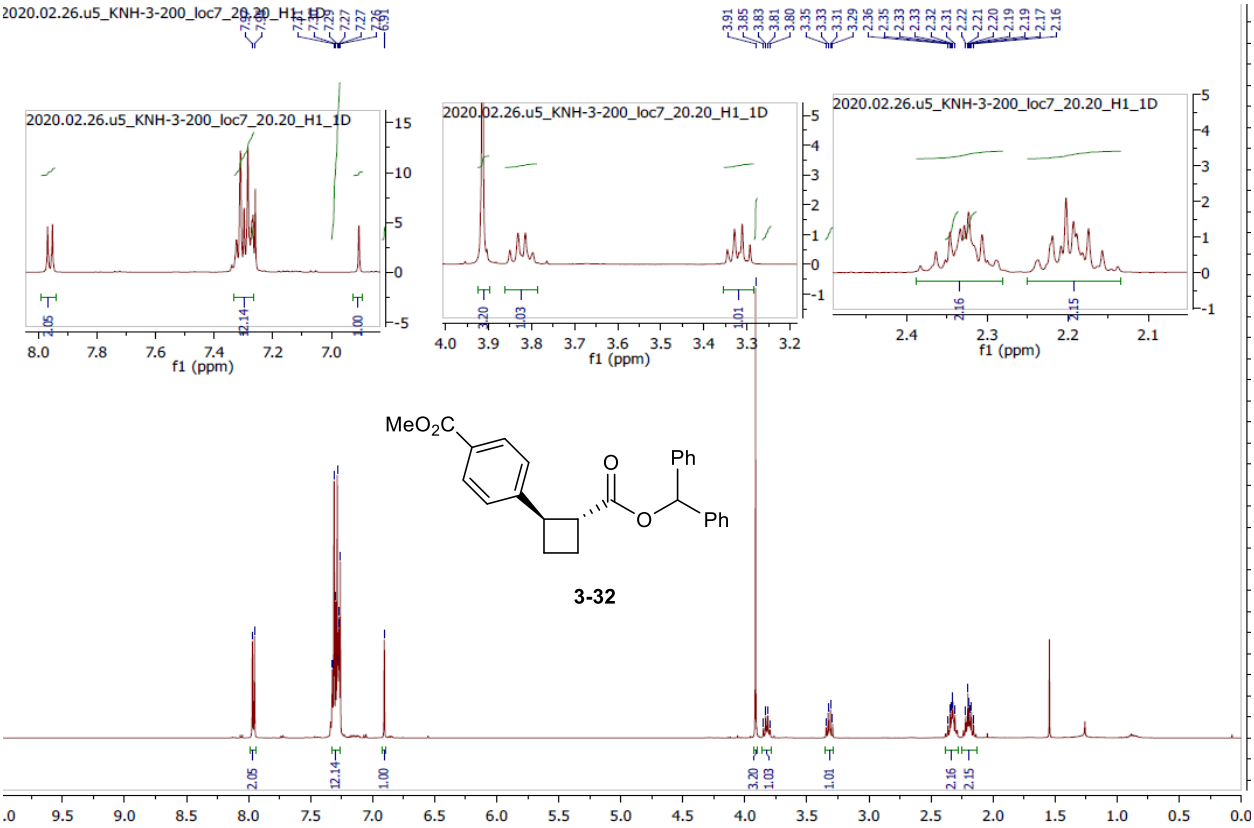
2020.02.26.u5_KNH-3-200_loc7_20.20_H1_1D
f1 (ppm)
MeO2C
O
Ph
O
Ph

3-32

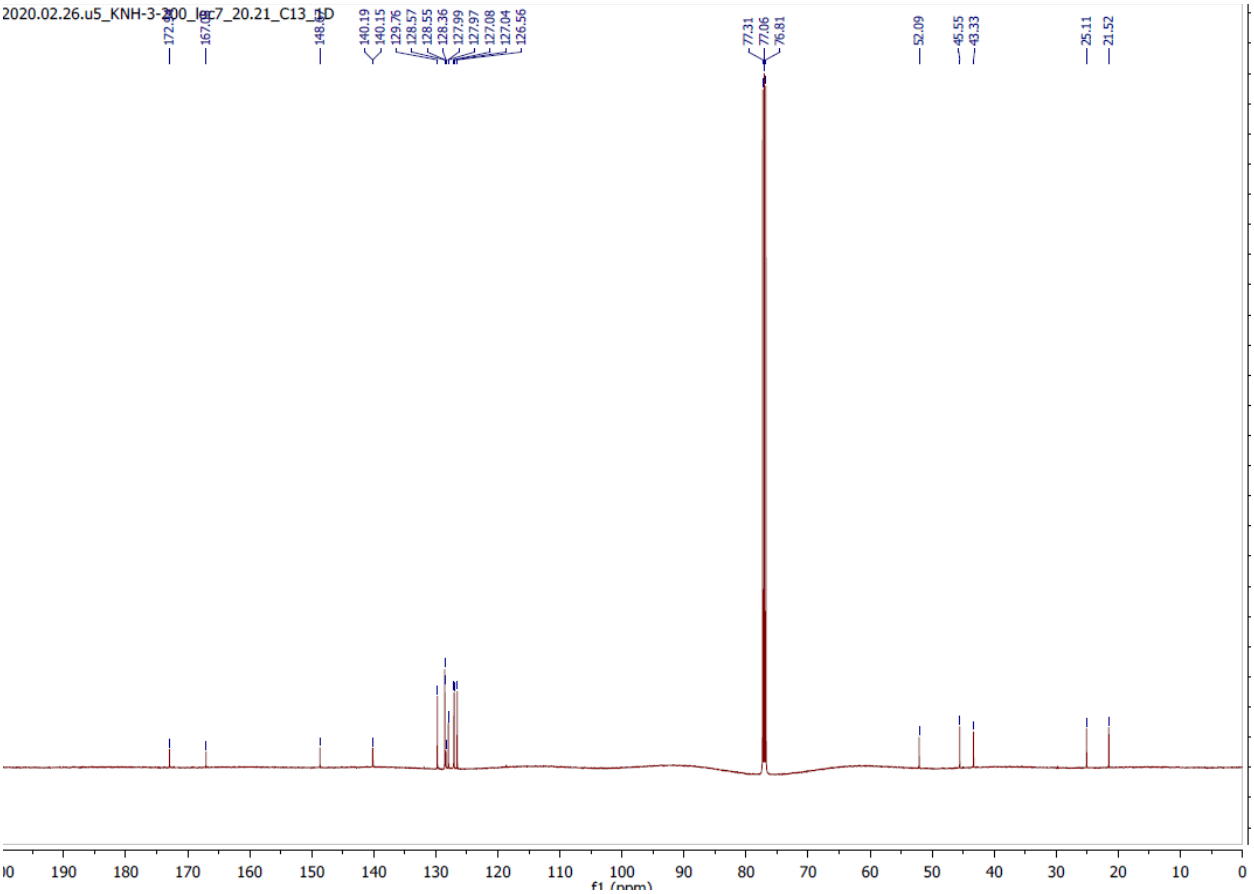
2020.02.26.u5_KNH-3-200_loc7_20.21_C13_1D
f1 (ppm)

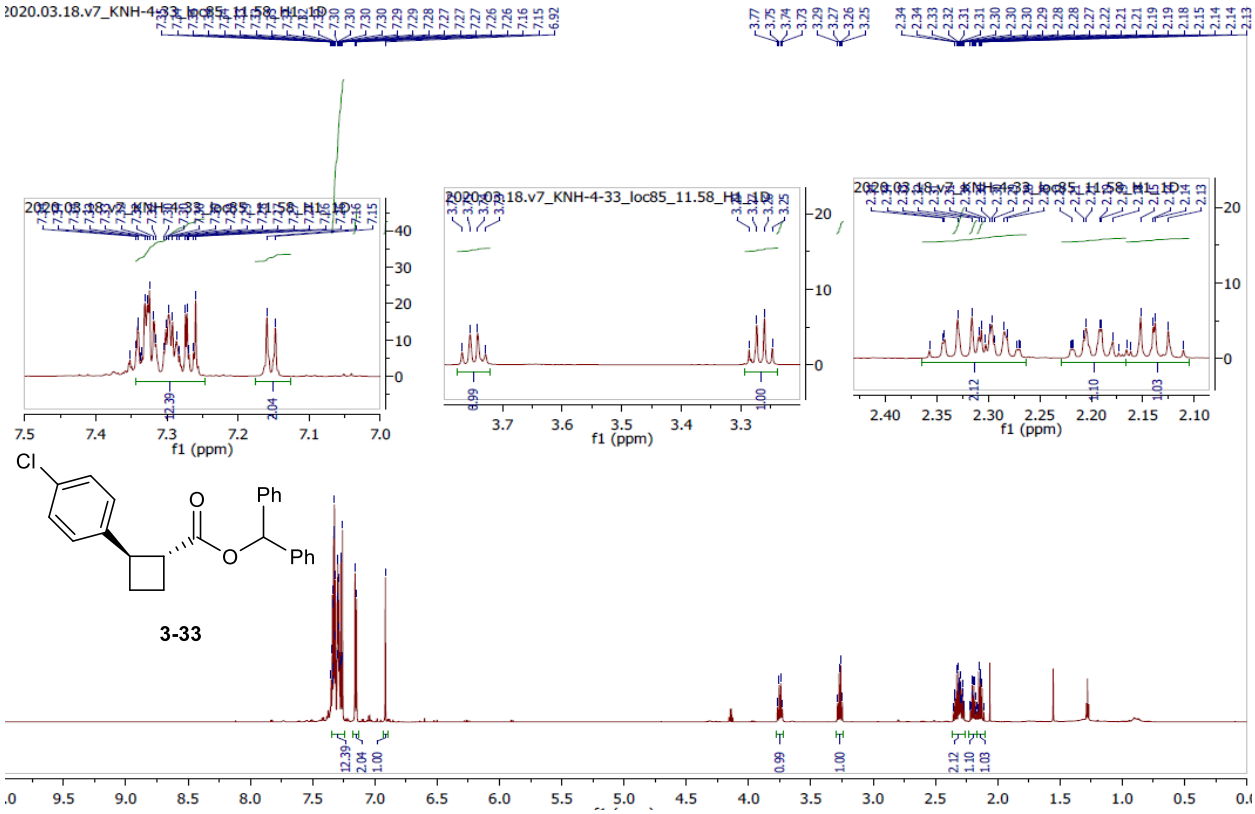
2020.03.18.v7_KNH-4-33_loc85_11.58_H1_1D
f1 (ppm)
Cl
O
Ph
O
Ph
3-33

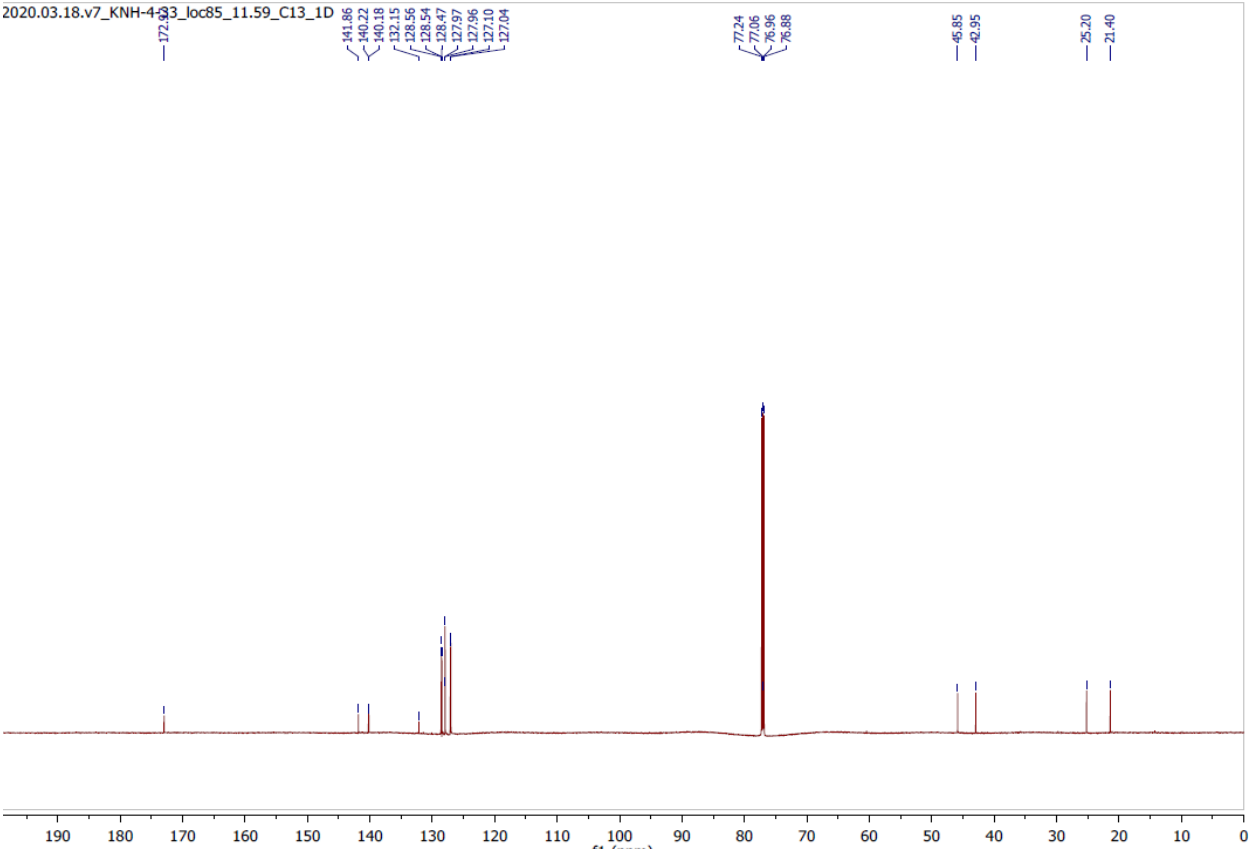
2020.03.18.v7_KNH-4-33_loc85_11.59_C13_1D

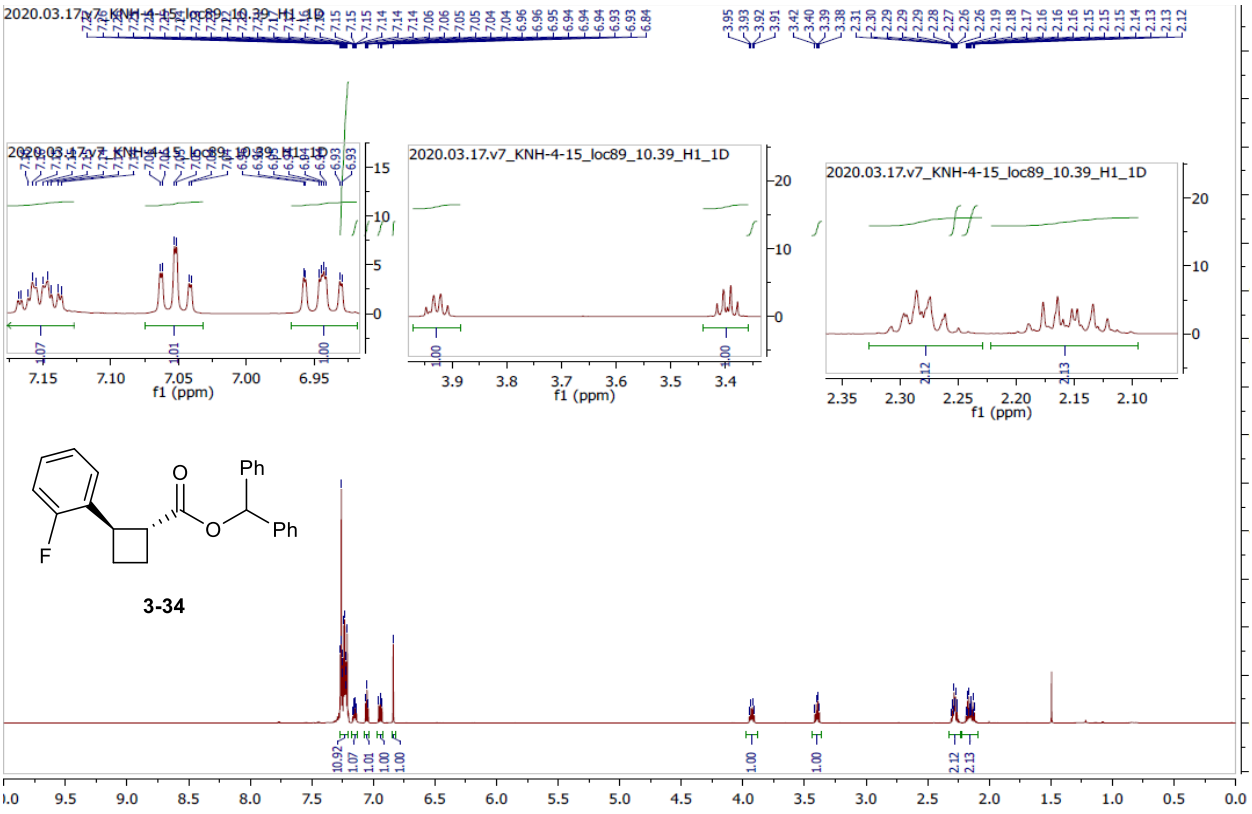
2020.03.17.v7_KNH-4-15_loc89_10.39_H1_1D
f1 (ppm)
O
Ph
O
Ph
F

3-34

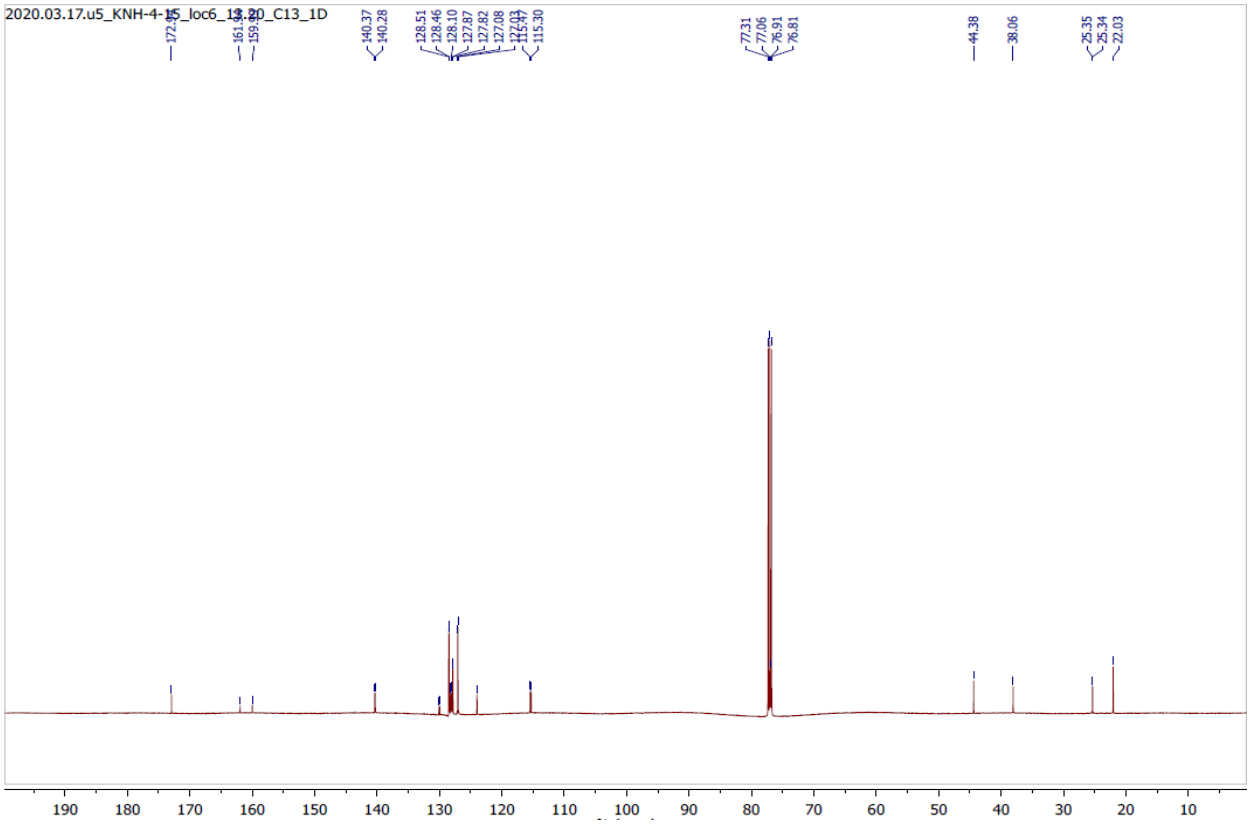
2020.03.17.u5_KNH-4-15_loc6_13.20_C13_1D

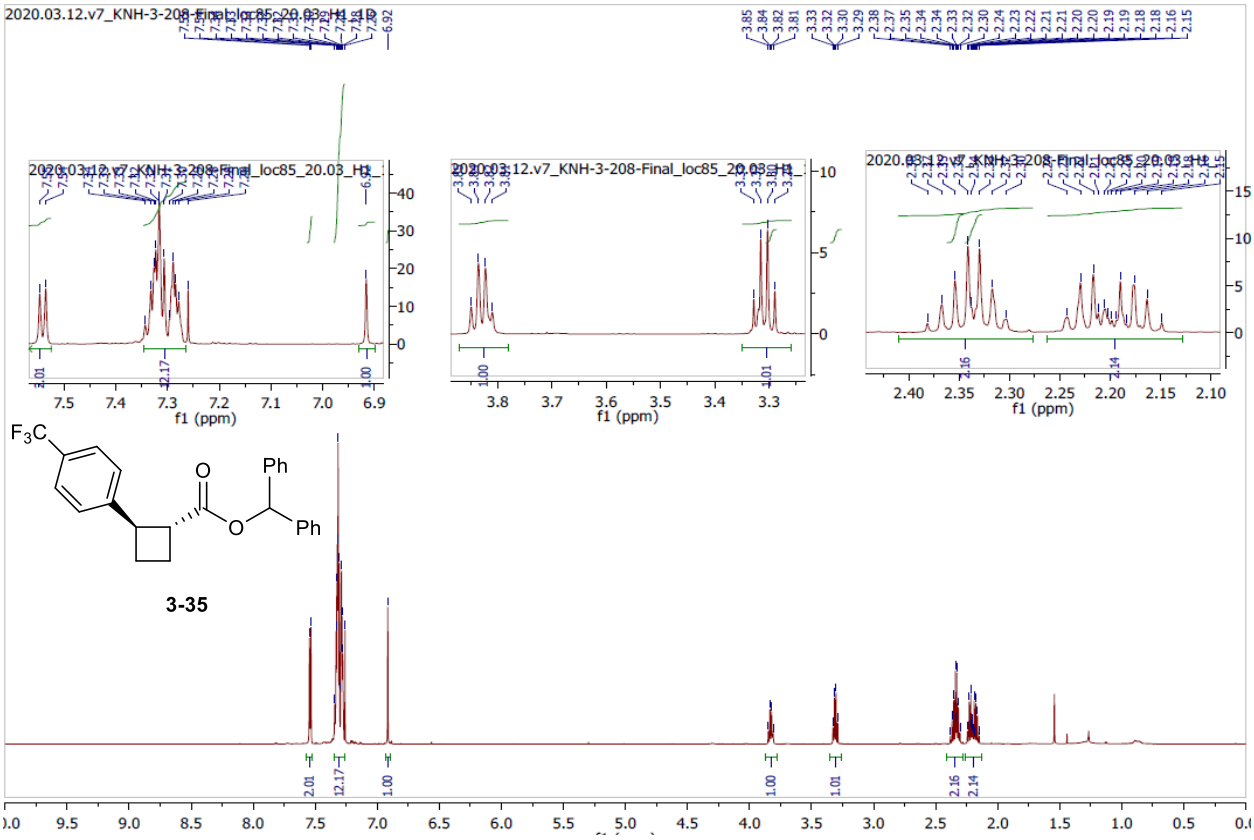
2020.03.12.v7_KNH-3-208-Final_loc85_20.03_H1
F3C
O
Ph
O
Ph
3-35
f1 (ppm)

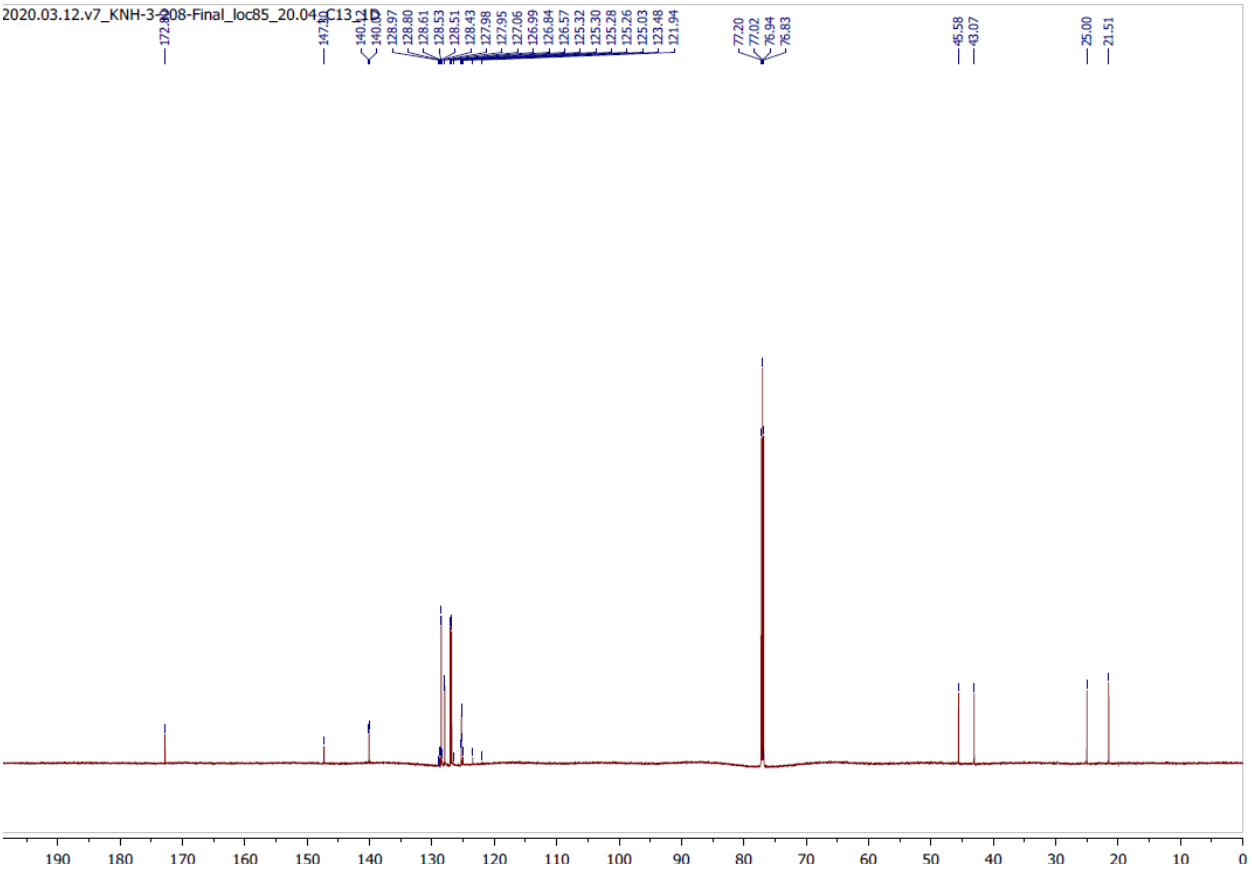
2020.03.12.v7_KNH-3-208-Final_loc85_20.04_C13_1D

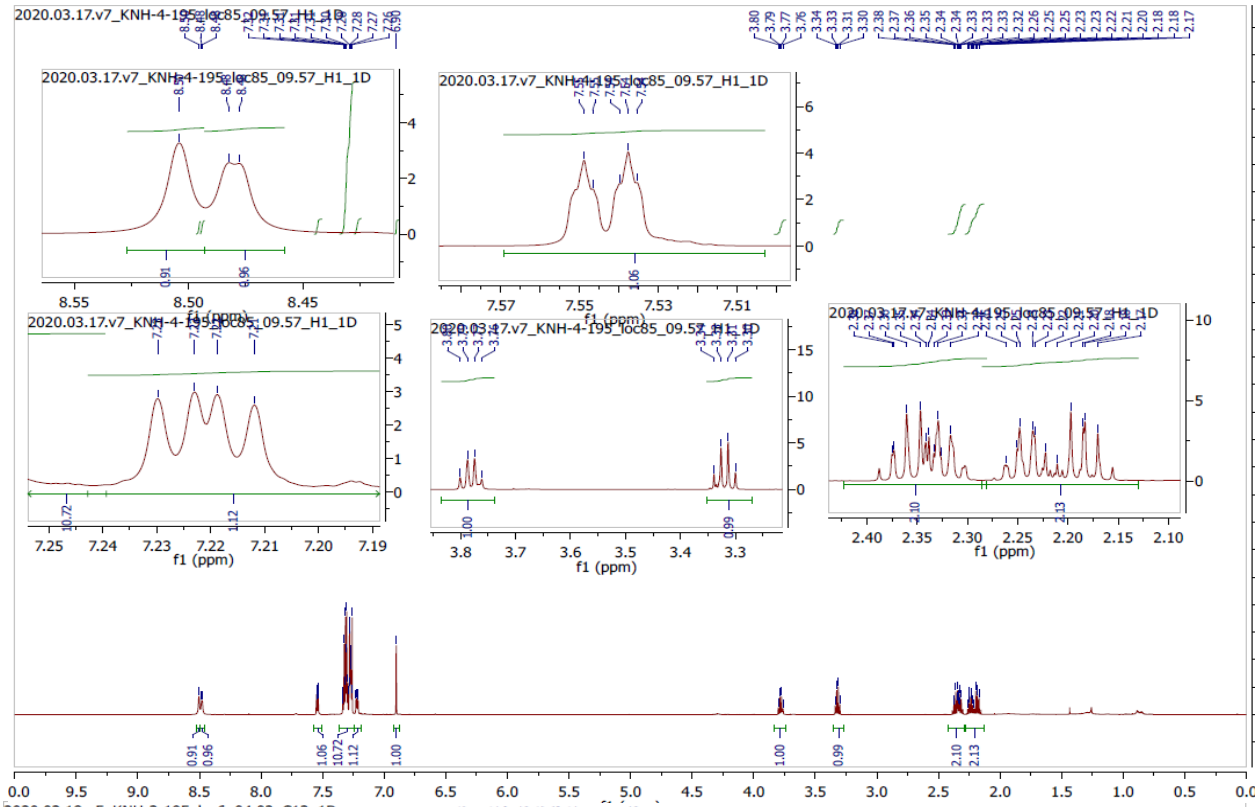

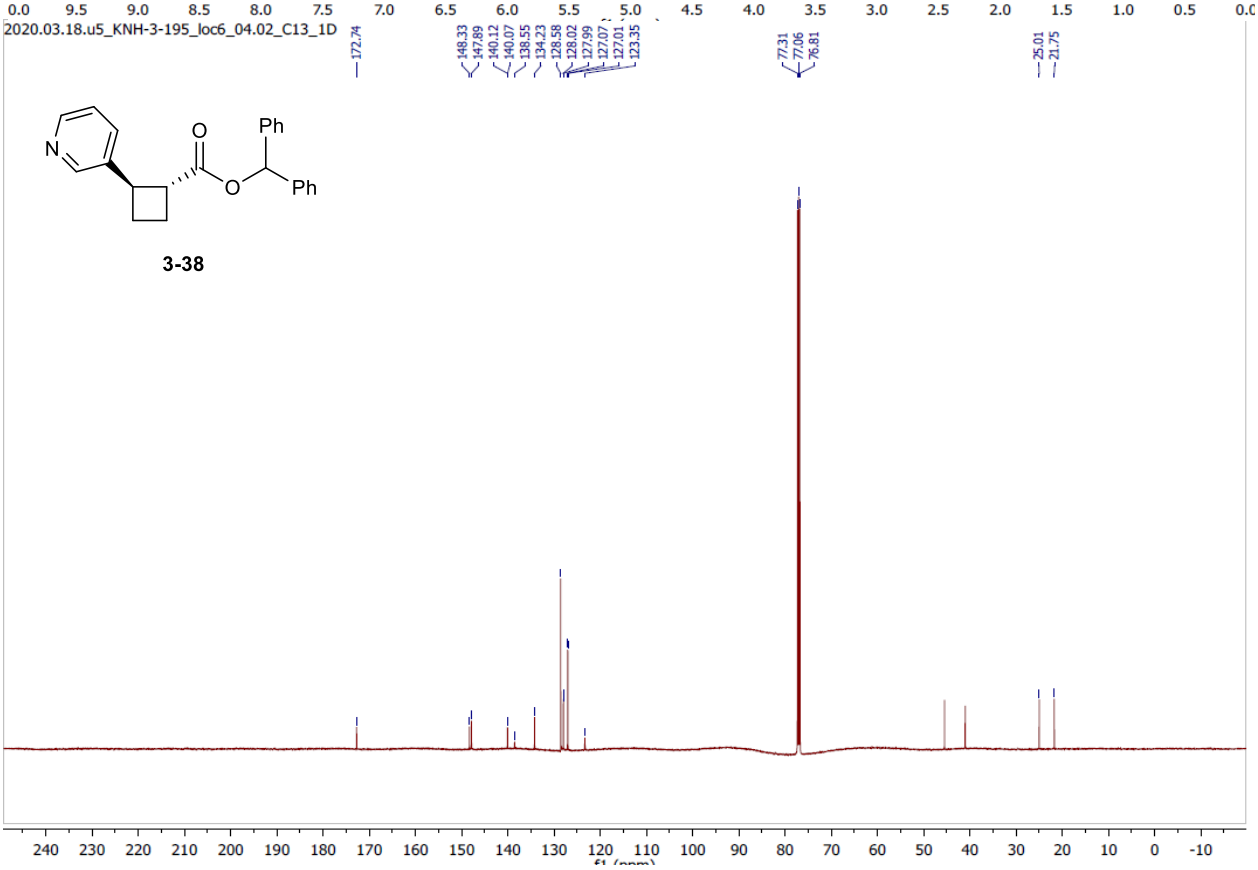

3-38

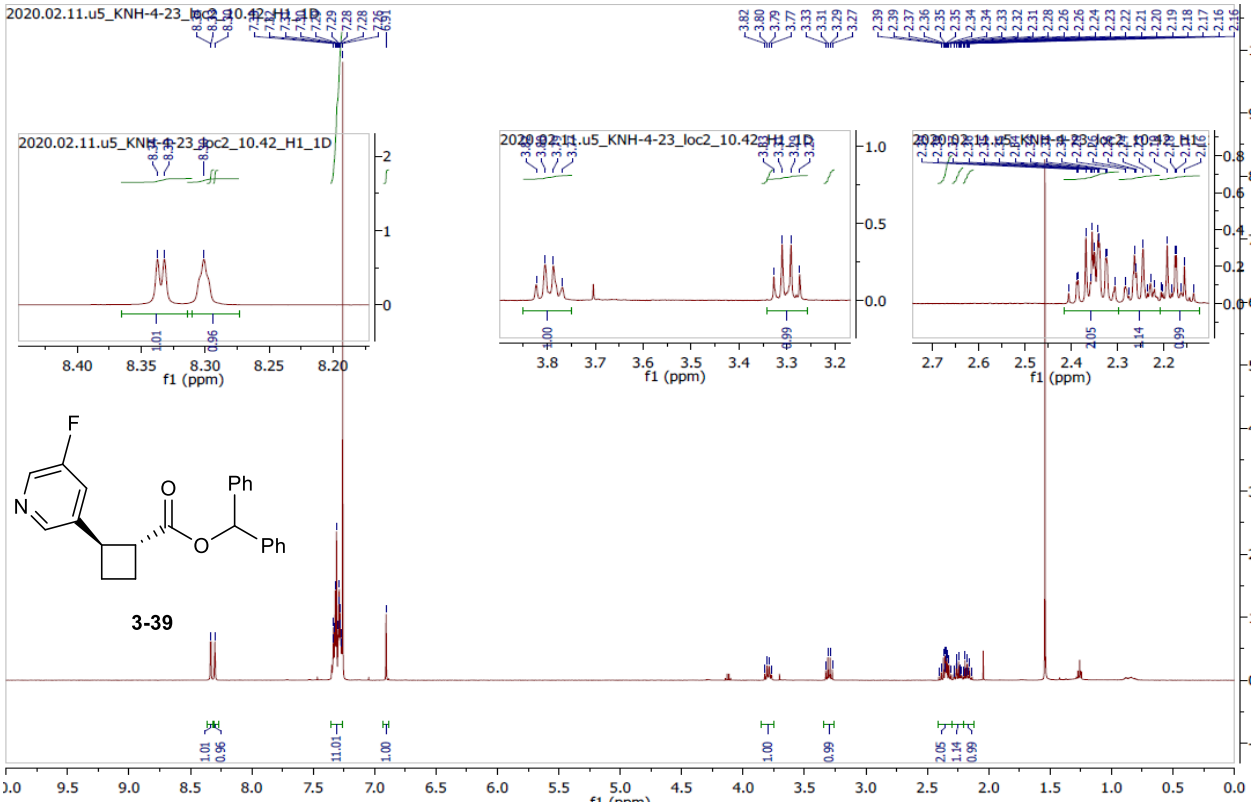
2020.02.11.u5_KNH-4-23_loc2_10.42_H1_1D
F
N
O
O
Ph
Ph
3-39
f1 (ppm)

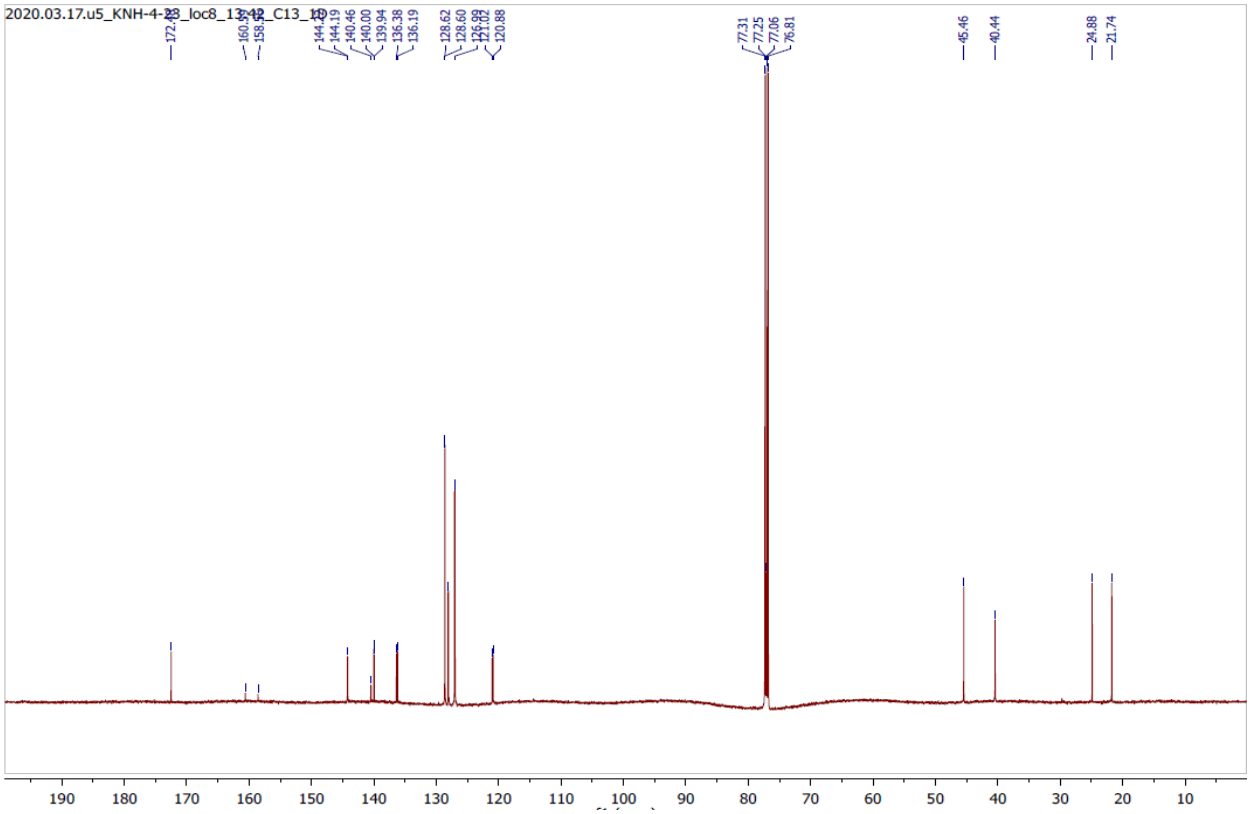
2020.03.17.u5_KNH-4-23_loc8_13.42_C13_1D
f1 (ppm)

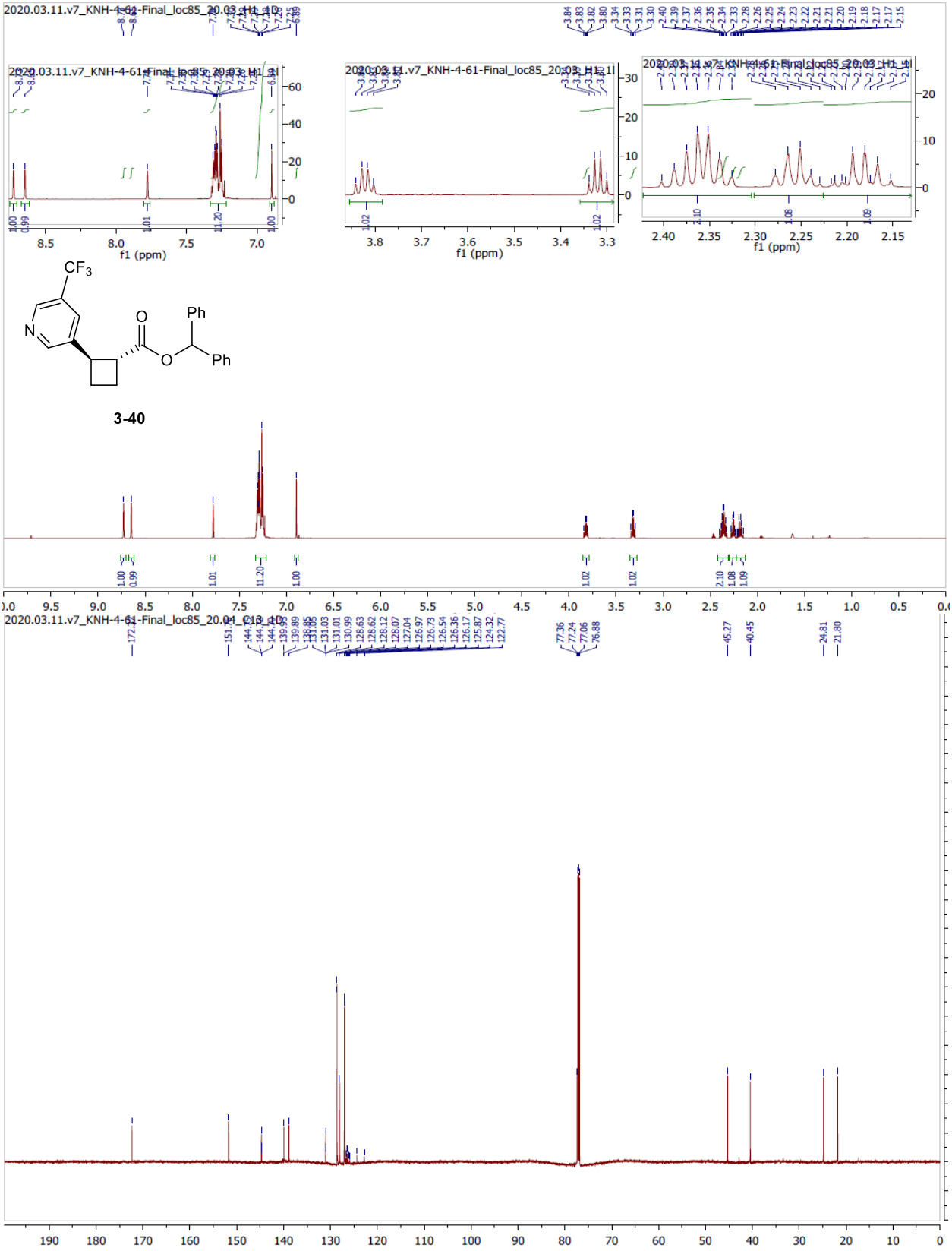
2020.03.11.v7_KNH-4-61-Final_loc85_20.03_H1_1D
2020.03.11.v7_KNH-4-61-Final_loc85_20.03_C13_1D
f1 (ppm)
CF3
N
O
O
Ph
Ph
3-40

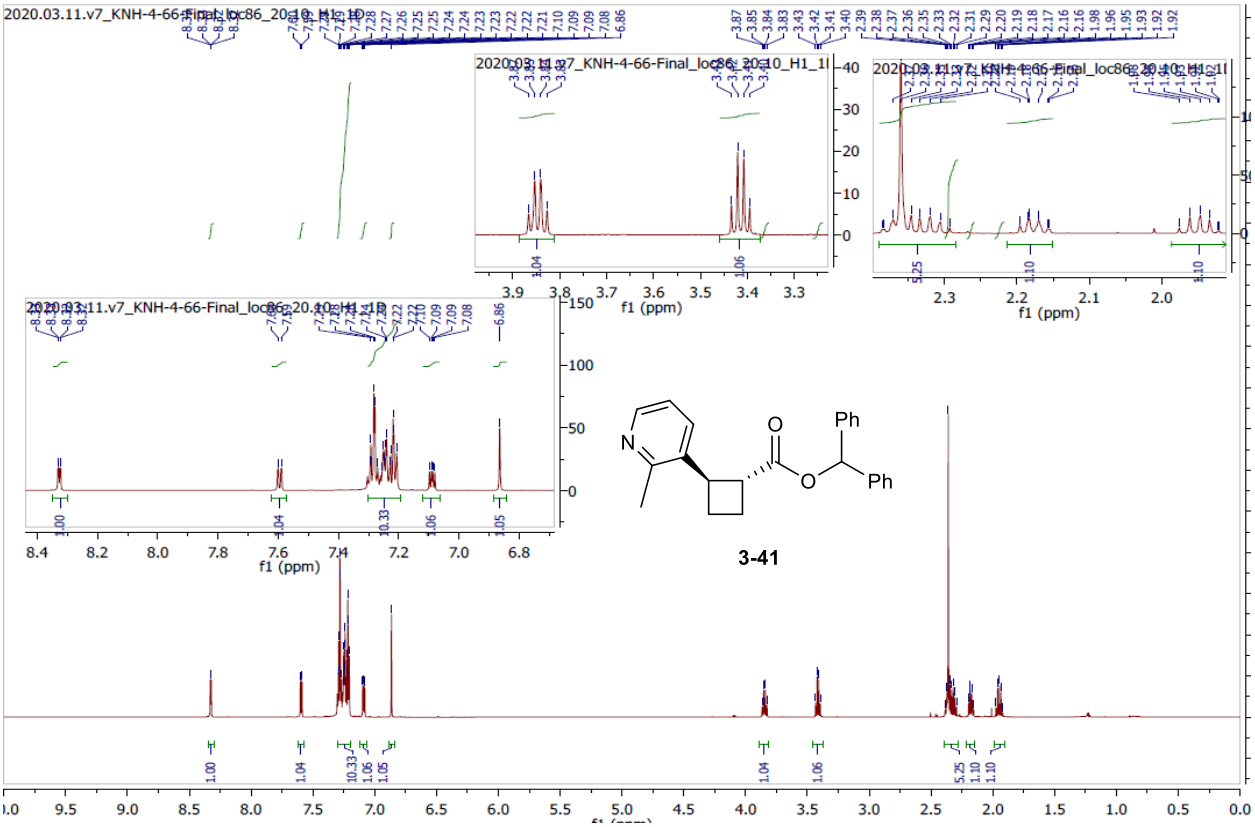
3-41

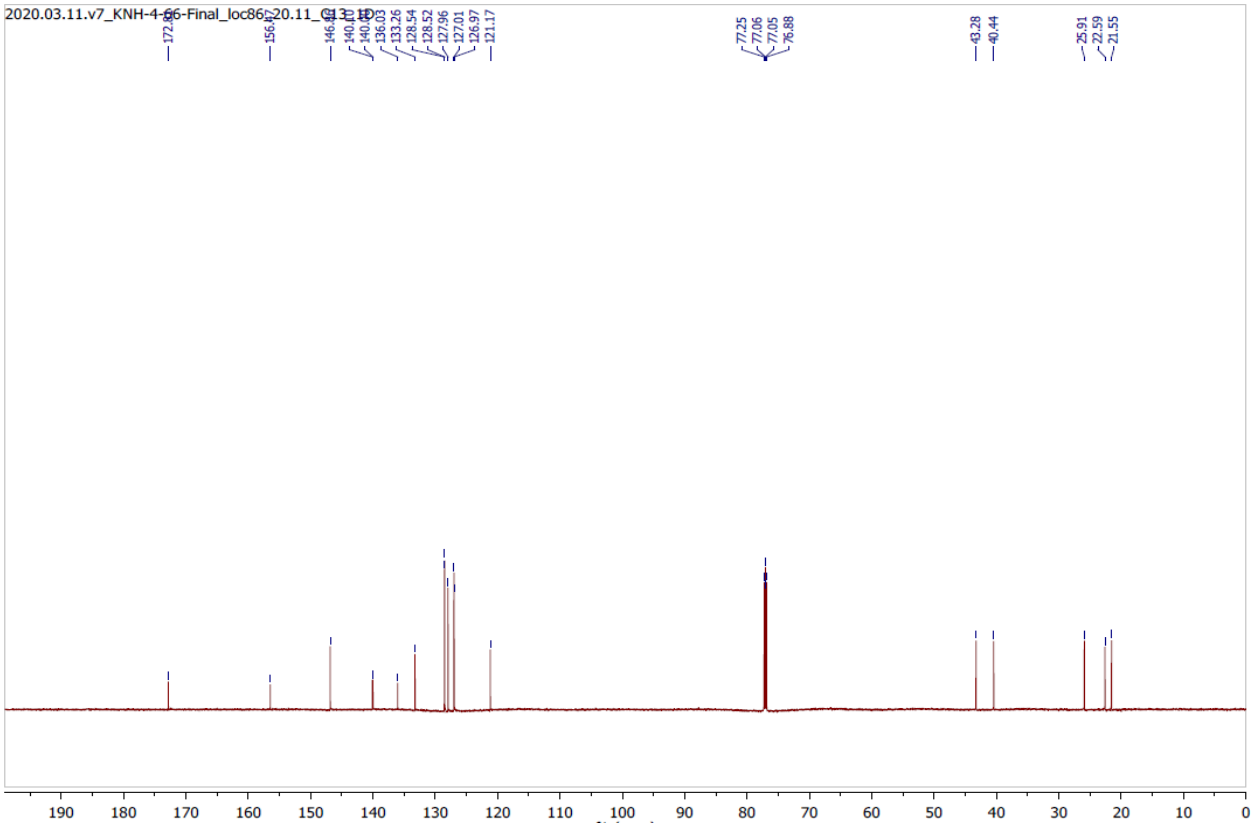

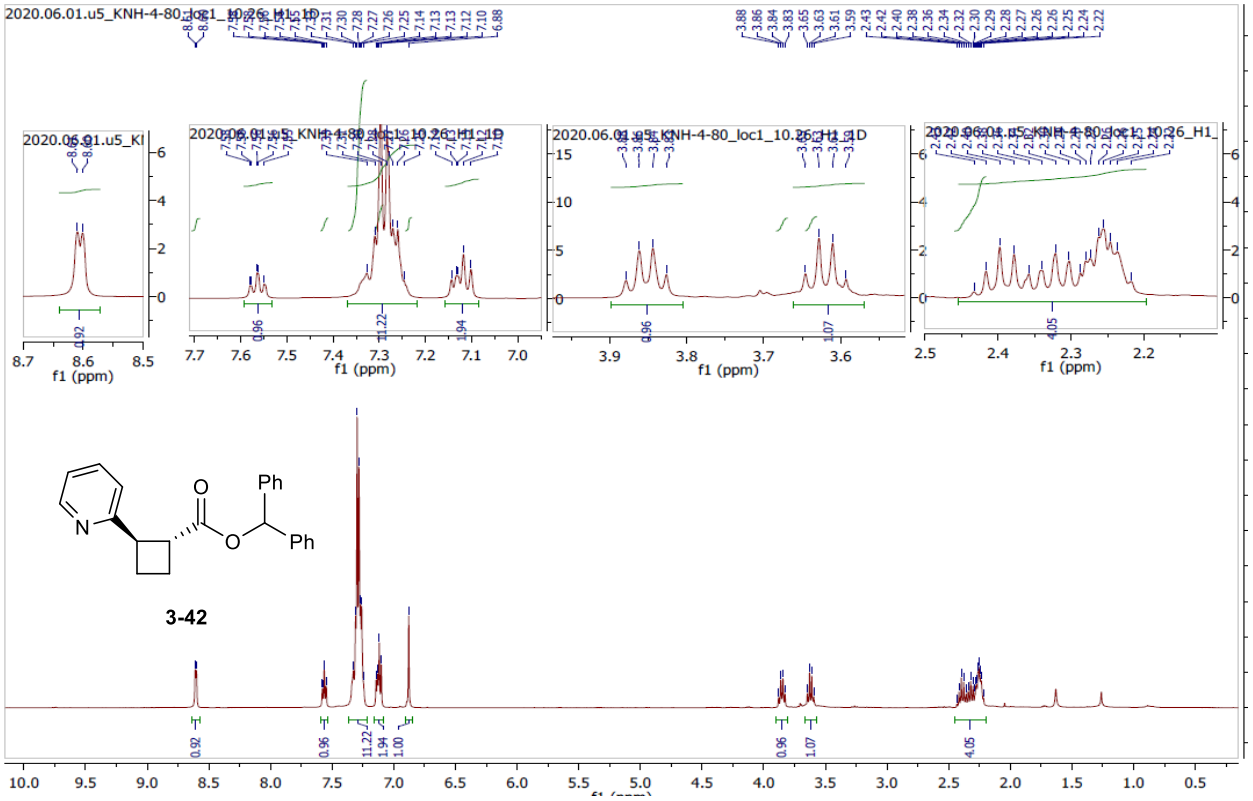
3-42

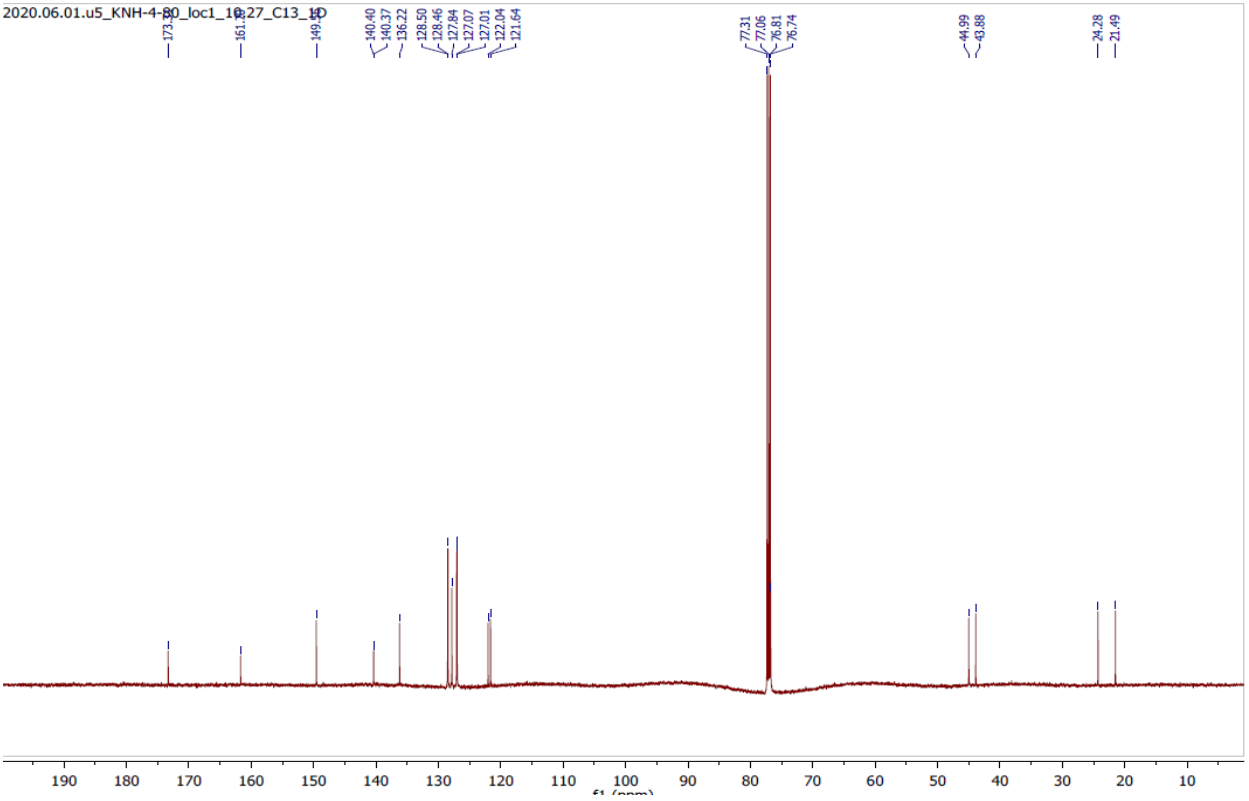

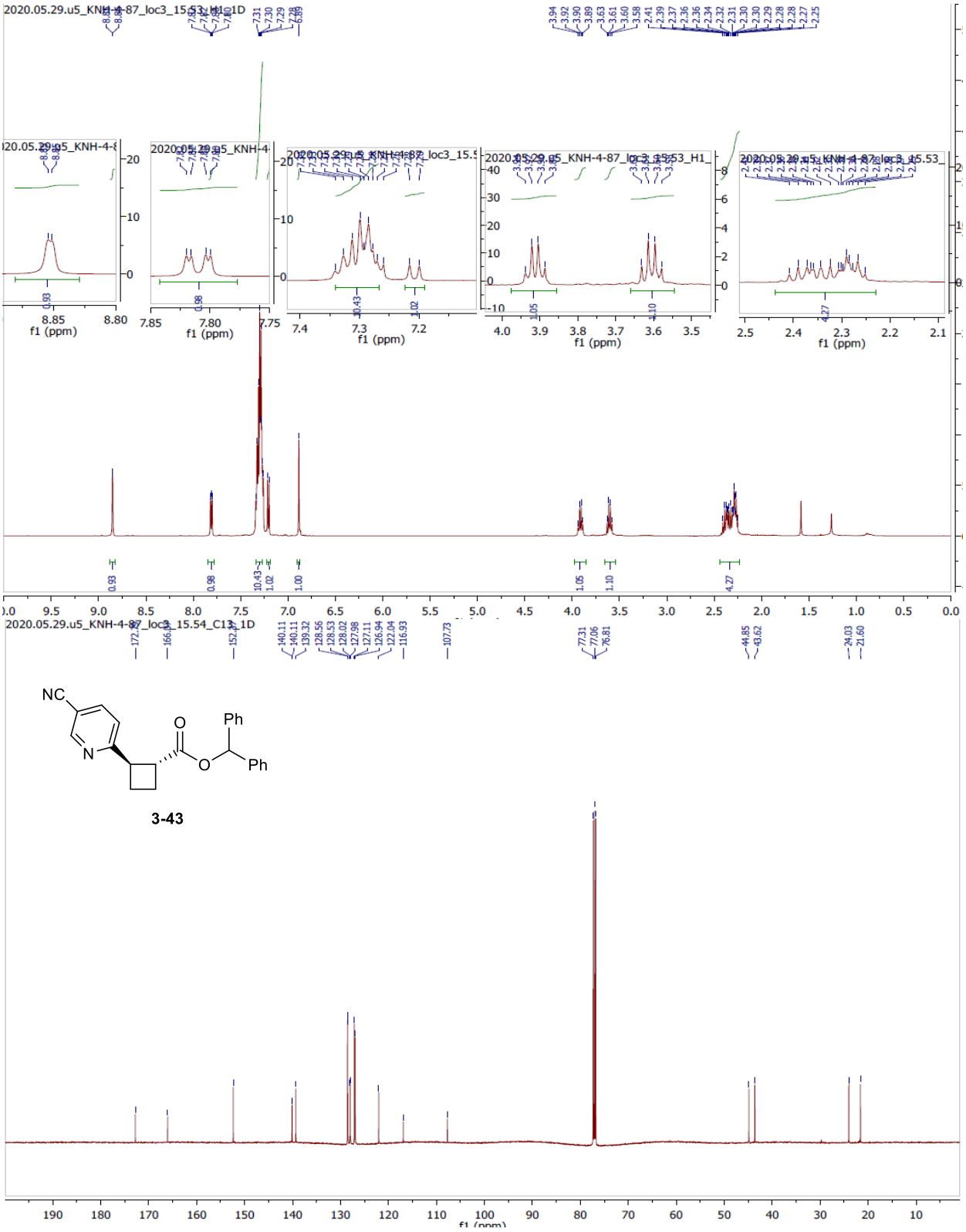
NC
N
O
O
Ph
Ph
3-43

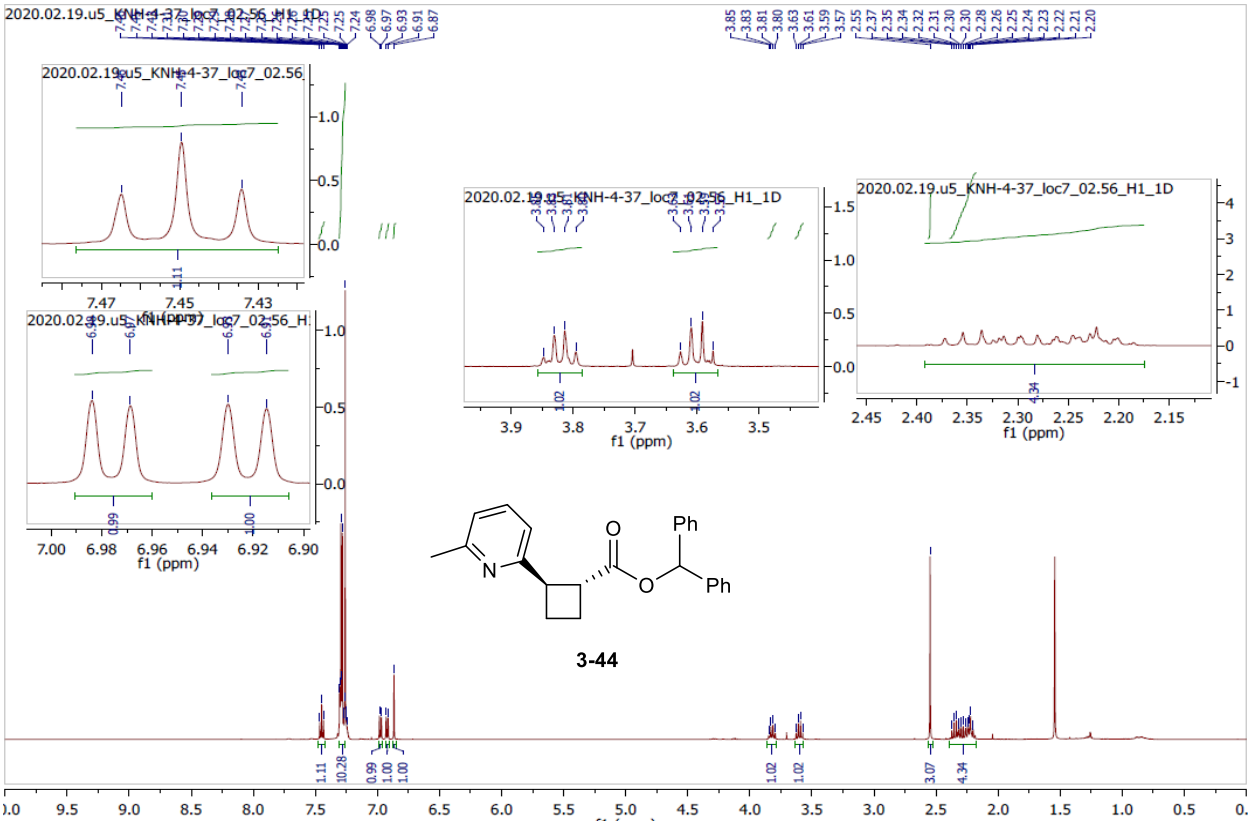
2020.02.19.u5_KNH-4-37_loc7_02.56_H1_1D
f1 (ppm)
O
Ph
N
O
Ph

3-44

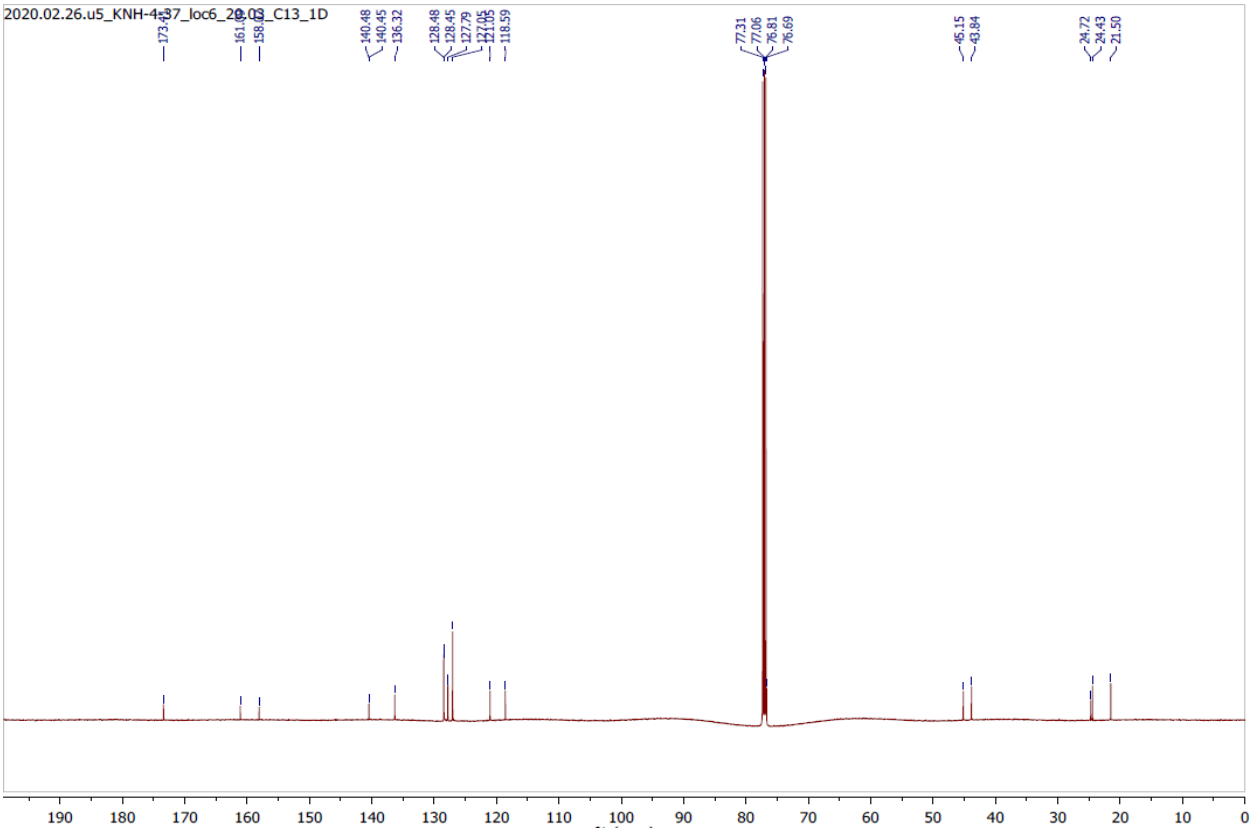
2020.02.26.u5_KNH-4-37_loc6_20.03_C13_1D

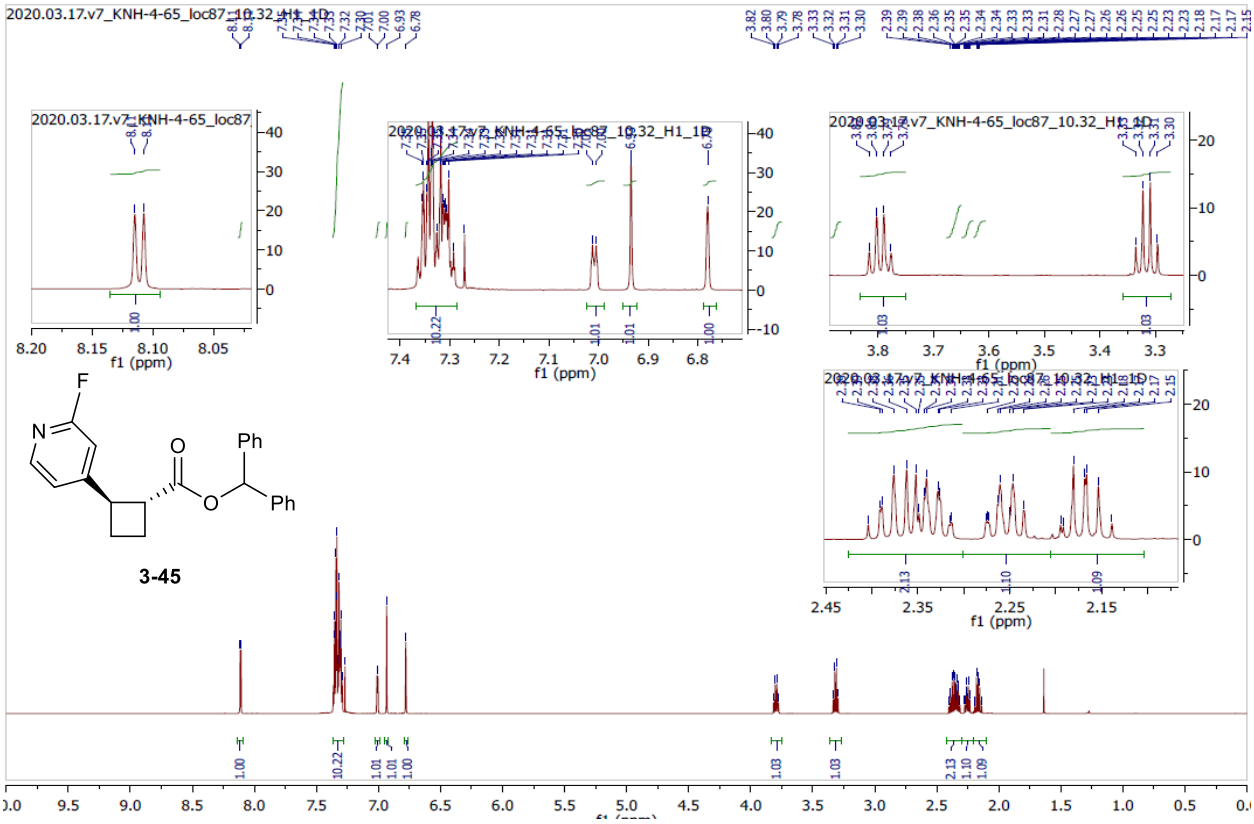
2020.03.17.v7_KNH-4-65_loc87_10.32_H1_1D
F
N
O
O
Ph
Ph
3-45
f1 (ppm)

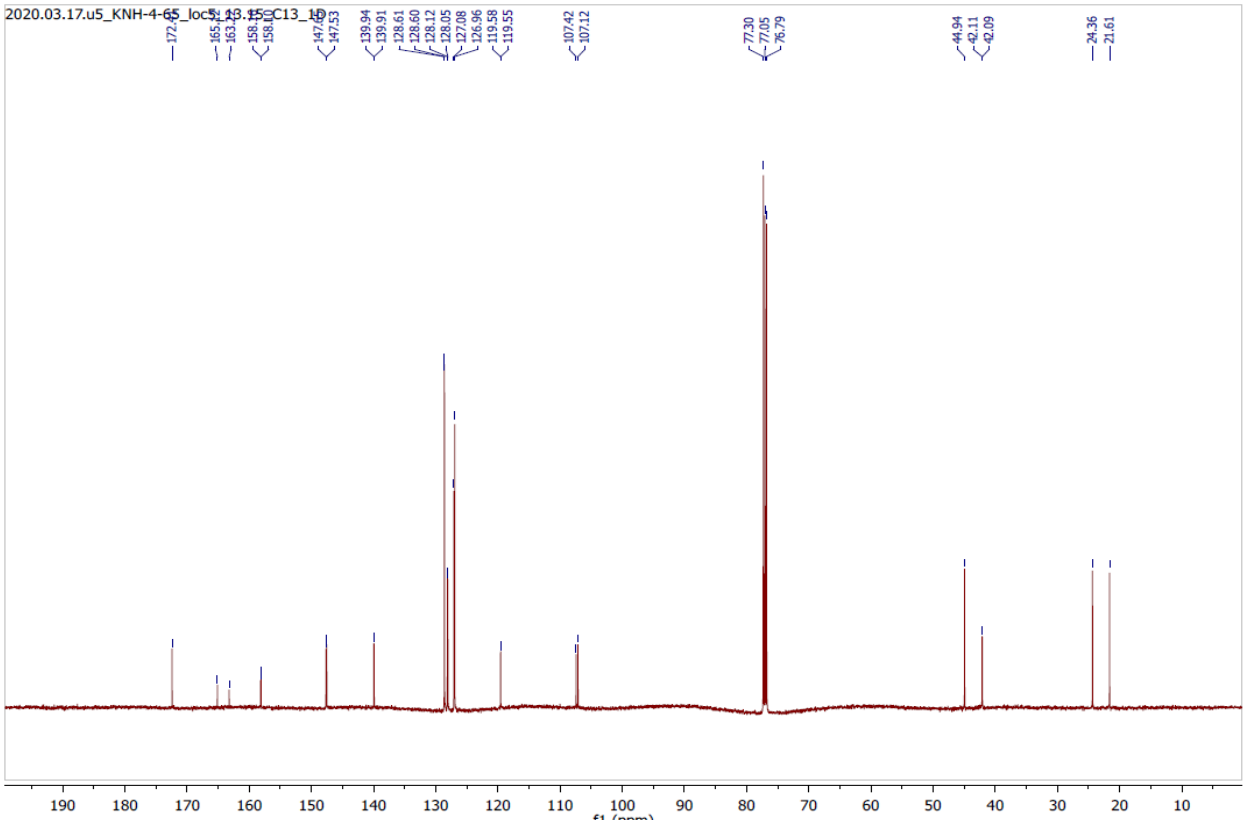
2020.03.17.u5_KNH-4-65_loc87_13.15_C13_1D
f1 (ppm)

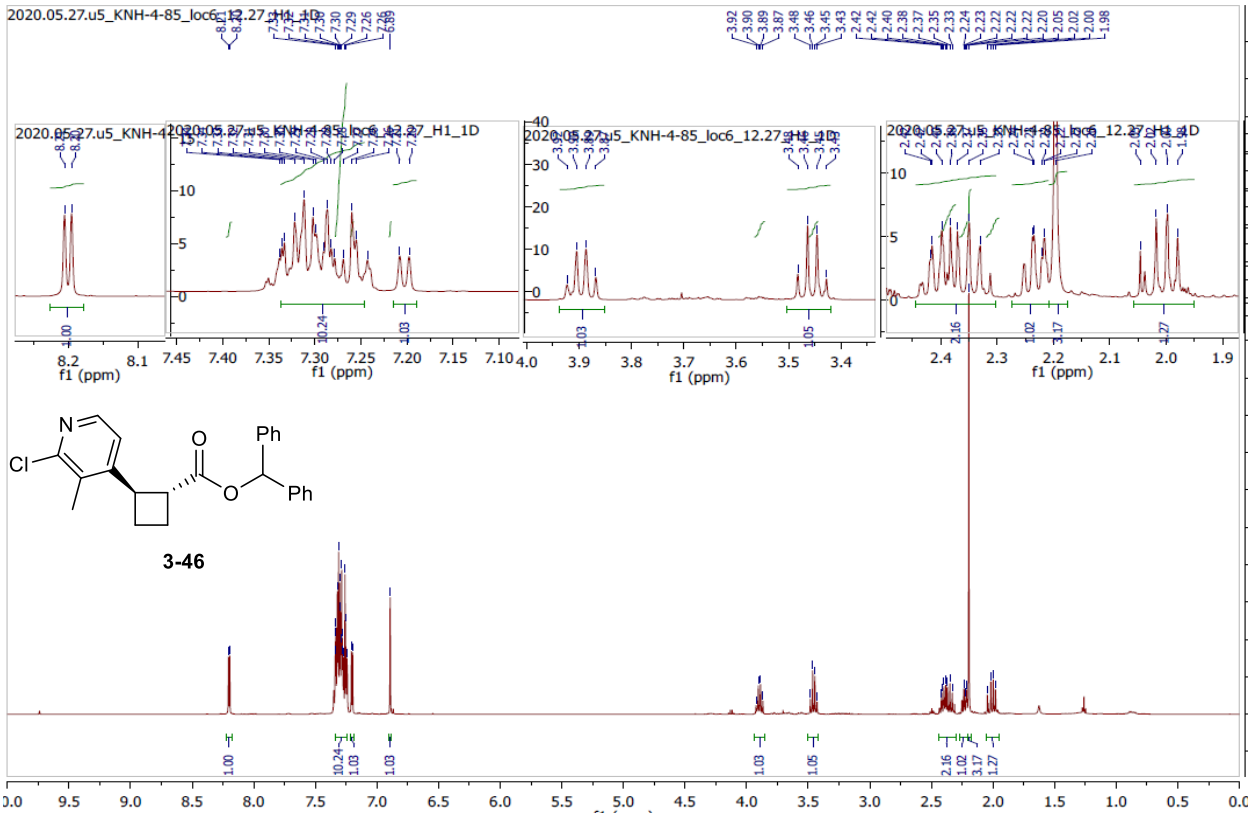
2020.05.27.u5_KNH-4-85_loc6_12.27_H1_1D
f1 (ppm)
N
Cl
O
O
Ph
Ph
3-46

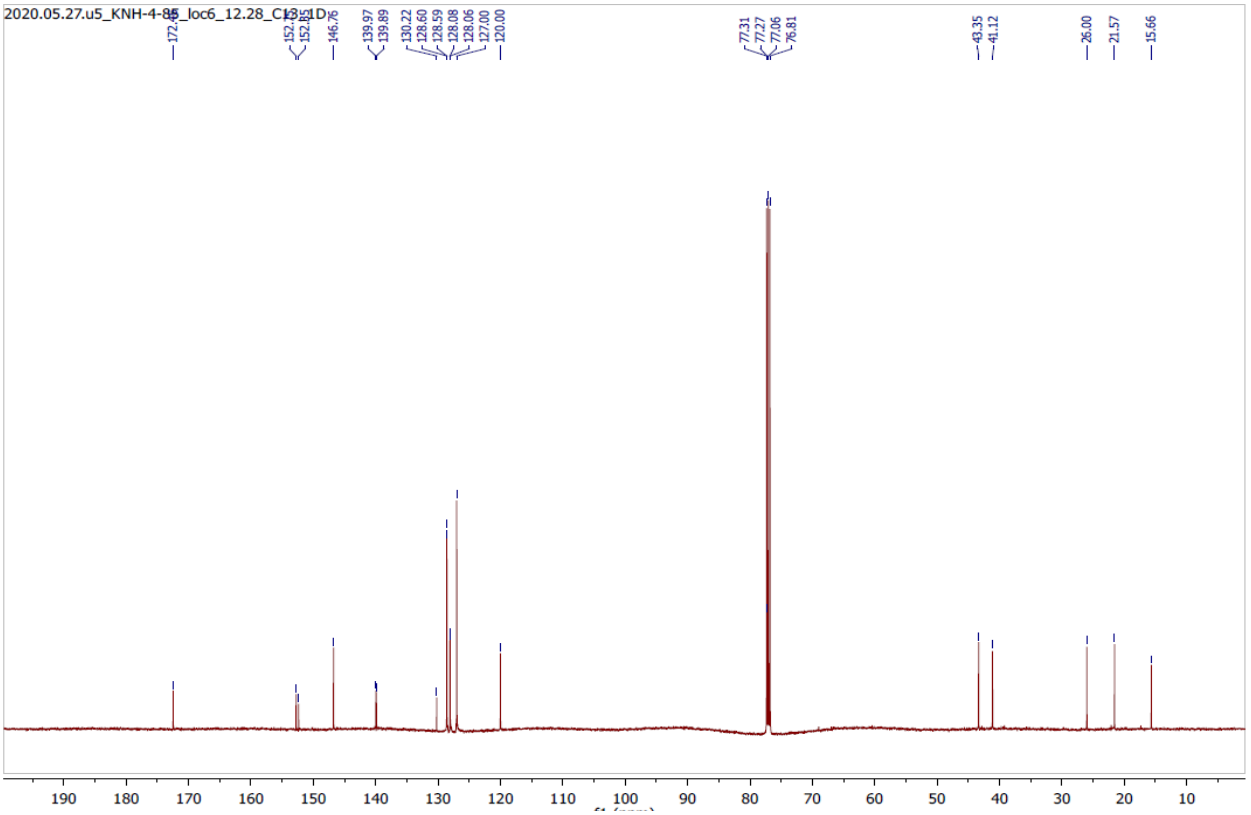
2020.05.27.u5_KNH-4-85_loc6_12.28_C13_1D
f1 (ppm)

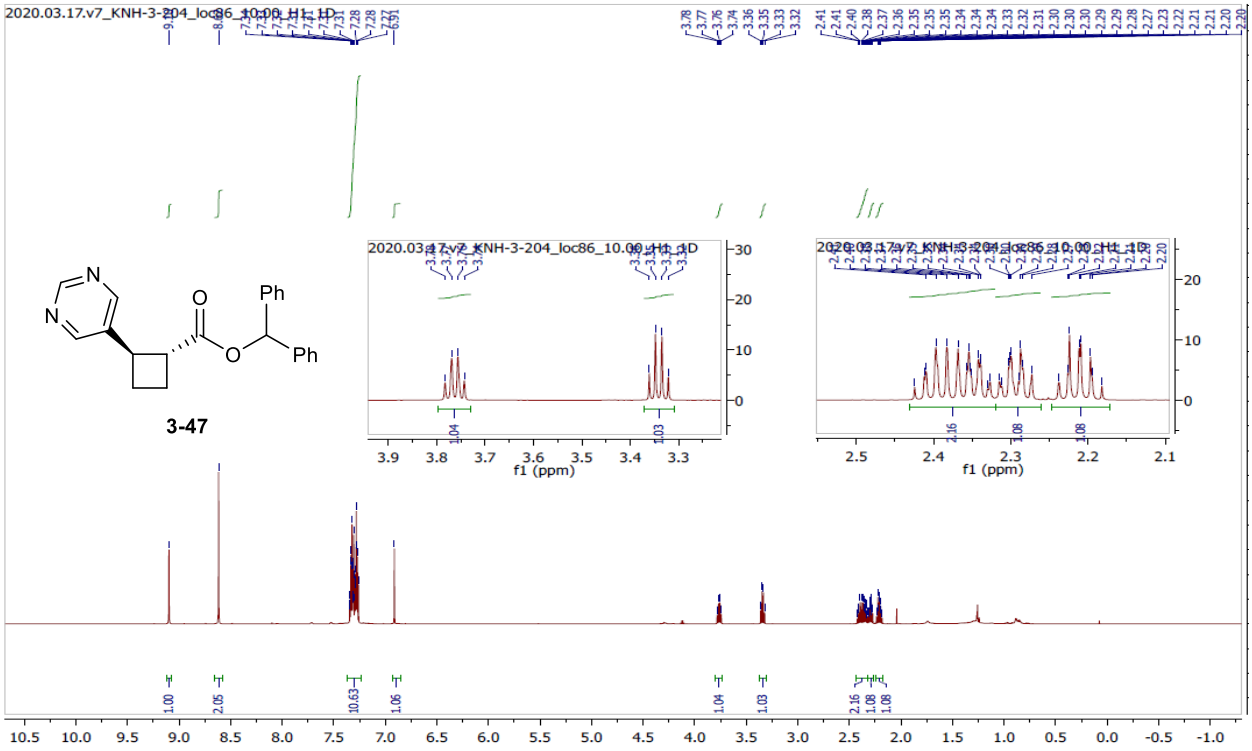
2020.03.17.v7_KNH-3-204_loc86_10.00_1H_1D
3-47
f1 (ppm)

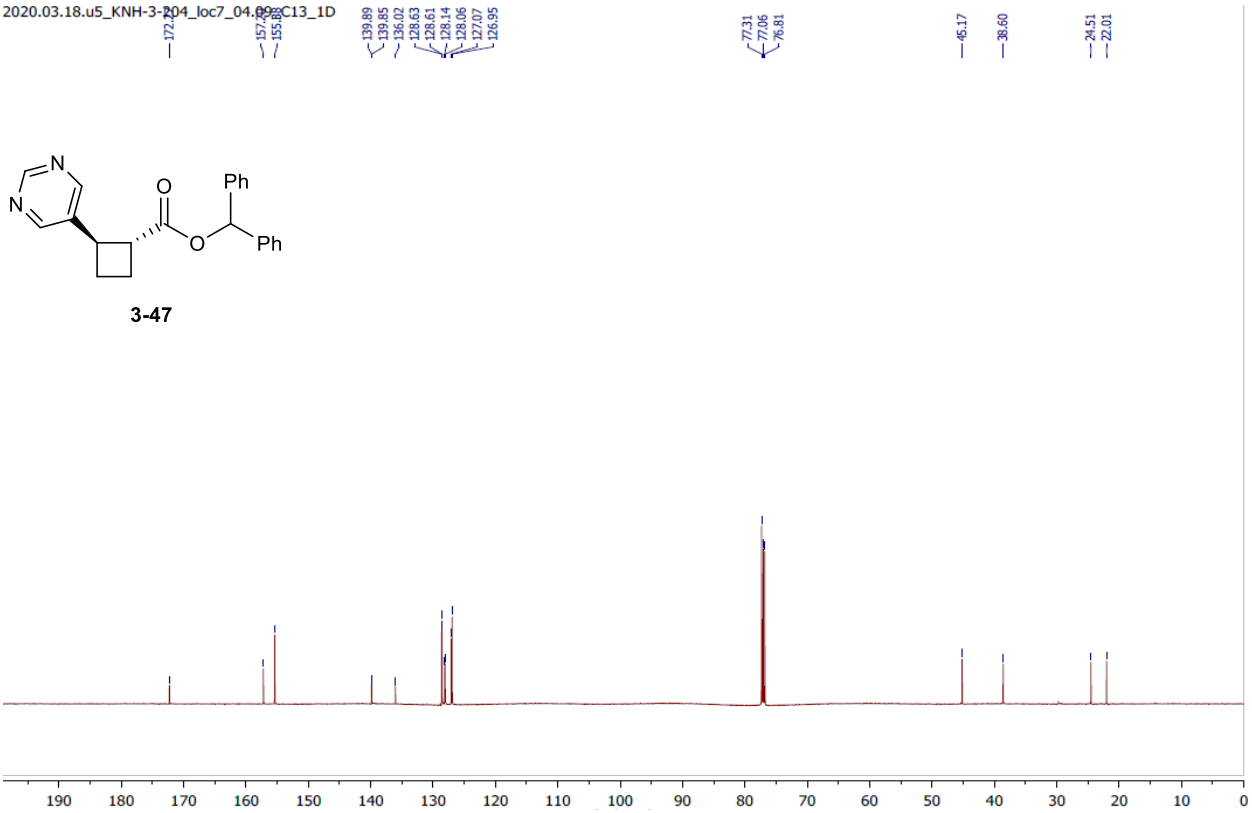
2020.03.18.u5_KNH-3-204_loc7_04.09_C13_1D
3-47

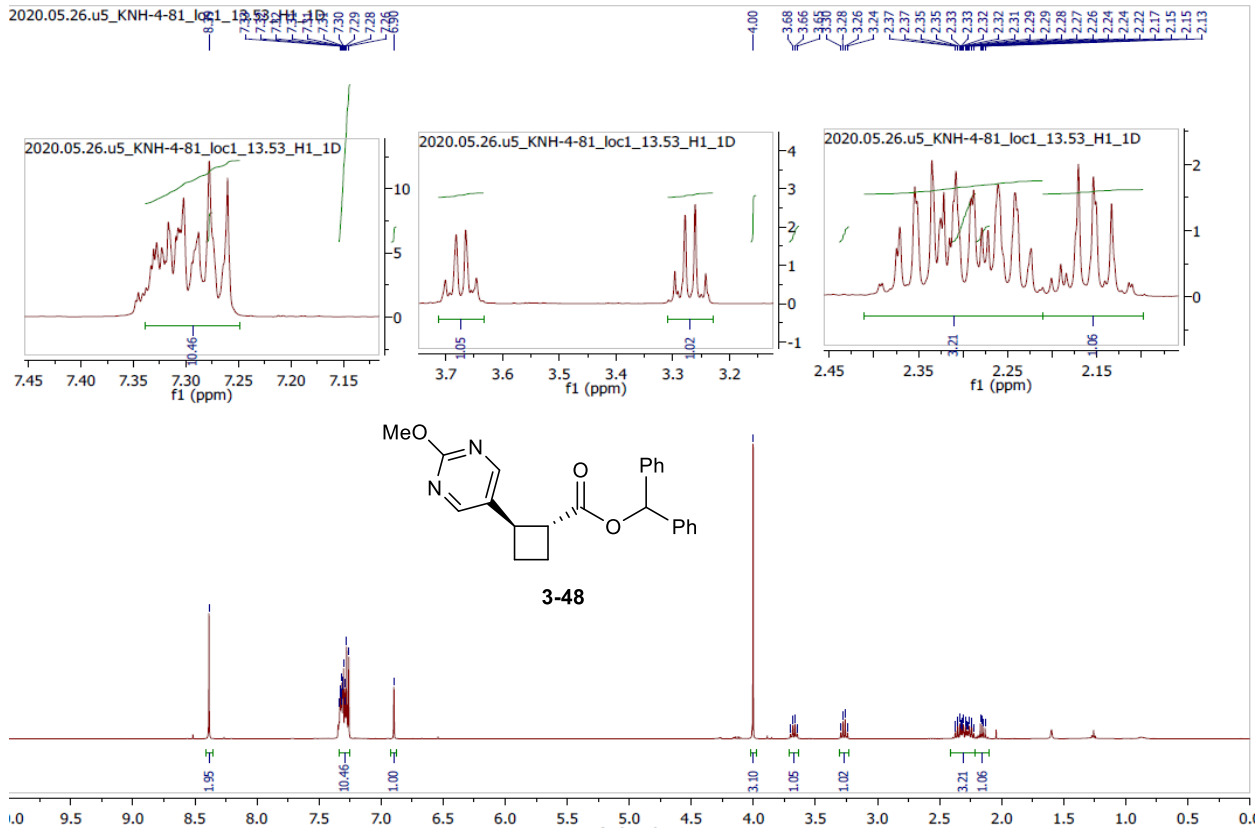
2020.05.26.u5_KNH-4-81_loc1_13.53_H1_1D
f1 (ppm)

MeO
N
N
O
O
Ph
Ph

3-48

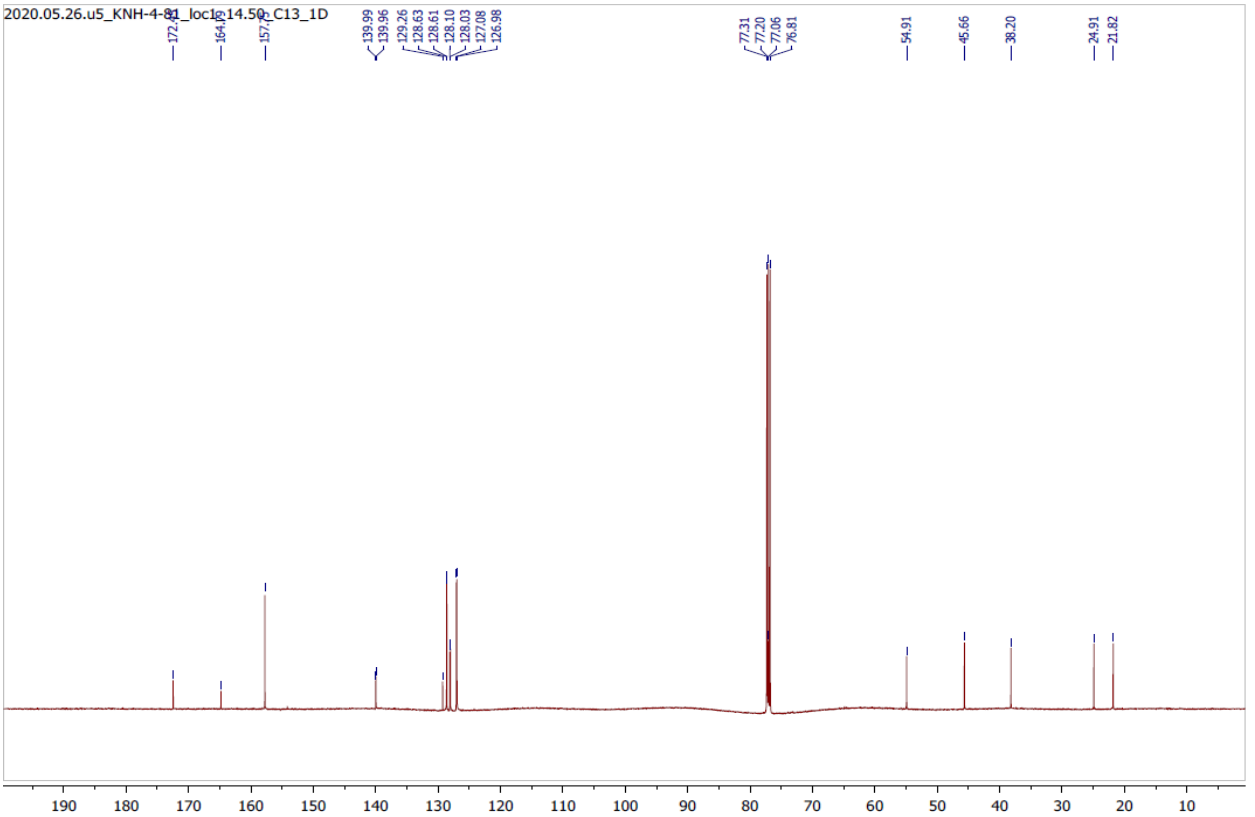
2020.05.26.u5_KNH-4-81_loc1_14.50_C13_1D
f1 (ppm)

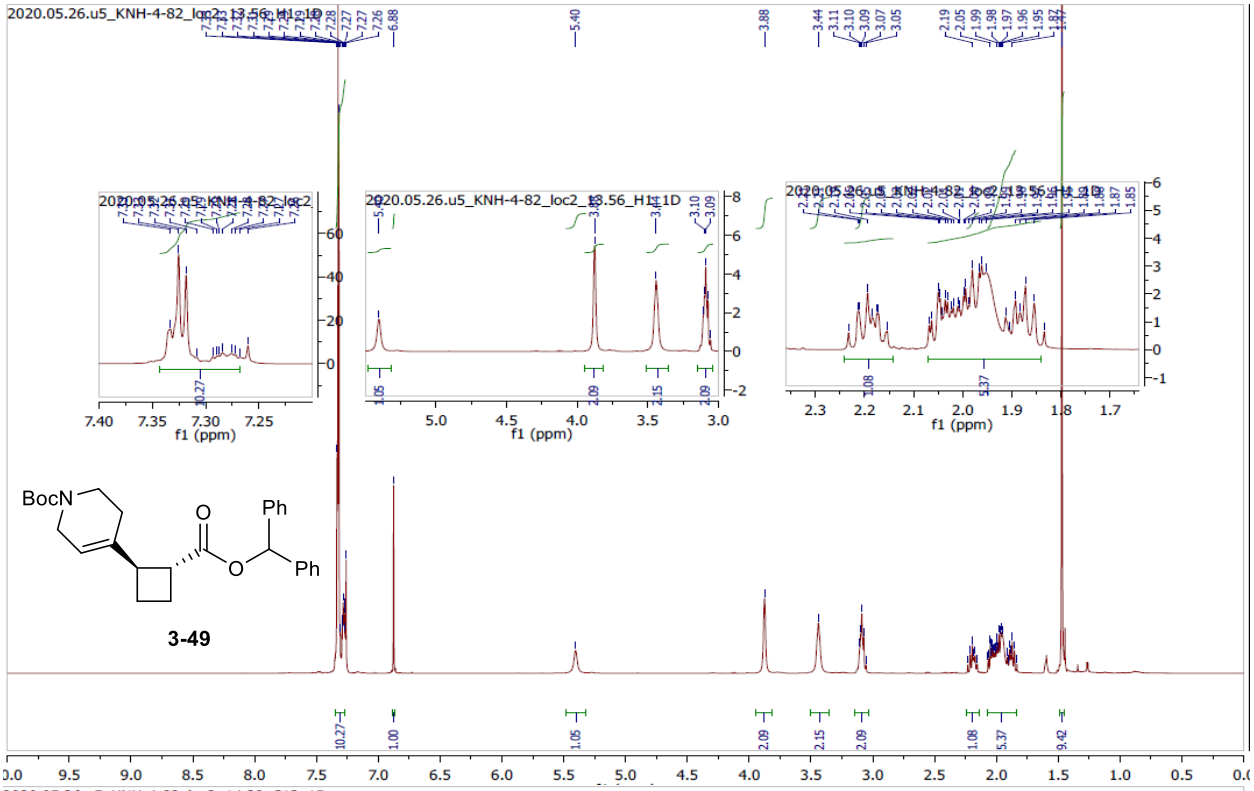
2020.05.26.u5_KNH-4-82_loc2_13.56_H1_1D
BocN
O
O
Ph
Ph
3-49
f1 (ppm)

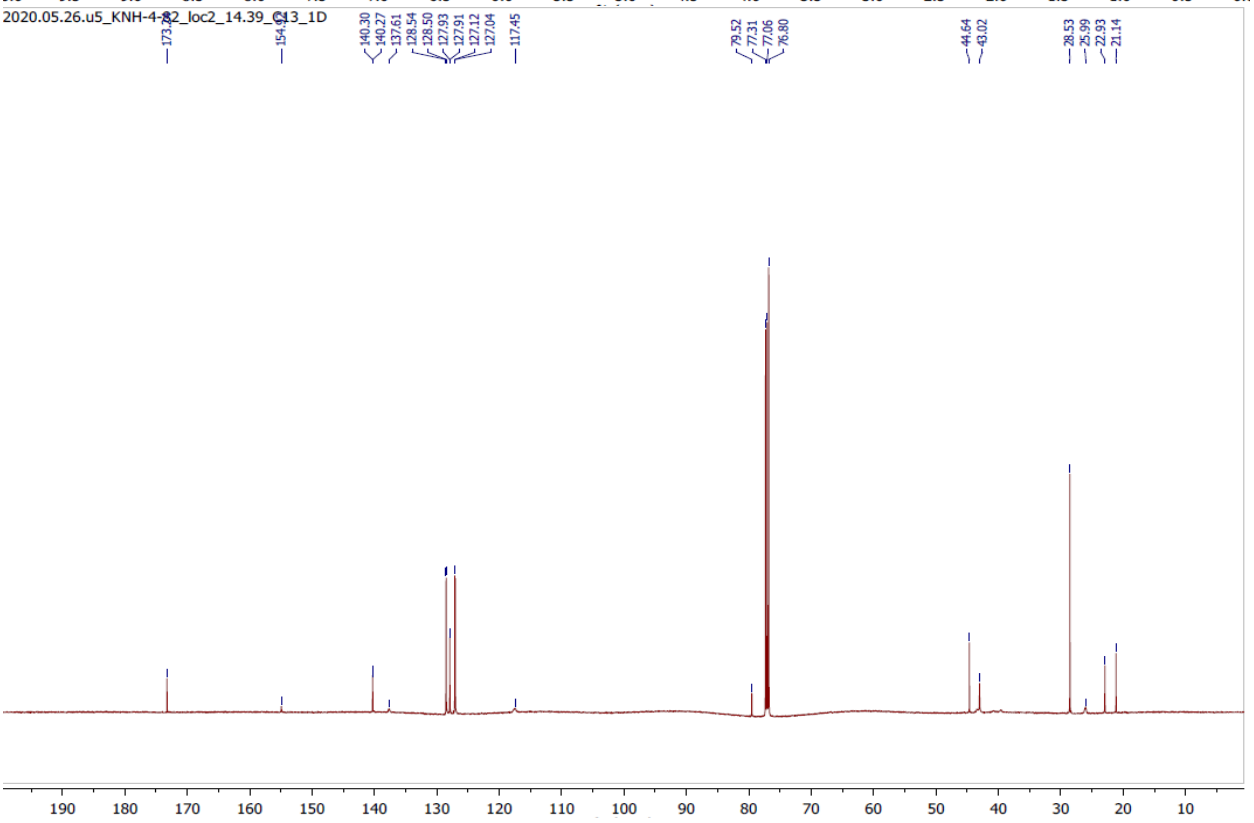
2020.05.26.u5_KNH-4-82_loc2_14.39_C13_1D

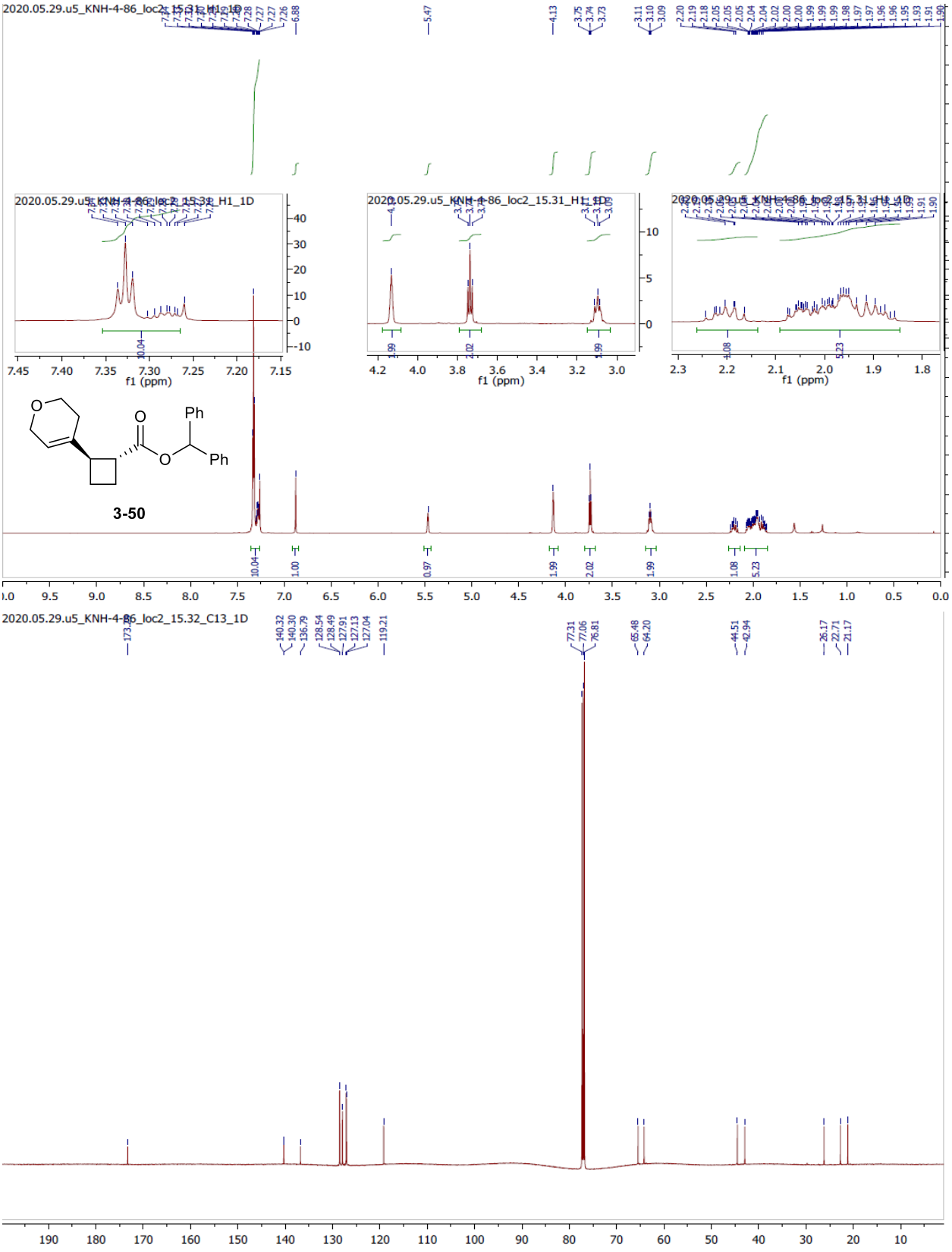
2020.05.29.u5_KNH-4-86_loc2_15.31_H1_1D
f1 (ppm)
O
O
O
Ph
Ph
3-50

2020.05.29.u5_KNH-4-86_loc2_15.32_C13_1D

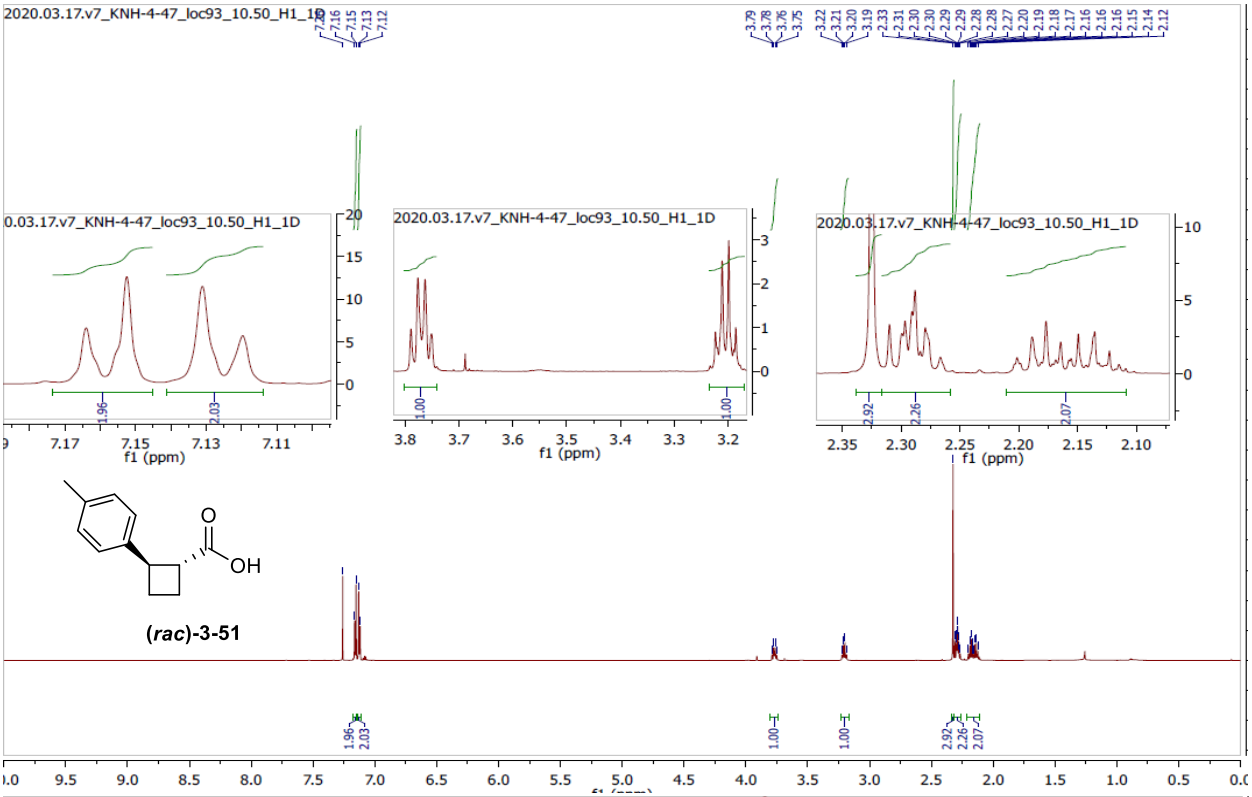
2020.03.17.v7_KNH-4-47_loc93_10.50_H1_1D
f1 (ppm)
O
OH
(rac)-3-51

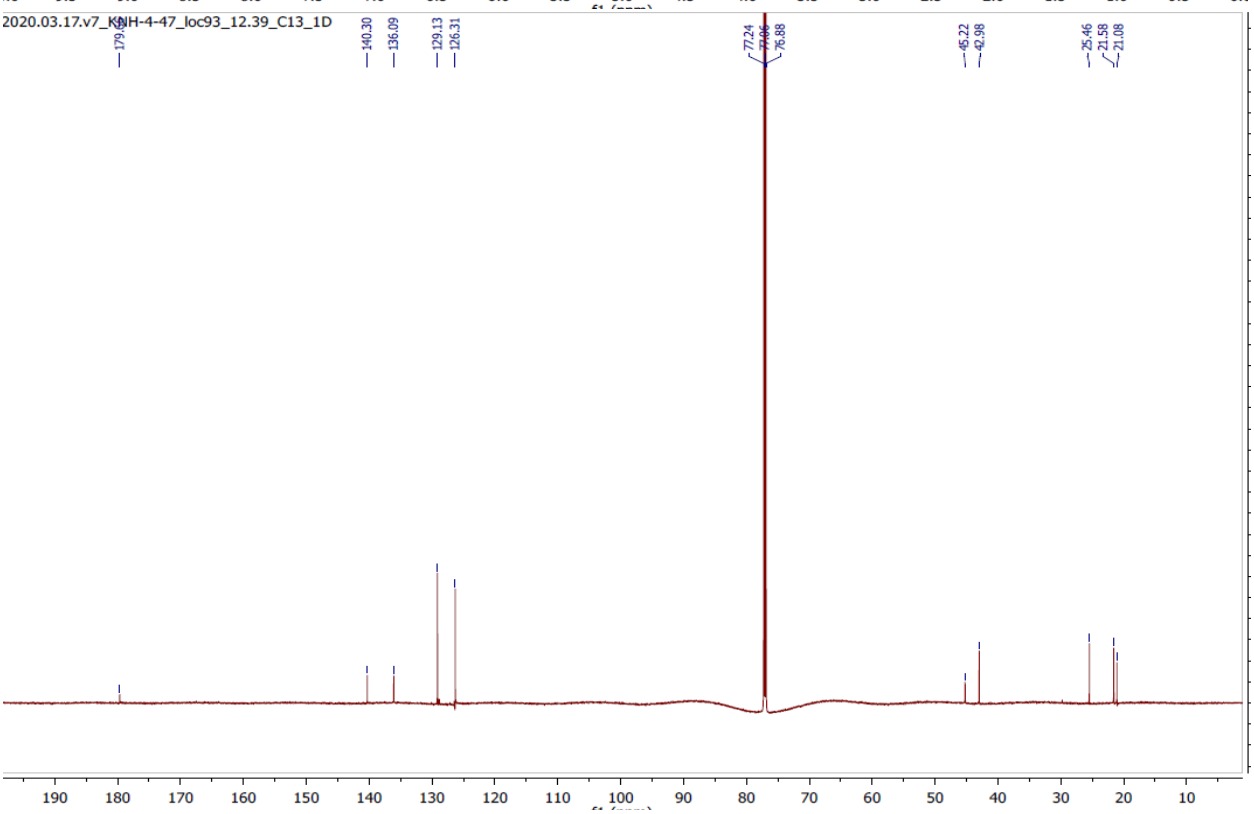
2020.03.17.v7_KNH-4-47_loc93_12.39_C13_1D
f1 (ppm)

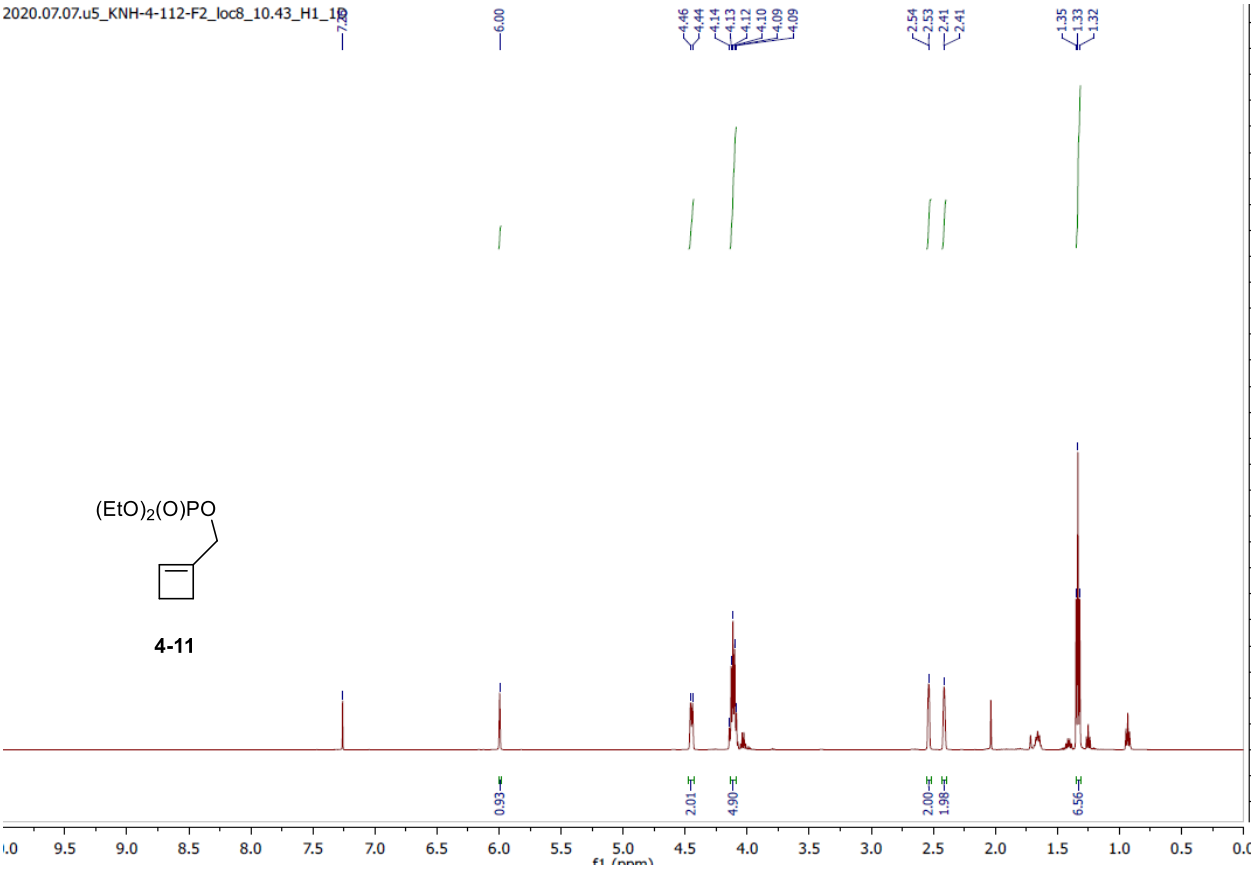
2020.07.07.u5_KNH-4-112-F2_loc8_10.43_H1_1D
(EtO)2(O)PO
4-11

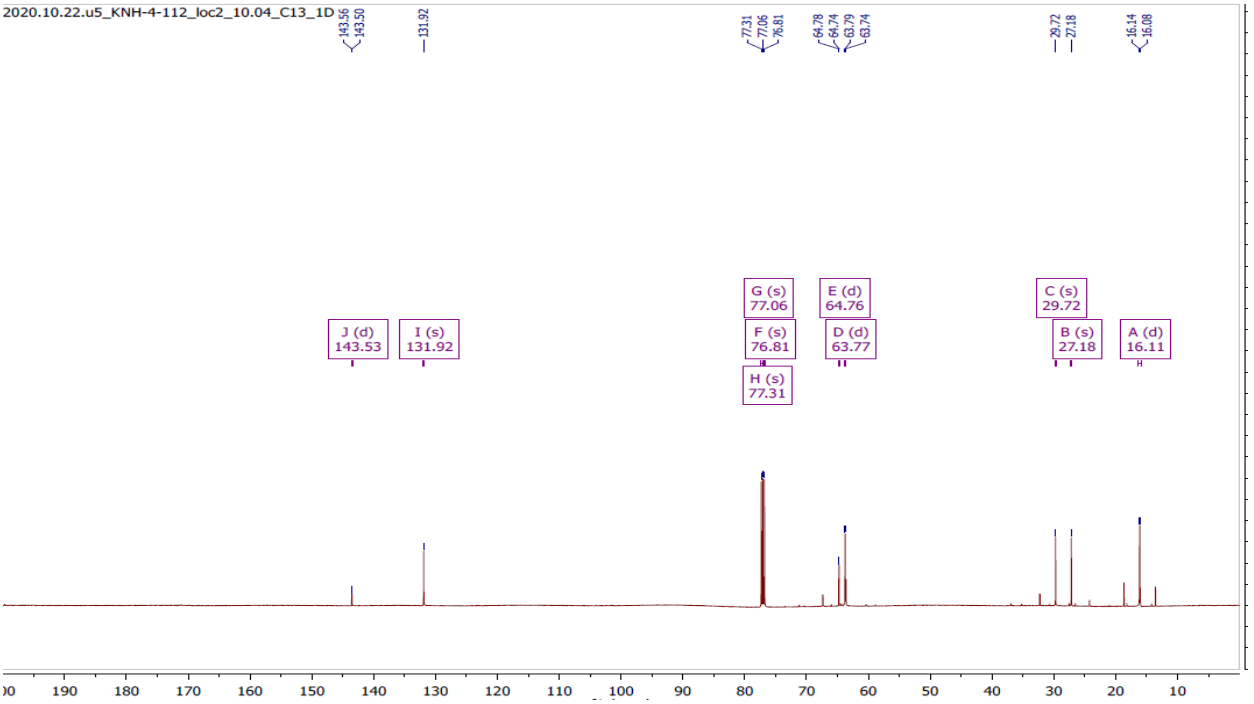
2020.10.22.u5_KNH-4-112_loc2_10.04_C13_1D
J (d) 143.53
I (s) 131.92
G (s) 77.06
F (s) 76.81
H (s) 77.31
E (d) 64.76
D (d) 63.77
C (s) 29.72
B (s) 27.18
A (d) 16.11

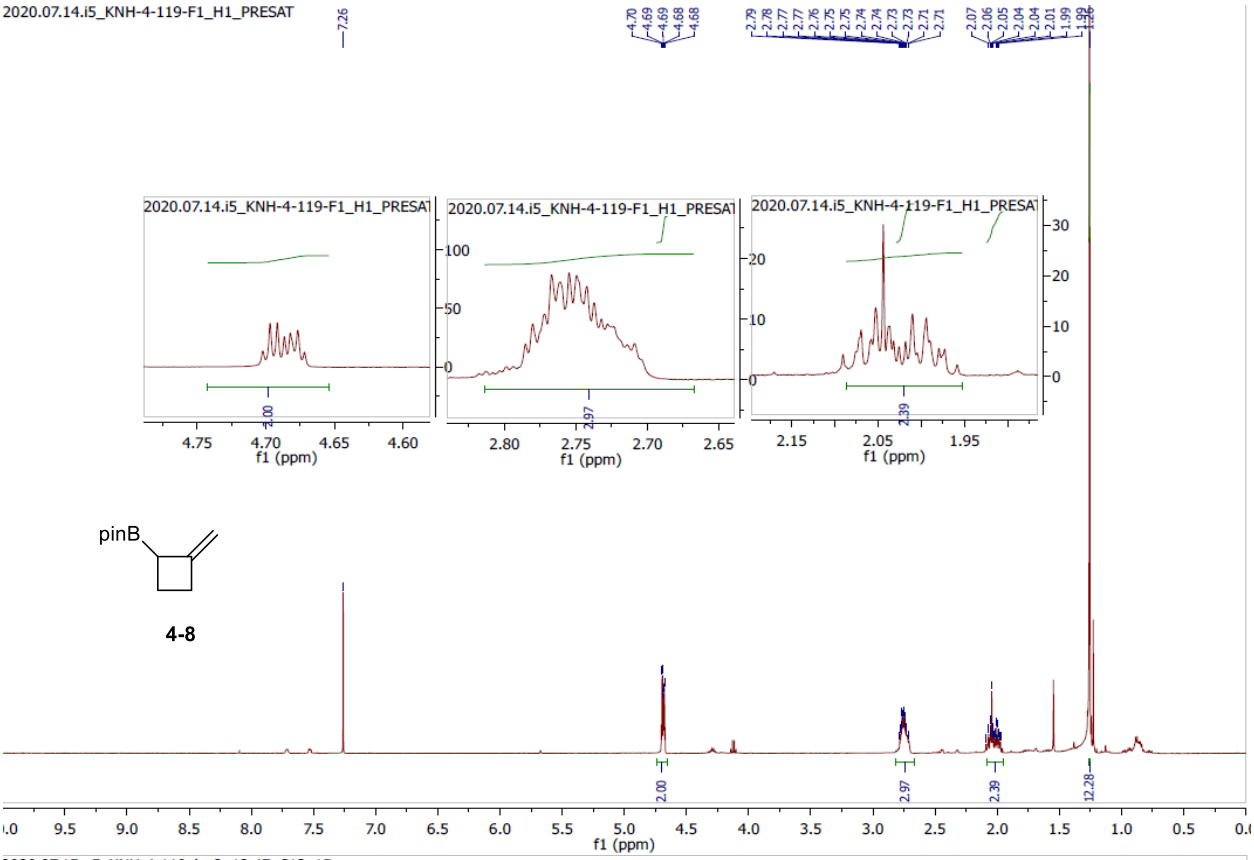
2020.07.14.i5_KNH-4-119-F1_H1_PRESAT
pinB
4-8
f1 (ppm)

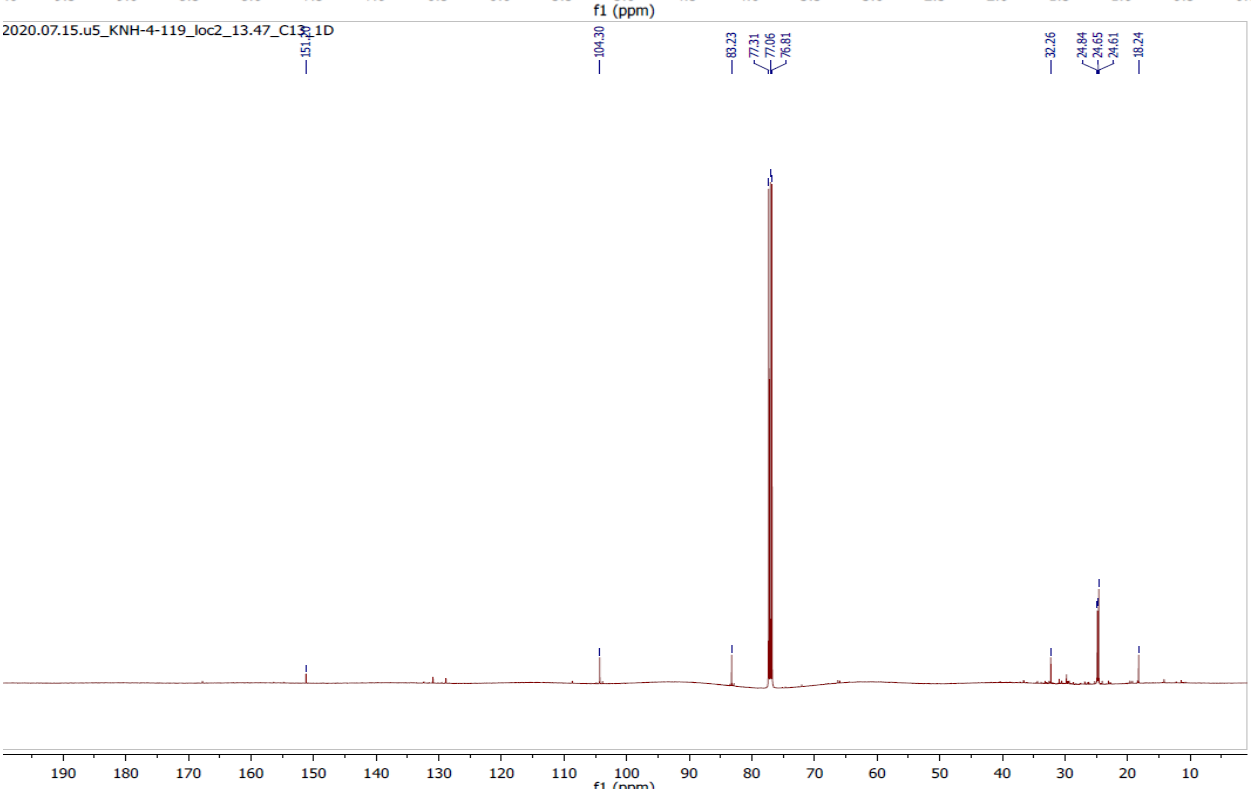
2020.07.15.u5_KNH-4-119_loc2_13.47_C13_1D
f1 (ppm)

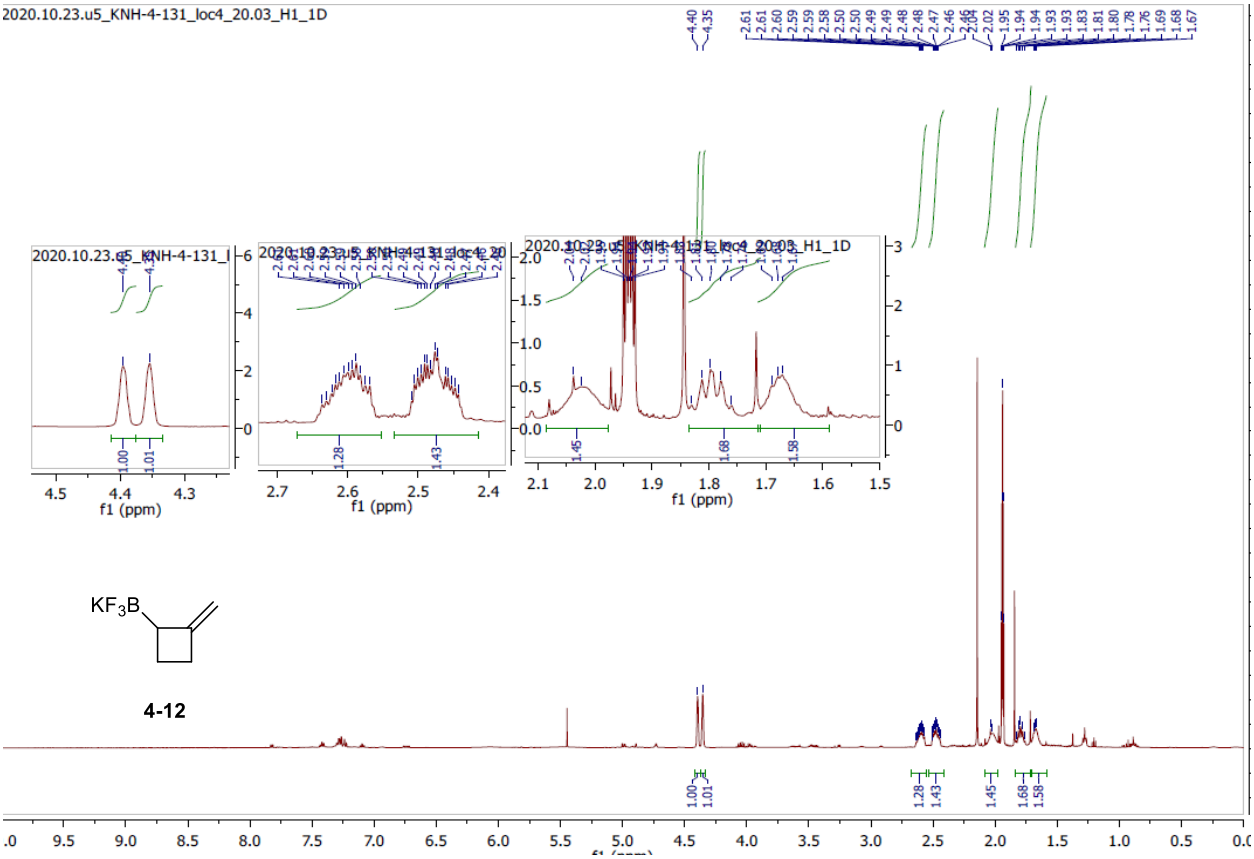
2020.10.23.u5_KNH-4-131_loc4_20.03_H1_1D
KF3B
4-12

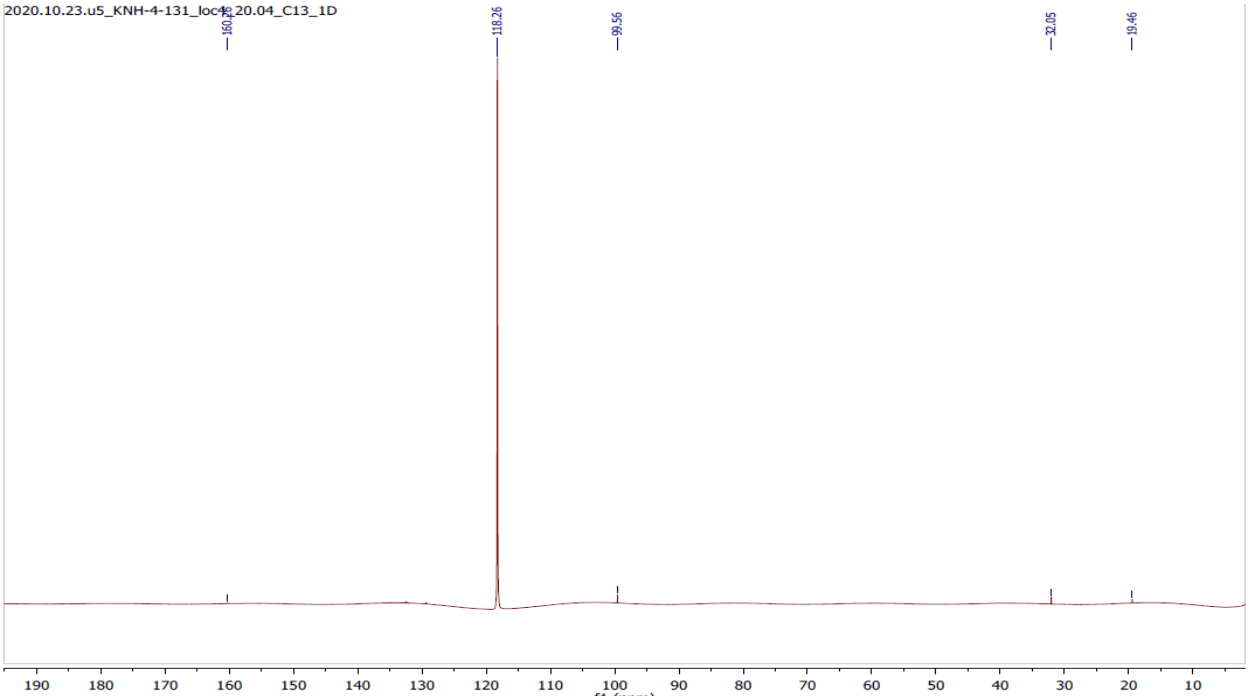
2020.10.23.u5_KNH-4-131_loc4_20.04_C13_1D

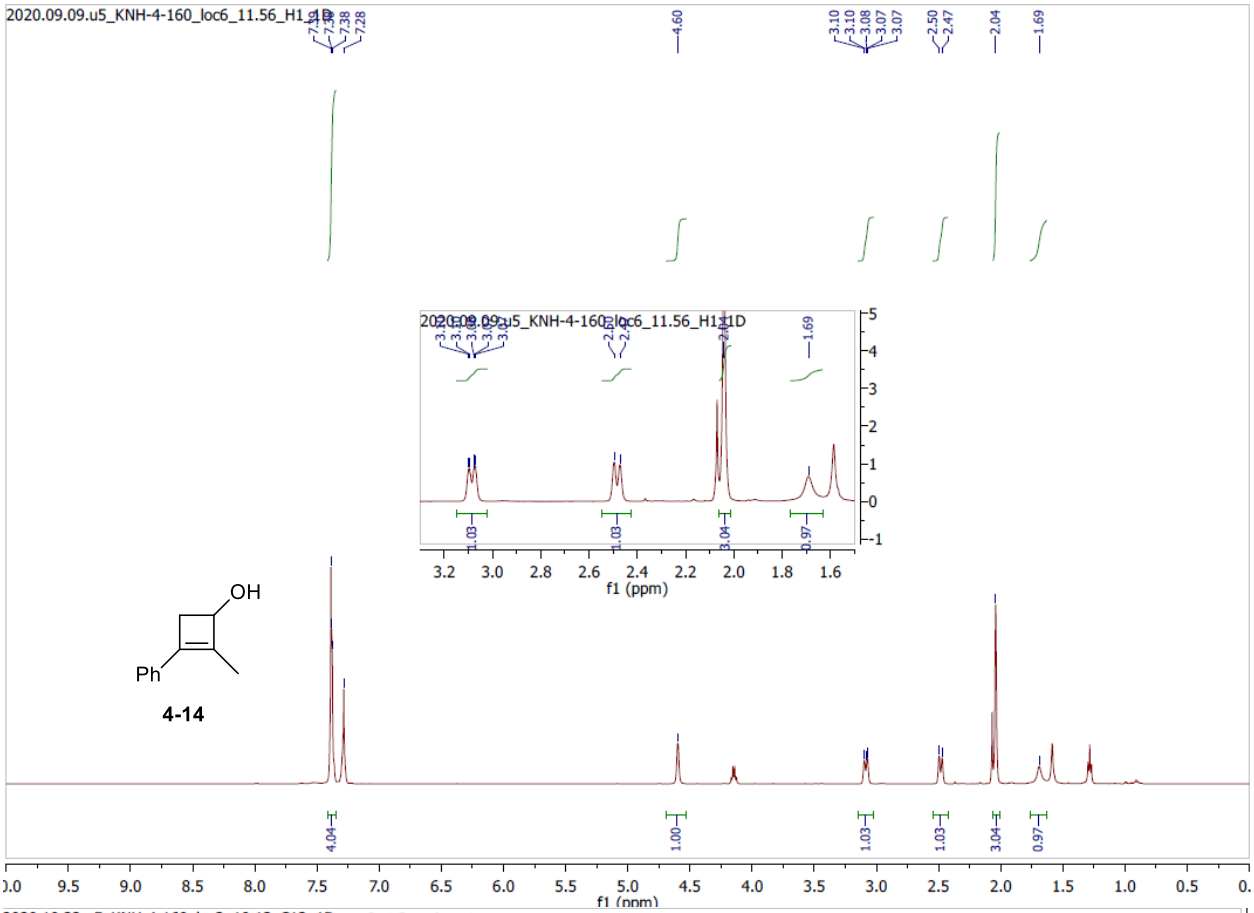
2020.09.09.u5_KNH-4-160_loc6_11.56_H1_1D
OH
Ph
4-14
f1 (ppm)

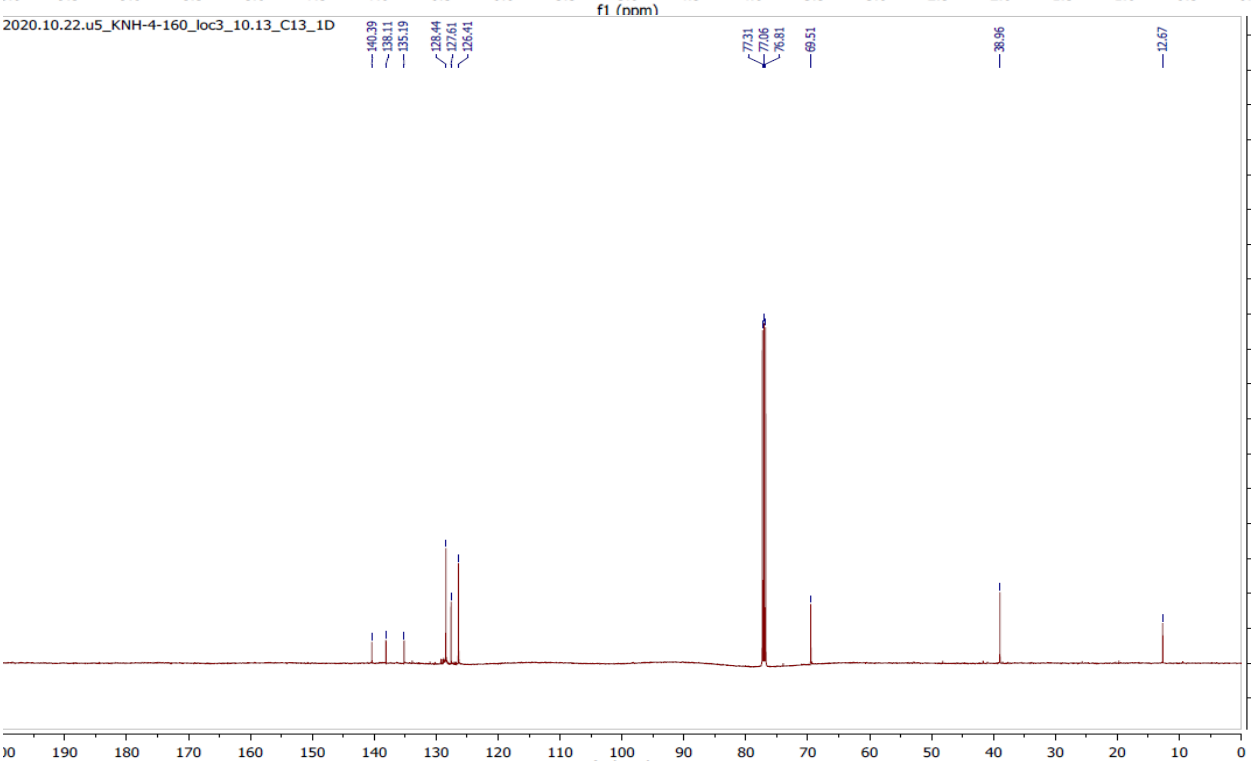
2020.10.22.u5_KNH-4-160_loc3_10.13_C13_1D

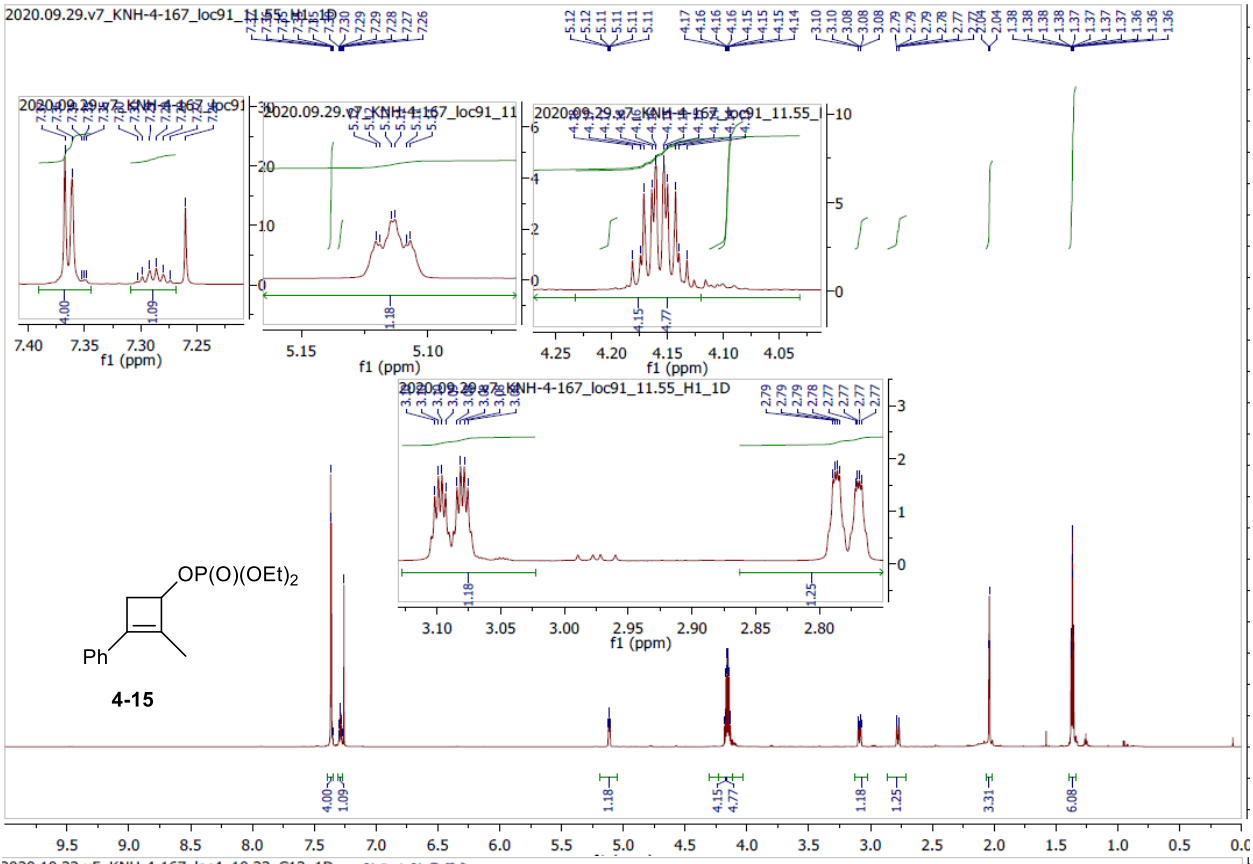
2020.09.29.v7_KNH-4-167_loc91_11.55_H1_1D
OP(O)(OEt)2
Ph
4-15

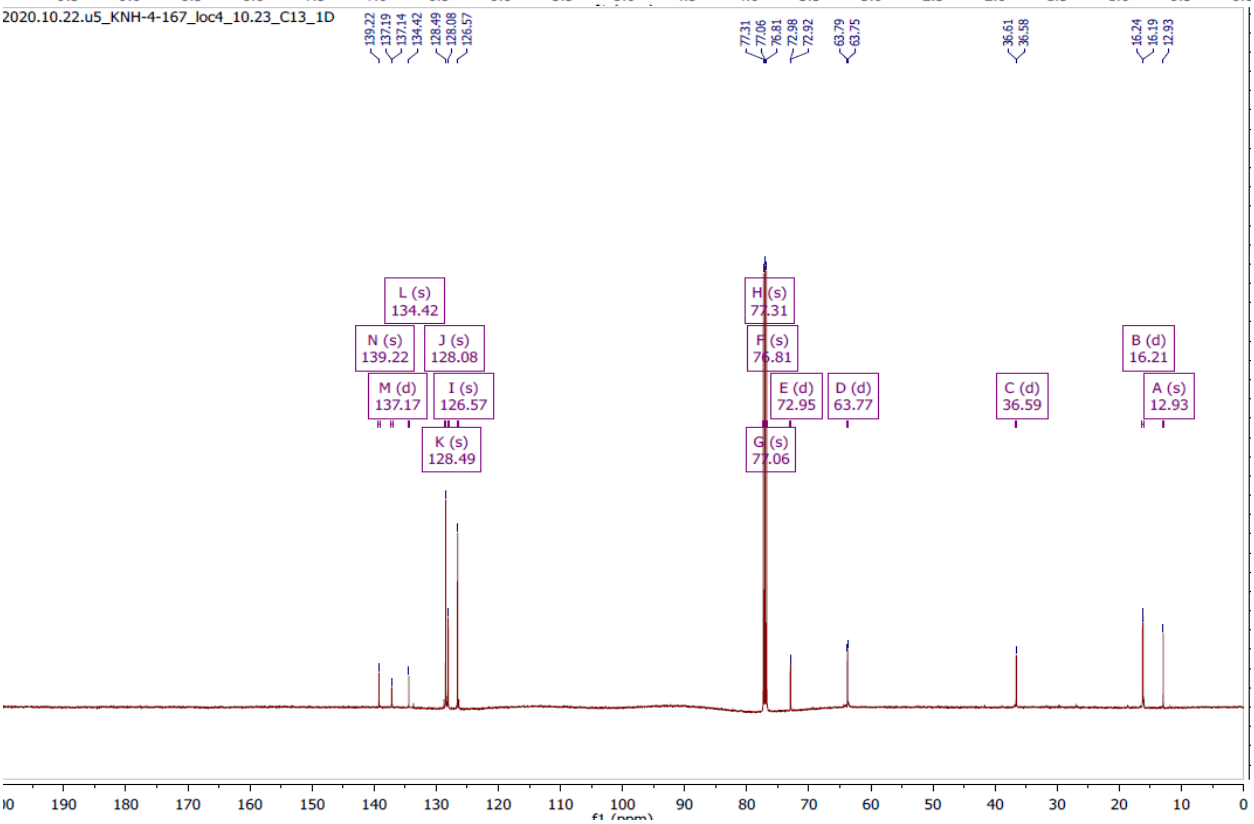
2020.10.22.u5_KNH-4-167_loc4_10.23_C13_1D
L (s) 134.42
N (s) 139.22
J (s) 128.08
M (d) 137.17
I (s) 126.57
K (s) 128.49
H (s) 77.31
F (s) 76.81
E (d) 72.95
D (d) 63.77
G (s) 77.06
C (d) 36.59
B (d) 16.21
A (s) 12.93

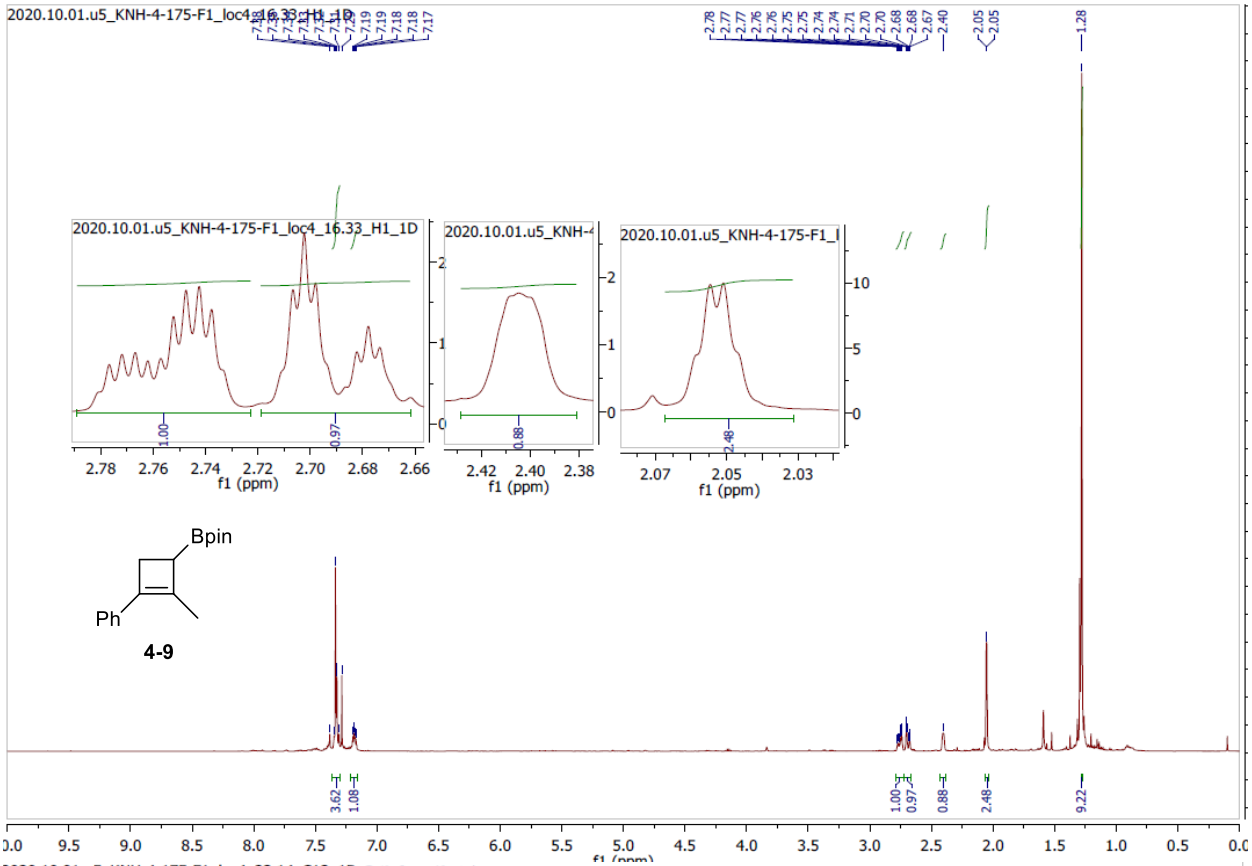
2020.10.01.u5_KNH-4-175-F1_loc4_16.33_H1_1D
Bpin
Ph
4-9

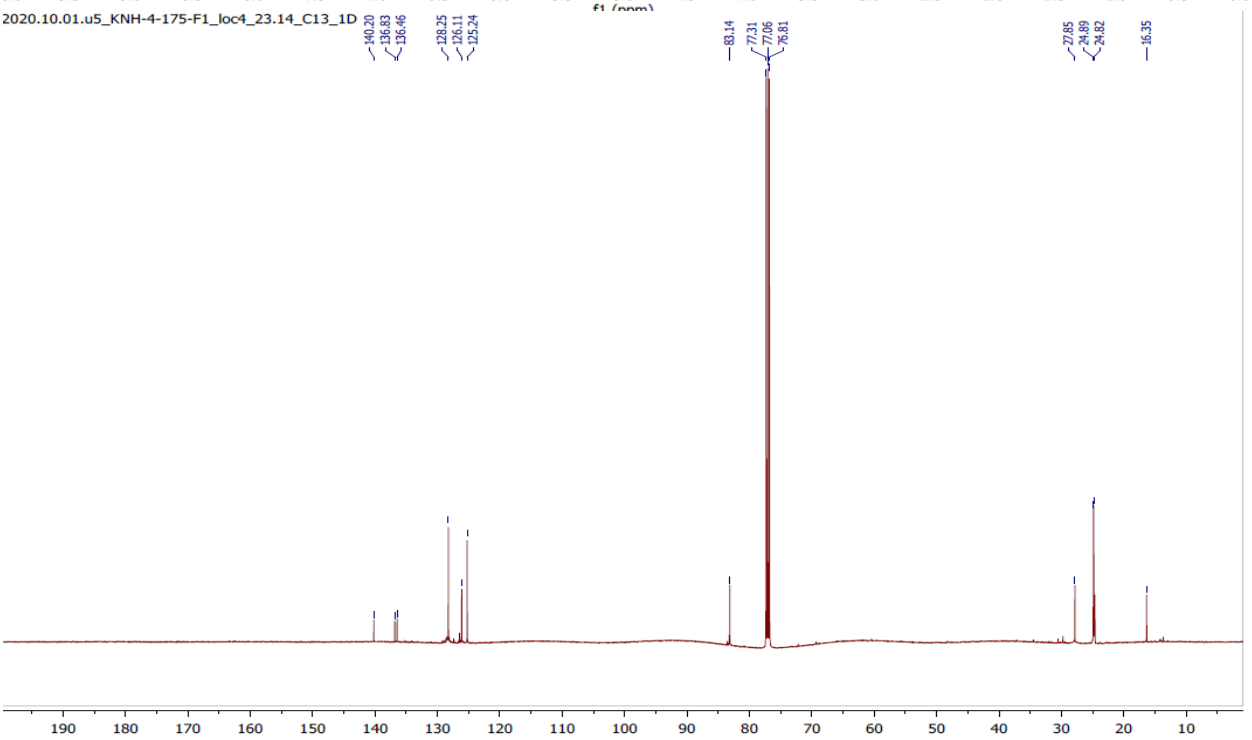
2020.10.01.u5_KNH-4-175-F1_loc4_23.14_C13_1D

Appendix 2. HPLC chromatograms for enantioenriched compounds

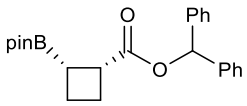

2-30

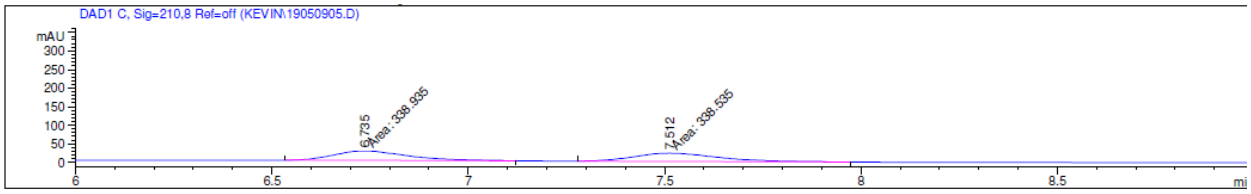


```
================================================================================
                          Area Percent Report
================================================================================

Sorted By             :      Signal
Multiplier            :      1.0000
Dilution              :      1.0000
Use Multiplier & Dilution Factor with ISTDs


Signal 1: DAD1 C, Sig=210,8 Ref=off

Peak RetTime Type  Width     Area      Height     Area
  #   [min]        [min]   [mAU*s]     [mAU]       %
----|-------|----|-------|----------|----------|--------|
   1   6.735 MM    0.2191  338.93533   25.78599  50.0295
   2   7.512 MM    0.2521  338.53519   22.38333  49.9705
```

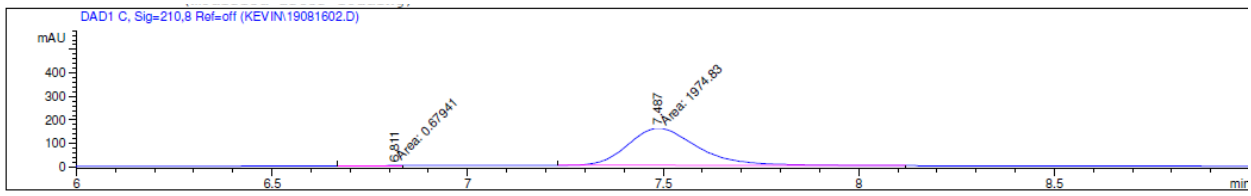


```
================================================================================
                          Area Percent Report
================================================================================

Sorted By             :      Signal
Multiplier            :      1.0000
Dilution              :      1.0000
Use Multiplier & Dilution Factor with ISTDs


Signal 1: DAD1 C, Sig=210,8 Ref=off

Peak RetTime Type  Width     Area      Height     Area
  #   [min]        [min]   [mAU*s]     [mAU]       %
----|-------|----|-------|----------|----------|--------|
   1   6.811 MM    0.1056 6.79410e-1 1.07183e-1   0.0344
   2   7.487 MM    0.2074 1974.82715  158.66473  99.9656
```

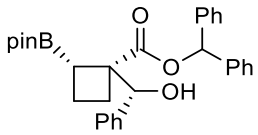

2-35

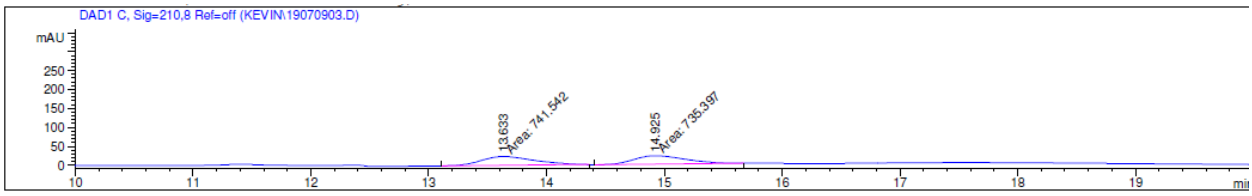


```
================================================================
                    Area Percent Report
================================================================

Sorted By             :      Signal
Multiplier            :      1.0000
Dilution              :      1.0000
Use Multiplier & Dilution Factor with ISTDs


Signal 1: DAD1 C, Sig=210,8 Ref=off

Peak RetTime Type  Width     Area      Height     Area
  #   [min]        [min]   [mAU*s]     [mAU]       %
----|-------|----|-------|----------|----------|--------|
   1  13.633 MM    0.5225  741.54211   23.65463  50.2080
   2  14.925 MM    0.5260  735.39703   23.30118  49.7920
```

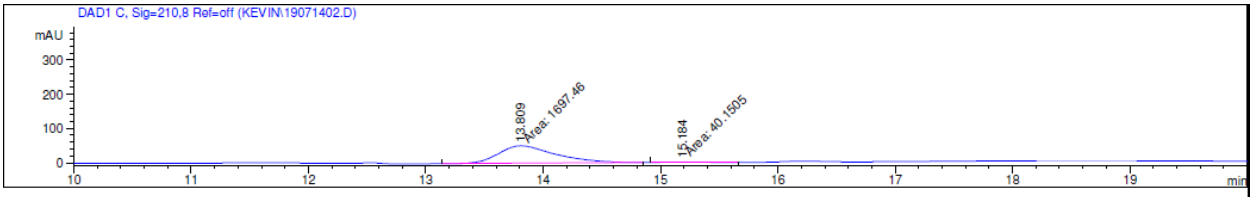


```
================================================================
                    Area Percent Report
================================================================

Sorted By             :      Signal
Multiplier            :      1.0000
Dilution              :      1.0000
Use Multiplier & Dilution Factor with ISTDs


Signal 1: DAD1 C, Sig=210,8 Ref=off

Peak RetTime Type  Width     Area      Height     Area
  #   [min]        [min]   [mAU*s]     [mAU]       %
----|-------|----|-------|----------|----------|--------|
   1  13.809 MM    0.5588 1697.45972   50.63028  97.6893
   2  15.184 MM    0.4221   40.15052    1.58520   2.3107
```

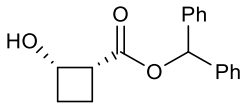

2-36

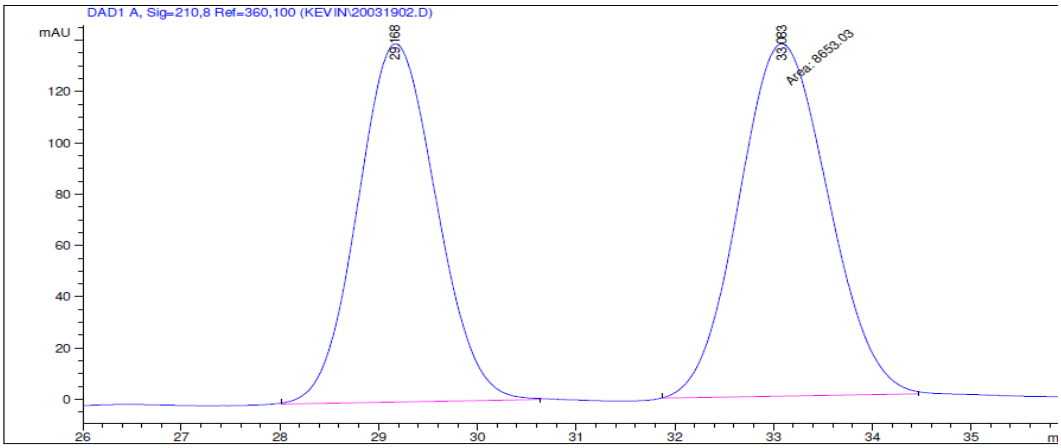


```
================================================================================
                          Area Percent Report
================================================================================

Sorted By             :      Signal
Multiplier            :      1.0000
Dilution              :      1.0000
Use Multiplier & Dilution Factor with ISTDs


Signal 1: DAD1 A, Sig=210,8 Ref=360,100

Peak RetTime Type  Width     Area      Height     Area
  #   [min]      [min]   [mAU*s]      [mAU]       %
----|-------|----|-------|----------|----------|--------|
   1  29.168 BB    0.8509 7727.98535  139.79703  48.9430
   2  33.083 MM    1.0083 8061.78027  133.25230  51.0570

Totals :                  1.57898e4   273.04933
```

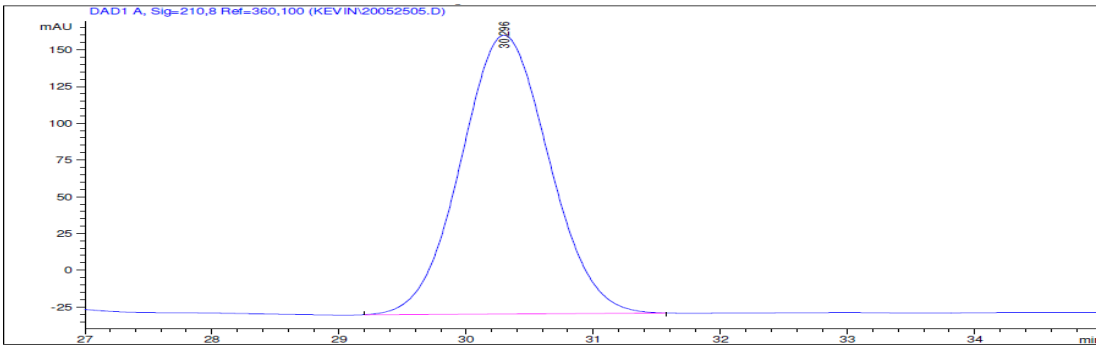


```
================================================================================
                          Area Percent Report
================================================================================

Sorted By             :      Signal
Multiplier            :      1.0000
Dilution              :      1.0000
Use Multiplier & Dilution Factor with ISTDs


Signal 1: DAD1 A, Sig=210,8 Ref=360,100

Peak RetTime Type  Width     Area      Height     Area
  #   [min]      [min]   [mAU*s]      [mAU]       %
----|-------|----|-------|----------|----------|--------|
   1  30.296 BB    0.7475 9127.59375  189.64552 100.0000
```

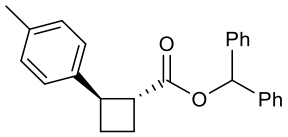

3-29

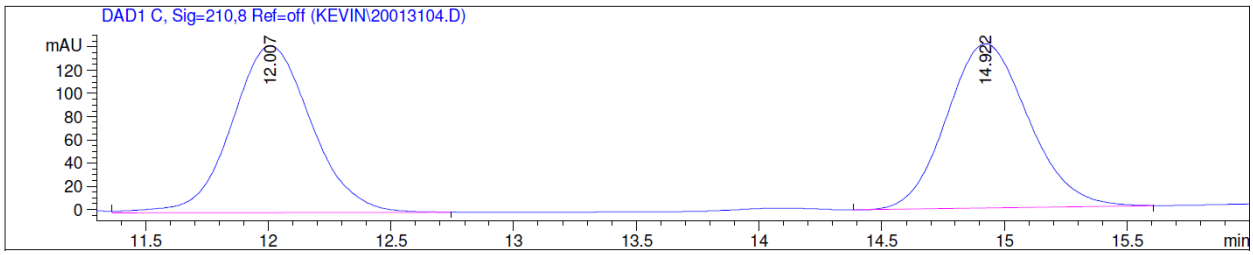

Signal 1: DAD1 C, Sig=210,8 Ref=off

Peak #	RetTime [min]	Type	Width [min]	Area [mAU*s]	Height [mAU]	Area %
1	12.007	VB	0.3502	3254.72192	143.75056	49.7420
2	14.922	VB	0.3610	3288.48657	141.58412	50.2580

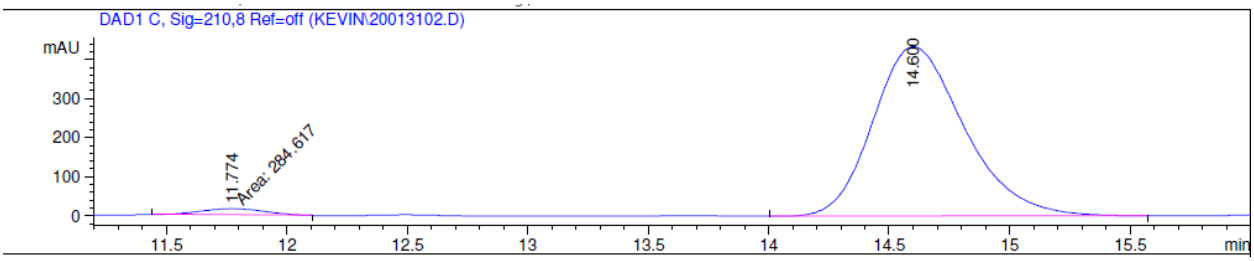

Signal 1: DAD1 C, Sig=210,8 Ref=off

Peak #	RetTime [min]	Type	Width [min]	Area [mAU*s]	Height [mAU]	Area %
1	11.774	MM	0.3018	284.61731	15.71935	2.4287
2	14.600	VB	0.4040	1.14342e4	433.10620	97.5713

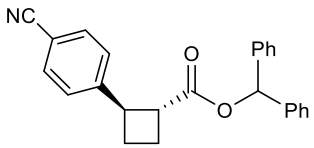

3-28

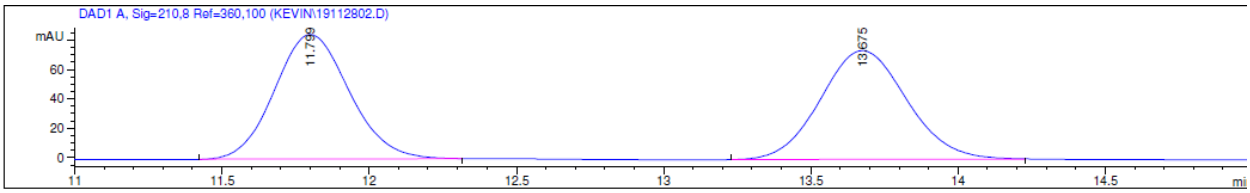


```
=====================================================================
                      Area Percent Report
=====================================================================

Sorted By             :      Signal
Multiplier            :      1.0000
Dilution              :      1.0000
Use Multiplier & Dilution Factor with ISTDs


Signal 1: DAD1 A, Sig=210,8 Ref=360,100

Peak RetTime Type  Width     Area      Height     Area
  #   [min]        [min]   [mAU*s]     [mAU]       %
----|-------|----|-------|----------|----------|--------|
   1  11.799 BB    0.2746 1506.85242   85.10081  49.7719
   2  13.675 BB    0.3208 1520.66125   74.29865  50.2281
```

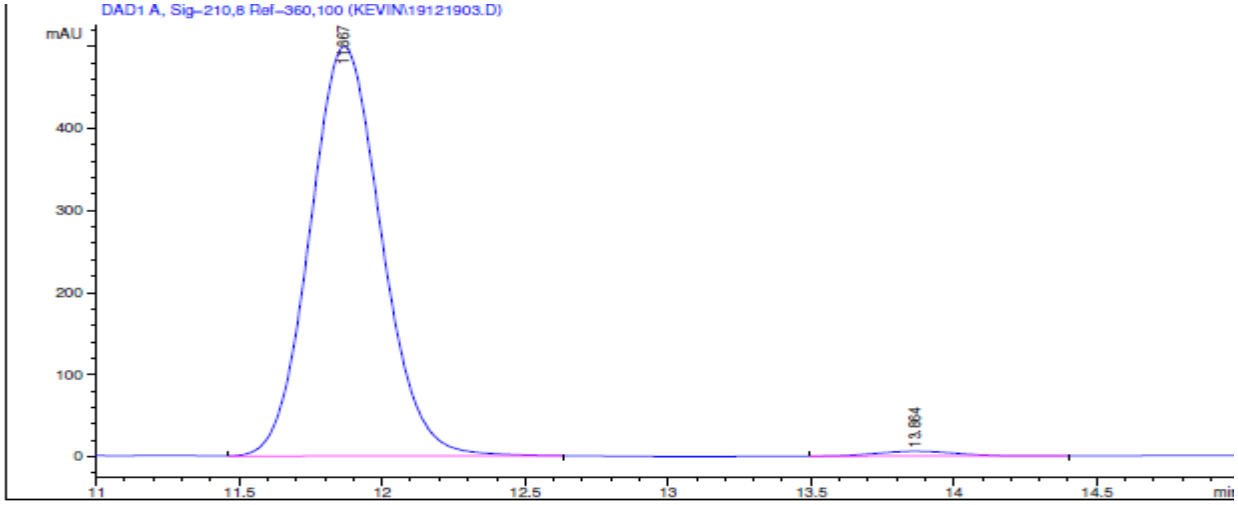


```
=====================================================================
                      Area Percent Report
=====================================================================

Sorted By             :      Signal
Multiplier            :      1.0000
Dilution              :      1.0000
Use Multiplier & Dilution Factor with ISTDs


Signal 1: DAD1 A, Sig=210,8 Ref=360,100

Peak RetTime Type  Width     Area      Height     Area
  #   [min]        [min]   [mAU*s]     [mAU]       %
----|-------|----|-------|----------|----------|--------|
   1  11.867 BB    0.2712 8696.18750  499.39111  98.7005
   2  13.864 BP    0.3035  114.49145    5.97561   1.2995
```

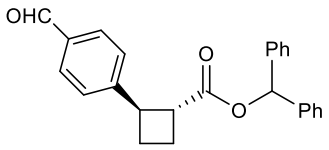

3-30

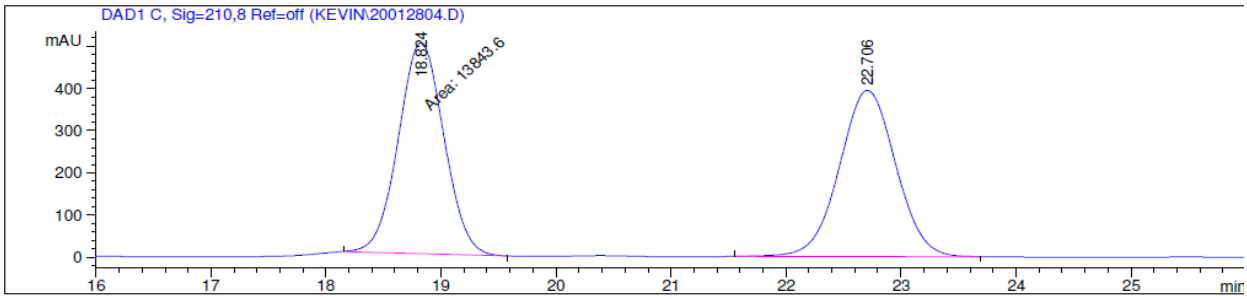


```
=====================================================================
                      Area Percent Report
=====================================================================

Sorted By             :      Signal
Multiplier            :      1.0000
Dilution              :      1.0000
Use Multiplier & Dilution Factor with ISTDs


Signal 1: DAD1 C, Sig=210,8 Ref=off

Peak RetTime Type  Width     Area      Height     Area
  #   [min]        [min]   [mAU*s]     [mAU]       %
----|-------|----|-------|----------|----------|--------|
   1  18.824 MM    0.4605 1.38436e4   501.00601  50.6435
   2  22.706 BB    0.5314 1.34918e4   394.10715  49.3565
```

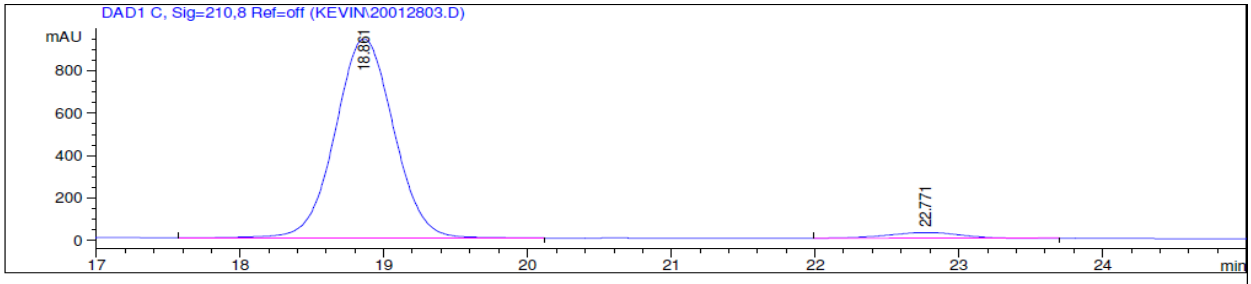


```
=====================================================================
                      Area Percent Report
=====================================================================

Sorted By             :      Signal
Multiplier            :      1.0000
Dilution              :      1.0000
Use Multiplier & Dilution Factor with ISTDs


Signal 1: DAD1 C, Sig=210,8 Ref=off

Peak RetTime Type  Width     Area      Height     Area
  #   [min]        [min]   [mAU*s]     [mAU]       %
----|-------|----|-------|----------|----------|--------|
   1  18.861 VB    0.4413 2.66884e4   939.78638  96.5033
   2  22.771 BP    0.5193  967.03058   27.56447   3.4967
```

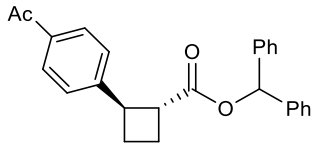

3-31

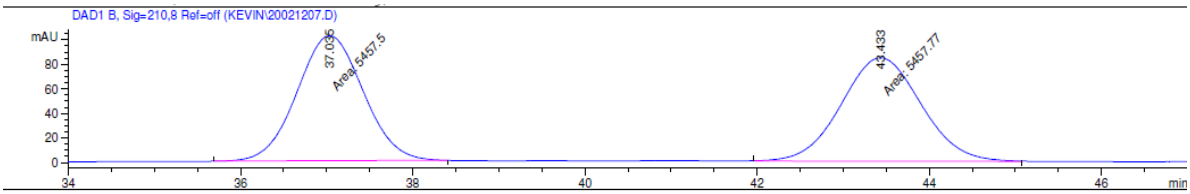


```
=====================================================================
                      Area Percent Report
=====================================================================

Sorted By             :      Signal
Multiplier            :      1.0000
Dilution              :      1.0000
Use Multiplier & Dilution Factor with ISTDs


Signal 1: DAD1 B, Sig=210,8 Ref=off

Peak RetTime Type  Width     Area      Height     Area
  #   [min]       [min]    [mAU*s]     [mAU]       %
----|-------|----|-------|----------|----------|--------|
   1  37.035 MM    0.8919 5457.50342  101.98620  49.9988
   2  43.433 MM    1.0769 5457.77441   84.46430  50.0012
```

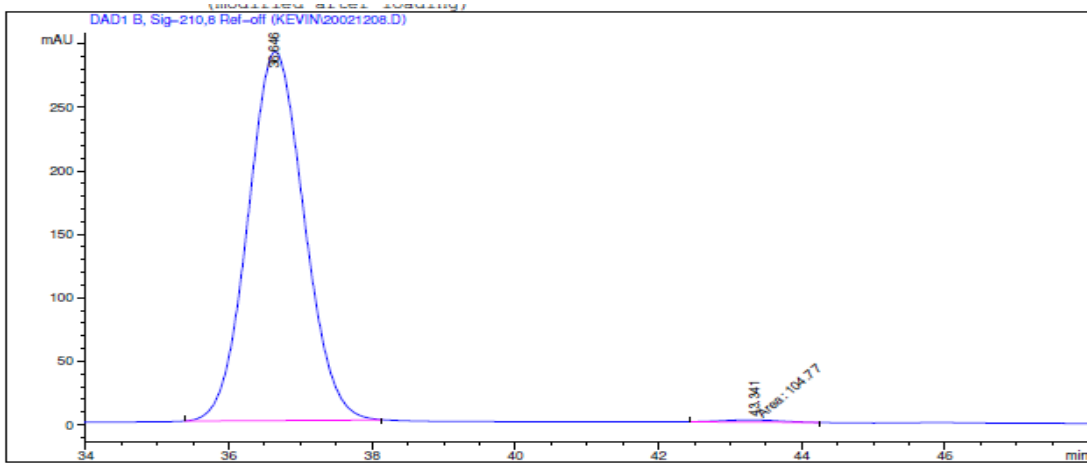


```
=====================================================================
                      Area Percent Report
=====================================================================

Sorted By             :      Signal
Multiplier            :      1.0000
Dilution              :      1.0000
Use Multiplier & Dilution Factor with ISTDs


Signal 1: DAD1 B, Sig=210,8 Ref=off

Peak RetTime Type  Width     Area      Height     Area
  #   [min]       [min]    [mAU*s]     [mAU]       %
----|-------|----|-------|----------|----------|--------|
   1  36.646 BB    0.8185 1.58723e4  290.92920  99.3442
   2  43.341 MM    0.9634  104.76960    1.81247   0.6558
```

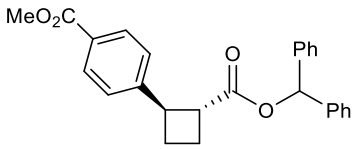

3-32

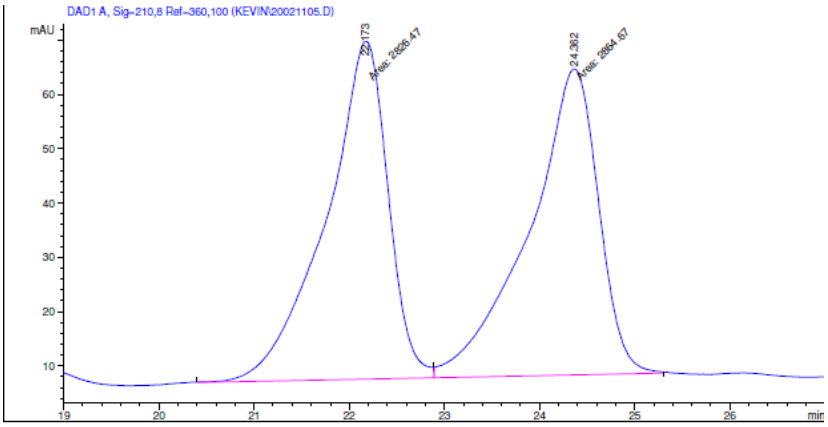


```
================================================================
                      Area Percent Report
================================================================

Sorted By             :      Signal
Multiplier            :      1.0000
Dilution              :      1.0000
Use Multiplier & Dilution Factor with ISTDs


Signal 1: DAD1 A, Sig=210,8 Ref=360,100

Peak RetTime Type  Width     Area      Height     Area
  #   [min]        [min]   [mAU*s]     [mAU]       %
----|-------|----|-------|----------|----------|--------|
   1  22.173 MF    0.7567 2826.46582   62.25505  49.6644
   2  24.362 FM    0.8470 2864.66724   56.36612  50.3356
```

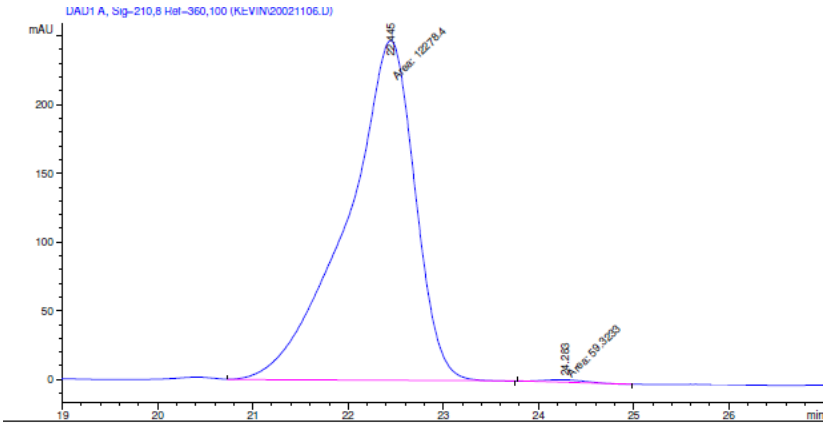


```
================================================================
                      Area Percent Report
================================================================

Sorted By             :      Signal
Multiplier            :      1.0000
Dilution              :      1.0000
Use Multiplier & Dilution Factor with ISTDs


Signal 1: DAD1 A, Sig=210,8 Ref=360,100

Peak RetTime Type  Width     Area      Height     Area
  #   [min]        [min]   [mAU*s]     [mAU]       %
----|-------|----|-------|----------|----------|--------|
   1  22.445 MM    0.8282 1.22784e4   247.09607  99.5192
   2  24.283 MM    0.5124   59.32329     1.92949   0.4808
```

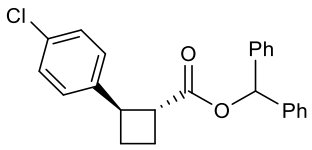

3-33

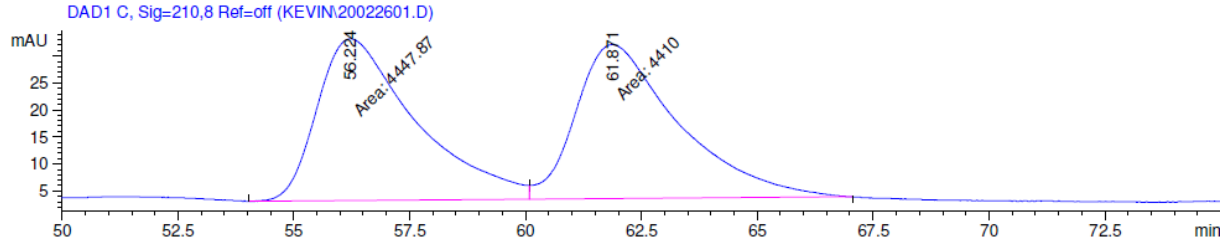

Signal 3: DAD1 C, Sig=210,8 Ref=off

Peak #	RetTime [min]	Type	Width [min]	Area [mAU*s]	Height [mAU]	Area %
1	56.224	MF	2.4714	4447.87305	29.99521	50.2138
2	61.871	FM	2.5721	4409.99951	28.57564	49.7862

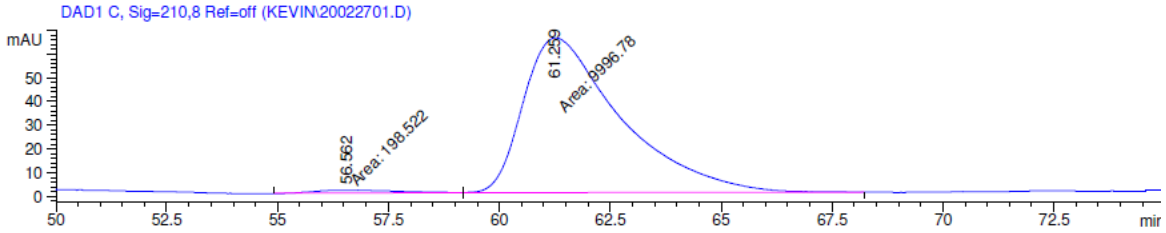

Signal 3: DAD1 C, Sig=210,8 Ref=off

Peak #	RetTime [min]	Type	Width [min]	Area [mAU*s]	Height [mAU]	Area %
1	56.562	MF	2.2852	198.52179	1.44787	1.9472
2	61.259	FM	2.5487	9996.78223	65.37131	98.0528

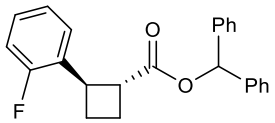

3-34

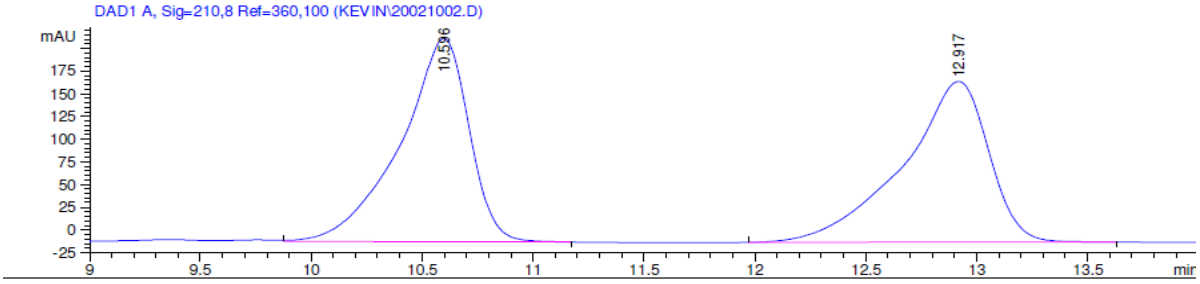


```
================================================================================
                          Area Percent Report
================================================================================

Sorted By             :      Signal
Multiplier            :      1.0000
Dilution              :      1.0000
Use Multiplier & Dilution Factor with ISTDs


Signal 1: DAD1 A, Sig=210,8 Ref=360,100

Peak RetTime Type  Width     Area      Height      Area
  #   [min]        [min]   [mAU*s]     [mAU]       %
----|-------|----|-------|----------|----------|--------|
   1  10.596 VB    0.3094 4829.03809  224.07419  50.2778
   2  12.917 BB    0.3844 4775.67480  177.21220  49.7222
```

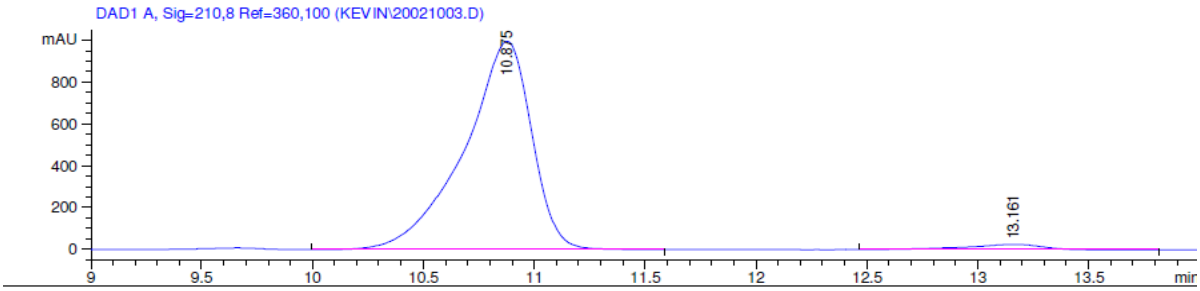


```
================================================================================
                          Area Percent Report
================================================================================

Sorted By             :      Signal
Multiplier            :      1.0000
Dilution              :      1.0000
Use Multiplier & Dilution Factor with ISTDs


Signal 1: DAD1 A, Sig=210,8 Ref=360,100

Peak RetTime Type  Width     Area      Height      Area
  #   [min]        [min]   [mAU*s]     [mAU]       %
----|-------|----|-------|----------|----------|--------|
   1  10.875 VB    0.3061 2.10324e4  996.88617  97.0063
   2  13.161 BP    0.3586  649.07684   25.87707   2.9937
```

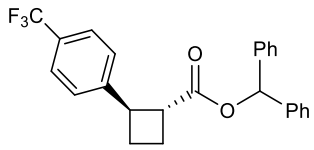

3-35

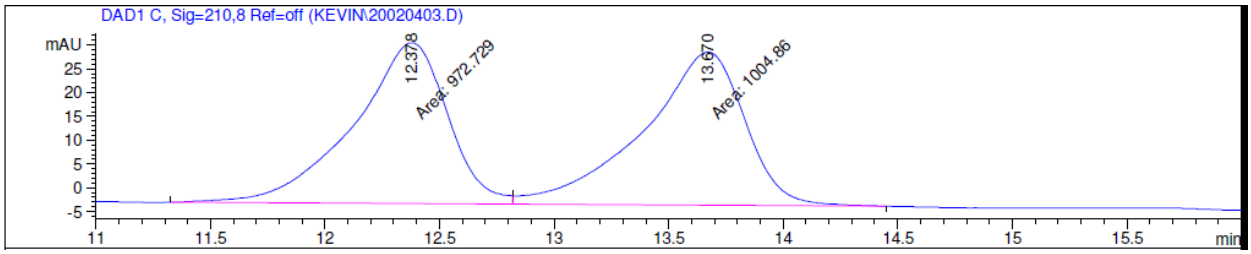

Peak #	RetTime [min]	Type	Width [min]	Area [mAU*s]	Height [mAU]	Area %
1	12.378	MF	0.4783	972.72876	33.89450	49.1876
2	13.670	FM	0.5191	1004.85889	32.26589	50.8124

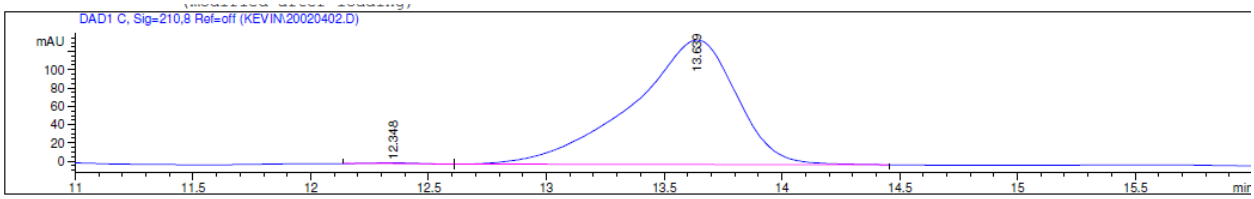


```
=====================================================================
                    Area Percent Report
=====================================================================

Sorted By             :      Signal
Multiplier            :      1.0000
Dilution              :      1.0000
Use Multiplier & Dilution Factor with ISTDs


Signal 1: DAD1 C, Sig=210,8 Ref=off

Peak RetTime Type  Width     Area      Height     Area
  #   [min]        [min]   [mAU*s]     [mAU]       %
----|-------|----|-------|----------|----------|--------|
   1  12.348 PP    0.1968   14.39819    1.01931   0.3431
   2  13.639 VB    0.4323 4182.25977  136.16374  99.6569
```

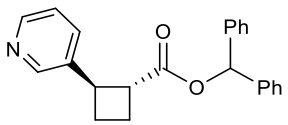

3-38

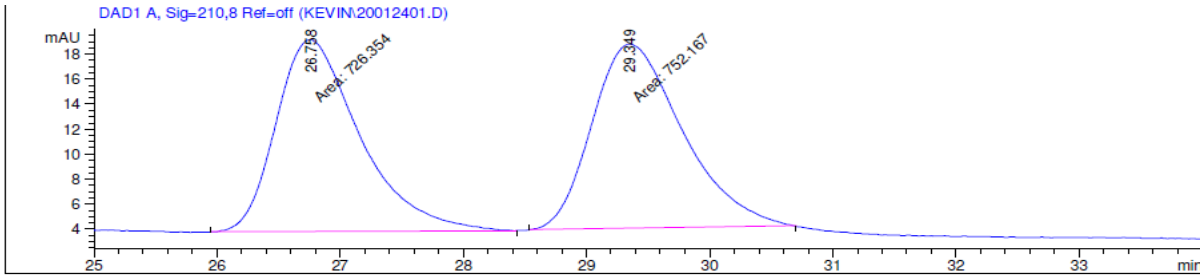


```
=====================================================================
                      Area Percent Report
=====================================================================

Sorted By             :      Signal
Multiplier            :      1.0000
Dilution              :      1.0000
Use Multiplier & Dilution Factor with ISTDs


Signal 1: DAD1 A, Sig=210,8 Ref=off

Peak RetTime Type  Width     Area      Height     Area
  #   [min]        [min]   [mAU*s]     [mAU]       %
----|-------|----|-------|----------|----------|--------|
   1  26.758 MM    0.7884  726.35382   15.35530  49.1271
   2  29.349 MM    0.8505  752.16705   14.73936  50.8729
```

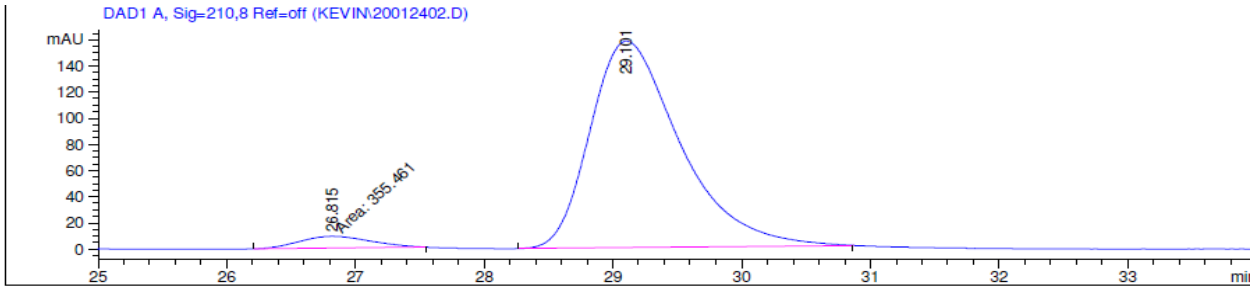


```
=====================================================================
                      Area Percent Report
=====================================================================

Sorted By             :      Signal
Multiplier            :      1.0000
Dilution              :      1.0000
Use Multiplier & Dilution Factor with ISTDs


Signal 1: DAD1 A, Sig=210,8 Ref=off

Peak RetTime Type  Width     Area      Height     Area
  #   [min]        [min]   [mAU*s]     [mAU]       %
----|-------|----|-------|----------|----------|--------|
   1  26.815 MM    0.6535  355.46149    9.06609   4.4131
   2  29.101 BB    0.7353 7699.26758  157.79402  95.5869
```

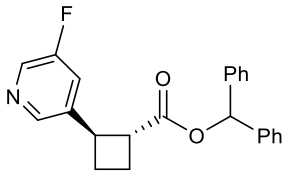

3-39

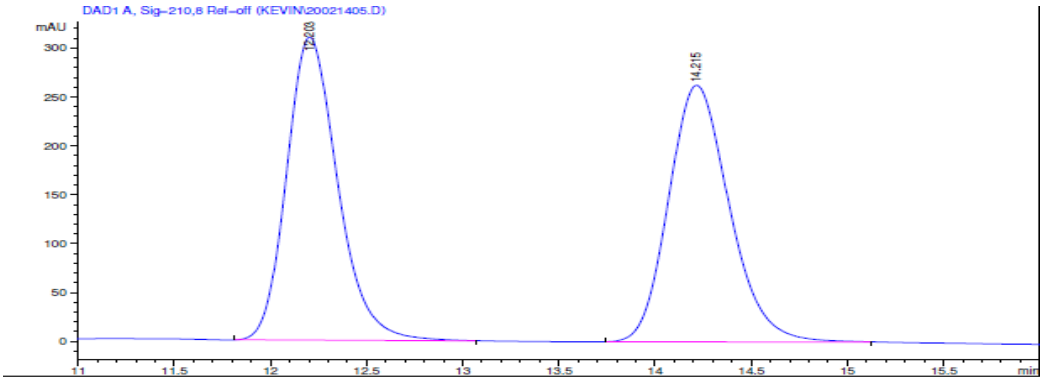


```
================================================================
                    Area Percent Report
================================================================

Sorted By             :      Signal
Multiplier            :      1.0000
Dilution              :      1.0000
Use Multiplier & Dilution Factor with ISTDs


Signal 1: DAD1 A, Sig=210,8 Ref=off

Peak RetTime Type  Width     Area      Height     Area
  #   [min]      [min]    [mAU*s]     [mAU]       %
----|-------|----|------|----------|----------|--------|
   1  12.203 PB    0.2839 5737.04688  309.99011  49.8066
   2  14.215 BB    0.3410 5781.59033  262.50348  50.1934
```

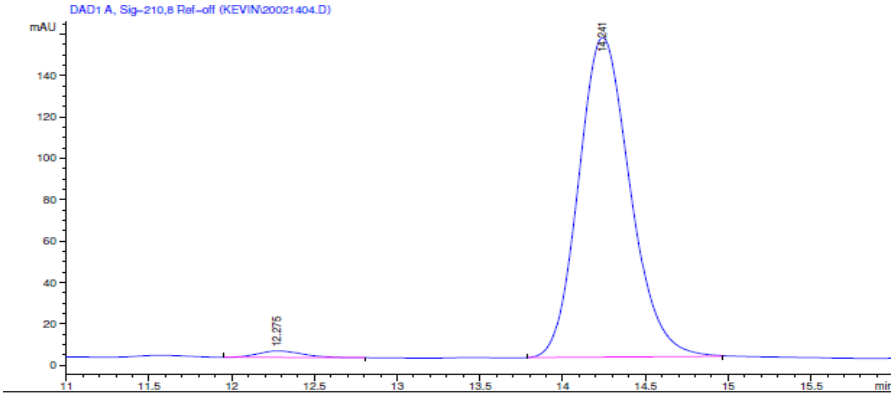


```
================================================================
                    Area Percent Report
================================================================

Sorted By             :      Signal
Multiplier            :      1.0000
Dilution              :      1.0000
Use Multiplier & Dilution Factor with ISTDs


Signal 1: DAD1 A, Sig=210,8 Ref=off

Peak RetTime Type  Width     Area      Height     Area
  #   [min]      [min]    [mAU*s]     [mAU]       %
----|-------|----|------|----------|----------|--------|
   1  12.275 PB    0.2655   61.09200    3.18931   1.7939
   2  14.241 BB    0.3346 3344.49707  154.49200  98.2061
```

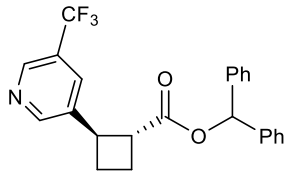

3-40

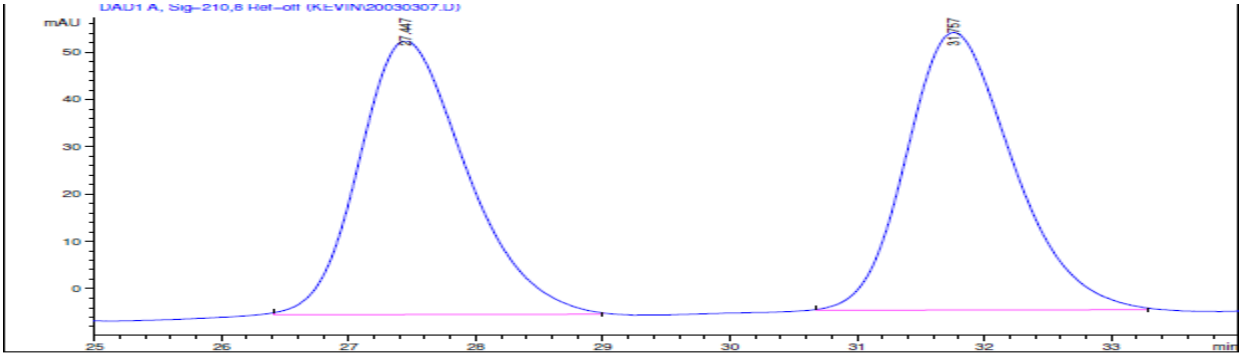


```
================================================================================
                          Area Percent Report
================================================================================

Sorted By             :      Signal
Multiplier            :      1.0000
Dilution              :      1.0000
Use Multiplier & Dilution Factor with ISTDs

Signal 1: DAD1 A, Sig=210,8 Ref=off

Peak RetTime Type  Width     Area      Height     Area
   #   [min]     [min]    [mAU*s]     [mAU]      %
----|-------|----|-------|----------|----------|--------|
   1  27.447 BB    0.8627 3407.80884   57.89916  49.9226
   2  31.757 BB    0.8793 3418.37109   58.70631  50.0774
```

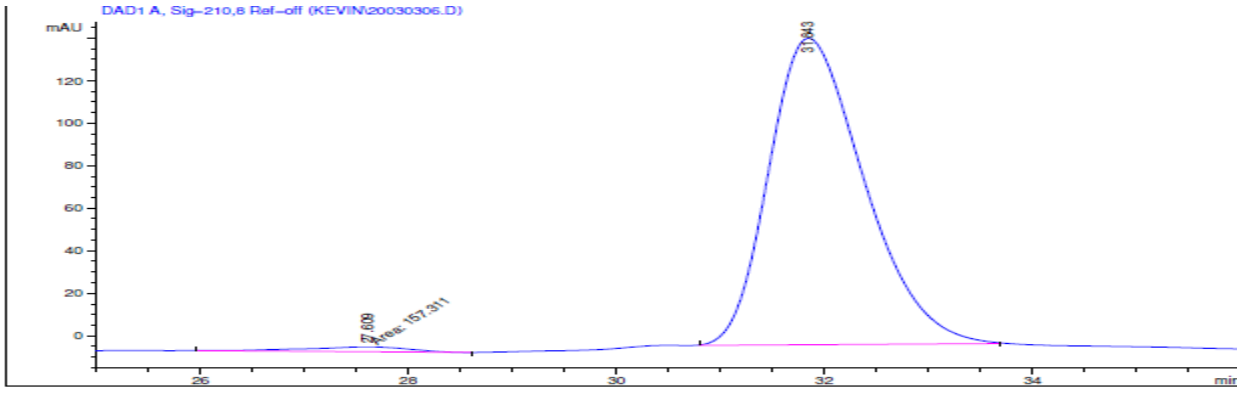


```
================================================================================
                          Area Percent Report
================================================================================

Sorted By             :      Signal
Multiplier            :      1.0000
Dilution              :      1.0000
Use Multiplier & Dilution Factor with ISTDs

Signal 1: DAD1 A, Sig=210,8 Ref=off

Peak RetTime Type  Width     Area      Height     Area
   #   [min]     [min]    [mAU*s]     [mAU]      %
----|-------|----|-------|----------|----------|--------|
   1  27.609 MM    1.1260  157.31065    2.32852   1.6843
   2  31.843 BB    0.9487 9182.37500  144.23482  98.3157
```

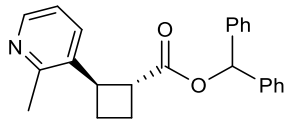

3-41

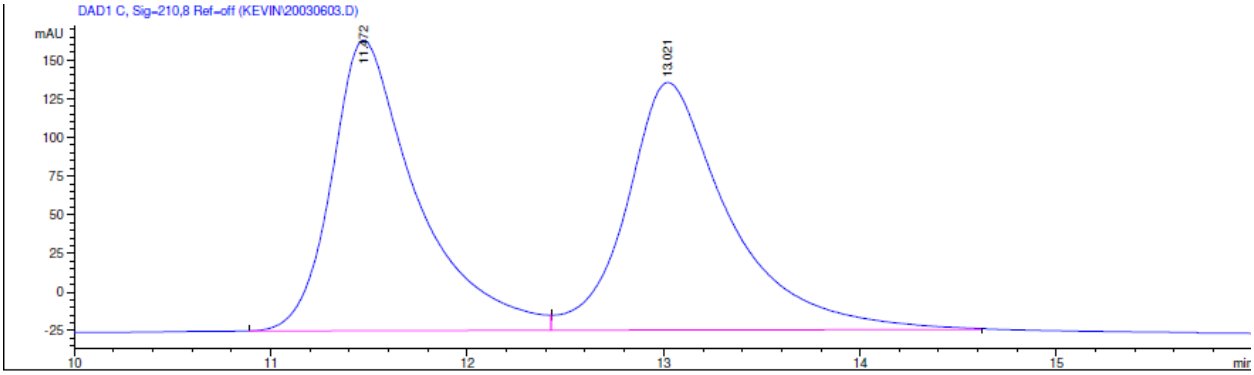

Peak #	RetTime [min]	Type	Width [min]	Area [mAU*s]	Height [mAU]	Area %
1	11.472	BV	0.4343	5706.88770	187.92270	49.3744
2	13.021	VB	0.5285	5851.49463	160.07845	50.6256

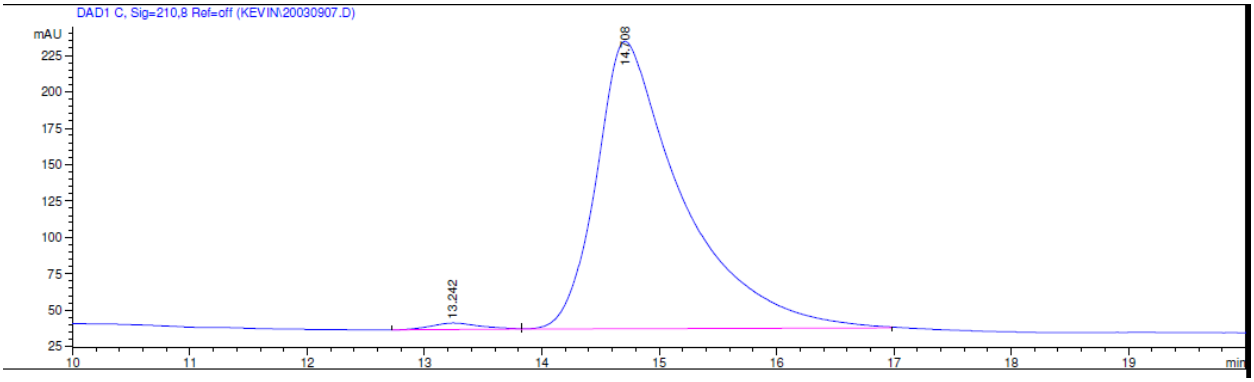

Peak #	RetTime [min]	Type	Width [min]	Area [mAU*s]	Height [mAU]	Area %
1	13.242	BV	0.4085	137.76208	4.58559	1.3472
2	14.708	VB	0.7136	1.00879e4	197.61600	98.6528

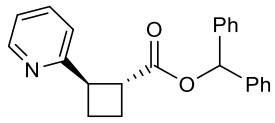

3-42

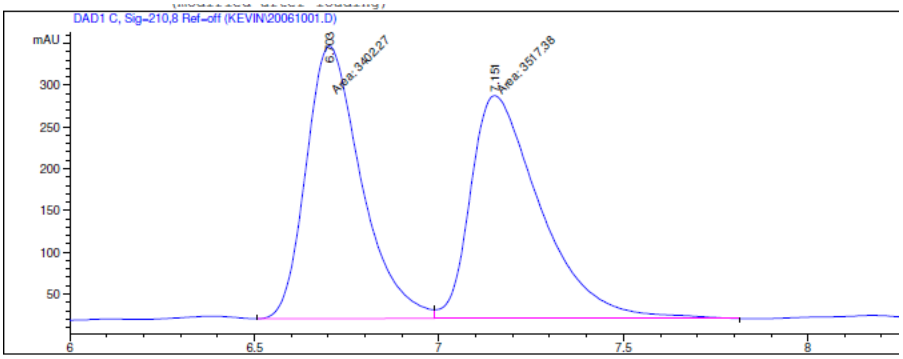


```
------------------------------------------------------------------------
                        Area Percent Report
------------------------------------------------------------------------

Sorted By             :      Signal
Multiplier            :      1.0000
Dilution              :      1.0000
Use Multiplier & Dilution Factor with ISTDs


Signal 1: DAD1 C, Sig=210,8 Ref=off

Peak RetTime Type  Width     Area      Height     Area
  #   [min]        [min]   [mAU*s]     [mAU]       %
----|-------|----|-------|----------|----------|--------|
   1   6.703 MF    0.1735 3402.27368  326.75452  49.1683
   2   7.151 FM    0.2194 3517.37793  267.24792  50.8317
```

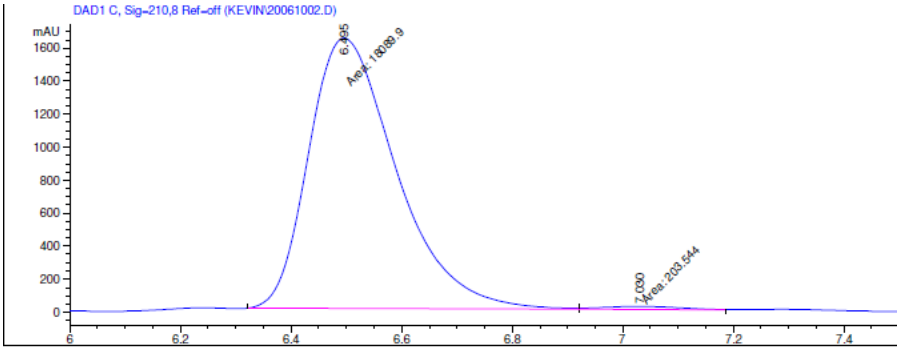


```
------------------------------------------------------------------------
                        Area Percent Report
------------------------------------------------------------------------

Sorted By             :      Signal
Multiplier            :      1.0000
Dilution              :      1.0000
Use Multiplier & Dilution Factor with ISTDs


Signal 1: DAD1 C, Sig=210,8 Ref=off

Peak RetTime Type  Width     Area      Height     Area
  #   [min]        [min]   [mAU*s]     [mAU]       %
----|-------|----|-------|----------|----------|--------|
   1   6.495 MF    0.1837 1.80899e4  1641.16272  98.8873
   2   7.030 FM    0.1705  203.54419   19.89349   1.1127
```

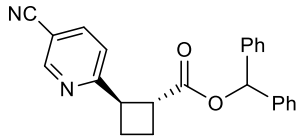

3-43

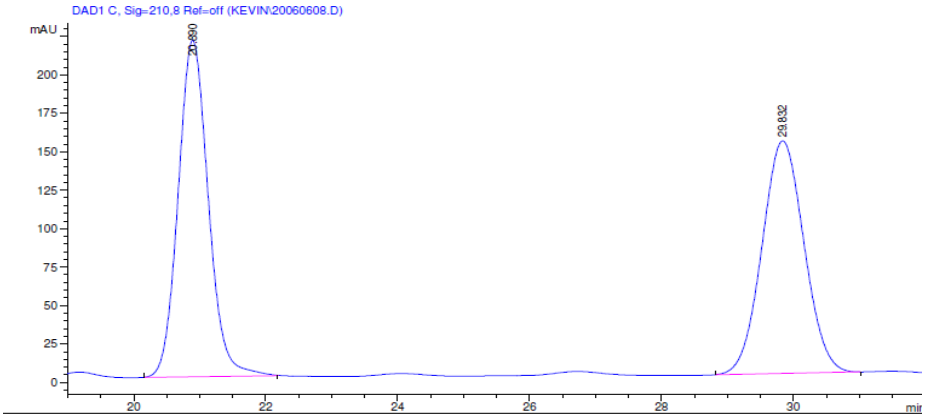


```
================================================================
                    Area Percent Report
================================================================

Sorted By             :      Signal
Multiplier            :      1.0000
Dilution              :      1.0000
Use Multiplier & Dilution Factor with ISTDs


Signal 1: DAD1 C, Sig=210,8 Ref=off

Peak RetTime Type  Width     Area      Height     Area
  #   [min]        [min]    [mAU*s]     [mAU]       %
----|-------|----|-------|----------|----------|--------|
   1  20.890 BB    0.4930 6962.96045  218.96371  50.9269
   2  29.832 BB    0.6890 6709.49219  151.39722  49.0731
```

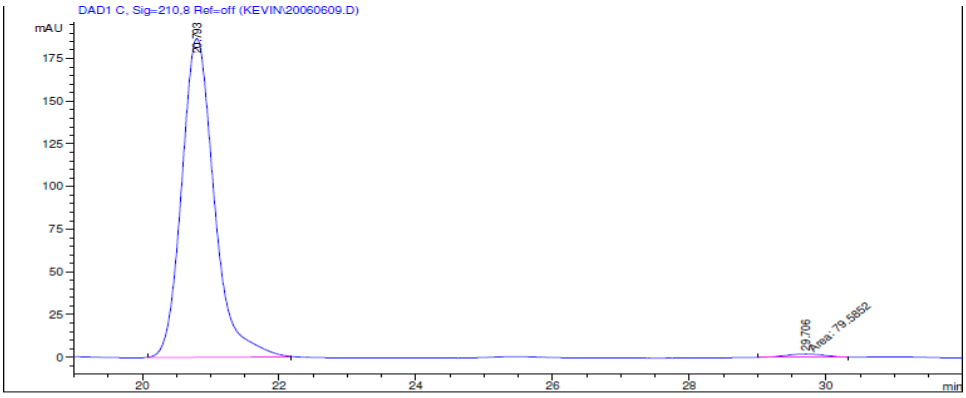


```
================================================================
                    Area Percent Report
================================================================

Sorted By             :      Signal
Multiplier            :      1.0000
Dilution              :      1.0000
Use Multiplier & Dilution Factor with ISTDs


Signal 1: DAD1 C, Sig=210,8 Ref=off

Peak RetTime Type  Width     Area      Height     Area
  #   [min]        [min]    [mAU*s]     [mAU]       %
----|-------|----|-------|----------|----------|--------|
   1  20.793 BB    0.5064 6192.01660  186.93507  98.7310
   2  29.706 MM    0.6599   79.58517    2.01004   1.2690
```

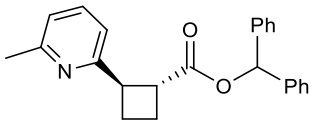

3-44

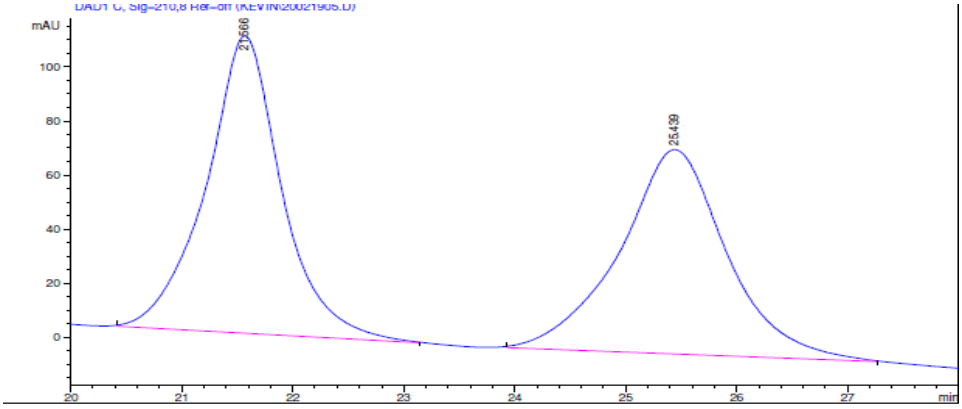


```
================================================================
                    Area Percent Report
================================================================

Sorted By             :      Signal
Multiplier            :      1.0000
Dilution              :      1.0000
Use Multiplier & Dilution Factor with ISTDs


Signal 1: DAD1 C, Sig=210,8 Ref=off

Peak RetTime Type  Width     Area      Height     Area
  #   [min]        [min]   [mAU*s]     [mAU]       %
----|-------|----|-------|----------|----------|-------|
   1  21.566 BB    0.6819 5220.46729  109.95131  50.7680
   2  25.439 BB    0.9456 5062.52441   75.57009  49.2320
```

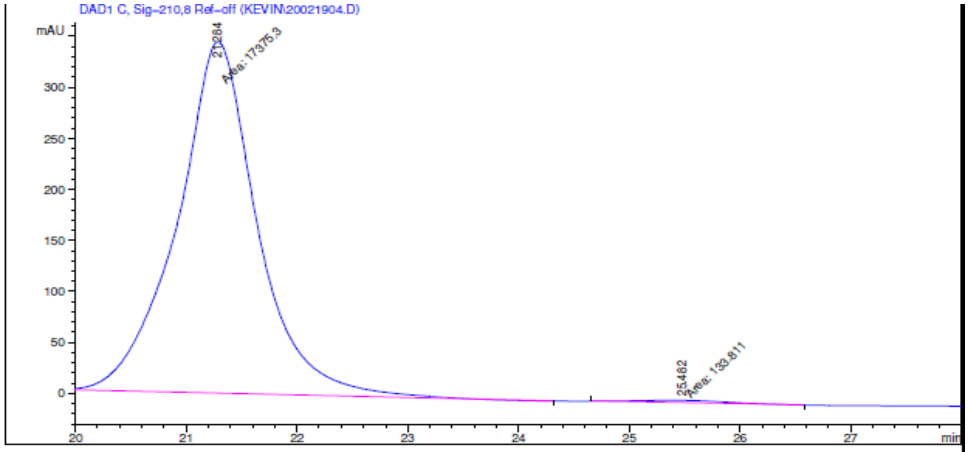


```
================================================================
                    Area Percent Report
================================================================

Sorted By             :      Signal
Multiplier            :      1.0000
Dilution              :      1.0000
Use Multiplier & Dilution Factor with ISTDs


Signal 1: DAD1 C, Sig=210,8 Ref=off

Peak RetTime Type  Width     Area      Height     Area
  #   [min]        [min]   [mAU*s]     [mAU]       %
----|-------|----|-------|----------|----------|-------|
   1  21.284 MM    0.8405 1.73753e4  344.55701  99.2358
   2  25.482 MM    0.9190  133.81087   2.42662   0.7642
```

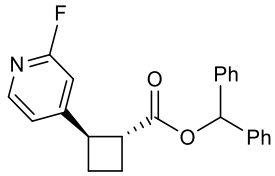

3-45

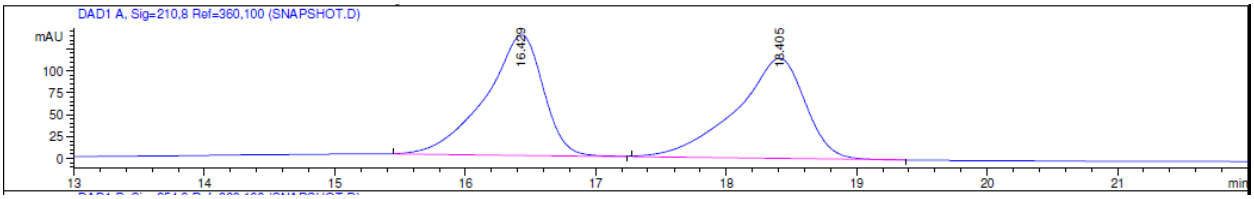

Signal 1: DAD1 A, Sig=210,8 Ref=360,100

Peak #	RetTime [min]	Type	Width [min]	Area [mAU*s]	Height [mAU]	Area %
1	16.429	BB	0.4450	4265.07373	137.82112	50.2524
2	18.405	BP	0.5281	4222.22266	114.53684	49.7476

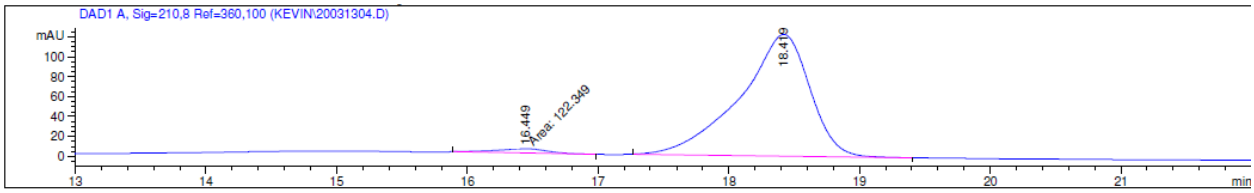


```
=====================================================================
                      Area Percent Report
=====================================================================

Sorted By             :      Signal
Multiplier            :      1.0000
Dilution              :      1.0000
Use Multiplier & Dilution Factor with ISTDs


Signal 1: DAD1 A, Sig=210,8 Ref=360,100

Peak RetTime Type  Width     Area      Height     Area
  #   [min]        [min]   [mAU*s]     [mAU]       %
----|-------|----|-------|----------|----------|--------|
   1  16.449 MM    0.4614  122.34883    4.41921   2.6189
   2  18.419 BB    0.5336 4549.47852  122.41017  97.3811
```

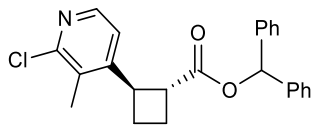

3-46

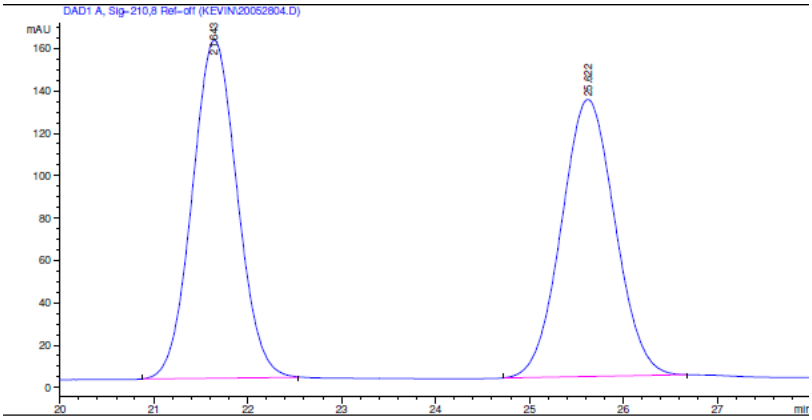


```
================================================================================
                              Area Percent Report
================================================================================

Sorted By             :      Signal
Multiplier            :      1.0000
Dilution              :      1.0000
Use Multiplier & Dilution Factor with ISTDs


Signal 1: DAD1 A, Sig=210,8 Ref=off

Peak RetTime Type  Width     Area      Height     Area
  #   [min]      [min]    [mAU*s]     [mAU]       %
-----|-------|----|-------|----------|----------|--------|
   1  21.643 BB    0.5182 5313.86377  159.68048  50.5739
   2  25.622 BB    0.6153 5193.25977  130.78677  49.4261
```

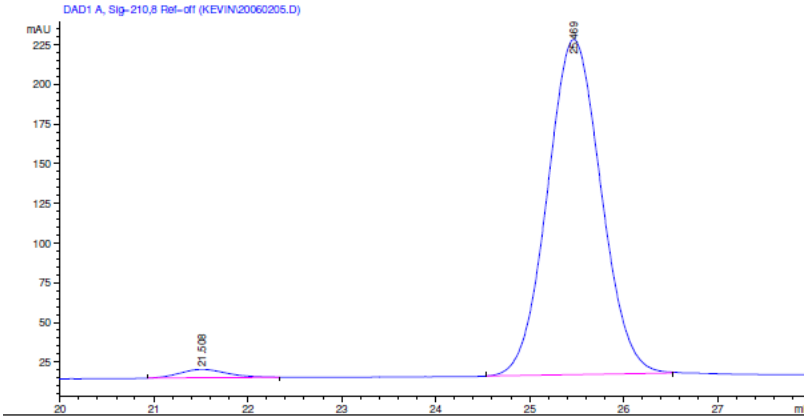


```
================================================================================
                              Area Percent Report
================================================================================

Sorted By             :      Signal
Multiplier            :      1.0000
Dilution              :      1.0000
Use Multiplier & Dilution Factor with ISTDs


Signal 1: DAD1 A, Sig=210,8 Ref=off

Peak RetTime Type  Width     Area      Height     Area
  #   [min]      [min]    [mAU*s]     [mAU]       %
-----|-------|----|-------|----------|----------|--------|
   1  21.508 BB    0.5108  189.26196    5.34906   2.2086
   2  25.469 BB    0.6207 8380.06641  211.30482  97.7914
```

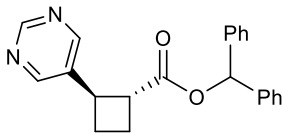

3-47

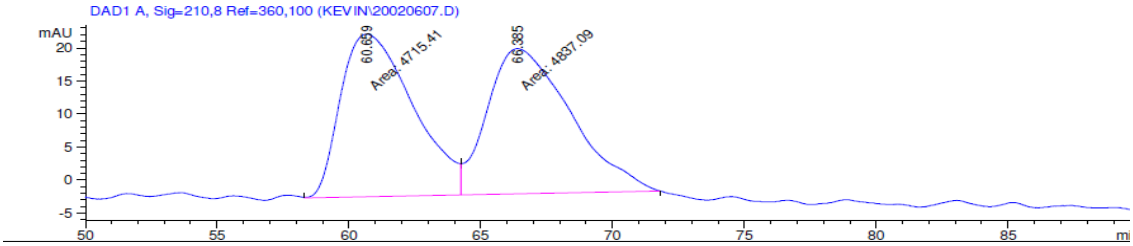


```
================================================================================
                          Area Percent Report
================================================================================

Sorted By             :      Signal
Multiplier            :      1.0000
Dilution              :      1.0000
Use Multiplier & Dilution Factor with ISTDs


Signal 1: DAD1 A, Sig=210,8 Ref=360,100

Peak RetTime Type  Width     Area      Height     Area
  #   [min]        [min]   [mAU*s]     [mAU]       %
----|-------|----|-------|----------|----------|--------|
   1  60.659 MF    3.1884 4715.40723   24.64869  49.3631
   2  66.385 FM    3.6563 4837.09131   22.04899  50.6369
```

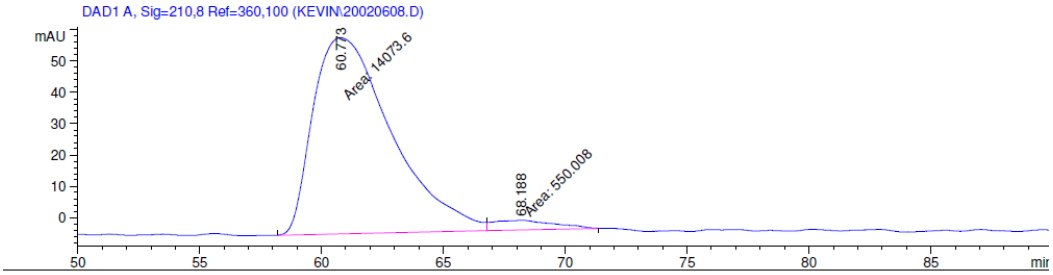


```
================================================================================
                          Area Percent Report
================================================================================

Sorted By             :      Signal
Multiplier            :      1.0000
Dilution              :      1.0000
Use Multiplier & Dilution Factor with ISTDs


Signal 1: DAD1 A, Sig=210,8 Ref=360,100

Peak RetTime Type  Width     Area      Height     Area
  #   [min]        [min]   [mAU*s]     [mAU]       %
----|-------|----|-------|----------|----------|--------|
   1  60.773 MF    3.7434 1.40736e4   62.66026  96.2389
   2  68.188 FM    2.9050  550.00800    3.15554   3.7611
```

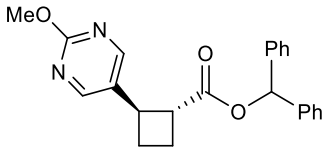

3-48

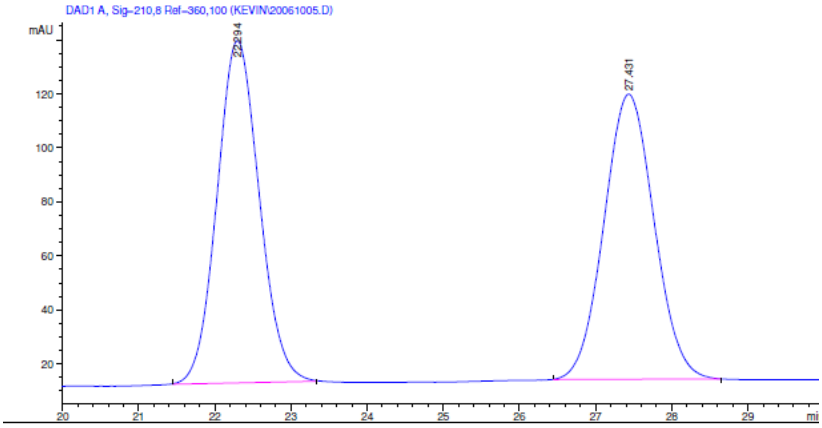


```
================================================================
                    Area Percent Report
================================================================

Sorted By             :      Signal
Multiplier            :      1.0000
Dilution              :      1.0000
Use Multiplier & Dilution Factor with ISTDs


Signal 1: DAD1 A, Sig=210,8 Ref=360,100

Peak RetTime Type  Width     Area      Height     Area
  #   [min]        [min]   [mAU*s]     [mAU]       %
----|-------|----|-------|----------|----------|--------|
   1  22.294 BB    0.5981 4890.29346  126.76913  50.2137
   2  27.431 BB    0.7092 4848.66602  105.69913  49.7863
```

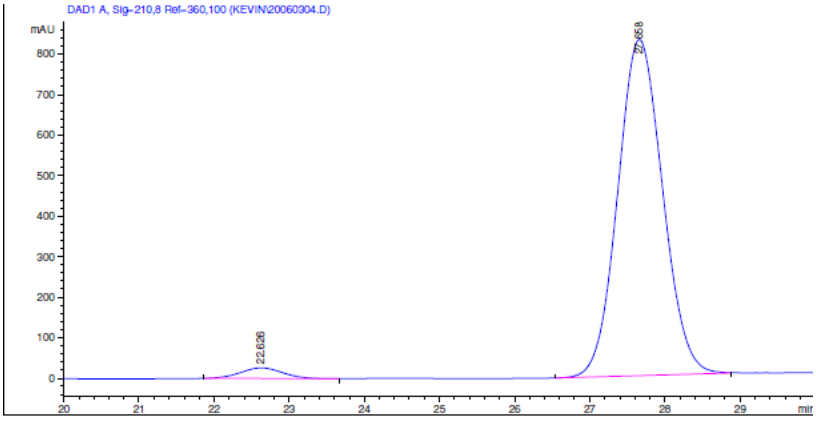


```
================================================================
                    Area Percent Report
================================================================

Sorted By             :      Signal
Multiplier            :      1.0000
Dilution              :      1.0000
Use Multiplier & Dilution Factor with ISTDs


Signal 1: DAD1 A, Sig=210,8 Ref=360,100

Peak RetTime Type  Width     Area      Height     Area
  #   [min]        [min]   [mAU*s]     [mAU]       %
----|-------|----|-------|----------|----------|--------|
   1  22.626 BP    0.6004 1043.63184   26.33164   2.9448
   2  27.658 PB    0.6497 3.43958e4   829.66534  97.0552
```

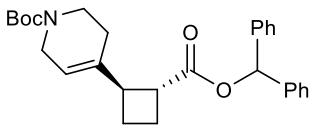

3-49

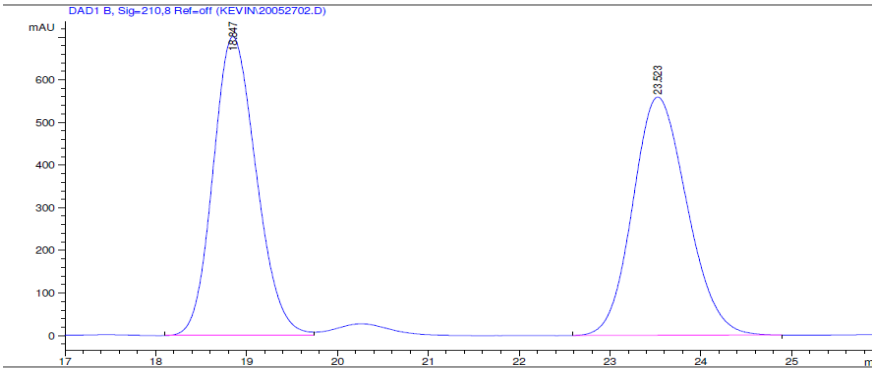


```
================================================================
                    Area Percent Report
================================================================

Sorted By             :      Signal
Multiplier            :      1.0000
Dilution              :      1.0000
Use Multiplier & Dilution Factor with ISTDs

Signal 1: DAD1 B, Sig=210,8 Ref=off

Peak RetTime Type  Width     Area      Height     Area
  #   [min]        [min]   [mAU*s]     [mAU]       %
----|-------|----|-------|----------|----------|--------|
   1  18.847 BV    0.5130 2.31418e4   701.31799  49.8751
   2  23.523 BB    0.6475 2.32577e4   558.90216  50.1249
```

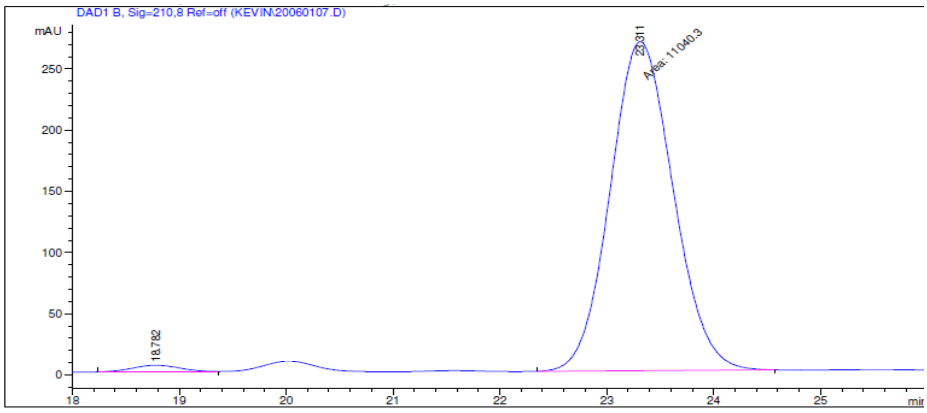


```
================================================================
                    Area Percent Report
================================================================

Sorted By             :      Signal
Multiplier            :      1.0000
Dilution              :      1.0000
Use Multiplier & Dilution Factor with ISTDs

Signal 1: DAD1 B, Sig=210,8 Ref=off

Peak RetTime Type  Width     Area      Height     Area
  #   [min]        [min]   [mAU*s]     [mAU]       %
----|-------|----|-------|----------|----------|--------|
   1  18.782 BV    0.4623  164.97887    5.34244   1.4723
   2  23.311 MM    0.6843 1.10403e4   268.90387  98.5277
```

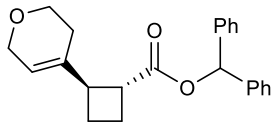

3-50

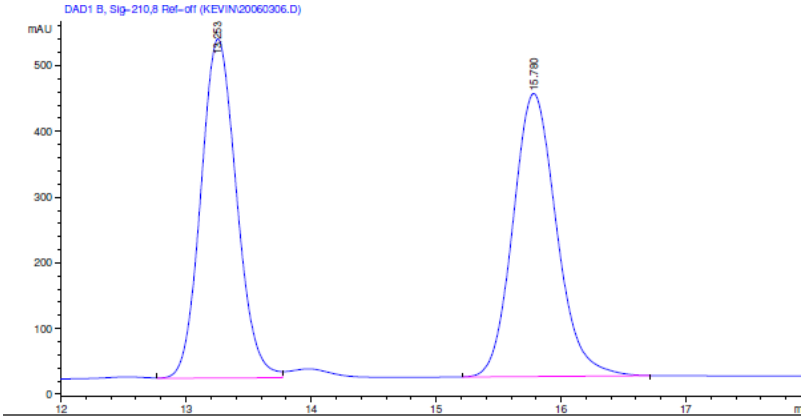


```
================================================================
                    Area Percent Report
================================================================

Sorted By             :      Signal
Multiplier            :      1.0000
Dilution              :      1.0000
Use Multiplier & Dilution Factor with ISTDs


Signal 1: DAD1 B, Sig=210,8 Ref=off

Peak RetTime Type  Width     Area      Height     Area
  #   [min]       [min]   [mAU*s]     [mAU]       %
----|-------|----|-------|----------|----------|--------|
   1  13.253 VV     0.3075 1.02423e4   516.16986  49.5423
   2  15.780 BB     0.3745 1.04315e4   430.83478  50.4577
```

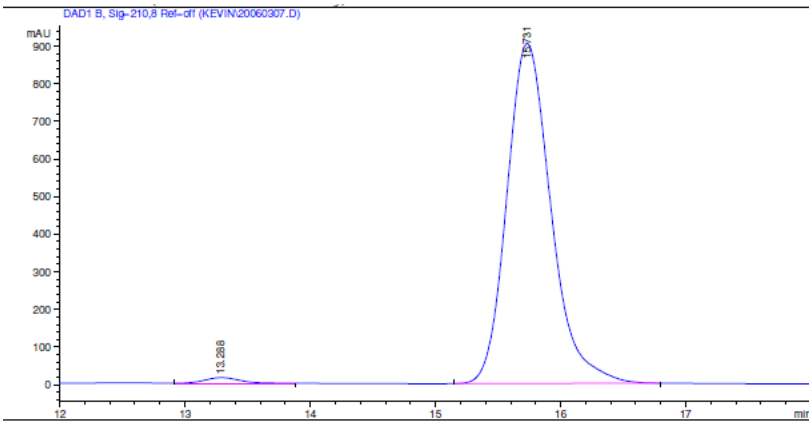


```
================================================================
                    Area Percent Report
================================================================

Sorted By             :      Signal
Multiplier            :      1.0000
Dilution              :      1.0000
Use Multiplier & Dilution Factor with ISTDs


Signal 1: DAD1 B, Sig=210,8 Ref=off

Peak RetTime Type  Width     Area      Height     Area
  #   [min]       [min]   [mAU*s]     [mAU]       %
----|-------|----|-------|----------|----------|--------|
   1  13.288 PB     0.3011  292.13834   15.00712   1.2996
   2  15.731 BB     0.3781 2.21866e4   904.67749  98.7004
```